

# Contributions to the Theory of Atoms and Molecules in Strong Electromagnetic Fields

Sølve Selstø

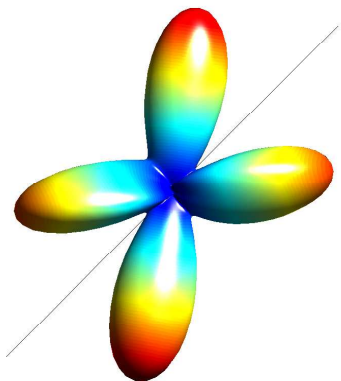
The degree of Philosophiae Doctor



University of Bergen, Norway  
2006



# Contributions to the Theory of Atoms and Molecules in Strong Electromagnetic Fields



Sølve Selstø

Dissertation for the degree of philosophiae doctor

June 2006



Department of Physics and Technology  
University of Bergen



*Når eg ser din himmel, eit verk av dine fingrar,  
månen og stjernene som du har sett der,  
kva er då eit menneske, sidan du kjem det i hug,  
eit menneskebarn, sidan du tek deg av det?*

**Salme 8,4-5.**

*When I consider your heavens, the work of your fingers,  
the moon and the stars, which you have set in place,  
what is man that you are mindful of him,  
the son of man that you care for him?*

**Psalm 8,3-4.**



# Acknowledgements

From the very beginning I would like to stress that this thesis is the product of various collaborations and by no means the work of one man alone. I have been very fortunate to be surrounded by excellent people and very competent researchers. I am truly grateful and honoured for having had the pleasure of being part of this environment – both professionally and socially.

My advisers Prof. Jan Petter Hansen and Prof. Ladislav Kocbach has both done more than what can ever be expected from any adviser. Jan Petter has been able to engage himself in my progress in spite of being tied up with many other obligations at work. The many fruitful and passionate discussions between Ladislav and me will certainly be remembered with love.

However, the one person I have had the pleasure of working the most with is Dr. Morten Førre. The countless hours discussing practically anything has resulted in, among other things, lots of good and interesting physics – at least in my opinion. You are a very important friend and an admirable scientist, Morten.

Gratitude is also owed to Prof. Fernando Martín García for letting me work with him and his group at la Universidad Autónoma de Madrid throughout the year 2004. A lot of state of the art research is done at his group, and I am thankful for having been introduced to this. Also, I deeply appreciate all the support and aid my fellow Ph. D. students in Madrid has provided me – both scientifically, practically and socially. ¡Sois muy, muy amables todos, Paula, Patricia, Lara, Christinas, Ines, Jorge, Luisfe, Felipe, Fran, Goar, Jose Luis, Luis, Omar, Romulo, Sergio, Zaki – todos!. In particular, Dr. Alicia Palacios Cañas deserves special thanks for the very patient and long lasting help she has provided.

My colleges in Bergen has truly been a great support. They have provided a good atmosphere which makes it easy to enjoy work. Doors have always been open for discussions and asking favours. Thank you, Ingrid (Sundvor), Ingrid (Ofte), Victoria, Lene, Nazila, Atle, Gaute, Ingjald, Joakim, Raymond, Suhail, Tore and Trygve!

I would like to thank the Norwegian Research Council, NordForsk, the Department of Physics and Technology and the University for financial support and good working conditions.

During the course of this work I have had the pleasure and privilege of working with various researchers from other European universities in addition to UiB and UAM. In particular, a lot of "constructive interference" has take place between Lars Bojer Madsen and Thomas Kim Kjeldsen in Århus and our group here in Bergen. Thomas has made important contributions in resolving numerical challenges. Also, working with Prof. James McCann in Belfast and Prof. Valentin Ostrovsky and Michail Volkov in St. Petersburg has been very agreeable.

All my other friends deserves a lot of credit for being there. And finally, I feel deep gratitude towards my exceptional family, my parents Haldis and Arvid and my sister Annlaug, for their invaluable love and support. Takk!



# Contents

<b>1</b>	<b>Introduction</b>	<b>1</b>
<b>2</b>	<b>The Schrödinger Equation</b>	<b>3</b>
2.1	The Hydrogen Atom . . . . .	4
2.2	The Non-Local Nature of Quantum Mechanics . . . . .	6
<b>3</b>	<b>The Interaction between Light and Matter</b>	<b>7</b>
3.1	Euler-Lagrange Formalism . . . . .	8
3.2	The Dipole Approximation . . . . .	9
3.2.1	Separability of the Schrödinger Equation . . . . .	10
3.2.2	Alternative Formulations of the Hamiltonian . . . . .	11
3.3	Non-Dipole Effects . . . . .	12
3.3.1	The non-dipole form of the Kramers-Henneberger Hamiltonian . . . . .	12
3.3.2	Separation of the two-particle Hamiltonian in the presence of a spatially dependent field . . . . .	13
3.4	Classical Dynamics . . . . .	15
<b>4</b>	<b>Solving the Schrödinger Equation</b>	<b>17</b>
4.1	The Landau-Zener Model . . . . .	17
4.1.1	The two state case . . . . .	18
4.1.2	The multi-state case . . . . .	20
4.2	Basis Expansion . . . . .	21
4.2.1	B-spline basis sets . . . . .	22
4.3	The Split Operator Method . . . . .	23
4.3.1	Propagation in imaginary time . . . . .	25
4.3.2	Practical examples challenges . . . . .	26
<b>5</b>	<b>Introduction to the Papers</b>	<b>31</b>
<b>6</b>	<b>Summary and Outlook</b>	<b>35</b>
<b>7</b>	<b>Scientific Results</b>	<b>41</b>

<b>A Derivation of the Non-Dipole Form of the Kramers-Henneberger Hamiltonian</b>	<b>143</b>
<b>B Separation of the Schrödinger Equation for Two Particles in a Spatially Dependent Field</b>	<b>145</b>

# List of Papers

- Paper I** *Dynamics of H(2p) ionization in ultrashort strong laser pulses.*  
T. Birkeland, M. Førre, J. P. Hansen, and S. Selstø, Journal of Physics B **37**, 4205 (2004).
- Paper II** *Exact Nondipole Kramers-Henneberger Form of the Light-Atom Hamiltonian: An Application to Atomic Stabilization and Photoelectron Energy Spectra.*  
M. Førre, S. Selstø, J. P. Hansen, and L. B. Madsen, Physical Review Letters **95**, 043601 (2005).
- Paper III** *Strong Orientation Effects in Ionization of H<sub>2</sub><sup>+</sup> by Short, Intense, High-Frequency Light Pulses.*  
S. Selstø, M. Førre, J. P. Hansen, and L. B. Madsen, Physical Review Letters **95**, 093002 (2005).
- Paper IV** *Atoms and Molecules in Strong, High-frequency Fields.*  
J. P. Hansen, M. Førre, S. Selstø, and I. Sundvor, Proceedings, 2nd International Conference on Developments in Atomic, Molecular and Optical Physics with Applications, Delhi, India 2006.
- Paper V** *Geometrical dependence in photoionization of H<sub>2</sub><sup>+</sup> in high-intensity, high-frequency, ultrashort laser pulses.*  
S. Selstø, J. F. McCann, M. Førre, J. P. Hansen, and L. B. Madsen, Physical Review A, **73**, 033407 (2006).
- Paper VI** *Nondipole Ionization Dynamics of Atoms in Super-Intense, High-Frequency, Attosecond Pulses*  
M. Førre, J. P. Hansen, L. Kocbach, S. Selstø and L. B. Madsen, Physical Review Letter in print, 2006.
- Paper VII** *Four-State (Two-Spin) Non-Stationary Models.*  
V. N. Ostrovsky, M. V. Volkov, J. P. Hansen, and S. Selstø, Submitted to Physical Review.

- Paper VIII** *Coherent Single-Electron Transport between Coupled Quantum Dots.*  
S. Selstø, and M. Førre, Submitted to Physical Review.
- Paper IX** *Electron angular distribution in resonance enhanced two-photon ionization of  $H_2^+$  by ultrashort laser pulses*  
S. Selstø, A. Palacios, J. Fernández, and F. Martín, to be submitted to  
Physical Review.

# Chapter 1

## Introduction

In 1960 Theodore Harold Maiman reported the first working laser (1). Although interesting to scientist, few people could have predicted the usefulness of this new technology. In the early days it was said to be "a solution looking for a problem". At present, however, numerous such problems have been found. In our every day life lasers are encountered for instance when listening to CD-s and watching DVD-films, talking on the phone, on the dance floor, when going to the supermarket and during traffic controls. Maybe the most important applications are the ones that are *not* encountered every day, though. For example, laser technology is widely used within medicine and science.

The main application of lasers in medicine is various kinds of surgery. There are also applications to diagnostics (2). Within science, it proves very useful for measurements. For instance, very precise measurements of distances can be performed – on almost any scale. Lasers are used for spectroscopy, i.e. measuring the energies of microscopic systems, and with short pulses, one is able to monitor chemical reactions on the actual time scale of the reaction. Other interesting applications are laser cooling and optical tweezing. Finally, one hope for the future is that energy may be produced by fusion of small nuclei in combinations of very strong laser fields (3).

The acronym "laser" stands for "light amplification by stimulated emission of radiation". Contrary to "ordinary light", laser light is coherent and practically monochromatic, i.e. it contains only one wavelength. Typically it is very focused, so that the intensity of the radiation may be extremely high. Over the years different techniques have been used to make lasers. Maiman used a silver coated rod of ruby, which is an example of a solid state-state laser. Nowadays, semiconductor lasers are most common. The newest and maybe most impressive contribution to the family is the free electron laser, which uses a relativistic beam of electrons. With the improved technology, the intensity, the shortness of the pulses and the photon energy of lasers are also improved (5). Lasers with photon energies of about 100 eV and pulse duration as low as 250 as has been demonstrated (6), and intensities can reach beyond  $10 \text{ TW/cm}^2$ .

It is expected that, as the intensity and frequency of laser pulses become increasingly high, we will acquire new knowledge about the interaction between matter and light. Much theoretical effort has been made during the last decades in order to describe both atoms and molecules in strong attosecond laser fields.

For very high-frequency laser fields the oscillations of the field may be fast even on the atomic scale. This, in turn may cause electrons to experience some time-average effect of the field rather than the instantaneous one. This may be related to the phenomenon of atomic stabilisation (7).

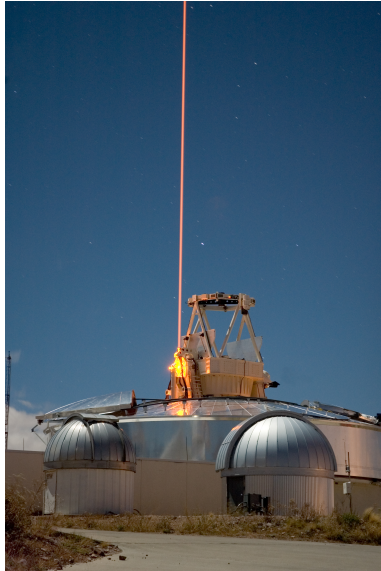


Figure 1.1: This picture is from Starfire Optical Range on Kirtland Air Force Base, New Mexico, USA (4). The laser is used to eliminate atmospheric distortions in order to get as clear images as possible of objects in space.

Another issue raised by both the shortness of the wavelength of the field and its high intensity, is the importance of the magnetic interaction. In many cases, the spatial dependence of the laser field may be neglected so that it is adequately described by a homogeneous electric field. However, as intensities and frequencies increase, this approximation breaks down.

Both these issues are central parts of the present work. The thesis contains six chapters. Chapter 2 is a brief introduction to the Schrödinger equation, which is the starting point for most of the results presented. Chapter 3 describes the interaction between matter and light, and methods used to solve the time dependent Schrödinger equation are briefly outlined in chapter 4. The scientific papers, which are found in chapter 7, constitute the main part of the thesis. Each of the these papers are introduced in chapter 5. Chapter 6 contains a summary of what has been done along with a few ideas about the direction of future work.

In most of the papers and in parts of the thesis atomic units are used. They are defined by choosing Planck's constant divided by  $2\pi$ ,  $\hbar = 1.05 \cdot 10^{-34}$  Js, as the unit of angular momentum, the Bohr radius,  $a_0 = 4\pi\varepsilon_0\hbar^2/m_e e^2 = 5.29 \cdot 10^{-11}$  m, as the unit of length and the electron mass,  $m_e = 9.1 \cdot 10^{-31}$  kg, as the unit of mass. Atomic units are practical since this choice simplify the relevant equations considerably, and the magnitudes of the quantities become moderate on the atomic scale. However, they have the disadvantage that for most people they are not easily related to quantities encountered in every day life, as is the case for the SI-units.

# Chapter 2

## The Schrödinger Equation

At the end of the 19th century and in the beginning of the last one, various discoveries forced scientist to change their understanding of nature in a profound way. The consequences reached far beyond the realm of mere physics. For instance, the Michelson Morley experiment showed that the speed of light is the same regardless of the observer's velocity relative to the light source, which, in turn, lead Albert Einstein to put forward his famous theory of special relativity in 1905 (8; 9). With this theory, space and time could no longer be considered two separate, absolute concepts; measurements of lengths or time intervals are modified by the movement of the observer.

This was not the only revolutionary hypothesis put forward by Einstein this year. Among other things he was also able to explain the photo-electric effect (10), in which he claims that charges are liberated to carry current by absorbing light-quanta – one at a time – of a certain energy which is given by the wavelength of the light. However, the idea of light as consisting of small quanta does not originate from Einstein. It was first introduced by Max Planck in order to explain the spectrum of black body radiation (11). Planck intended this idea to be no more than a mathematical tool. He was even disappointed to learn that his "trick" turned out to change our understanding of light completely. The traditional understanding of light as waves was no longer sufficient; it had to be acknowledged that sometimes light behaves as particles. This new insight in the nature of light was soon to have consequences for our understanding of matter as well.

Bohr was among the very first to try and formulate the principles of quantum mechanics. His model of the hydrogen atom was able to explain the Rydberg formula for the spectral emission lines from hydrogen gas through the relation (12)

$$E_n = -\frac{me^4}{2(4\pi\varepsilon_0)^2\hbar^2} \frac{1}{n^2}, \quad (2.1)$$

which was already known to agree very well with measured spectra. Here  $E_n$  is the energy of the atom in state number  $n$ ,  $e$  is the elementary charge and  $\varepsilon_0$  is the permittivity of free space. Although the Bohr model is considered obsolete nowadays, he should be accredited for having formulated the idea of a discretised energy spectrum of atoms.

In 1923 Luis de Broglie, inspired by Planck, Einstein and Bohr, among others, made the bold step of suggesting, in his Ph. D. thesis, that since light turns out to be particles as well as waves, also matter may behave as waves as well as particles. Few years later, his hypothesis was confirmed by experiments made by C. J. Davisson and L. H. Germer (13) and by G. P. Thomson (14).

All these observations paved the way for a completely new understanding of matter and its interactions. However, it was not at all trivial to formulate a theory that could embrace these new phenomena in a consistent manner. The process that finally lead to the formulation of quantum mechanics is an excellent example of the fruitfulness of cooperation and exchange of ideas. Many letters were written and hours of discussions took place – not the least in Niels Bohr’s institute in Copenhagen.

Erwing Schrödinger was convinced that if particles are to be considered waves, they should be described by a wave equation. In 1926 he developed and presented these ideas in a famous series of six papers (15). His first published version of the equation for a particle in a static potential reads

$$\Delta\psi + \frac{8\pi^2m}{h^2}(E - V)\psi = 0 \quad (2.2)$$

Here  $\Delta = \nabla^2$  is the Laplace operator, the eigenvalue  $E$  is the energy and  $V$  is the potential. He considered the particle to be represented by a standing wave. For the hydrogen atom the solution of this equation leads to the Bohr formula, Eq. (2.1), for the energies.

In fact, before this Schrödinger had already developed a relativistic version of the equation. This was not published, however, because the energies predicted did not coincide with the Sommerfeld correction to the Bohr formula (16). Schrödinger’s relativistic equation is actually the time independent version of the equation now known as the Klein-Gordon-Foch equation, which is valid for particles of spin zero.

In the following papers Schrödinger incorporated the description of an electric field in his wave equation, developed formalism for describing more complex systems, showed how perturbation theory could be applied to quantum mechanics, and finally formulated the dynamic generalisation of Eq. (2.2) (17). For a single particle the time-dependent Schrödinger equation may be written

$$\left\{ -\frac{\hbar^2}{2m}\nabla^2 + V(\mathbf{r}, t) \right\} \Psi(\mathbf{r}, t) = i\hbar \frac{\partial}{\partial t} \Psi(\mathbf{r}, t). \quad (2.3)$$

Shortly before Schrödinger published his wave equation, Werner Heisenberg had formulated another theory of quantum mechanics called *matrix mechanics*. This was shown by Schrödinger to be equivalent to his wave mechanical formulation.

Schrödinger’s equation gained acceptance rather quickly. However, its *meaning* was to be subject to intense debate. Specifically, how was the wave function  $\Psi$  to be interpreted? Max Born suggested that the square of the absolute value of the wave function,  $|\Psi|^2$  represents the probability density of finding the particle at position  $\mathbf{r}$ . These ideas were developed further by Bohr in cooperation with Heisenberg, among others.

## 2.1 The Hydrogen Atom

We will very briefly consider the solutions of the stationary Schrödinger equation for the hydrogen atom. For this system, Eq. (2.2) may be written

$$\left\{ -\frac{\hbar^2}{2m}\nabla^2 - \frac{e^2}{4\pi\varepsilon_0 r} \right\} \psi(\mathbf{r}) = E\psi(\mathbf{r}). \quad (2.4)$$

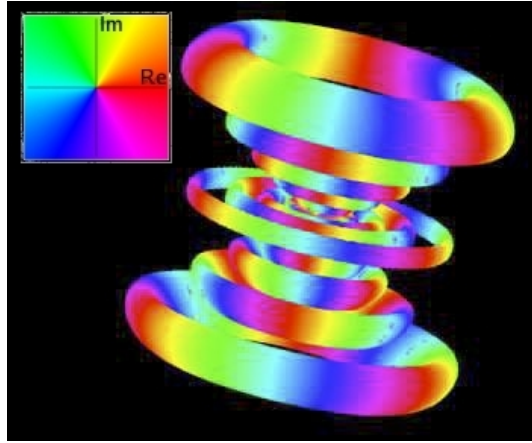


Figure 2.1: The wave function of a highly excited hydrogen bound state with quantum numbers  $n = 10$ ,  $l = 5$  and  $m = 3$ . The picture is taken from Ref. (18). The picture shows an isosurface of the absolute value of the wave function. The colours encode the phase according to the colour circle convention in the upper left corner. The diameter of this structure is about  $3 \cdot 10^{-8}$  m.

For a hydrogen atom the equation is analytically solvable. One discrete set of solutions for energies below zero, i.e. *bound states*, may be written as

$$\psi_{nlm} = R_{n,l}(r) Y_{l,m}(\theta, \varphi). \quad (2.5)$$

The radial part  $R_{n,l}$  is proportional to  $\rho^l e^{-\rho/2} L_{n+l}^{2l+1}(\rho)$  where  $\rho = 2r/na_0$  and  $L^j$  are associated Laguerre polynomials, and the angular part  $Y_{l,m}(\theta, \varphi)$  is proportional to  $P_l^{|m|}(\cos \theta) e^{im\varphi}$  where  $P_l^m$  are associated Legendre functions.

The quantum numbers  $n$ ,  $l$  and  $m$  are related to the energy (through Eq. (2.1)), the angular momentum of the system and the projection of the angular momentum on some pre-chosen axis, respectively. An example of such a wave function is illustrated in Fig. 2.1. Obtaining the energy spectrum of atomic hydrogen in such a consistent manner may be considered the first great triumph of Schrödinger's wave equation.

For unbound system the energy is no longer quantised, and the eigenfunctions,  $\psi_{k,l,m} = R_{k,l}(r) Y_{l,m}(\theta, \phi)$ , constitute a continuous basis in which the wave number  $k = \sqrt{2mE/\hbar}$  may have any positive value.

The quantum numbers  $l$ , and  $m$  are subject to the constraints  $l = 0, 1, \dots, n$  and  $m = -l, -l + 1, \dots, l$ , respectively. Consequently,  $n^2$  states corresponds to the same energy  $E_n$ . This high degree of *degeneracy* is a consequence of the special nature of the  $\sim 1/r$ -potential. Since it is spherically symmetric, all three components of the angular momentum are conserved. Furthermore, another spatial vector, namely the Runge-Lenz vector, is also conserved. In group theoretical terms, this is a manifestation of the  $SO(4)$ -symmetry (19).

For system with more than one electron, the degree of symmetry is strongly reduced due to the interaction between the electrons.

## 2.2 The Non-Local Nature of Quantum Mechanics

Einstein was very displeased about the direction quantum mechanics had taken. He felt that, although it may be *correct*, it could not possibly be a *complete* theory. He was particularly unhappy about the probabilistic, non-deterministic nature of the theory<sup>1</sup>. In order to "prove" its inadequacy, he and two of his colleagues formulated what they considered to be a paradox in which two particles, according to quantum mechanics, could have 100 % correlated, yet undecided, physical quantities at arbitrarily large separation (20). Thus, a measurement on one of the particles would completely determine the outcome of a measurement of the same quantity on the other particle instantly, which Einstein claimed to be in violation of the principle of relativity; no information can travel faster than the speed of light. They drew the conclusion that there had to be more to know about the system than what quantum mechanics was able to predict.

The correlation mentioned above arises from what is called *entanglement*; a system of, say, two particles is *not* described by the combination of the state of each one of them but rather by some global, common state. Schrödinger, who introduced the term "entanglement", said, referring to this phenomenon: "I would not call that *one* but rather *the* characteristic trait of quantum mechanics, the one that enforces its entire departure from classical lines of thought" (23).

In the early 1980s, one was able to investigate the issue of the EPR-paradox experimentally. Earlier, John Bell had shown that if we, inspired by Einstein, assumed that the correlation between seemingly entangled particle was due to some local *hidden variables*, measurements would be correlated in a different way than predicted by quantum mechanics. He suggested an experiment, which Alan Aspect and coworkers were able to perform. They found a very good agreement with the predictions of quantum mechanics (22).

Another manifestation of the non-local nature of dynamical, microscopic systems is interference. In classical mechanics, a system starts out in a well defined initial state and evolves uniquely into another. In quantum mechanics, however, the initial state is not precisely known – in the classical sense, and we may think of the system as following several separate evolutions simultaneously. When the amplitudes of these distinct "paths" interfere with each-other, the phases gives raise to an interference effect that does not have any classical analogue. The multiple path Landau-Zener model, which is described later in this thesis, may serve as an illustrative example of this phenomenon.

In addition to the heavy impact on physics and our understanding of nature, every day life has also felt the consequences of modern physics – for better and for worse. Inventions such as lasers (with all its applications), transistors and integrated circuits, nuclear magnetic resonance imaging (MRI), nuclear energy and weapons and GSM-navigation are all results of these theories. At present much effort is made in order to obtain control of quantum systems through manipulating them with electromagnetic fields. These efforts may enable us, among other things, to obtain optical control of chemical reactions, nano-fabrication and handling information on a quantum level. Our dream is that this may open new doors within medicine, information technology and energy production. This *may* make us better equipped to make conditions for life on earth more sustainable. In doing so, however, we should *not* wait until these new technologies are available.

---

<sup>1</sup>The famous claim "God does not play dice" was put forward by Einstein in this context. Bohr's response is both simple and wise: "Who are you to tell God what to do?"

# Chapter 3

## The Interaction between Light and Matter

The electromagnetic field is governed by the well known Maxwell equations. In differential form they read

$$\nabla \cdot \mathbf{E} = \frac{1}{\epsilon_0} \rho \quad (3.1)$$

$$\nabla \cdot \mathbf{B} = 0 \quad (3.2)$$

$$\nabla \times \mathbf{E} = -\frac{\partial}{\partial t} \mathbf{B} \quad (3.3)$$

$$\nabla \times \mathbf{B} = \mu_0 \mathbf{J} + \mu_0 \epsilon_0 \frac{\partial}{\partial t} \mathbf{E}, \quad (3.4)$$

where  $\mathbf{E}$  and  $\mathbf{B}$  is the electric and magnetic field, respectively,  $\rho$  is the charge density, and  $\mathbf{J}$  is the current density.

By expressing the fields by the vector potential,  $\mathbf{A}$ , and the scalar potential  $\varphi$ ,

$$\mathbf{E} = -\frac{\partial}{\partial t} \mathbf{A} - \nabla \varphi \quad (3.5)$$

$$\mathbf{B} = \nabla \times \mathbf{A}, \quad (3.6)$$

Eqs. (3.2) and (3.3) are automatically satisfied. The vector and scalar potentials are found by substituting Eqs. (3.5) and (3.6) into Eqs. (3.1) and (3.4). However, this does not determine the potentials completely; we may impose further restrictions which do not affect the physics. There are several possible ways of doing this, which are referred to as *gauges*. Here we will use the Coulomb gauge restriction, which demands that the divergence of the vector potential is zero:

$$\nabla \cdot \mathbf{A} = 0 \quad (3.7)$$

If we limit ourselves to free fields, i.e. with no charge nor current, the scalar potential is zero, and the vector potential (in the Coulomb gauge) is given by

$$c^2 \nabla^2 \mathbf{A} = \frac{\partial^2}{\partial t^2} \mathbf{A}, \quad (3.8)$$

which is the well known wave equation. Here  $c = (\epsilon_0 \mu_0)^{-1/2}$  is the speed of light. One is easily persuaded that any linear combination of functions of form  $\mathbf{f}(\omega t - \mathbf{k} \cdot \mathbf{r})$  such that  $\omega/|\mathbf{k}| = c$  is a solution of Eq. (3.8). Hence, the general solution may be written as

$$\mathbf{A}(\mathbf{r}, t) = \int d^3k \sum_{\lambda=1}^2 \{a(\mathbf{k}, \lambda) \exp[i(\omega t - \mathbf{k} \cdot \mathbf{r})] + a^*(\mathbf{k}, \lambda) \exp[-i(\omega t - \mathbf{k} \cdot \mathbf{r})]\} \varepsilon_{\hat{\mathbf{k}}, \lambda}. \quad (3.9)$$

The polarisation vectors  $\varepsilon_{\hat{\mathbf{k}}, \lambda}$ ,  $\lambda = 1, 2$ , are orthogonal to each other and to the propagation direction  $\hat{\mathbf{k}}$ . The three components of  $\mathbf{k}$  may be discretised by imposing a cavity on the system.

In quantum mechanics, the electromagnetic field, as well as the system of matter particles, is described by a state vector in its own Hilbert space. Furthermore, the field, as any physical quantity, is represented by operators. In the case of the vector potential, which gives the physical quantities  $\mathbf{E}$  and  $\mathbf{B}$ , we let the expansion coefficients  $a^{(*)}(\mathbf{k}, \lambda)$  become operators. The  $a(\mathbf{k}, \lambda)$ -s are the annihilation operators, which reduce the number of field quanta in the mode given by the momentum  $\mathbf{k}$  and polarisation  $\lambda$  by one. Accordingly,  $a^*(\mathbf{k}, \lambda) \rightarrow a^\dagger(\mathbf{k}, \lambda)$  is the creation operator, which increases the number of quanta, i.e. photons, in the mode by one.

However, for strong fields, the number of photons in a mode may be so high, in the order of  $10^6$  or more, that any basis representation of the photon states would be unfeasible. On the other hand, according to the correspondence principle of Bohr (24), for high quantum numbers, classical physics should be reproduced. Hence, we should be able to describe the field classically in the following, i.e.  $\mathbf{A}$  will be a scalar quantity, not an operator. A rigorous proof of the validity of this approximation for strong fields is found in Ref. (25).

Alternatively, this procedure may be justified by the ideas of Briggs and Rost (26). They have shown that for some small quantum system coupled to another much larger<sup>1</sup> system, the larger one may be described classically in the interaction. Furthermore, based on the same idea, they are able to deduce the time dependent Schrödinger equation from the time independent one with a statistical description of the interaction. This semi-classical approach has a long history within collision physics (27).

We will now turn to the issue of how the interaction between the (classical) electromagnetic field and matter is described.

### 3.1 Euler-Lagrange Formalism

The starting point is the classical Euler-Lagrange formalism (28). In this context, the classical Hamiltonian function for a particle with mass  $m$  is given by

$$H = \frac{1}{2m} \sum_{i=1}^3 p_i \dot{q}_i + V, \quad (3.10)$$

where  $p_i$  are the components of the generalised momenta,  $q_i$  are the generalised coordinates and  $V$  is some external potential.

---

<sup>1</sup>What is meant by "larger" is defined very precisely by an asymmetry condition on the energies of the systems.

The generalised momentum is defined by the Lagrangian function  $\mathcal{L}$ ,

$$p_i = \frac{\partial \mathcal{L}}{\partial \dot{q}_i}. \quad (3.11)$$

The Lagrangian is to be chosen such that it reproduces Newton's second law with the Lorentz force,

$$m\ddot{\mathbf{r}} = q(\mathbf{E} + \mathbf{v} \times \mathbf{B}), \quad (3.12)$$

through the Euler-Lagrange equation,

$$\frac{d}{dt} \frac{\partial \mathcal{L}}{\partial \dot{q}_i} - \frac{\partial \mathcal{L}}{\partial q_i} = 0. \quad (3.13)$$

This is achieved with

$$\mathcal{L} = \frac{1}{2}mv^2 - V + q\mathbf{v} \cdot \mathbf{A}. \quad (3.14)$$

Here  $q$  is the charge of the particle and  $\mathbf{v}$  is its velocity.

Inserting Eqs. (3.14) and Eq. (3.11) into Eq. (3.10), we arrive at the Hamiltonian

$$H = \frac{1}{2m}(\mathbf{p} - q\mathbf{A})^2 + V(\mathbf{r}) = H_0 + H_I \quad (3.15)$$

where  $H_0 = 1/2m p^2 + V$  is the Hamiltonian of the unperturbed particle and the interaction is given by

$$H_I = -\frac{q}{m}\mathbf{A} \cdot \mathbf{p} + \frac{q^2}{2m}A^2. \quad (3.16)$$

## 3.2 The Dipole Approximation

For monochromatic light the wavelength may be much larger than the extension of the system at hand. For instance, red light has a wavelength of about 700 nm, whereas the typical size of a molecule in the ground state is about 1 nm. In such cases, when the extension of the atomic system is not greatly increased by the interaction, the spatial variation of the field may be neglected. This corresponds to a zeroth order expansion in the spatial variables of the field,

$$\exp[i(\omega t - \mathbf{k} \cdot \mathbf{r})] = \exp[i\omega t] + \mathcal{O}(\omega r/c).$$

When this approximation is applied to Eq.(3.15), it is referred to as the *dipole approximation*.

This approximation is widely used. However, as the wavelength grows shorter and the field grows stronger, non-dipole effects may come into play. Part of this work is devoted to the study of such effects.

It should be noted that large atomic system does not necessarily imply significant non-dipole effects since dynamics in many cases primarily takes place near the nucleus.

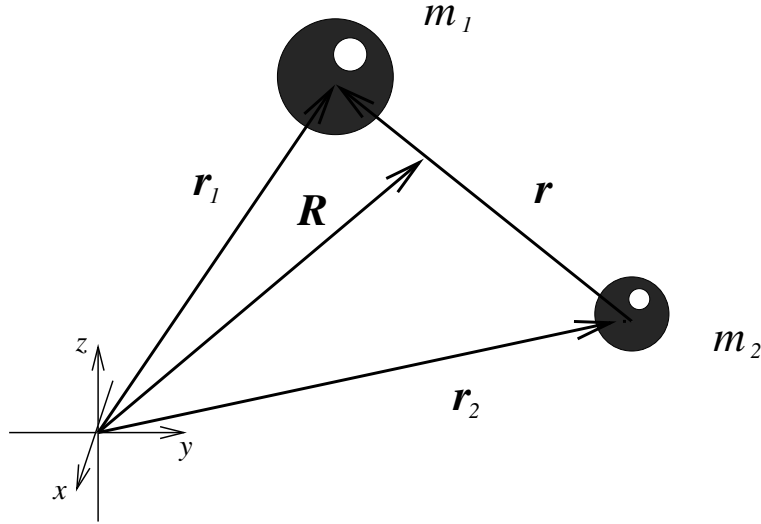


Figure 3.1: The coordinates of the two particles,  $\mathbf{r}_1$  and  $\mathbf{r}_2$ , along with the centre of mass and relative coordinates  $\mathbf{R}$  and  $\mathbf{r}$ .

### 3.2.1 Separability of the Schrödinger Equation

When solving the time dependent Schrödinger equation for, e.g., the hydrogen atom or a hydrogen like atom in an electromagnetic field, it is usually assumed that the proton may be considered fixed, and the only dynamics is that of the electron relative to the position of the nucleus. This seems reasonable considering the large ratio between the proton and the electron masses. However, for any system of two charged particles, the Schrödinger equation is easily reduced to an effective one particle equation when the dipole approximation applies.

For two particles in the field  $\mathbf{A}$ , Eq. (3.15) is straightforwardly generalised:

$$H = \frac{1}{2m_1}(\mathbf{p}_1 - q_1\mathbf{A}(\mathbf{r}_1, t))^2 + \frac{1}{2m_2}(\mathbf{p}_2 - q_2\mathbf{A}(\mathbf{r}_2, t))^2 + \frac{q_1q_2}{|\mathbf{r}_1 - \mathbf{r}_2|}. \quad (3.17)$$

We define a new set of coordinates, namely the centre of mass (CoM) coordinates and the relative coordinates, by

$$\left. \begin{array}{l} \mathbf{R} = \frac{1}{M}(m_1\mathbf{r}_1 + m_2\mathbf{r}_2) \\ \mathbf{r} = \mathbf{r}_1 - \mathbf{r}_2 \end{array} \right\} \Leftrightarrow \left. \begin{array}{l} \mathbf{r}_1 = \mathbf{R} + \frac{m_2}{M}\mathbf{r} \\ \mathbf{r}_2 = \mathbf{R} - \frac{m_1}{M}\mathbf{r} \end{array} \right\} \quad (3.18)$$

The coordinates are illustrated in Fig. 3.1.

The corresponding generalised momenta,  $\mathbf{P}$  and  $\mathbf{p}$ , respectively, are still given by Eq. (3.11). By expressing the Hamiltonian in these coordinates and neglecting the spatial dependence of the field, the Hamiltonian may be separated in three parts:  $H_R$ , corresponding to the  $\mathbf{R}$ -coordinate,  $H_r$ , corresponding to the  $\mathbf{r}$ -coordinate, and  $H_t$ , which is purely time dependent. Specifically we have:

$$\begin{aligned} H &= H_R + H_r + H_t \\ H_R &= \frac{P^2}{2M} - \frac{Q}{M}\mathbf{A}(t) \cdot \mathbf{P} \end{aligned} \quad (3.19)$$

$$\begin{aligned} H_r &= \frac{p^2}{2\mu} - \frac{\tilde{q}}{\mu} \mathbf{A}(t) \cdot \mathbf{p} + V_C(r) \\ H_t &= (A(t))^2 \left( \frac{Q^2}{2M} + \frac{\tilde{q}^2}{2\mu} \right). \end{aligned}$$

where the total mass  $M$  and the reduced mass  $\mu$  are defined by

$$M \equiv m_1 + m_2, \quad (3.20)$$

$$\mu \equiv \frac{m_1 m_2}{m_1 + m_2}, \quad (3.21)$$

and the total charge  $Q$  and the reduced charge  $\tilde{q}$  are defined by

$$Q \equiv q_1 + q_2, \quad (3.22)$$

$$\tilde{q} \equiv \frac{1}{M} (q_1 m_2 - q_2 m_1) = \mu \left( \frac{q_1}{m_1} - \frac{q_2}{m_2} \right), \quad (3.23)$$

respectively. The last term in Eq. (3.19) may be removed by a trivial phase transformation of the wave function.

With the Hamiltonian reduced to separate terms depending only on  $\mathbf{R}, \mathbf{P}$  and  $\mathbf{r}, \mathbf{p}$ , respectively, the separation is trivial. As we will see later, separation is less trivial when the spatial dependence of the field is taken into consideration.

### 3.2.2 Alternative Formulations of the Hamiltonian

The form of the Hamiltonian Eq. (3.15) is commonly referred to as *velocity gauge*. This reflects the fact that the generalised momentum is shifted compared to the canonical momentum,  $m\mathbf{v}$ , by  $q\mathbf{A}$  which corresponds to the momentum of a classical free particle in the presence of the electric field  $\mathbf{E} = -\dot{\mathbf{A}}$ .

Within the dipole approximation, there are various ways to formulate the the Hamiltonian of the interaction. In general, by imposing some norm conserving (unitary) transformation  $T$  on the state  $|\Psi\rangle$ ,

$$|\Psi'\rangle \equiv T|\Psi\rangle,$$

the Hamiltonian may be brought from  $H$  to  $H'$ , which has generic form

$$H' = THT^\dagger + i\dot{T}T^\dagger. \quad (3.24)$$

In the following we will consider two other forms of the interaction, which constitute alternatives to the velocity gauge, namely the *length gauge* description and the *Kramers-Henneberger frame*.

#### The length gauge

If the unitary phase transformation

$$T_l = \exp(-iq\mathbf{r} \cdot \mathbf{A}(t)) \quad (3.25)$$

(in atomic units) is applied to Eqs. (3.15) and (3.24), the new Hamiltonian will be

$$H_l = \frac{1}{2m} p^2 + V(\mathbf{r}) - qr \cdot \mathbf{E}. \quad (3.26)$$

In this case the interaction,  $-qr \cdot \mathbf{E}$ , has a somewhat more intuitive form than in velocity gauge: It is the potential energy of a dipole of charges  $\pm q$  at separation  $\mathbf{r}$  in the presence of the electric field  $\mathbf{E}$ . This is the origin of the term "dipole approximation".

In this formalism, the canonical and generalised momenta coincide,  $\mathbf{p} = m\mathbf{v}$ . It is also possible to arrive at Eq. (3.26) through the Lagrangian function by adjusting the vector and scalar potential in a way that does not change  $\mathbf{E}$  nor  $\mathbf{B}$ , i.e. by performing a gauge transformation – hence the name length *gauge*.

### Kramers-Henneberger frame

The Kramers-Henneberger (KH) form of the Hamiltonian is obtained by the transformation (in atomic units)

$$T_{\text{KH}} = \exp(-i\boldsymbol{\alpha}(t) \cdot \mathbf{p}), \quad (3.27)$$

$$\boldsymbol{\alpha} \equiv \frac{q}{m} \int_{t_0}^t \mathbf{A}(t') dt', \quad (3.28)$$

which is a translation (24). The resulting Hamiltonian reads

$$H_{\text{KH}} = \frac{1}{2m} p^2 + V(\mathbf{r} - \boldsymbol{\alpha}) + \frac{q^2}{2m} A^2. \quad (3.29)$$

This description of the interaction was first derived by Pauli (29), and later by Kramers and Henneberger (30; 31), after whom it is named. In literature, one will also find that it is called *acceleration gauge*, which is somewhat misleading since it, contrary to the length gauge, cannot be achieved by a gauge transformation (32).

The interaction is induced by the time dependent translation  $\boldsymbol{\alpha}$  of the position vector  $\mathbf{r}$ . This corresponds to a reference frame that follows the path of a classical free particle in the field. Rather than the direct influence from the field, the particle "experiences" a moving potential.

As we will see, it is possible to generalise this description in order to include non-dipole effects.

## 3.3 Non-Dipole Effects

Of course, no magnetic effects can be described with a vector potential independent of the spatial variables (see Eq. (3.6)). In the velocity gauge, Eq. (3.15), the spatial dependence of the field may be fully accounted for in a straightforward manner. But the description in the length gauge is not that straight forward without the dipole approximation (33). When it comes to the KH frame, the transition is somewhat more cumbersome than in the dipole case. However, we will demonstrate here that it may still be done.

### 3.3.1 The non-dipole form of the Kramers-Henneberger Hamiltonian

We will take the vector potential to be represented by a linearly polarised field of the form

$$\mathbf{A}(\eta) = A(\eta)\boldsymbol{\varepsilon} \quad (3.30)$$

where  $\boldsymbol{\varepsilon} \equiv [\varepsilon_x, \varepsilon_y, \varepsilon_z]$  is a unit vector in the direction of the polarisation, and  $\eta$  is defined by

$$\eta \equiv \omega t - \mathbf{k} \cdot \mathbf{r}. \quad (3.31)$$

The Coulomb gauge restriction, Eq. (3.7), is here equivalent to

$$\mathbf{k} \cdot \mathbf{r} = k_x \varepsilon_x + k_y \varepsilon_y + k_z \varepsilon_z = 0. \quad (3.32)$$

The form of the transformation, Eq. (3.27), is maintained, but translation  $\boldsymbol{\alpha}$  is slightly redefined as compared to Eq. (3.28):

$$\boldsymbol{\alpha}(\eta) = \frac{q}{\omega m} \int_{\eta_0}^{\eta} \mathbf{A}(\eta') d\eta'. \quad (3.33)$$

In fact, it is not obvious that the transformation  $T_{\text{KH}} = \exp(-\boldsymbol{\alpha}(\eta) \cdot \mathbf{p})$  actually is a translation since  $\boldsymbol{\alpha}$  now depends on spatial variables in addition to time. However, within the Coulomb gauge restriction we find that indeed  $T_{\text{KH}} V(\mathbf{r}) T_{\text{KH}}^\dagger = V(\mathbf{r} - \boldsymbol{\alpha})$ . The transformation of the kinetic energy term,  $T p^2 / 2m T^\dagger$ , gives raise to three new terms.

All in all the final Hamiltonian in the generalised Kramers-Henneberger frame reads

$$\begin{aligned} H_{\text{KH}} = & \frac{1}{2m} p^2 + V(\mathbf{r} - \boldsymbol{\alpha}(\eta)) + \frac{1}{2m} (A(\eta))^2 - \\ & \frac{1}{2m} \left( k^2 (\boldsymbol{\alpha}'(\eta) \cdot \mathbf{p})^2 + ik^2 \boldsymbol{\alpha}''(\eta) \cdot \mathbf{p} + 2(\boldsymbol{\alpha}'(\eta) \cdot \mathbf{p})(\mathbf{k} \cdot \mathbf{p}) \right). \end{aligned} \quad (3.34)$$

In many cases the three last terms may be neglected. By comparing their magnitude to the kinetic energy terms of the same form, we find that a sufficient criterion for this is given by

$$\frac{|q| E_{\max}}{\omega mc} \ll 1, \quad (3.35)$$

where  $E_{\max}$  is the maximum amplitude of the electric field ( $E_{\max} = \omega A_{\max}$ ). In App. A for all details are given.

The above formalism is easily generalised to a circularly polarised field and to any number of particles.

### 3.3.2 Separation of the two-particle Hamiltonian in the presence of a spatially dependent field

We have already seen that within the dipole approximation, the two-particle Schrödinger equation is easily reduced from a six dimensional to an effective three dimensional equation. With a spatially dependent field, which would necessarily depend on both the CoM coordinate  $\mathbf{R}$  and the relative coordinate  $\mathbf{r}$ , this is not possible in the general case (see Eqs. (3.17) and (3.18) or Ref. (34)). However, by expanding the vector potential to first order, we may find cases in which separation is permissible. For simplicity, we let the linearly polarised field of Eq. (3.30) propagate along the  $x$  axis. To first order in  $\omega x/c$  and  $\omega X/c$ , the field at positions  $\mathbf{r}_1$  and  $\mathbf{r}_2$  are given by

$$\mathbf{A}(\mathbf{r}_1, t) \approx \mathbf{A}_0(t) + \frac{1}{c} \mathbf{E}_0(t) \left( X + \frac{m_2}{M} x \right) \quad (3.36)$$

and

$$\mathbf{A}(\mathbf{r}_2, t) \approx \mathbf{A}_0(t) + \frac{1}{c} \mathbf{E}_0(t) \left( X - \frac{m_1}{M} x \right), \quad (3.37)$$

respectively, where the time-only dependent fields  $A_0$  and  $E_0$  are the respective fields evaluated at the origin. Keeping only terms of first order, the velocity gauge Hamiltonian reads

$$H = H' + h' + \left( \frac{Q^2}{2M} + \frac{\tilde{q}^2}{2\mu} \right) A_0^2 - \frac{\tilde{q}}{M} \mathbf{P} \cdot \mathbf{E}_0 \frac{x}{c} - \frac{\tilde{q}}{\mu} \mathbf{P} \cdot \mathbf{E}_0 \frac{X}{c} \quad (3.38)$$

with

$$H' \equiv \frac{1}{2M} P^2 - \frac{Q}{M} \mathbf{P} \cdot \left( \mathbf{A}_0 + \mathbf{E}_0 \frac{X}{c} \right) + \left( \frac{Q^2}{M} + \frac{\tilde{q}^2}{\mu} \right) A_0 E_0 \frac{X}{c} \quad (3.39)$$

$$h' \equiv \frac{1}{2\mu} p^2 + V_C(r) - \frac{\tilde{q}}{\mu} \mathbf{P} \cdot \mathbf{A}_0 - \frac{q'}{\mu} \mathbf{P} \cdot \mathbf{E}_0 \frac{x}{c} + \left( \frac{Q\tilde{q}}{M} + \frac{\tilde{q}q'}{\mu} \right) A_0 E_0 \frac{x}{c}. \quad (3.40)$$

The total and reduced charges,  $Q$  and  $\tilde{q}$ , are already defined in Eqs. (3.22) and (3.23), respectively, whereas the effective charge  $q'$  is defined by

$$q' \equiv \frac{q_1 m_2^2 + q_2 m_1^2}{M^2}. \quad (3.41)$$

The two last terms of Eq. (3.38) prohibit separation. However, for a charged system ( $Q \neq 0$ ) in a strong field they may be neglected upon comparison to other non-dipole terms that do not include any momentum operator. This is related to the fact that for strong enough fields, the  $p$ -distribution in the velocity gauge has a narrow peak centred at the origin (35). This argument also applies to the distribution of the relative momentum  $\mathbf{p}$  in the direction of the field. For neutral systems, the effect of the second last term in Eq. (3.38) may be estimated by assuming thermal motion of the CoM (34). This way its effect may be compared to, e.g., the last term of Eq. (3.40) and neglected when the latter is dominant. The resulting effective one particle Schrödinger equation takes the form

$$i \frac{\partial}{\partial t} \psi(\mathbf{r}, t) = \left\{ \frac{1}{2\mu} p^2 + \frac{q_1 q_2}{r} + \frac{\tilde{q}}{\mu} \mathbf{P} \cdot \mathbf{A} + \left( \frac{Q\tilde{q}}{M} + \frac{\tilde{q}q'}{\mu} \right) A E \frac{x}{c} \right\} \psi(\mathbf{r}, t). \quad (3.42)$$

Another interesting observation is that when the reduced charge  $\tilde{q}$  vanish, as is the case, e.g., for a system consisting of two identical particles, the Schrödinger equation separates exactly (to first order in  $\omega x/c$ ). Recently Smirnova et al. demonstrated that, within the dipole approximation, a proton and a deuterium particle may be quasi bound by combined linearly and circularly polarised laser fields (3). This raises the question of whether inclusion of non-dipole effects makes binding of two protons feasible in a similar manner. With a linearly polarised field  $\mathbf{A}^\dagger$  polarised in the  $z$ -direction propagating in the  $x$  direction and a circularly polarised field  $\mathbf{A}^\circ$  polarised in the  $xy$  plane propagating in the  $z$  direction, the Schrödinger equation of system may be written as

$$i \frac{\partial}{\partial t} \Psi(\mathbf{r}, t) = \left\{ \frac{1}{m_p} p^2 + \frac{1}{r} - \frac{1}{m_p c} \mathbf{P} \cdot (\mathbf{E}^\circ z + \mathbf{E}^\dagger x) \right\} \Psi(\mathbf{r}, t), \quad (3.43)$$

where  $m_p$  is the proton mass and  $\mathbf{E}^{(\circ)} = -\dot{\mathbf{A}}^{(\circ)}$ .

## 3.4 Classical Dynamics

When describing complex systems, Monte Carlo methods, i.e. methods making use of arbitrary numbers, may be quite useful. The description of the interaction between microscopic systems and light is no exception. Furthermore, in surprisingly many cases adapted classical methods may be applied successfully to study atomic and molecular processes. The classical trajectory Monte Carlo (CTMC) method is an example of such a method. In this scheme, the dynamics is given by classical equations, i.e. Newton's second law. A large number of initial positions and momenta are chosen at random from some initial distribution. Then the classical equations corresponding to each of these initial conditions are solved, and the results are obtained by investigating the whole set of such solutions. There are various ways of constructing initial distributions. One possible choice is the micro-canonical distribution in which the energy of each set of initial conditions is fixed. Specifically, the initial coordinates  $\mathbf{r}_0, \mathbf{p}_0$ , subject to the condition  $1/2 p_0^2 + V(\mathbf{r}_0)$ , are substituted by a new set of coordinates in which the distribution is uniform. This method was introduced by Abrines and Percival in 1966 (36).

Ideally, the distribution of initial conditions should reassemble the quantum mechanical probability distribution as closely as possible – both in position and momentum space. For the micro-canonical distribution, this is impossible, however, since there is an outer limit to the classical position of a bound electron in a potential, and there are no such limit on the quantum mechanical wave function.

For a particle subject to the static potential  $V(\mathbf{r})$  and the external electric field  $\mathbf{E}(\mathbf{r}, t)$  and magnetic field  $\mathbf{B}(\mathbf{r}, t)$ , Newton's second law may be written as a set of coupled ordinary differential equations:

$$\begin{aligned}\dot{\mathbf{r}} &= \mathbf{v} \\ \dot{\mathbf{v}} &= \frac{q}{m}(\mathbf{E} + \mathbf{v} \times \mathbf{B}) - \frac{1}{m}\nabla V.\end{aligned}\tag{3.44}$$

This classical problem is of course much less costly to solve than the quantum mechanical one – also for relatively large sets of initial conditions.

Again referring to the system of quasi bound proton and deuterium, Ref. (3), the above method has been used to investigate the effect of non-dipole terms in binding of bare nuclei (37). These calculations indicate that inclusion of spatial variables in the fields have detrimental effect on the binding of the system. However, we will demonstrate later that this detrimental effect is less pronounced in a fully quantum mechanical description.



# Chapter 4

## Solving the Schrödinger Equation

When solving the Schrödinger equation, analytical solutions are desirable. In addition to being elegant, such solutions represent a very compact way of obtaining results which makes it easier to investigate how the outcome depends on the parameters involved. However, in most cases we are forced to settle for some numerical solution. A wide range of schemes for solving the Schrödinger equation numerically is available. In this chapter we will consider two of them and give practical examples of their application. We will start by considering an analytical method, though.

Throughout this chapter atomic units are used unless stated otherwise.

### 4.1 The Landau-Zener Model

In 1932 no less than four different scientists were able to find analytical solutions to the Schrödinger equation of a quantum system consisting of two states,  $|1\rangle$  and  $|2\rangle$  with some constant coupling  $V$  and linear difference in diagonal energy,  $\langle 2|H|2\rangle - \langle 1|H|1\rangle = bt$ . These four people, who used quite different approaches, where Ettore Majorana (38), Ernst Carl Gerlach Stückelberg (39), Lev Davidovich Landau (40) and Clarence Melvin Zener (41). However, usually only the last two has their names attached to the model.

The model provides an analytical expression for the probability of transition between the two states. Although derived for a very particular – and very small – system, it is widely used today. Reason being that the model invites us to an intuitive understanding of the dynamics which may easily be generalised and applied to larger systems. The underlying idea is that transitions between states take place more or less instantly as the energies, or potential curves, of the two states cross. For a system consisting of several states, transitions between crossing states take place with probability given by the LZ model, whereas the populations of all other states are assumed to be unaltered. An example of such a system to which the LZ model has been applied successfully is shown in Fig. 4.1 (43). It should be noted that in general the phases of the amplitudes of the states involved in crossings are important, not just the populations.

The assumption that transitions takes place at the instant of crossing may be motivated by turning to the basis consisting of instantaneous eigenstates of the time dependent Hamiltonian. We label these time dependent states  $|\chi_j(t)\rangle$  and define them by

$$H(t)|\chi_j(t)\rangle = \epsilon_j(t)|\chi_j(t)\rangle, \quad (4.1)$$

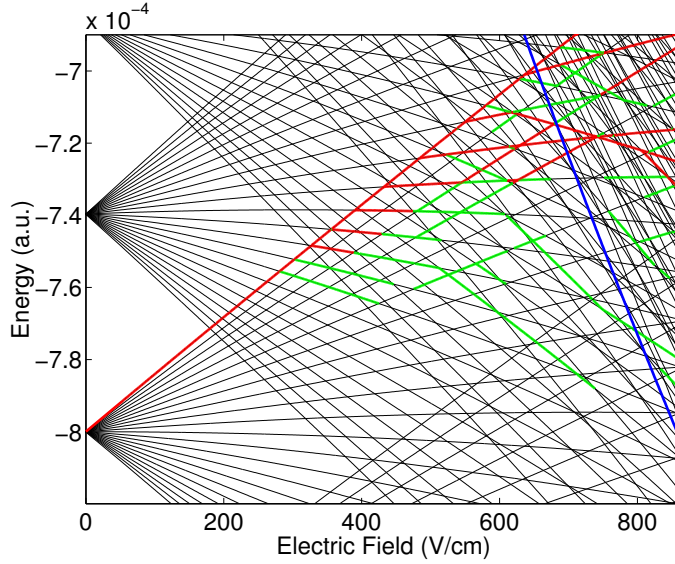


Figure 4.1: The energies of three sub-shell in a lithium atom in the presence of a dc field. The figure is taken from Ref. (43). The red curves correspond to states with population probability  $P$  larger than 1 %, whereas the the green curves correspond to  $0.5 \% \leq P \leq 1 \%$ . The classical ionisation limit is shown as a blue line.

where the  $\epsilon_j$ -s are the eigenenergies of  $H(t)$ . In this basis, which is referred to as the *adiabatic* basis, the potential curves in general exhibit an avoided crossing rather than a crossing according to the von Neumann-Wigner non crossing rule, see, e.g., Ref. (28). If we write the state as a linear combination of the adiabatic states as

$$|\Psi\rangle = \sum_j a'_j \exp\left(-i \int_{t_i}^t \epsilon_j(t') dt'\right) |\chi_j\rangle, \quad (4.2)$$

the Schrödinger equation is equivalent to

$$\frac{\partial}{\partial t} a'_k = \sum_{j \neq k} \frac{\langle \chi_k | \frac{\partial H}{\partial t} | \chi_j \rangle}{\epsilon_k - \epsilon_j} e^{-i \int_{t_i}^t \epsilon_j(t') dt'} a'_j(t). \quad (4.3)$$

From this we see that couplings, and hence the possibility of transitions, between the adiabatic states vanish when the energy separation between two states become large. Furthermore, the above expression together with the non-crossing rule, proves the adiabatic theorem, which says that if the Hamiltonian varies slowly with time,  $\partial H / \partial t \approx 0$ , a system that starts out in the  $n$ 'th eigenstate will remain in the  $n$ th state (42).

In the following we will outline the relevant concepts of the LZ model a bit more precisely.

### 4.1.1 The two state case

We start out by a two state system, which in some basis has a linear energy difference and constant coupling. We will refer to this basis as the *diabatic* basis. We may write the Schrödinger equation

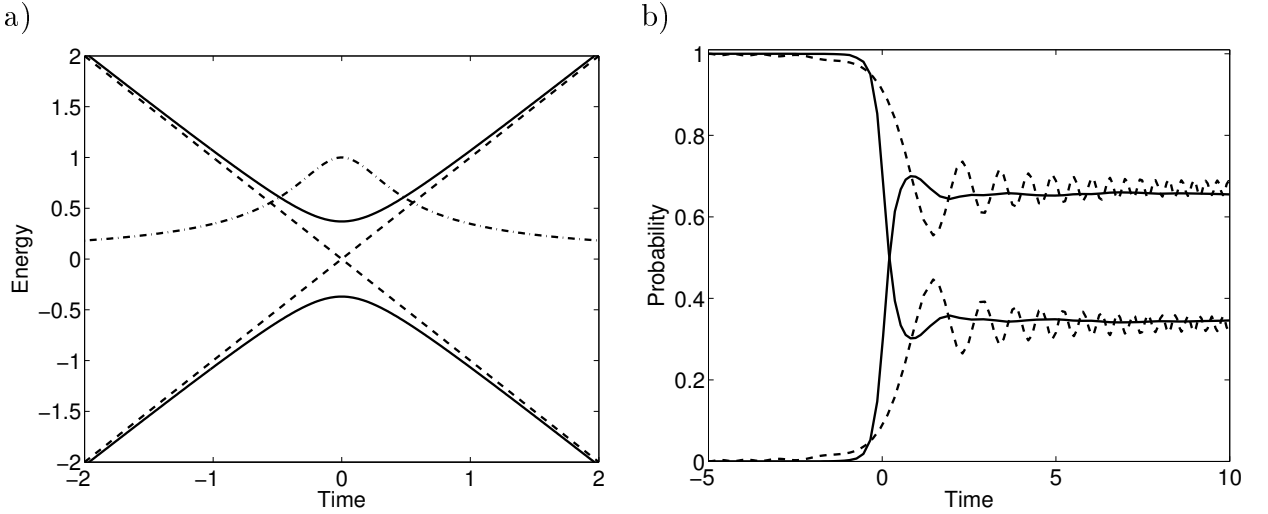


Figure 4.2: *a)* The diabatic (dashed curve) and adiabatic (full curve) diagonal energies. The absolute value of the Lorentzian shaped coupling is also included (dash-dotted curve). *b)* The populations of the two states as functions of time in the diabatic (dashed curve) and adiabatic basis (full curve). In this example we have  $b = 2$  a.u. and  $V = 0.37$  a.u..

as matrix equation,  $i\dot{\mathbf{c}} = H_D \mathbf{c}$ , with the Hamiltonian matrix

$$H_D = \begin{pmatrix} -\frac{1}{2}bt & V \\ V^* & \frac{1}{2}bt \end{pmatrix}, \quad (4.4)$$

The coupling  $V$  is assumed to be real in the following.

In the adiabatic basis, which is obtained by diagonalising the matrix (4.4), the Hamiltonian takes the form:

$$H_A = \begin{pmatrix} -\sqrt{(bt/2)^2 + V^2} & i\frac{bV}{b^2t^2+4V^2} \\ -i\frac{bV}{b^2t^2+4V^2} & \sqrt{(bt/2)^2 + V^2} \end{pmatrix}. \quad (4.5)$$

The diagonal energies within both bases are illustrated in Fig. 4.2 *a*. The adiabatic diagonal energies and basis states coincide with the diabatic ones in the limit  $t \rightarrow \pm\infty$ . At the instant when the diabatic curves cross, the splitting of the adiabatic curves gives the magnitude of the coupling:

$$\Delta\epsilon(t=0) = 2|V|. \quad (4.6)$$

The adiabatic coupling has a well localised Lorentzian shape, whereas it remains constant in the diabatic basis. It is evident that transitions take place much faster in the adiabatic basis than in the diabatic one. This is illustrated in Fig. 4.2 *b*.

In the adiabatic basis, the dynamics may be described through propagators in the form of  $2 \times 2$  matrices:

$$\mathbf{c}(t_f) = J(t_f, 0) S J(0, t_i) \mathbf{c}(t_i), \quad (4.7)$$

where  $\mathbf{c}(t) = (c_1, c_2)^T$  is defined by  $|\Psi(t)\rangle = c_1|\chi_1\rangle + c_2|\chi_2\rangle$ . The initial and final times,  $t_i$  and  $t_f$ , are to be chosen well separated from the crossing. Before and after the crossing, the only

time-evolution is the one corresponding to the adiabatic phase, given by the  $J$ -matrices:

$$J(t_2, t_1) \equiv \text{diag} \left\{ \int_{t_1}^{t_2} \epsilon_1(t') dt', \int_{t_1}^{t_2} \epsilon_2(t') dt' \right\}. \quad (4.8)$$

The transition matrix  $S$  reads

$$S^{(\pm)} = \begin{pmatrix} \sqrt{1-p} e^{i\alpha} & \pm \sqrt{p} \\ \mp \sqrt{p} & \sqrt{1-p} e^{-i\alpha} \end{pmatrix}, \quad (4.9)$$

where  $p$  is the probability of a non-adiabatic evolution (38; 39; 40; 41),

$$p \equiv \exp(-2\pi\delta), \quad \delta \equiv V^2/|b|, \quad (4.10)$$

and the Stokes phase,

$$\alpha \equiv \frac{\pi}{4} + \delta(\ln \delta - 1) - \arg[\Gamma(1 + i\delta)], \quad (4.11)$$

is the phase shift introduced by the crossing.

We emphasise that this description only applies to the adiabatic basis. In the diabatic basis, the phase shift that arises from the crossing is time-dependent.

The sign in Eq. (4.9) is crucial; care must be taken when choosing the right expression. It depends on both the signs of the parameters  $b$  and  $V$  and also the topology of the potential curves of the system.

### 4.1.2 The multi-state case

Within the framework of matrix propagators, the generalisation from two state to multi-state Landau-Zener (MLZ) theory is straightforward. Suppose a system of  $N$  states is subject to  $m$  crossings at times  $t_i$ ,  $i = 1, \dots, m$ . Then

$$\begin{pmatrix} c_1(t_f) \\ c_2(t_f) \\ \vdots \\ c_N(t_f) \end{pmatrix} = J(t_f, t_m) S_m J(t_m, t_{m-1}) S_{m-1} \cdots J(t_3, t_2) S_2 J(t_2, t_1) S_1 J(t_1, t_i) \begin{pmatrix} c_1(t_i) \\ c_2(t_i) \\ \vdots \\ c_N(t_i) \end{pmatrix}. \quad (4.12)$$

The  $S$ -matrices are constructed by inserting the elements of the  $2 \times 2$  matrix Eq. (4.9) in the entries corresponding to the adiabatic states involved in the avoided crossing, and the rest of it corresponds to the identity matrix. The  $J$ -matrices are constructed by a direct generalisation of Eq. (4.8).

In this propagation scheme, there are three kinds of phases involved, namely the adiabatic or dynamic phases given by the time integral of the adiabatic energies, the instantaneous phase shift  $\alpha$  and signs arising from "book-keeping" arguments. In some particular cases, these phases are unimportant. (44; 45). However, unless the system has some special topology, they all play a crucial role.

In order to be able to apply Eq. 4.12, it is crucial that the transition dynamics at one crossing do not interfere with the dynamics corresponding to the next one. From Eq. (4.5) we may find a

criterion for this. We define the interaction time  $\tau$  as the width of the Lorentzian coupling at 10 % of its maximum value,  $1/(b^2\tau^2 + 4V^2) = \frac{1}{10} \cdot 1/(4V^2)$ , which gives

$$\tau = 6 \left| \frac{V}{b} \right|. \quad (4.13)$$

By demanding that two consecutive couplings do not overlap considerably we arrive at

$$t_{n+1} - t_n > \frac{1}{2}(\tau_{n+1} + \tau_n) \quad \forall n. \quad (4.14)$$

Although this is only a necessary condition, not a sufficient one, we expect that it should serve at least as an estimate of the applicability of the MLZ model.

### Second order transitions

Obviously, if the coupling  $V$  in Eq. (4.4) vanishes, no transition takes place. Analogously, one may expect that no transitions will take place between two uncoupled crossing diabatic states in some system consisting of more than two states. However, this is not necessarily the case. The Hamiltonian matrix of such a diabatic system may still feature avoided crossings between the eigenenergies. The splitting will in general be of order  $\sim V^2$  as opposed to  $\sim V$ , cf. Eq. (4.6). From this a "pseudo-coupling" may be found and inserted into Eq. (4.10) in order to find the probability of such a second order transition. Although the transition probabilities between uncoupled diabatic states tend to be rather low, they may play a surprisingly crucial role. This is rather puzzling seen from the semi classical point of view in which propagation takes place only forward in time following diabatic energy curves between crossings with possible hopping between diabatic states at the crossings due to the coupling.

## 4.2 Basis Expansion

One very common way of solving the Schrödinger equation numerically, is to expand the wave function in some basis,  $|\Psi\rangle = \sum_{i=1}^N c_i |\phi_i\rangle$ , where the finite set of basis states  $\{|\phi_i\rangle\}$  to as large an extent as possible spans the relevant space. When doing so, the Schrödinger equation takes the form of a coupled set of ordinary differential equations, which can be expressed as a matrix equation. If the basis is orthonormal and the basis states are independent of time, the equation reads

$$i \frac{\partial}{\partial t} \mathbf{c} = \tilde{H}(t) \mathbf{c}, \quad (4.15)$$

with  $\mathbf{c} = (c_1, \dots, c_N)^T$  and  $\tilde{H}$  is a matrix with its elements given by  $\langle \phi_i | H(t) | \phi_j \rangle$ . This system of coupled first order differential equations may be solved by, e.g., the Runge-Kutta method (46). Of course, obtaining the couplings  $\langle \phi_i | H | \phi_j \rangle$  may be far from trivial.

In principle, for sufficiently large  $N$ , any set of basis states will do. However, we want to keep  $N$  as low as possible. Furthermore, maximum sparsity of the Hamiltonian matrix is desired in order to make the numerical solution as fast and stable as possible. Quite frequently a basis that solves some corresponding time independent Schrödinger equation is applied. Specifically, if the Hamiltonian can be written as  $H = H_0 + H'(t)$  where  $H_0$  does not depend on time, the eigenstates of  $H_0$  may be a good choice of basis.

### 4.2.1 B-spline basis sets

The method of basis expansion may be used in order to solve the time independent Schrödinger equation,  $H_0|\phi_i\rangle = \varepsilon_i|\phi_i\rangle$ , as well as the time dependent one. In that respect, b-splines is a popular choice of basis (47). These basis functions are piecewise polynomials which are non-zero only on some limited interval. They are defined on the interval  $[0, r_{\max}]$  by a knot sequence  $\{t_i\}$  consisting of  $N$  points on the interval. The  $i$ 'th b-spline of order  $k$  is given by the recursion formula

$$\begin{aligned} B_i^1(r) &= \begin{cases} 1, & t_i < r < t_{i+1} \\ 0, & \text{otherwise} \end{cases} \\ B_i^k(r) &= \frac{r - t_i}{t_{i+k-1} - t_i} B_i^{k-1}(r) + \frac{t_{i+k} - r}{t_{i+k} - t_{i+1}} B_{i+1}^{k-1}(r). \end{aligned} \quad (4.16)$$

Since these functions are non-zero only on a limited interval, the Hamiltonian matrix  $\tilde{H}_0$  becomes band-diagonal. The degree of differentiability of the basis functions is given by the order  $k$ , as well as the width of the diagonal band of the Hamiltonian matrix.

The basis is very flexible in the sense that different parts of space may be given particular significance by an appropriate choice of knot sequence. In this way, by expanding the position wave function on a basis consisting of spherical harmonics for the angular part and b-splines for the radial part,

$$\begin{aligned} \psi_n(r, \theta, \phi) &= \sum_{l,m} \frac{f_{l,m}^n(r)}{r} Y_{l,m}(\Omega) \\ f_{l,m}^n(r) &= \sum_i c_{i,lm}^n B_i^k(r), \end{aligned} \quad (4.17)$$

the eigenfunctions of both atoms and molecules may be found to a very high degree of precision (48; 49; 50).

### Angular spectra for the photo electron of $\text{H}_2^+$

The procedure described above has been applied to find the angular distribution of the photo electron of the hydrogen molecular ion ionised by a linearly laser field oriented along the internuclear axis. The internuclear separation is assumed to be fixed at  $R = 2$  a.u.. The eigenstates are found using a set of b-splines of order  $k = 8$  with 220 knot-points distributed linearly from 0 to  $r_{\max} = 60$  a.u.. The continuum states, representing outgoing waves, are subject to the boundary condition that the angular momentum quantum number  $l$  become well defined for the continuum states in the limit  $r \rightarrow \infty$ . This is imposed through Lippmann-Schwinger formalism (48).

Having obtained the adequate eigenfunctions, couplings may be calculated and the time dependent Schrödinger equation is solved.

The angular distribution of the electron of  $\text{H}_2^+$  after being ionised by a laser pulse may be written as

$$\frac{dP_I}{d\Omega} = \int d\varepsilon \left| \sum_l i^{-l} e^{-i\sigma_l} Y_{lm}(\Omega) \langle \psi_{\varepsilon lm} | \Psi_f \rangle \right|^2. \quad (4.18)$$

Here  $\varepsilon = k_e^2/2$  is the electron energy,  $\sigma_l \equiv \arg \Gamma(l + 1 + i2/k_e)$  is the Coulomb phase shift, and  $\psi_{\varepsilon lm}$  is the continuum state corresponding to an outgoing wave with energy  $\varepsilon$ , azimuthal quantum

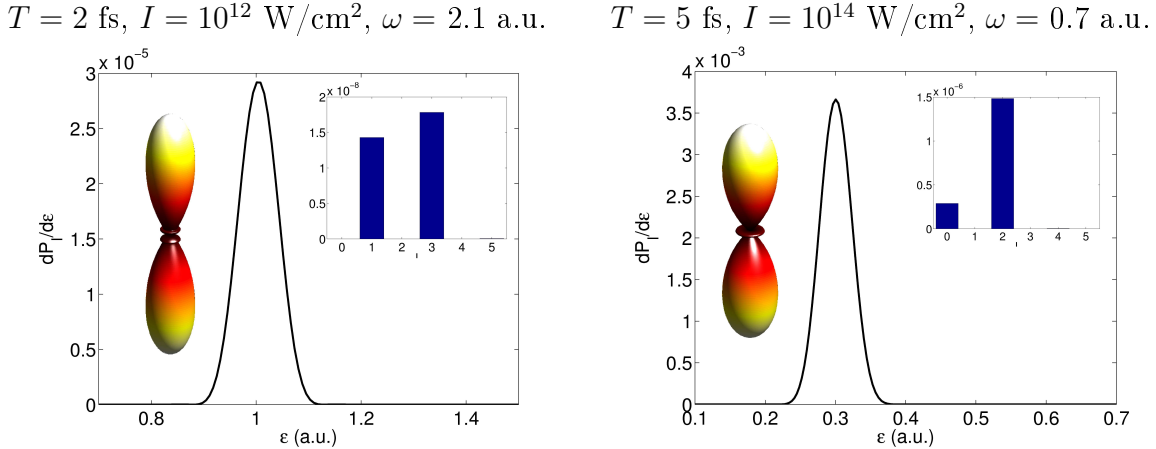


Figure 4.3: The energy distribution of the photo electron from a  $\text{H}_2^+$  molecule exposed to a laser pulse in the fixed nuclei approximation. The left panel is for a one photon transition, whereas the right panel corresponds to a two photon transition. Also inserted in the figure are the distribution between the final channels and the angular distribution.

number  $m$ , which is conserved in this particular process, and asymptotic angular momentum quantum number  $l$ . The final amplitudes  $\langle \psi_{\varepsilon lm} | \Psi_f \rangle$  correspond directly to the amplitudes in Eq. (4.15).

The angular distribution, along with the energy and channel distribution, for processes in which the electron in the ground state  $\Sigma_g$  is ionised by absorption of one photon and by two photons is shown in Fig. 4.3. In representing the energy distribution of the photo electron,  $dP_I/d\varepsilon$ , the amplitudes must be multiplied by the proportionality factor between the true continuum states and the box normalised continuum states, which is simply the square root of the density of states in the box. Also the distributions within the final  $l$ -channels are shown. We see that, in accordance with the dipole selection rules, only odd  $l$ -s are populated by one photon absorption and only even  $l$ -s are populated in the two photon process. The two-photon angular distribution is essentially a  $d$ -wave, whereas the outgoing wave is a mixture of  $p$  and  $f$ -waves in the one photon case.

### 4.3 The Split Operator Method

Formally, the solution of the Schrödinger equation may be written as

$$\Psi(t) = \hat{T} \exp \left( -i \int_{t_0}^t H(t') dt' \right) \Psi(t_0), \quad (4.19)$$

where  $\hat{T}$  indicates that the products in the expansion of the exponential operator should be time ordered (24). If we neglect time ordering and split the time interval into sub intervals of length  $\Delta t$ ,

$$\Psi(t + \Delta t) \approx \exp(-iH(t)\Delta t) \Psi(t), \quad (4.20)$$

the error made in each time step is of order  $\Delta t^2$  and proportional to the time derivative of the Hamilton operator (51). In practical implementations the appearance of both kinetic energy  $T$

and potential energy  $V$  in the exponent may be troublesome to handle. Therefore we would like to split the propagator into products corresponding to the distinct parts of the Hamiltonian. The error in doing so is minimised by "sandwiching" the propagator of the potential by half steps of the kinetic energy operator, i.e. by writing  $\Psi(t + \Delta t) \approx e^{-iT\Delta t/2} e^{-iV\Delta t} e^{-iT\Delta t/2} \Psi(t)$ ,  $H = T + V$ . In doing this an error of order  $\Delta t^3$  is introduced (52).

This method has been developed further in order to describe dynamical systems of cylindrical symmetry in spherical coordinates (53) and finally to describe any three dimensional system in spherical coordinates (54). The method is widely used in this work, so it merits being reviewed in detail.

The Schrödinger equation of one particle subject to some time dependent potential  $W(\mathbf{r}, t)$  may be written in the following form:

$$i \frac{\partial}{\partial t} \Phi(\mathbf{r}, t) = \left\{ \frac{1}{2m} \frac{\partial^2}{\partial r^2} + \frac{L^2}{2mr^2} + V_S(r) + W(\mathbf{r}, t) \right\} \Phi(\mathbf{r}, t). \quad (4.21)$$

$\Phi$  is the reduced wave function,  $r\Psi(\mathbf{r}, t)$ ,  $V_S$  is any spherically symmetric part of the potential and  $L$  is the angular momentum operator.

The reduced wave function is expanded in spherical harmonics,

$$\Phi(r, \Omega, t) = \sum_l^{l_{\max}} \sum_{m=-l}^l f_{lm}(r, t) Y_{lm}(\Omega). \quad (4.22)$$

In order to minimise errors, the propagator is constructed as

$$U(t + \Delta t, t) = e^{-iA\Delta t/2} e^{-iB\Delta t/2} e^{-iW(t)\Delta t} e^{-iB\Delta t/2} e^{-iA\Delta t/2}, \quad (4.23)$$

with

$$A = \frac{1}{2m} \frac{\partial^2}{\partial r^2}, \quad (4.24)$$

$$B = \frac{L^2}{2mr^2} + V_S(r). \quad (4.25)$$

Correspondingly, propagating the wave function from time  $t$  to  $t + \Delta t$  is performed in five steps. The first one is multiplication with  $e^{-iA\Delta t/2}$ . This part only operates on the radial part of the wave function. By Fourier transforming the radial functions, the operator  $\partial^2/\partial r^2$  amounts to simply multiplying by  $k^2$ . Afterwards, the new radial functions are constructed by an inverse Fourier transform. Very fast numerical routines for doing so are available.

The second step is very simple since the spherical harmonics are eigenfunctions of  $L^2$ . Specifically,  $e^{-iB\Delta t/2} f_{lm} Y_{lm} = f_{lm} \exp[-i(l(l+1)/2mr^2 + V_S(r))] Y_{lm}$ .

The most time consuming part of the propagation is the third one,  $e^{-iW\Delta t}$ . The entire wave function  $\Phi$  must be constructed from Eq. (4.22) and then multiplied by the exponential operator. Afterwards, the new radial parts  $f_{lm}$  must be obtained, which is done by projecting of the new  $\Phi$  on spherical harmonics,

$$f_{lm}(r) = \int \Phi(r, \Omega) Y_{lm}^*(\Omega) d\Omega \approx \sum_n w_n \Phi(r, \Omega_n) Y_{lm}^*(\Omega_n). \quad (4.26)$$

Angular grid points  $\{\Omega_n\}$  and the corresponding weights  $\{w_n\}$  of the quadrature are provided by Sloan and Wommersley (55). See Fig. 4.4.

The fourth and fifth step consist in repeating the second and third ones, respectively.

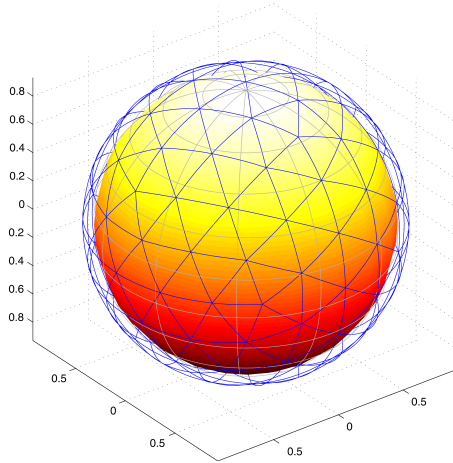


Figure 4.4: The angular grid points of a grid consisting of 122 points. As we see, the points are distributed rather uniformly on the sphere. The Image is provided by Prof. Ladislav Kocbach (56).

### 4.3.1 Propagation in imaginary time

For certain systems, such as the hydrogen atom, analytical expressions for the bound states are accessible. But in general these wave functions are not that easily constructed. In such cases, any propagation scheme may provide at least the ground state by a very simple modification, namely substituting time by *imaginary time*,  $t \rightarrow \tau = -it$ . The time propagator given by the time independent Hamiltonian  $H_0$  is modified accordingly:

$$\Psi(t) = e^{-iH_0 t} \Psi_0 \rightarrow e^{-H_0 \tau} \Psi_0, \quad (4.27)$$

where  $\Psi_0$  is some test function with a non-vanishing projection on the ground state. This state may always be written as a linear combination of eigenstates of  $H_0$ ,  $\Psi_0 = \sum_n c_n \phi_n$  with  $H_0 \phi_n = \varepsilon_n \phi_n$ . Consequently,  $\Psi(\tau) = \sum_n c_n e^{-i\varepsilon_n \tau} \phi_n$ . The amplitude of all excited states die out exponentially faster than that of the ground state  $\phi_0$ . Therefore, after a short "time", the only surviving state is the ground state.

The energy of the ground state is easily found from the norms of the wave functions of two consecutive time steps. Assuming that it has already converged rather close to the ground state, we have  $\Psi(\tau + \Delta\tau) = e^{-H_0 \Delta\tau} \Psi(\tau) \approx e^{-\varepsilon_0 \Delta t} \Psi(\tau)$ . Thus

$$\varepsilon_0 = -\frac{1}{2\Delta\tau} \ln \left( \frac{\langle \Psi(\tau + \Delta\tau) | \Psi(\tau + \Delta\tau) \rangle}{\langle \Psi(\tau) | \Psi(\tau) \rangle} \right). \quad (4.28)$$

The convergence towards the ground state can be checked by monitoring this value. An example of such a convergence is illustrated in Fig. 4.7. When the ground state energy of the system is known in advance, it provides a test of the accuracy of the numerical parameters at hand.

In principle, this method may be used to find excited states as well. By removing any projection of lower lying states at each time step, the resulting wave function should be the desired excited state.

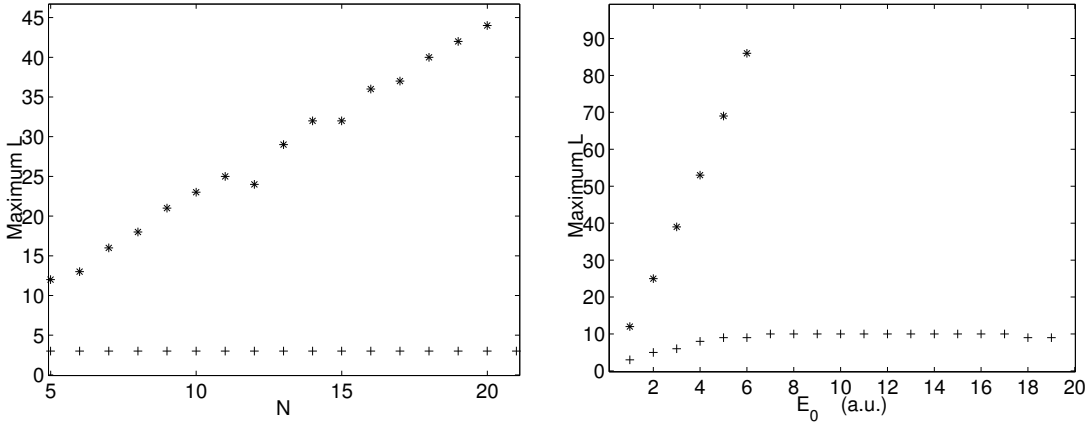


Figure 4.5:  $l_{\max}$ , the number of  $l$ -s needed to achieve convergent results, in the length gauge (\*) and the Kramers-Henneberger frame (+) as a function of the number of optical cycles (left) and maximum field strength (right) for a hydrogen atom initially prepared in the  $2p$  state exposed to a linearly polarised laser field. The figures are taken from paper I in this thesis.

### 4.3.2 Practical examples challenges

The split operator method is very useful and seemingly quite powerful. In principle, any three dimensional dynamic system of one effective particle may be described by this method; any interaction may be implemented in the  $W(\mathbf{r}, t)$ -potential. However, an interaction given by a scalar operator is much more easily implemented than non scalar ones. Specifically, for interaction with electromagnetic fields, the length gauge, Eq. (3.26), and KH form of the interaction, Eq. (3.29), is preferable to the velocity gauge, Eq. (3.15), which involves the operator  $\mathbf{A} \cdot \mathbf{p} = -i\mathbf{A} \cdot \nabla$ .

In the following some of the possibilities and challenges of the method will be illuminated by briefly outlining some particular applications.

#### The hydrogen atom in laser fields

When describing a hydrogen atom in an electromagnetic field in the length gauge, the Coulomb potential may be included in the spherical part of the potential,  $V_S$  in Eqs. (4.21) and (4.25). In the KH frame the translated Coulomb potential,  $1/|\mathbf{r} + \int_{t_0}^t \mathbf{A}(t') dt'|$ , is included in the time dependent potential  $W$ . As it turns out, for strong fields much lower  $l_{\max}$  is needed in order to obtain convergence in the latter case than in the length gauge. In Fig. 4.5 we see that the numbers of  $l$ -s needed in the length gauge seems to increase linearly with both field strength and pulse duration, whereas it is more or less constant in the KH frame.

A problem that must always be tackled in atomic and molecular physics, is the singularity of the Coulomb potential,  $V = 1/r$ . Since the field is calculated directly in this method, some finite value must be assigned to  $V(r = 0)$ . One way of avoiding this problem, is to impose a softening,  $V \rightarrow 1/\sqrt{r^2 + s^2}$ . However, this may change the dynamics of the system rather dramatically (57). In this work, the problem has been minimised by arranging the geometry relative to the angular grid-points, such that the singularity is encountered as little as possible.

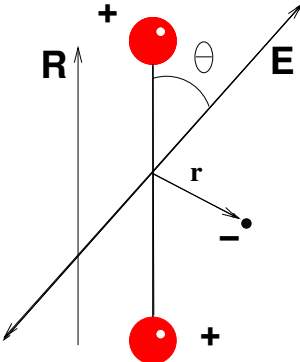


Figure 4.6: The geometry of the system of a  $\text{H}_2^+$  molecule exposed to a linearly polarised laser field. The protons are separated by the distance  $R$  and the angle between the internuclear axis and the electric field of the laser define the orientation angle  $\theta$ .

### Dynamics involving the hydrogen molecular ion

In the fixed nuclei approximation, the Hamiltonian of an  $\text{H}_2^+$  molecule exposed to a linearly polarised field is given in atomic units by

$$H_l = -\frac{1}{2}\nabla^2 - \frac{1}{|\mathbf{r} - \mathbf{R}/2|} - \frac{1}{|\mathbf{r} + \mathbf{R}/2|} + \mathbf{r} \cdot \mathbf{E}(t)$$

in the length gauge and by

$$H_{\text{KH}} = -\frac{1}{2}\nabla^2 - \frac{1}{|\mathbf{r} - \mathbf{R}/2 + \boldsymbol{\alpha}|} - \frac{1}{|\mathbf{r} + \mathbf{R}/2 + \boldsymbol{\alpha}|}$$

in the Kramers-Henneberger frame, cf. Eqs. (3.26), (3.28) and (3.29). See Fig. 4.6. Since the Coulomb potential is not isotropic, both the Coulomb potential and the interaction with the field is incorporated in the potential  $W$  in Eq. (4.21) in both gauges.

Although an analytical expression for the ground state of this system is known (58), it is more convenient to construct it by propagation in imaginary time. In Fig. 4.3.2 the energy calculated from Eq. (4.28) is shown as a function of the imaginary time  $\tau$ . The convergence towards the ground state energy is seen to be very fast.

In order to find the final ionisation probability an absorber is imposed on the boundary of the grid. The remaining wave function is propagated until the norm is converged, so that the ionisation probability is found as  $P_I = 1 - \int_{\text{grid}} |\Psi|^2 dV$ .

As mentioned, the projection of the explicit wave function  $\Phi(r, \Omega)$  onto spherical harmonics is the most time consuming part of the propagation. Therefore the scheme may be "speeded up" considerably if we are able to calculate the matrix elements of type  $\langle l'm'|W|lm\rangle$ . Furthermore, since numerical integration over the angles is avoided, the precision of the method is improved, and truncation errors induced by the coupling to  $l$ -values higher than  $l_{\max}$  may be removed.

Specifically, for the case of a  $\text{H}_2^+$  molecule in an electromagnetic field of arbitrary orientation in the length gauge, this can be done analytically by expanding the Coulomb potential in spherical harmonics and performing subsequent Euler rotations of the interaction term in order to align

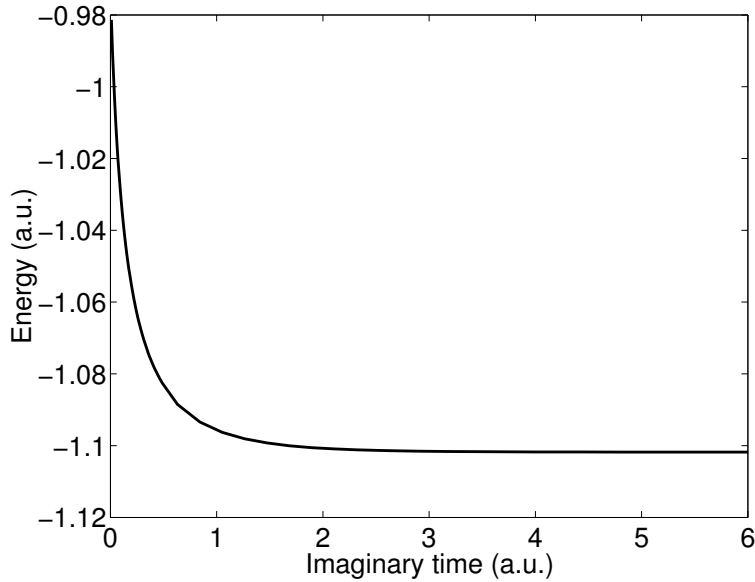


Figure 4.7: The convergence towards the ground state energy for a  $\text{H}_2^+$  molecule at internuclear separation  $R = 2$  a.u..

it with the quantisation axis (59). In this way, also the problem related to the singularities is avoided since the potential is always finite and still consistent with the  $l_{\max}$  of Eq. (4.22).

### Binding bear nuclei: Non-dipole effects

As mentioned previously, it has been demonstrated that, within the dipole approximation, deuterium and proton may be quasi bound by a combined circularly and linearly polarised laser field (3) and that classical calculations indicate that this binding does not sustain inclusion of non-dipole effects (60).

The Hamilton operator for the system, with the circularly polarised field  $\mathbf{A}^\circ$  propagating in the  $z$ -direction and the linearly polarised field  $\mathbf{A}^\dagger$  polarised in the  $z$ -direction and propagating in the  $x$ -direction may be written in the Kramers-Henneberger form as

$$H = \frac{3}{2m_p} p^2 + \frac{1}{|r - \boldsymbol{\alpha}_0|} + \frac{1}{2m_p c} \mathbf{A}_0 \cdot \mathbf{E}_0^\dagger x, \quad (4.29)$$

where  $m_p$  is the proton mass and  $\boldsymbol{\alpha} = 1/2m_p \int_{t_i}^t \mathbf{A}_0(t') dt' \hat{\mathbf{z}}$ . The index "0" indicates that the fields are evaluated at  $\mathbf{r} = \mathbf{0}$ . The details of the separation in relative and centre of mass coordinates are explained in App. B.

In this particular case, the linearly polarised field is much stronger and has a higher frequency than the circular one, so that only non-dipole terms arising from this field is included. This is done by expanding the field to first order in  $\mathbf{k}^\dagger \cdot \mathbf{r}$ .

Using a Cartesian version of the split-operator scheme, it is found that inclusion of non-dipole effects does have a certain detrimental effect on the binding of the system, but not to such an extent that binding is not feasible. This is illustrated in Fig. 4.8.

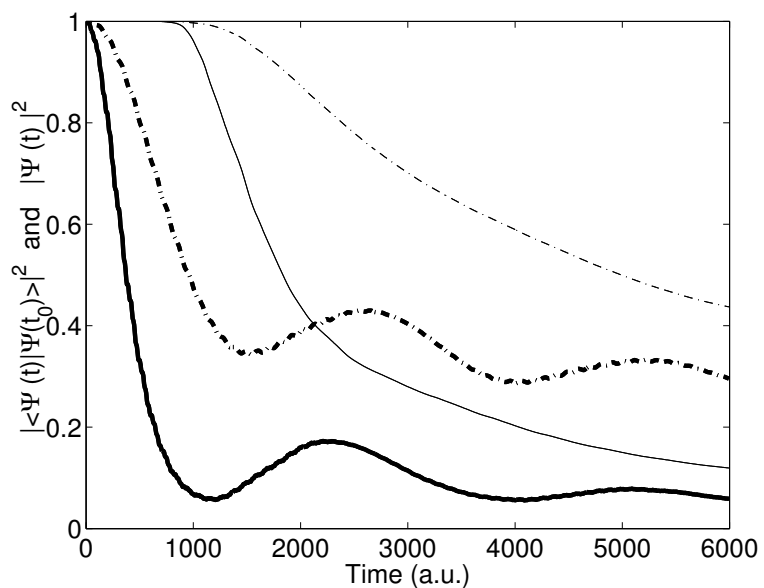


Figure 4.8: The norm of the wave function (thin lines) and the projection on the initial state (thick lines) as functions of time with the dipole approximation (dash-dotted curves) and without the dipole approximation (full curves). The field strengths are  $E^\circ = 33$  a.u. for the circularly polarised field and  $E^\parallel = 260$  a.u. for the linearly polarised field, and the frequencies are  $\omega^\circ = 0.060$  a.u. and  $\omega^\parallel = 0.11$  a.u., respectively. This image is based on a calculation by Ingrid Sundvor.



# Chapter 5

## Introduction to the Papers

The present scientific results are all products of teamwork. Many of the underlying ideas have emerged from discussions and interaction between various people so that they cannot be accredited one single person.

The content of the papers may seem somewhat diverse. However, they are all, in some way, related to the dynamic interaction between matter and light. In the following the content of each one of them will be briefly outlined, and my specific contributions in each case – in addition to taking part in writing the papers – is indicated.

*Paper I* concerns geometrical dependencies in photo-ionisation of a hydrogen atom initially prepared in the  $2p$ ,  $m = 0$  state. It is found that for high photon energy, the ionisation probability features a very strong dependence of the angle between the quantisation axis and the polarisation of the laser field. This dependence is explained as a consequence of the multi photon channel closing due to an effectively lower binding energy for the perpendicular geometry than the for the parallel one. This hypothesis is confirmed by investigating the energy spectra of the photo-electron.

My specific contribution to this work is mainly modifying the computer codes used to describe this system.

*Paper II* addresses some of the same issues as the previous one. By investigating the energy spectra of photo-electrons from hydrogen atoms initially prepared in the ground state, it is found that multi-photon-ionisation is suppressed as the field strength increases. This explains the mechanism of atomic stabilisation. At sufficiently high intensity, the electron only "experiences" the time independent zeroth order Floquet component of the Coulomb potential in the Kramers-Henneberger frame. Furthermore, the non-dipole version of the Kramers-Henneberger frame Hamiltonian is presented. It is demonstrated that atomic stabilisation prevails inclusion of non-dipole effects, contrary to what others have claimed, and that the photoelectrons have low energy in this regime.

In this work I have worked out the non-dipole form of the Kramers-Henneberger Hamiltonian.

*Paper III*, as paper I, addresses the issue of orientational dependence in photo-ionisation.

This time the system is the hydrogen molecular ion, however. Also in this case, for high photon energy, very strong dependence on geometry is found. Specifically, at polarisation parallel to the internuclear axis, the ionisation probability exhibits oscillatory behaviour as a function of the internuclear distance. As the field strength increases, the ionisation probability ceases to increase, i.e. the system is stabilised. As the angle between the polarisation and internuclear axis is varied, the oscillations are reduced and vanish at perpendicular polarisation. This phenomenon is explained in terms of interference between outgoing waves originating from each of the scattering centres (protons). This idea is also able to explain the angular distribution of the photo-electron.

In this case, obtaining the numerical results and presenting them graphically has been done by myself.

*Paper IV* is a proceeding to the 2nd International Conference on Developments in Atomic, Molecular and Optical Physics with Applications in Delhi, India 2006. It may be considered a brief summary of the results of the three preceding articles. Furthermore, results concerning the nuclear motion in photo-ionisation of  $H_2^+$  are presented. Three such methods are considered, namely the fixed nuclear approximation, classical description of the nuclear motion, and full quantum mechanical description.

*Paper V* is an elaboration and continuation of paper III. Specifically, the photo-electron spectra are investigated in more detail through a Fourier transform of the outgoing wave function after the interaction. The model of two interfering outgoing waves is developed further to include Coulomb scattering by the other scattering centre. This way, the angular distributions predicted by the model agree quantitatively with the ones obtained from the *ab initio* calculations. Finally, the importance of the initial distribution of the internuclear separations is considered.

As in the case of paper III, the *ab initio* calculations have been performed by myself, as well as presenting them. This includes the method of finding the photo-electron spectra through a Fourier transform.

In *paper VI* non-dipole effects in photo-ionisation of the hydrogen atom is investigated. The before mentioned non-dipole form of the Kramers-Henneberger frame is applied. Clear manifestations of the magnetic field are found by investigating the angular distribution of the photo-electron. The angular distribution has a third lobe in addition to the two which are present also in the dipole approximation. The non-dipole effects are reproduced by classical calculations.

In *Paper VII* we investigate the applicability of the Landau-Zener model to a four level system, which may, e.g., consist of two spin-1/2 particles exposed to a magnetic field. Special emphases is put on cases of exact solvability. Furthermore, the importance of interference effects and second order transitions is demonstrated.

Numerical solutions to the specific examples are provided by myself. However, my main contribution to this paper has been on the application of the Multi-state Landau-Zener model to systems of multiple paths and describing the consequent interference effect in addition to investigating the significance of second order crossings.

*Paper VIII* describes the transport of an electron between adjacent quantum dots using a linearly polarised oscillating field in the radio frequency regime. The process is understood within a simple four level model, which I have solved analytically. The framework of the Landau-Zener model is applied, although the parameters predicted by this model does not apply to this particular system.

*Paper IX* addresses some of the same issues as those of papers III and V, namely the angular distribution of the electron arising from photon ionisation of the hydrogen molecular ion. The method is quite different, however. In this case, the Schrödinger equation is solved as described in Sect. 4.2.1 using a basis set consisting of b-spines and spherical harmonics. The dynamics is contained within the  $\Sigma$  ( $m = 0$ )-symmetry, and the dynamics include description of nuclear vibration. It is demonstrated that the angular distribution of the photo electron ionised by two photons is strongly altered when the ionisation process involves resonant transitions between bound electronic states.

The distributions displayed in the article are calculated by myself from calculations involving nuclear vibration performed by Dr. Alicia Palacios. Furthermore, solving the Schrödinger equation in the fixed nuclei approximation, used for comparison with the proton kinetic energy integrated angular distributions, has been done by me.



# Chapter 6

## Summary and Outlook

The main focus in this work has been the dynamics of atoms and molecules in the presence of intense, short, high frequency laser fields. Within this scope special emphasis has been put on geometrical aspects. It has been found that the relative orientation of the linearly polarised field is quite significant – both for atoms and diatomic molecules. Furthermore, in the latter case, also the internuclear separation is crucial. For both hydrogen and the hydrogen molecular ion, the dependence is understood theoretically. For the molecule it has been shown that it may be understood as a consequence of interference and refraction of two outgoing partial waves.

Some more fundamental theoretical concepts have been investigated as well. First of all, we have considered the general applicability of the Landau-Zener model and found that its generalisation to systems of many states and crossings can be done. Careful treatment of phase-interference effects is necessary in the general case. It has also been found that transitions at second order avoided crossings may be significant, which is rather puzzling from a semi-classical point of view. The framework of the Landau-Zener model has also been applied to describe coherent electron transport between adjacent quantum dots.

Furthermore, effort has been made in order to describe non-dipole effects in the interaction with the electromagnetic field. We have found that for very strong fields in the high frequency regime, the magnetic field causes the angular distribution of the photo electron from an atom to feature a three lobe shape rather than a two lobe shape, as would be the situation in the dipole approximation. We have also demonstrated that the phenomena of atomic stabilisation sustains inclusion of non-dipole terms.

Another aspect of these non-dipole terms is their importance to the separability of the Schrödinger equation. In general, these terms prohibit separation. However, in some cases separation may be performed – either approximatively or exactly to first order in the spatial variables of the field. The question of separability will be investigated further by numerical calculations.

Since  $H_2^+$  has been much investigated in this work, the two electron system  $H_2$  represents a natural step forward. The *ab initio* description of this system is far more complex than the one with only one electron – not just because the dimensionality is increased from three to six, or seven if internuclear vibration is to be included, but also because electron correlation and entanglement are introduced.

On the other hand, the *reduction* of one electron from  $H_2^+$  to  $H_2^{2+}$  is also an interesting challenge. We have found that two protons, for which the relative motion does not have any dipole interaction with any external field, first order spatial terms *does* induce an interaction. This raises

the question of whether this system may be bound by a combination of strong electromagnetic fields in a manner analogous to that for proton - deuterium.

# Bibliography

- [1] T. H. Maiman, Nature (London) **187**, 493 (1960).
- [2] Tuan Vo-Dinh (ed.), *Biomedical Photonics*, CRC press, Boca Raton, sections IV and V (2003).
- [3] O. Smirnova, M. Spanner, and M. Ivanov, Phys. Rev. Lett **90**, 243001 (2003).
- [4] URL: <http://en.wikipedia.org/wiki/Laser>
- [5] U. Keller, Nature (London) **424**, 831 (2003).
- [6] R. Kienberger, E. Goulielmakis, M. Uiberacker, A. Baltuska, V. Yakovlev, F. Bammer, A. Scrinzi, Th. Westerwalbesloh, U. Kleineberg, U. Heinzmann, M. Drescher, and F. Krausz, Nature (London) **427**, 817 (2004).
- [7] M. Gavrila, J. Phys. B **35**, R147 (2002).
- [8] A. Einstein, Annalen der Physik **17**, 891 (1905).
- [9] A. Einstein, Annalen der Physik **18**, 639 (1905).
- [10] A. Einstein, Annalen der Physik **17**, 132 (1905).
- [11] M. Planck, Annalen der Physik **4**, 553 (1901).
- [12] N. Bohr (1913), Philosophical Magazine **26**, 1 (1913);  
N. Bohr (1913), Philosophical Magazine **26**, 476 (1913);  
N. Bohr (1913), Philosophical Magazine **26**, 857 (1913).
- [13] C. Davisson, and L. H. Germer, Phys. Rev. **30**, 705 (1927).
- [14] G. P. Thomson, Proc. Royal Soc. London A **2026**, 600 (1928).
- [15] E. Schrödinger, Annalen der Physik **79**, 361 (1926);  
E. Schrödinger, Annalen der Physik **79**, 489 (1926);  
E. Schrödinger, Annalen der Physik **79**, 734 (1926);  
E. Schrödinger, Annalen der Physik **80**, 437 (1926);  
E. Schrödinger, Annalen der Physik **81**, 109 (1926).

- [16] R. Eisberg, and R. Resnick, R. *Quantum Physics of Atoms, Molecules, Solids, Nuclei, and Particles*, 2nd ed. Wiley, New York, pp. 114-117 (1985).
- [17] W. Moore, *A life of Erwin Schrödinger*, University Press, Camebridge (1994).
- [18] URL: <http://www.kfunigraz.ac.at/imawww/vqm/articles/avs/AVS.html>
- [19] M. J. Engelfield, *Group Theory and the Coulomb Problem*, Wiley, New York (1972).
- [20] A. Einstein, B. Podolsky, and N. Rosen, Phys. Rev. **47**, 777 (1935).
- [21] J. S. Bell, Physics **1**, 195 (1964);  
J. S. Bell, Rev. Mod. Phys. **38**, 447 (1966).
- [22] A. Aspect, J. Dalibard, and G. Roger, Phys. Rev. Lett. **49**, 1804 (1982).
- [23] E. Schrödinger, Proc. Camb. Phil. Soc. **31**, 555 (1935).
- [24] E. Merzbacher, *Quantum Mechanics* (3rd edition), John Wiley & Sons, New York, (1998).
- [25] M. H. Mittelman, *Introduction to the Theory of Laser-Atom Interactions*, Plenum Press, New York (1982).
- [26] J. S. Briggs, and J. M. Rost, Eur. Phys. J. D **10**, 311 (2000).
- [27] J. Bang, and J. M. Hansteen, K. Dansk. Vidensk. Selsk. Mat.-Fys. Meddr. **31** No 13, 1 (1959).
- [28] B. H. Bransden, and C. J. Joachain, *Physics of atoms and molecules*, Longman, Essex (1983).
- [29] W. Pauli, and M. Fierz, Nuovo Cimento **15**, 167 (1938).
- [30] H. A. Kramers, *Collected Scientific Papers*, North-Holland, Amsterdam, p. 866 (1965).
- [31] W. C. Henneberger, Phys. Rev. Lett. **21**, 838 (1968).
- [32] L. B. Madsen, Phys. Rev. A **65**, 053417 (2002).
- [33] R. Laudon, *The quantum theory of light*, 2nd ed. Clarendon Press, Oxford (1983).
- [34] H. R. Reiss, Phys. Rev. A **19**, 1140 (1979).
- [35] J. R. Vázquez de Aldana, N. J. Kylstra, L. Roso, P. L. Knight, A. Patel, and R. A. Worthington, Phys. Rev. A **64**, 013411 (2001).
- [36] R. Abrines, and I. C. Precival, Proc. Phys. Soc. London **88**, 861 (1966).
- [37] J. P. Hansen, and L. B. Madsen, Phys. Rev. A **71**, 045402 (2005).

- [38] E. Majorana, Nuovo Cimento **9**, 43 (1932).
- [39] E. C. G. Stueckelberg, Helvetica Physica Acta **5**, 369 (1932).
- [40] L. D. Landau, Phys. Z. Soviet Union **2**, 46 (1932).
- [41] C. Zener, Proc. Royal Society A **137**, 696 (1932).
- [42] D. J. Griffiths, *Introduction to Quantum Mechanics*, Prentice Hall, New Jersey (1995).
- [43] M. Førre, and J. P. Hansen, Phys. Rev. A **67**, 053402 (2003).
- [44] M. V. Volkov, and V. N. Ostrovsky, J. Phys.- B **37**, 4069 (2004).
- [45] V. N Ostrovsky, and H. Nakamura, J. Phys. A **30**, 6939 (1997);  
Yu. N. Demkov, and V. N. Ostrovsky, J. Phys. B **34**, 2419 (2001).
- [46] M. Abramowitz, and I. A. Stegun (ed.), *Handbook of mathematical functions*, Dove Publications, New York (1970).
- [47] C. de Boor, *A Practical Guide to Splines*, Springer, New York (2001).
- [48] F. Martín, J. Phys. B **32**, R197 (1999).
- [49] A. Palacios, H. Bachau, and F. M. Martín Garcia, Phys. Rev. Lett. **96**, 143001 (2006).
- [50] J. L. Sanz-Vicario, E. Lindroth, and N. Brandefelt, Phys. Rev. A **66**, 052713 (2002).
- [51] Tore Birkeland, *Numerical aspects of time dependent quantum mechanics with applications to laser ionization of Hydrogen*, Master thesis, University of Bergen (2004).
- [52] M. D. Feit, J. A. Fleck, Jr., and A. Steiger, J. Comput. Phys. **47**, 412 (1982).
- [53] M. R. Hermann, and J. A. Fleck, Phys Rev. A **38**, 6000 (1988).
- [54] J. P. Hansen, T. Sørevik, and L. B. Madsen, Phys. Rev. A **68**, 031401(R) (2003).
- [55] I. H. Sloan, and R. S. Womersley, Adv. Comput. Math.,  
URL: <http://www.maths.unsw.edu.au/rsw/Sphere/> (2003).
- [56] ICPEAC 2003, Stockholm On-line Book of Abstracts, Abstract Th155  
URL: <http://atomlx04.physto.se/icpeac/webpdffiles/Th155.pdf>.
- [57] G. L. Ver Steeg, K. Bartschat, and I. Bray, J. Phys. B **36**, 3325 (2003).
- [58] J. C. Slater, *Quantum theory of molecules and solid. Vol. 1: Electronic structure of molecules*, McGraw Hill, New York (1963).

- [59] T. K. Kjeldsen, L. B. Madsen, and J. P. Hansen, submitted to Phys. Rev. Lett.
- [60] L. B. Madsen, and J. P. Hansen, Phys. Rev. A **71**, 045402 (2005).
- [61] A. Bugacov, M. Pont, and R. Shakeshaft, Phys. Rev. A **48**, R4027 (1993).
- [62] K J Meharg, J S Parker, and K T Taylor, J. Phys. B **38**, 237 (2005).

# Chapter 7

## Scientific Results



# Paper I

Tore Birkeland, Morten Førre, Jan Petter Hansen and Sølve Selstø

**Dynamics of H(2p) ionization in ultrashort strong laser pulses**

*Journal of Physics B* **37**, 4205 (2004).



# Dynamics of H(2p) ionization in ultrashort strong laser pulses

T Birkeland, M Førre, J P Hansen and S Selstø

Department of Physics and Technology, University of Bergen, N-5007 Bergen, Norway

Received 27 July 2004

Published 12 October 2004

Online at [stacks.iop.org/JPhysB/37/4205](http://stacks.iop.org/JPhysB/37/4205)

doi:10.1088/0953-4075/37/20/014

## Abstract

The ionization dynamics of an initially excited aligned H(2p,  $m = 0$ ) atom exposed to short intense laser pulses is studied in the non-perturbative regime based on a three-dimensional numerical solution of the time-dependent Schrödinger equation on a spherical grid. The laser pulse is given a linear polarization vector which defines an angle  $\theta$  with the symmetry axis of the initial 2p state. Strong orientation effects for ionization are found as a function of polarization direction for high laser frequencies. The angular distribution of the photo-electron spectrum shows two characteristic features related to ionization dynamics and interference of parallel versus perpendicular states with respect to the polarization direction of the field. For high enough field intensities, the ionization probability saturates below unity. In this limit, the angular electronic distribution is insensitive to the laser polarization direction. Another characteristic feature is a complete suppression of multiphoton peaks which results in kinetic emission spectra dominated by slow electrons.

(Some figures in this article are in colour only in the electronic version)

## 1. Introduction

In recent years, the experimental tools to study dynamical processes of atom and molecule interactions with electromagnetic fields have improved dramatically. For example, attosecond laser pulses with phase control are now realized [1] and open for imaging of ultrafast dynamics such as time-dependent Auger processes [2] or nuclear dynamics [3]. Other examples involve preparation of aligned molecules [4] and momentum recoil analysis of fragmenting products [5, 6] utilizing real studies of reaction dynamics to a degree which only a few years ago were at the ‘gedanken’ level.

In order to interpret and understand the basic underlying quantum mechanics, the need to solve the time-dependent Schrödinger equation in parallel with the experimental progress is strengthened [7]. This requires development and evaluation of numerical methods for

increasingly complex systems with a corresponding increasing number of degrees of freedom. For linear polarized laser light interacting with spherically symmetric ground state atoms, the symmetry reduction to two effective degrees of freedom has resulted in a variety of methods [8] which has been applied to a range of phenomena such as above threshold ionization (ATI) [9], dynamic stabilization (DS) [10] and high harmonic generation [11]. A few groups, however, have reported related studies with broken cylindrical symmetry, e.g., atomic stabilization in intense circular polarized light [12, 13] molecular dynamics [14] and interaction with excited hydrogen [15].

Analogous to such studies of light–matter interactions with circular polarized light, interactions between initially aligned atoms or molecules in general need a full three-dimensional analysis as well [16]. An example is here the ability of a diatomic molecule to ionize as a function of the angle between the (linear) laser polarization vector and the molecular internuclear axis. A strong alignment dependence on the ionization probability of diatomic molecules exposed to femtosecond laser pulses was recently experimentally demonstrated [17]. On the theoretical side, molecular alignment effects and the interplay between nuclear and electronic dynamics has only been studied within perturbation schemes [18, 19] or low-dimensional models [20, 21].

Concerning alignment and increasingly intense laser fields, it is well known that the ionization probability of ground state atoms at some point may start to decrease, or alternatively saturate at a level below 1 [10]. The geometrical aspects of this process for aligned atoms have only been briefly documented previously [15].

The present paper has two main components (i) an analysis of numerical methods and (ii) an application of the best method to calculate the ionization probability and the energy spectrum of an initially excited hydrogen atom in the 2p state with vanishing angular momentum around the quantization axis. The atom is exposed to a 5-cycle laser pulse with frequency either in the XUV region or in the UV region. The linear polarization vector defines in both cases an angle  $\theta$  with the quantization axis. An extremely strong orientation effect is predicted for the XUV radiation, whereas the UV light produces a much more modest orientation effect. This is in contrast to calculations of similar orientation effects in diatomic molecules [25] and indicates that new orientation effects might be observed for diatomic  $\Pi$  state molecules in contrast to  $\Sigma$  state molecules [17].

The calculations are based on a three-dimensional spectral split step method. The method is shown to behave very efficiently in the Kramers–Henneberger frame for strong pulsed laser fields. It is based on an original two-dimensional formulation by Hermann and Fleck [22] which was recently extended to three dimensions [23]. The paper is organized as follows: in the following section, the numerical method is described. In section 3, the calculations are presented and the results are interpreted. Atomic units,  $m_e = \hbar = e = 1$ , are used unless otherwise stated.

## 2. Three-dimensional spectral method

A hydrogen atom interacting with the classical electromagnetic field is conveniently described by the semi-classical Hamiltonian,

$$H = \frac{1}{2}[\mathbf{p} + \mathbf{A}(\mathbf{r}, t)]^2 - \frac{1}{r}, \quad (1)$$

where  $\mathbf{A}(\mathbf{r}, t)$  is the electromagnetic vector potential. In the present formulation we assume the dipole approximation to be valid, i.e. the wavelength of the radiation is much larger than the extent of the atom. For moderate intensity, laser frequency and pulse duration, this is

an excellent approximation. However, for the highest intensities in section 3, it has been shown that non-dipole effects start to become important [24]. When the dipole approximation applies,  $\mathbf{A}(\mathbf{r}, t) \approx \mathbf{A}(t)$ , and when introducing spherical coordinates the effective Hamiltonian can be expressed in the so-called *velocity gauge*,

$$H(\mathbf{r}, t) = -\frac{1}{2} \frac{\partial^2}{\partial r^2} + \frac{\mathbf{L}^2(\Omega)}{2r^2} + V_v(r, \Omega, t) = H_0 + V_v(r, \Omega, t), \quad (2)$$

with

$$V_v(r, \Omega, t) = -\frac{1}{r} + \mathbf{A}(t) \cdot \nabla. \quad (3)$$

Here  $\Omega = (\theta, \phi)$  denotes the spherical angles. This Hamiltonian governs the time evolution of the reduced wavefunction  $\Phi(\mathbf{r}, t) = r\Psi(\mathbf{r}, t)$ . The squared term of the vector potential of equation (2) contributes in the dipole approximation to the wavefunction only as a global phase factor. This factor is routinely removed by the transformation  $\Psi_v(\mathbf{r}, t) \rightarrow \Psi_v(\mathbf{r}, t) e^{-i/2 \int_0^t \mathbf{A}^2(t') dt'}$ . The velocity gauge is a frequently used starting point for perturbation theories [25] as well as non-perturbative treatments [26].

An alternative formulation which is explicitly based on the physical electric and/or magnetic fields is obtained by the transformation

$$\Psi_l(\mathbf{r}, t) = U_{v \rightarrow l} \Psi_v(\mathbf{r}, t) \quad (4)$$

with,  $U_{v \rightarrow l} = e^{-ir \cdot \mathbf{A}(t)}$ . Since the electric field is related to the vector potential by,  $\mathbf{E}(\mathbf{r}, t) = -\partial_t \mathbf{A}(\mathbf{r}, t)$ , we obtain the *length gauge* Hamiltonian  $H = H_0 + V_l(r, \Omega, t)$  where the potential is given by,

$$V_l(r, \Omega, t) = -\frac{1}{r} + \mathbf{E}(\mathbf{r}, t) \cdot \mathbf{r}. \quad (5)$$

Alternatively, the laser pulse may be described from the accelerated frame [27] following the motion of a free electron in the field. The frame transformation is defined by  $U_{v \rightarrow a} = e^{-i\mathbf{p} \cdot \alpha(t)}$  which gives the Kramers–Henneberger (KH) frame Hamiltonian,  $H = H_0 + V_a(r, \Omega, t)$ , with

$$V_a(r, \Omega, t) = -\frac{1}{|\mathbf{r} + \alpha(t)|}. \quad (6)$$

The quantity  $\alpha(t)$  is the electron field displacement vector defined by  $\alpha(t) = \int_0^t \mathbf{A}(t') dt'$ . In the KH frame, the effect of the laser is thus ‘seen’ from the position of the electron as a nucleus oscillating with the characteristic frequency of the laser pulse. We note that the KH transformation is closely related to the electronic translational factors (ETF) applied to almost all non-perturbative two-centre descriptions of ion–atom collisions where the ETF factors not only ensure Galilean invariance of the theory, but also strongly limit the number of states needed to describe electron capture processes [28].

In light–matter interactions, the KH frame has played a decisive role for the development of an understanding of adiabatic stabilization [10]. We summarize here briefly the method of approach: assume for the moment that the Hamiltonian is perfectly periodic. Then from Floquet theory, a complete set of complex time-dependent eigenfunctions (quasi-stationary states) of the KH Hamiltonian can be constructed as follows:

$$\psi^{(\eta)}(r, \Omega, t) = e^{-iE^{(\eta)}t} \sum_{n=0}^{\infty} \phi_n^{(\eta)}(r, \Omega) e^{-in\omega t} \quad (7)$$

where  $E^{(\eta)}$  is the complex ‘quasi-energy’ of these states. Insertion of this expansion, together with a Fourier expansion of the time-dependent potential of equation (6),

$$V_a(r, \Omega, t) = V_{\text{KH}} + \sum_{n \neq 0} V_n(r, \Omega) e^{in\omega t}, \quad (8)$$

into the Schrödinger equation in the KH frame, leads to an infinite set of time-independent coupled differential equations for the components  $\phi_n^{(\eta)}$  and the complex eigenvalues  $E^{(\eta)}$ ,

$$\left( \frac{1}{2} \mathbf{p}^2 + V_{\text{KH}} - (E^{(\eta)} + n\omega) \right) \phi_n^{(\eta)} = - \sum_{m \neq 0} V_m \phi_{m+n}^{(\eta)}. \quad (9)$$

The zero-order term  $V_{\text{KH}}$  represents the time average of the potential over a period, i.e.

$$V_{\text{KH}} = \frac{1}{T} \int_T V_a(r, \Omega, t) dt, \quad (10)$$

with  $T$  being the period of the laser. In the high-frequency limit ( $\omega \rightarrow \infty$ ) the zero-order part of equation (9) dominates, and the set of Floquet equations reduces to one single [29],

$$\left( \frac{1}{2} \mathbf{p}^2 + V_{\text{KH}} - E^{(\eta)} \right) \phi_0^{(\eta)} = 0, \quad (11)$$

with the formal solution

$$\psi^{(\eta)}(r, \Omega, t) = e^{-iE^{(\eta)}t} \phi_0^{(\eta)}(r, \Omega). \quad (12)$$

In this limit, the atom is completely stable against multiphoton ionization, i.e. for  $\omega \rightarrow \infty$  the electron does not feel the rapid oscillations of the nucleus, but only its average value over a period. A *sufficient* criterion for stabilization is,  $\omega \gg |W_0(E_0)|$ , where  $|W_0(E_0)|$  is the binding energy of the lowest eigenenergy state in the field. From this criterion, stabilization can occur when the external frequency is higher than internal (field free) frequencies of the electron. Adiabatic development from an initial field-free state to the ground state of  $V_{\text{KH}}$  when the field is on and back again is then possible. And in this very simple picture, the atom is completely stable against ionization. It was shown by Pont and Gavrila [30] that the ground state of the  $V_{\text{KH}}$  potential becomes less bound with increasing field strength. Hence, for a given frequency the stabilization process strengthens as the laser intensity increases.

From a modelling point of view, different physical processes are most efficiently described in different physical frames. In general, the description should start from a point which minimizes the perturbation and thus keeps the number of computational operations to a minimum. Thus, none of the equivalent descriptions of dipole limited light–atom interactions, equations (3), (5) and (6), is optimal for all kinds of laser frequencies, intensities and pulse durations. With  $\mathbf{r}$  and  $\mathbf{p}_l$  the conjugate variables describing position and momentum in the length gauge, the corresponding conjugate variables of the velocity gauge are  $\mathbf{r}$  and  $\mathbf{p}_v = \mathbf{p}_l - \mathbf{A}$ . This may lead to fewer states required to describe the wavefunction in situations where  $p_l \simeq A$ , as has been shown in basis state expansions [26]. Unfortunately, however, the velocity gauge cannot be easily implemented in the numerical split step scheme below.

A comparison between the numerical properties of the velocity and length gauge with the KH frame has to the best of our knowledge not been carried out. By inspection however, the KH frame seems to be a natural frame for impulsive strong field processes, as strong field strengths will only reduce the magnitude of the Coulomb potential. Apart from regions in space where  $\mathbf{r} \simeq \alpha$ , the KH frame thus minimizes the magnitude of the perturbation. The present scheme allows for direct implementation of both the length gauge and the KH frame Hamiltonians. In the following, we will compare the computational requirements necessary

to obtain frame invariance of the numerical results between the two Hamiltonians with the potentials in equations (5) and (6), respectively. The vector potential is here given by,

$$\mathbf{A}(t) = \frac{E_0}{\omega} \sin^2 \left( \frac{t\pi}{T_{\text{pulse}}} \right) \sin(\omega t) \mathbf{u}_p. \quad (13)$$

This pulse ensures that the dc component of the field is zero. Furthermore, by keeping  $T_{\text{pulse}}$  an integer number  $n$  of laser cycles,  $T_{\text{pulse}} = 2\pi n/\omega$ , we are also guaranteed that the field displacement is zero at  $t = T_{\text{pulse}}$ . This makes a direct comparison of the wavefunction before and after the pulse possible without any additional transformations of the states [31].

In the simplest split step operator formulation, the wavefunction can be propagated from time  $t$  to  $t + \Delta t$ , with  $\Delta t$  small [32, 22] by,

$$\Phi(\mathbf{r}, t + \Delta t) \approx e^{-i\Delta t A/2} e^{-i\Delta t B/2} e^{-i\Delta t V_{l/a}(\mathbf{r}, t)} e^{-i\Delta t B/2} e^{-i\Delta t A/2} \Phi(\mathbf{r}, t) \quad (14)$$

with  $A = -\frac{1}{2} \frac{\partial^2}{\partial r^2}$  and  $B = \frac{L^2(\Omega)}{2r^2}$ . The overall numerical error per time step is here  $\mathcal{O}(\Delta t^2)$ . A common misunderstanding is to assume the global error of the scheme above to be  $\mathcal{O}(\Delta t^3)$  which is the splitting error. This is however only true for time-independent Hamiltonians. For time-dependent Hamiltonians there is already a  $\Delta t^2$  error in the time evolution operator defined by  $\Psi(t_f) = T(t_f, t_0)\Psi(t_0)$ , since,

$$T(t_f, t_0) = e^{-i(t_f-t_0)H} + \frac{i}{2} \frac{\partial H}{\partial t} (t_f - t_0)^2 + \mathcal{O}(t_f - t_0)^3. \quad (15)$$

The second-order term is normally small for most laser processes. For short pulses towards attosecond duration, however, it is clear that this term is important and becomes the leading source of error.

Following Hansen *et al* [23], the trick is now to expand the wavefunction in orthonormal polynomials which is partly diagonal in  $A$  and  $B$ . By expanding in spherical harmonics,

$$\Phi(r_i, \Omega_{jk}, t) = \sum_{l=0}^{L_{\max}} \sum_{m=-l}^l f_{lm}(r_i, t) Y_{lm}(\Omega_{jk}), \quad (16)$$

we obtain,

$$f_{lm}(r_i, t) = \sum_{jk} w_{jk} Y_{lm}^*(\Omega_{jk}) \Phi(r_i, \Omega_{jk}, t), \quad (17)$$

with abscissas and weights  $(\Omega_{jk}, w_{jk})$  recently published in tabular form [33]. The sum is truncated at  $l = L_{\max}$ , where  $L_{\max}$  is chosen sufficiently large to assure convergence of the numerical scheme. The radial space is also truncated at  $r_{\max}$  which is set large enough to cover the spatial extension of the wavefunction at all times during the pulse. With the present expansion the operator  $B$  simply reduces to a phase multiplication of each angular function by  $\exp[i\Delta t l(l+1)/4r_i^2]$ . The operator  $A$  is correspondingly calculated by expanding each radial basis function in its Fourier components which reduce to another set of multiplications accompanied by two fast Fourier transformations. Following the action of these operators the wavefunction  $\Phi$  is calculated at each grid point and the exponential potential operator  $e^{-i\Delta t V_{l/a}(r_i, \Omega_{jk}, t)}$  can act by straightforward multiplication.

The present method is ideal for ‘near spherical’ problems which restrict the number of necessary radial basis functions and keeps  $L_{\max}$  to a minimum. It also has some built-in numerical advances such as providing an efficient parallel code [34], and it can be applied to the length gauge as well as the KH frame without extra programming.

The post-processing work needed to produce physical quantities following a numerical algorithm should also be considered. In the present scheme, this work is minimized since the

projection onto field-free eigenstates is particularly simple. For ionization, for example, the hydrogenic free particle wavefunctions can be expanded in the spherical harmonics,

$$\phi_c(k, r, \Omega) = \sum_{l=0}^{\infty} \sum_{m=-l}^l i^l e^{i\sigma_l} R_l(k, r) Y_{lm}(\Omega) Y_{lm}^*(\Omega_k). \quad (18)$$

Here  $k = \sqrt{2E}$  is the wavenumber of the wavefunction,  $\Omega_k$  is the spherical angle of the outgoing wave and  $R_l(k, r)$  is a real radial wavefunction. Furthermore,  $\sigma_l$  is the Coulomb phase required to satisfy the boundary condition as  $r \rightarrow \infty$  and  $\sigma_l = \arg \Gamma(l + 1 + \frac{i}{k})$ . For an infinitely large  $r$ -space,  $k$  is a continuous variable, while here the discrete  $k$ -spectrum is directly obtained from maximum box size of the simulation,  $r_{\max}$ . The radial free particle Coulomb waves,  $K_l(k, r)$ , are found by iterative solution of

$$\frac{1}{2} k^2 K_{k,l}(r) = \left( -\frac{d^2}{dr^2} + \frac{l(l+1)}{2r^2} - \frac{1}{r} \right) K_{k,l}(r) \quad (19)$$

with boundary values  $K_{k,l}(0) = K_{k,l}(r_{\max}) = 0$  where  $K_{k,l}(r) = r R_l(k, r)$ . It is then a matter of computational power to find the Coulomb waves for all valid values of  $k_i$  up to a chosen  $k_{\max}$ , and all values of  $l \leq L_{\max}$ . We must ensure that  $k_{\max}$  is sufficiently high so that the probability of ionization to higher energies than  $E_{\max} = k_{\max}^2/2$  is negligible.

Having found the radial Coulomb waves the energy distribution of the ionized electron is given as

$$\frac{dP_I(k_i)}{dk} = \frac{1}{\Delta k_i} \sum_{l,m} \left| \int_0^{r_{\max}} K_{k_i,l}(r) f_{lm}(r) dr \right|^2. \quad (20)$$

We then easily calculate the total ionization probability by taking the sum over all discrete values of  $E(k_i) = k_i^2/2$ . Furthermore, the angular ionization distribution is given by

$$\frac{dP_I(\Omega)}{d\Omega} = \sum_{k_i} \left| \sum_{l,m} (-i)^l e^{-i\sigma_l} Y_{lm}(\Omega_k) \int_0^{r_{\max}} K_{k_i,l}(r) f_{lm}(r) dr \right|^2. \quad (21)$$

Thus, as long as  $r_{\max}$  is chosen large enough all measurable quantities can be directly calculated by simple one-dimensional integrals involving the final wavefunction directly.

We now return to the question of which frame is the most efficient for short laser pulses. In figure 1, we show the highest populated  $l$ -value for calculations in the length gauge and the KH frame, respectively, for a 5-cycle pulse, cf equation (13), with increasing intensity (upper figure) and an  $N$  cycle pulse with fixed intensity (lower figure). By highest populated  $l$  is meant the  $l$  value in equation (16) which is such that the probability for populating any higher state is always smaller than  $10^{-3}$  during the pulse. Thus, the highest populated  $l$  value gives a direct indication of the maximum  $l$  needed to obtain convergence. By comparison, it is clear that the KH frame outmatches completely the length gauge in computational power. Both as a function of intensity and as a function of pulse length with fixed intensity, we observe that the KH frame stabilizes at a small number  $L_{\max} \simeq 10$  as a necessary upper limit for the expansion in equation (16). The length gauge on the other hand requires increasingly higher value of  $L_{\max}$  with increasing number of optical cycles and/or increasing intensity, and it will thus rapidly become prohibitive for three-dimensional calculations.

The KH frame combined with a spherical expansion thus becomes very efficient for non-perturbative laser–atom or laser–molecule simulations. We therefore apply the KH frame to the calculations in the following section. We have also checked the results by performing some of the calculations in the length gauge, and frame invariance within 1% was obtained for all cases.

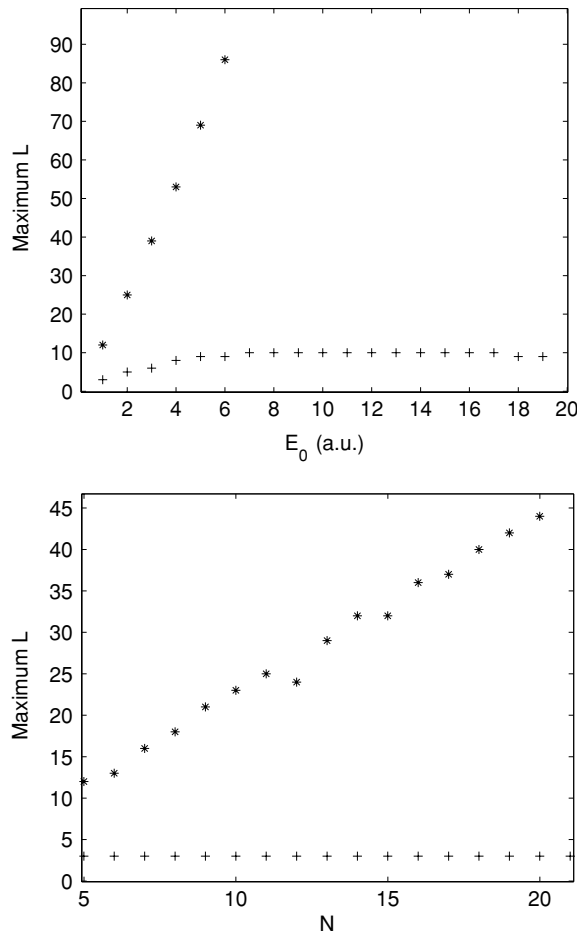


**Figure 1.** Upper: highest populated  $l$  as a function of field strength for a 5 cycle pulse with  $\omega = 1.0$ . Lower: highest populated  $l$  as a function of pulse length with  $E_0 = 2.0$ , and the pulse length is given by  $T_{\text{pulse}} = N2\pi/\omega$ . Both panels: ‘+’ Kramers–Henneberger frame calculations; ‘\*’ Length-gauge calculations.

### 3. Results and discussion

We here report results from three-dimensional calculations of the ionization probabilities and characteristics of a H(2p) atom based on the outlined method of the previous section. The initial state is aligned along the  $z$  axis with magnetic quantum number  $m = 0$ , and exposed to a linearly polarized laser pulse defining an arbitrary angle with the initial quantization axis of the atom. The motivation behind the calculations is twofold; (i) to contribute to a more complete understanding of dynamical stabilization of excited atoms in intense laser fields and (ii) to investigate the geometrical aspects of ionization from aligned quantum states. As such, the latter point is related to ionization of aligned diatomic molecules as well as excited atomic states.

The calculations are carried out for 5-cycle pulses in the non-perturbative intensity regime. Two typical laser frequencies are applied,  $\omega = 1.0$  (45 nm) and  $\omega = 0.11$  (400 nm) which

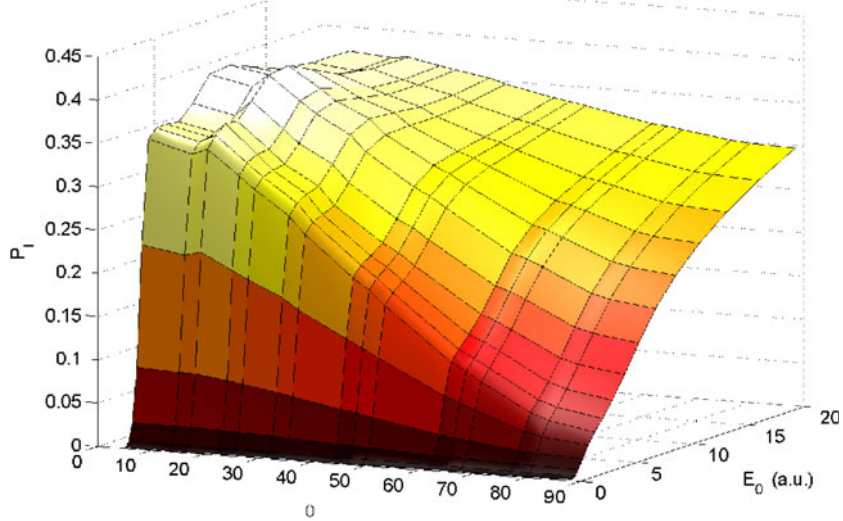


**Figure 2.** Ionization probability for  $2p(m = 0)$  hydrogen as a function of laser polarization  $\theta$  and electric field strength  $E_0$  for  $\omega = 1.0$ .

allow us to study the electronic response in a high frequency pulse of attosecond duration (760 as) versus the response to more conventional pulsed laser frequency in the femtosecond range (7 fs). The intensity ranges were set to  $0 < E_0 < 20$  ( $0 < I < 1.4 \times 10^{19} \text{ W cm}^{-2}$ ) and  $0 < E_0 < 0.1$  ( $0 < I < 3.4 \times 10^{14} \text{ W cm}^{-2}$ ) for the high and low frequency pulse, respectively. Other parameters of the calculations are,  $L_{\max} = 12$ ,  $r_{\max} = 300$ , 1024 radial grid points and the time step  $\Delta t = 0.01$ . An absorbing boundary was used to remove unphysical high-frequency components. These components of the wavefunction carry initially a very small amplitude such that they do not destroy norm conservation significantly when damped at first contact with the boundary. The extension of the grid was always kept large enough to assure that the norm of the wavefunction remains very close to unity at the end of the pulse.

In figure 2, the ionization probability following a 5-cycle pulse with  $\omega = 1.0$  is shown as function of the electric field intensity and the angle between the H(2p) symmetry axis and the polarization vector of the electric field, cf equation (13). The ionization probability is seen to depend critically on the angle  $\theta$  for field strengths  $1 < E_0 < 10$  with favoured ionization at small angles. At  $E_0 = 1$  for example, the ionization probability is around ten times larger for  $\theta \simeq 0$  compared to  $\theta \simeq 90^\circ$ . From a simple classical picture of an initial oscillating charge it seems reasonable with preferred orientation for  $\theta = 0$ , even if the laser frequency is much larger than the natural frequency of the electron, a phenomenon well known from fast ion–atom collisions [35]. In both cases, ionization is enhanced for minimum momentum transfer which is initially present in the parallel case. Another interesting aspect of figure 2 is that dynamic stabilization is most pronounced at small angles. Here the ionization probability reaches a maximum around  $E_0 = 10$  and from there on decreases with increasing intensity. For larger values of  $\theta$ , however, the ionization probability always increases with field intensity.

In figure 3, the ionization probability for a corresponding 5-cycle pulse with  $\omega = 0.11$  is shown as function of field intensity in a comparable intensity region with respect to ionization probability. For this frequency we observe a much smaller angular ionization dependence,

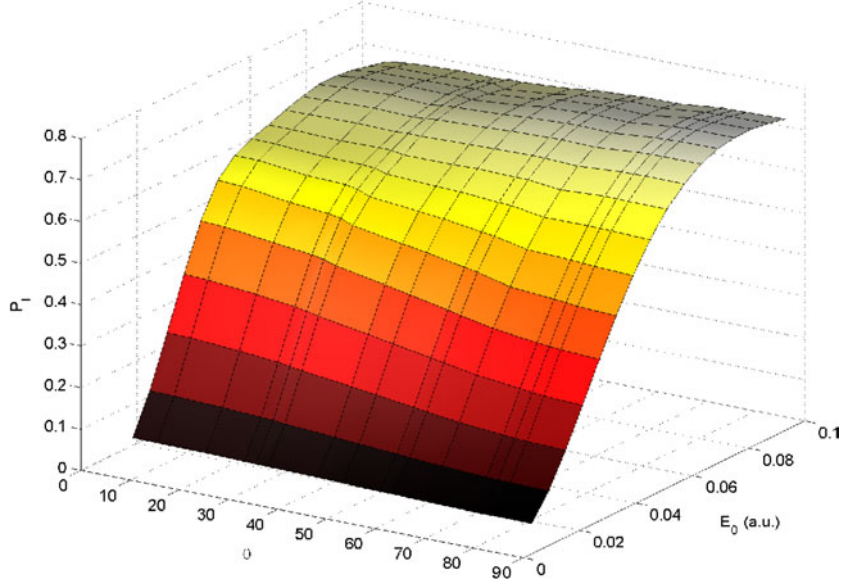


**Figure 3.** Ionization probability for  $2p(m = 0)$  hydrogen as a function of laser polarization  $\theta$  and electric field strength  $E_0$  for  $\omega = 0.11$ .

only about 30–40% in favour of small  $\theta$ -values around  $E_0 \simeq 0.02$ . For high intensities, the ionization probability is completely independent of  $\theta$  and the ionization probability stabilizes around 70%.

In figure 4, snapshots of the time development of the probability density are compared at corresponding times for the two pulses, i.e. after 1, 2 and 4 cycles. The left side shows  $\omega = 0.11$  and polarization angle  $\theta = 55^\circ$ . We observe that the wavefunction has instantly responded to the laser polarization direction which results in a distinct radiative pattern. The right side of figure 4 shows snapshots for  $\omega = 1.0$  and polarization angle  $\theta = 90^\circ$ . Here we observe that it does take several cycles for the oscillating field to release the electron.

The results in figures 2 and 3 are now interpreted by taking advantage of symmetry properties of the real spherical harmonics,

$$\begin{aligned} \tilde{Y}_{l0} &= Y_{l0} \\ \tilde{Y}_{lm} &= \frac{1}{\sqrt{2}}(Y_{lm} + (-1)^m Y_{l-m}) \quad (m > 0) \end{aligned} \quad (22)$$

$$\tilde{Y}_{l-m} = \frac{1}{\sqrt{2}}(Y_{lm} + (-1)^{m+1} Y_{l-m}) \quad (m < 0). \quad (23)$$

When the electric polarization vector defines the quantization axis the initial wavefunction can thus be decomposed into two decoupled components,

$$\Phi(r, \Omega, t = 0) = [\cos \theta \tilde{Y}_{10}(\Omega) + \sin \theta \tilde{Y}_{11}(\Omega)] R_{21}(r, t = 0), \quad (24)$$

where  $R_{nl}(r)$  is the hydrogenic radial wavefunction. The two components evolve independently, such that the wavefunction at a later time  $t$  can be written as

$$\Phi(r, \Omega, t) = \cos \theta \sum_{l=0}^{\infty} f_{l0}(r, t) \tilde{Y}_{l0}(\Omega) + \sin \theta \sum_{l=1}^{\infty} f_{l1}(r, t) \tilde{Y}_{l1}(\Omega). \quad (25)$$

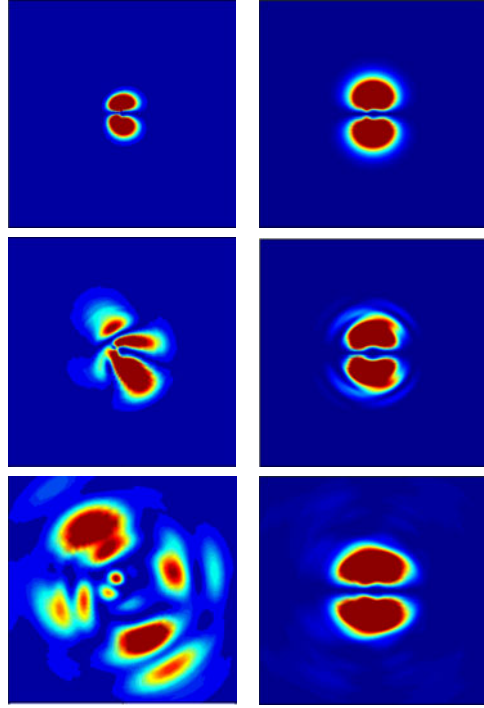


**Figure 4.** Snapshots of the probability density in the  $x$ - $z$  plane at three different times during the laser pulse. Left:  $\omega = 0.11$  and polarization angle  $\theta = 55^\circ$ . Right:  $\omega = 1.0$  and polarization angle  $\theta = 90^\circ$ . Upper: snapshot after 1 cycle. Middle: after 2 cycles. Bottom: after 4 cycles. The scale at the left (right) panel is  $\pm 50(\pm 30)$  in both directions.

The ionization probability may thus be expressed as

$$P_I(\theta, E_0) = p_0(E_0) \cos^2 \theta + p_1(E_0) \sin^2 \theta \quad (26)$$

with  $p_0$  and  $p_1$  being the corresponding ionization probabilities of the states  $|2p(m=0)\rangle_{\vec{u}_p}$  and  $|2p(m=1)\rangle_{\vec{u}_p}$ , defined with respect to the polarization direction of the field.

Now turning back to figure 2, equation (25) shows that the 1s state is symmetry forbidden when  $\theta = 90^\circ$  for a linearly polarized field, whereas its importance for the dynamics is proportional to  $\cos^2 \theta$  as the angle  $\theta$  is decreased. Hence, the stabilization dynamics will strongly depend on the relative population on the  $|2p(m=0)\rangle_{\vec{u}_p}$  and  $|2p(m=1)\rangle_{\vec{u}_p}$  states initially. For a given frequency, the  $2p(m=1)$  state stabilizes at a lower intensity than the  $2p(m=0)$  state. This is because the criterion for stabilization is fulfilled at lower intensities as long as the ground state in the field (1s state) is not populated during the period of the laser pulse. Similar considerations were made and exploited experimentally when atomic stabilization was first demonstrated in excited circular Rydberg states [36, 37]. These aspects explain the geometric variation of the ionization probability in figure 2. In fact, for  $\theta \sim 90^\circ$  the frequency is already so high compared to the binding energy of the lowest accessible eigenenergy state in the field that multiphoton ionization is strongly suppressed at all intensities, whereas for  $\theta \sim 0^\circ$  multiphoton processes occur for the lower field intensities. For the highest field strengths the effective binding energy ultimately becomes so low, independent of the polarization angle, that any dependence on  $\theta$  vanishes.

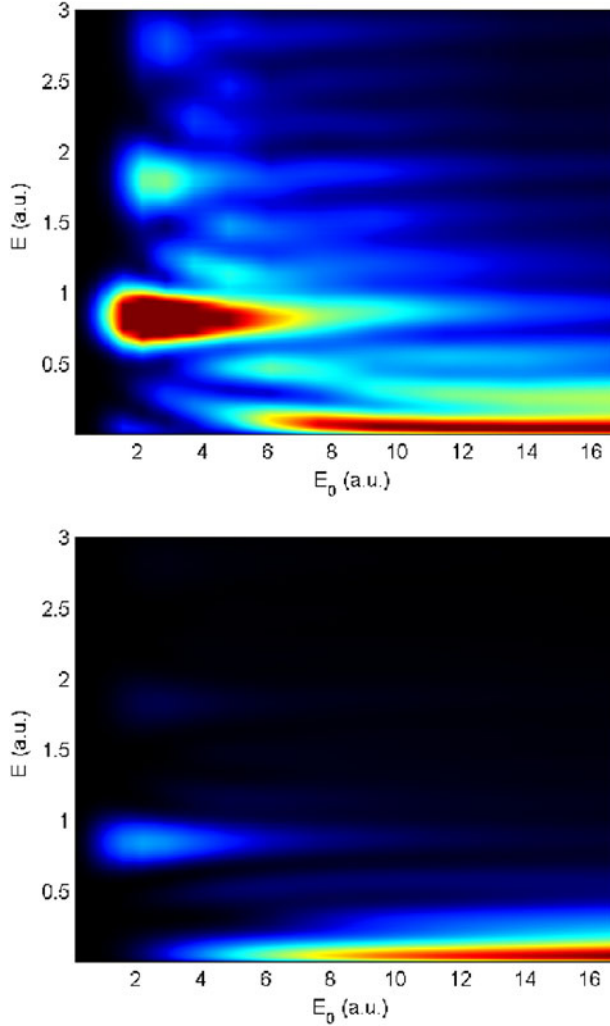


**Figure 5.** Upper: ionization probability density  $dP(E)/dk$  as a function of electric field strength  $E_0$  and energy of the ionized electron  $E = k^2/2$  for  $\omega = 1.0$ . The polarization angle is constant at  $\theta = 5^\circ$ . Lower: same as upper, but  $\theta = 88^\circ$ .

Figure 5 shows the ionization probability density  $dP(E)/dk$  versus electric field strength  $E_0$  and energy  $E$  of the ionized electrons for  $\omega = 1.0$ , and for  $\theta = 5^\circ$  and  $\theta = 88^\circ$ . A regular pattern of resonances corresponding to absorption of  $1\omega$ ,  $2\omega$  and  $3\omega$  from the field is present at lower intensities for the lower angle, whereas only a weak signature of the one-photon resonance is visible for orthogonal polarization. The smaller peaks/resonances in the probability density appearing between the main resonances in the figure cannot be attributed to multiples of  $\omega$ , but rather fractions of  $\omega$ . They are a result of the non-adiabatic turn-on/-off of the field and are especially prominent for short pulses, and can be expected to be rather independent of the detailed pulse shape [38]. All essential features from the above discussion concerning directional dependences on the stabilization are confirmed, i.e. multiphoton ionization is strongly suppressed as  $\theta \rightarrow 90^\circ$ , whereas it is contributing significantly for smaller angles for  $E_0 < 10$ . Another important feature of figure 5 is the

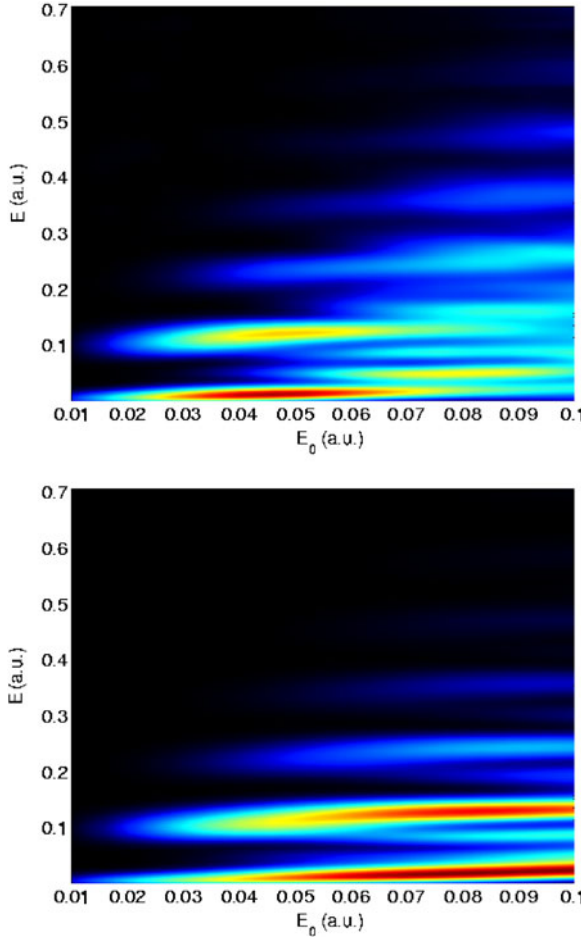


**Figure 6.** Ionization probability density  $dP(E)/dk$  as a function of electric field strength  $E_0$  and energy of the ionized electron  $E = k^2/2$  for  $\omega = 0.11$ . The polarization angle is constant at  $\theta = 5^\circ$ . Lower: same as upper, but  $\theta = 88^\circ$ .

characteristic energies of the released electrons at high field intensities. The signatures of integral number of photon absorption vanish leaving only low energy electrons.

Referring to figure 3, for the lower frequency,  $\omega = 0.11$ , the geometric effect on the ionization is less pronounced, but still the trend is the same as for  $\omega = 1.0$ . A possible explanation for the much weaker orientation dependence is that the frequency (and/or intensity) of the laser is too low to support significant stabilization, independent of the polarization of the field. Furthermore, we suggest that the remaining dominating process, multiphoton ionization, only depends weakly on  $\theta$ . The hypothesis is strengthened by comparison with figure 6, where  $dP(E)/dk$  versus the electric field amplitude  $E_0$  and energy  $E$  is shown for  $\omega = 0.11$ . Here multiphoton ionization processes are the dominating feature for all angles. The two spectra in figure 6 are similar, showing that the geometric effects are less important for ATI processes.

We now turn to the question whether the different  $\theta$  behaviour gives rise to correspondingly different angular distributions of the ionizing electrons. Returning to equation (25) we can

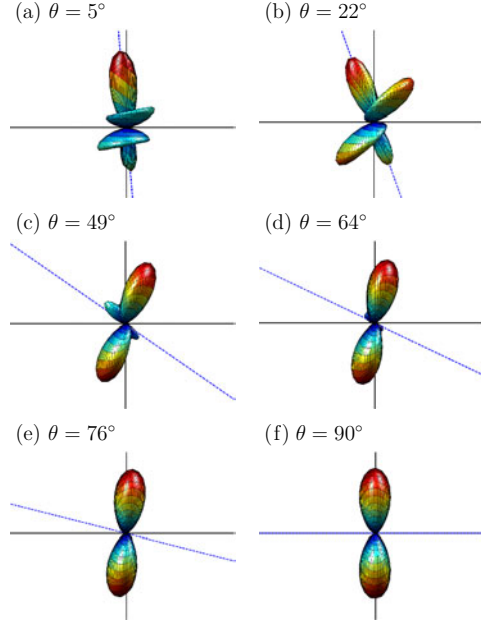


**Figure 7.** Angular ionization distribution,  $dP_I(\Omega)/d\Omega$ , for  $\omega = 1$  and  $E_0 = 9.3$  plotted in the  $x-z$  plane. The (blue) dashed line is the laser polarization direction  $\theta$ . The snapshots of figure 4 result in the emission spectrum (f) of this figure.

express the differential cross section as

$$\frac{dP_I(\Omega)}{d\Omega} = \sum_{k_i} \left| \sum_l (-i)^l e^{-i\sigma_l} (a_{k_i,l} \cos \theta \tilde{Y}_{l0}(\Omega_k) + a_{k_i,l} \sin \theta \tilde{Y}_{l1}(\Omega_k)) \right|^2 \quad (27)$$

with  $a_{l,k_i} = \int_0^{r_{\max}} K_{k_i,l}(r) f_{l0}(r) dr$  and  $b_{l,k_i} = \int_0^{r_{\max}} K_{k_i,l}(r) f_{l1}(r) dr$ . In general several angular momentum states are populated in the final state so further simplification cannot be easily performed. In figures 7 ( $\omega = 1.0$ ) and 8 ( $\omega = 0.11$ ), the angular electron spectrum is plotted for a series of  $\theta$ -values in the field intensity region where the angle dependence is most significant. In figure 7 we observe some interesting structures in the angular spectrum at small  $\theta$ -values. This is caused by strong population and mixing of  $l = 1, 2, 3$  states. At large  $\theta$ -values multiphoton ionization is suppressed and only  $l = 1$  remains significantly populated. From equation (27), we obtain a spectrum dominated by the  $\tilde{Y}_{l1}$  term, which is indeed seen in the lower parts of figure 7.

The electron spectrum for  $\omega = 0.11$  is completely different and dominated by the  $l = 2$  component for all angles. At small angles, the azimuthal quantum number  $m = 0$  determines the spectrum and at large angles  $m = \pm 1$  appears on an equal footing giving rise to the four-leaf clover shape. At intermediate angles, we observe the up-building of a ‘slippage angle’ between the major electron emission direction and the laser polarization vector. This slippage mechanism is also well known as rotational (or Coriolis) coupling from ion–atom collisions [39].

When comparing the two frequencies in figures 5, 7 with figures 6, 8, it is clear that ionization by high frequency pulses results in completely different characteristics than conventional laser frequencies:  $\Delta l = 0$  transitions dominate at high intensities resulting in angular spectra less sensitive to the laser polarization direction. The released electrons have

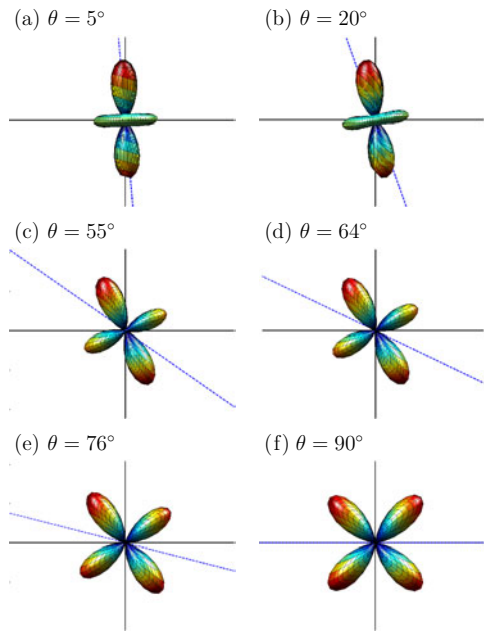


**Figure 8.** Angular ionization distribution,  $dP_I(\Omega)/d\Omega$ , for  $\omega = 0.11$  and  $E_0 = 0.04$  plotted in the  $x$ - $z$  plane. The (blue) dashed line is the laser polarization direction  $\theta$ . The snapshots of figure 4 result in the emission spectrum (c) of this figure.

an expected energy much lower than the energy corresponding to the central one-photon frequency.

#### 4. Concluding remarks

The ionization dynamics of an initially aligned H(2p) atom exposed to angle-specified linear polarized 5-cycle laser pulses with central frequencies in the XUV ( $\omega = 1.0$ ) and UV ( $\omega = 0.11$ ) regimes has been analysed in detail. The analysis is based on results from a fully non-perturbative solution of the time-dependent Schrödinger equation in the Kramers–Henneberger frame on a spherical grid. The results have been interpreted on the basis of symmetry resolved basis functions.

Strong orientation effects in total ionization probability as well as differential probabilities in ejection angles and energy have been found in the XUV regime. The ionization probability at moderate intensities is ten times larger for the parallel polarization vector,  $\theta = 0^\circ$ , than for perpendicular,  $\theta = 90^\circ$ . Dynamic stabilization is found to be most pronounced at high frequencies and for polarization vectors parallel to the initial 2p state. At high intensities, multiphoton ionization vanishes resulting in the release of slow electrons propagating in a direction mostly determined by the initial charge cloud direction. For UV light, the effect of total orientation dependence is much more modest where the well-known  $\Delta l = 1$  transition dominates the angular spectrum.

The geometrical results of this work are relevant for ongoing studies of ionization by aligned molecules [25] as well as the general understanding of atomic response to strong light sources of attosecond range duration. With rapid development of new intense laser sources,

an experiment measuring the kinetic electron spectrum from atoms can be directly compared with the present results.

### Acknowledgments

The present research has been sponsored by Norges Forskningsråd through the Nanomat and Notur programmes.

### References

- [1] Baltuška A *et al* 2003 *Nature* **421** 611
- [2] Drescher M *et al* 2002 *Nature* **419** 803
- [3] Milosevic N, Corkum P B and Brabec T 2004 *Phys. Rev. Lett.* **92** 013002
- [4] Peronne E, Poulsen M D, Bisgaard C Z, Stapelfeldt H and Seideman T 2003 *Phys. Rev. Lett.* **91** 043003
- [5] Weber Th *et al* 2001 *Phys. Rev. Lett.* **86** 224
- [6] Moshammer R *et al* 2000 *Phys. Rev. Lett.* **84** 447
- [7] Makris M G and Lambropoulos P 2004 *J. Phys. B: At. Mol. Opt. Phys.* **37** 2247
- [8] Lambropoulos P, Maragakis P and Zhang J 1998 *Phys. Rep.* **305** 1
- [9] Eberly J H, Javanainen J and Rzazewski K 1991 *Phys. Rep.* **204** 331
- [10] Gavrila M 2002 *J. Phys. B: At. Mol. Opt. Phys.* **35** R147
- [11] Schafer K J, Gaarde M B, Heinrich A, Biegert J and Keller U 2004 *Phys. Rev. Lett.* **92** 023003
- [12] Boca M, Muller H G and Gavrila M 2004 *J. Phys. B: At. Mol. Opt. Phys.* **37** 147
- [13] Bauer D and Ceccherini F 2002 *Phys. Rev. A* **66** 053411
- [14] Dundas D 2002 *Phys. Rev. A* **65** 023408
- [15] Gajda M, Piraux B and Rzazewsky K 1994 *Phys. Rev. A* **50** 2528
- [16] Andersen N, Gallagher J W and Hertel I V 1998 *Phys. Rep.* **165** 1
- [17] Litvinyuk I V *et al* 2003 *Phys. Rev. Lett.* **90** 233003
- [18] Zhao Z X, Tong X M and Lin C D 2003 *Phys. Rev. A* **67** 043404
- [19] Kjeldsen T K, Bisgaard C Z, Madsen L B and Stapelfeldt H 2003 *Phys. Rev. A* **68** 063407
- [20] Rotenberg B, Taieb R, Veniard V and Maquet A 2002 *J. Phys. B: At. Mol. Opt. Phys.* **35** L397
- [21] Feuerstein B and Thumm U 2003 *Phys. Rev. A* **67** 063408
- [22] Hermann M R and Fleck J A 1988 *Phys. Rev. A* **38** 6000
- [23] Hansen J P, Sørevik T and Madsen L B 2003 *Phys. Rev. A* **68** 031401(R)
- [24] Vázquez de Aldana J R and Roso L 1999 *Opt. Express* **5** 144
- [25] Kjeldsen T K and Madsen L B 2004 *J. Phys. B: At. Mol. Opt. Phys.* **37** 2033
- [26] Cormier E and Lambropoulos P 1996 *J. Phys. B: At. Mol. Opt. Phys.* **29** 1667
- [27] Pauli W and Fierz M 1938 *Nuovo Cimento* **15** 167  
Kramers H A 1956 *Collected Scientific Papers* (Amsterdam: North-Holland) p 866  
Henneberger W C 1968 *Phys. Rev. Lett.* **21** 838
- [28] Fritsch W and Lin CD 1991 *Phys. Rep.* **202** 1
- [29] Gavrila M 1992 *Atoms in Intense Laser Fields* ed M Gavrila (San Diego: Academic) p 435
- [30] Pont M and Gavrila M 1990 *Phys. Rev. Lett.* **65** 2362
- [31] Madsen L B 2002 *Phys. Rev. A* **65** 053417
- [32] Feit M D, Fleck J A and Steiger A 1982 *J. Comput. Phys.* **47** 412
- [33] Sloan I H and Wommersley R S 2003 *Adv. Comput. Math.* <http://www.maths.unsw.edu.au/rsw/Sphere/>
- [34] Hansen J P, Matthey T and Sørevik T 2003 A parallel split operator method for the time dependent Schrödinger equation *10th Euro PVM/MPI*
- [35] Aumayr F, Gieler M, Schweinzer J, Winther H and Hansen J P 1992 *Phys. Rev. Lett.* **68** 3277
- [36] de Boer M P, Hoogenraad J H, Vrijen R B, Constantinescu R C, Noordam L D and Muller H G 1993 *Phys. Rev. Lett.* **71** 3263  
de Boer M P, Hoogenraad J H, Vrijen R B, Constantinescu R C, Noordam L D and Muller H G 1994 *Phys. Rev. A* **50** 4085
- [37] van Druten N J, Constantinescu R C, Schins J M, Nieuwenhuize H and Muller H G 1997 *Phys. Rev. A* **55** 622
- [38] Dondera M, Muller H G and Gavrila M 2002 *Phys. Rev. A* **65** 031405
- [39] Kocbach L and Hansen J P 1990 *Phys. Scr.* **42** 317



# Paper II

Morten Førre, Sølve Selstø, Jan Petter Hansen and Lars Bojer Madsen

**Exact Nondipole Kramers-Henneberger Form of the Light-Atom Hamiltonian: An Application to Atomic Stabilization and Photoelectron Energy Spectra**

*Physical Review Letters* **95**, 043601 (2005).



# Exact Nondipole Kramers-Henneberger Form of the Light-Atom Hamiltonian: An Application to Atomic Stabilization and Photoelectron Energy Spectra

M. Førre,<sup>1</sup> S. Selstø,<sup>1</sup> J. P. Hansen,<sup>1</sup> and L. B. Madsen<sup>2</sup>

<sup>1</sup>*Department of Physics and Technology, University of Bergen, N-5007 Bergen, Norway*

<sup>2</sup>*Department of Physics and Astronomy, University of Aarhus, 8000 Aarhus, Denmark*

(Received 18 February 2005; published 21 July 2005)

The exact nondipole minimal-coupling Hamiltonian for an atom interacting with an explicitly time- and space-dependent laser field is transformed into the rest frame of a classical free electron in the laser field, i.e., into the Kramers-Henneberger frame. The new form of the Hamiltonian is used to study nondipole effects in the high-intensity, high-frequency regime. Fully three-dimensional nondipole *ab initio* wave packet calculations show that the ionization probability may decrease for increasing field strength. We identify a unique signature for the onset of this dynamical stabilization effect in the photoelectron spectrum.

DOI: [10.1103/PhysRevLett.95.043601](https://doi.org/10.1103/PhysRevLett.95.043601)

PACS numbers: 42.50.Hz, 32.80.Fb, 32.80.Rm

The general field of laser-matter interactions is characterized by impressive progress in light-source technology. Light sources with pulses of shorter and shorter duration and ever increasing intensities are being developed. Pulses containing only a few cycles and with a duration of less than 10 fs are now commercially available [1]. Intensities of  $10^{14}$  W/cm<sup>2</sup> are routinely provided, and intensities 2 orders of magnitude higher, reaching the field strength of the Coulomb interaction in atoms and molecules, are not unusual. Femtosecond laser pulses have been used to produce coherent extreme-ultraviolet pulses of attosecond duration, and the expression “attosecond metrology” [2] was coined for the investigation of matter with such short pulses [3]. Other developments include the large-scale intense free-electron laser projects at DESY (Hamburg, Germany) and SLAC (Stanford, USA). The TESLA test facility in Hamburg has begun operation in the far-ultraviolet regime and, e.g., a study of the interaction of intense soft x rays with atom clusters was reported [4]. The clusters absorbed energy much more efficiently than anticipated from existing models, and the physical mechanism responsible for the excess in the absorbed energy is currently subject to some controversy [5].

Typically the laser-atom interaction is described in the dipole approximation where several equivalent formulations exist; the most popular ones being the velocity gauge, the length gauge, and the Kramers-Henneberger frame [6]. It is, however, clear that the new light sources alluded to above pave the way for studies of atomic and molecular systems under extreme nonperturbative conditions [7]. In the case of atoms interacting with light from the vacuum-ultraviolet free-electron laser the dipole approximation cannot be expected to be valid [8]. Thus, motivated by the need to include the full  $\mathbf{k} \cdot \mathbf{r}$  term in the description of the light-matter interaction, we here revisit the question of equivalent formulations of electrodynamics.

We transform the exact nondipole minimal-coupling Hamiltonian for an atom in an explicitly time- and space-

dependent field into the rest frame of a classical free electron in the laser field. In the dipole approximation, this frame is known as the Kramers-Henneberger frame [9]. Our transformed exact nondipole Hamiltonian takes a simple form and is very useful for the discussion of strong-field dynamics. We apply it to the study of  $H$  in the high-intensity, high-frequency regime, and confirm the phenomenon of atomic stabilization, i.e., the possibility of having a decreasing ionization probability/rate with increasing intensity (for reviews see, e.g., [10]). Most importantly, we point out that the onset of the dynamic stabilization can be directly observed from electron energy spectra. [Atomic units (a.u.) with  $m_e = e = \hbar = 1$  are used throughout. All derivations are straightforwardly generalized to atoms and molecules involving more electrons.]

The minimal-coupling scheme determines the Hamiltonian for a charged particle in an electromagnetic field through the vector potential  $A(\eta)$  with  $\eta \equiv \omega t - \mathbf{k} \cdot \mathbf{r}$ , and  $\mathbf{k}$  the wave number. The scheme implies that the canonical momentum is obtained by  $\mathbf{p} \rightarrow \mathbf{p} - q\mathbf{A}$  and for an electron of charge  $q = -1$  in atomic units, we have  $\mathbf{p} + \mathbf{A}$ , and the time-dependent Schrödinger equation reads

$$i\partial_t\Psi_v(\mathbf{r},t) = \left[ \frac{1}{2}(\mathbf{p} + \mathbf{A}(\eta))^2 + V(\mathbf{r}) \right] \Psi_v(\mathbf{r},t), \quad (1)$$

where the subscript  $v$  refers to the velocity gauge. The advantage of this formulation is that the spatial dependence of the field is explicitly accounted for through its presence in the vector potential. A disadvantage is that the interaction is not expressed in terms of the physical  $E$  and  $B$  fields. Also numerically, the evaluation of the action of the  $\mathbf{A} \cdot \mathbf{p}$  term can be quite involved unless a diagonal representation of  $\Psi_v$  with respect to this operator is applied. Until now only the alternative multipole formulation of Power-Zienau-Woolley [6,11] has, in principle, kept the spatial dependence to all orders. The multipolar form represents the interaction in terms of the physical fields and the electron coordinate  $\mathbf{r}$ , but, as the name suggests, it is

inherently designed to provide an expansion of the light-matter interaction, and consequently very impractical if one wishes to retain  $\mathbf{k} \cdot \mathbf{r}$  to all orders.

Here, we transform the Schrödinger equation into a new form by applying a nondipole Kramers-Henneberger transformation. Let

$$\Psi_{\text{KH}} = U\Psi_v = \exp[i\boldsymbol{\alpha}(\eta) \cdot \mathbf{p}]\Psi_v, \quad (2)$$

where

$$\boldsymbol{\alpha}(\eta) \equiv \frac{1}{\omega} \int_{\eta_i}^{\eta} d\eta' \mathbf{A}(\eta') \quad (3)$$

represents the quiver motion relative to the laboratory frame of a classical free electron in the field. The Hamiltonian corresponding to the new point of view is obtained by taking the time derivative on both sides of (2), and by using (1) for  $\Psi_v$ , we obtain  $i\partial_t \Psi_{\text{KH}}(\mathbf{r}, t) = H_{\text{KH}} \Psi_{\text{KH}}(\mathbf{r}, t)$  with

$$H_{\text{KH}} = UH_vU^\dagger + i(\partial_t U)U^\dagger. \quad (4)$$

To evaluate the effect of the unitary translation operators in (4), we use the operator identity known as the Baker-Hausdorff lemma [12] and take advantage of the Coulomb gauge restriction  $[\mathbf{p}, \mathbf{A}] = 0$  and  $\mathbf{k} \cdot \mathbf{A} = 0$ . The resulting Hamiltonian reads

$$H_{\text{KH}} = \frac{p^2 + A^2}{2} + V(\mathbf{r} + \boldsymbol{\alpha}) + \frac{k^2}{2} \left( \frac{d\boldsymbol{\alpha}}{d\eta} \cdot \mathbf{p} \right)^2 + \frac{ik^2}{2} \frac{d^2\boldsymbol{\alpha}}{d\eta^2} \cdot \mathbf{p} + \left( \frac{d\boldsymbol{\alpha}}{d\eta} \cdot \mathbf{p} \right) (\mathbf{k} \cdot \mathbf{p}), \quad (5)$$

which holds for a general elliptically polarized field. Within the dipole approximation  $A$  and  $\boldsymbol{\alpha}$  are space independent, the last three terms are absent, and (5) reduces to the well-known result [9]. In the nondipole case, the importance of these terms is readily understood, e.g., in terms of their effect on a continuum wave function. The two terms proportional to  $k^2$  are of the order of  $E_0^2 v^2 / (\omega^2 c^2)$  and  $E_0 v / c^2$ , respectively, whereas the last term is of order  $E_0 v^2 / (\omega c)$ . We thus see that the effect of the dominant term on a wave function is reduced by a factor  $\sim E_0 / (\omega c)$  compared to the  $p^2$  term. The factor  $E_0 / \omega$  is precisely the quiver velocity of the electron  $v_{\text{quiver}}$ , so we expect that the last three terms may be neglected as long as  $v_{\text{quiver}}/c \ll 1$ . Whenever this condition is fulfilled, the nonrelativistic approach is automatically justified as well. As it turns out, for the field parameters considered here, the effect of the nondipole terms is effectively given by the spatial dependence of the vector potential in the  $A^2$  term.

As a first application of the new form of the Hamiltonian we consider the interaction with high-intensity, high-frequency fields. In this so-called stabilization regime [10], atoms may go through a region of decreasing ionization for increasing field strength. Stabilization was experimentally observed with Rydberg atoms [13]. With the development of new light sources, dynamic stabilization

of ground state atoms is, however, expected to be within experimental reach in the near future [14].

Nondipole terms were investigated in approximate ways earlier and found to have a detrimental effect on the stabilization [15,16]. The relative role of the different nondipole terms in (5) is now discussed for a two-dimensional model atom [16]. The ground state was exposed to a laser pulse propagating in the  $x$  direction and of linear polarization  $\mathbf{u}_p$  along the  $z$  axis corresponding to the vector potential  $\mathbf{A}(\eta) = \frac{E_0}{\omega} f(\eta) \sin(\eta) \mathbf{u}_p$  with  $f(\eta)$  the envelope and  $E_0$  the electric field amplitude. The wave function was propagated on a Cartesian grid by means of the split-step operator technique [17]. A 5-cycle laser pulse with central frequency  $\omega = 1$  a.u. (46 nm) corresponding to the pulse duration  $T = 760$  as, and with carrier-envelope  $f(\eta) = \sin^2(\frac{\pi\eta}{\omega T})$ , was employed. The intensity range was set to  $0 < I_0 < 1.4 \times 10^{19} \text{ W/cm}^2$ . Total ionization and ground state probability versus laser intensity is displayed in Fig. 1. The population not accounted for in the figure is left in excited states. The total effect of the last three terms in the Hamiltonian (5), as well as the spatial dependence of the quiver amplitude  $\boldsymbol{\alpha}(\mathbf{r}, t)$ , is so small that it cannot be resolved on the scale of Fig. 1.

We have, accordingly, justified that for the parameters under concern, it is a very accurate approach to apply the Hamiltonian (5), neglecting the last three additional kinetic energy terms arising from the transformation (2), to a fully three-dimensional study of ionization of a real ground state atom by intense short wave light field beyond the dipole approximation. We consider  $H(1s)$  exposed to 5-cycle laser pulses in the attosecond range with central frequencies  $\omega = 1$  a.u. and  $\omega = 2$  a.u.. The time-dependent Schrödinger equation is solved numerically based on a split-step operator approximation on a spherical grid as detailed elsewhere [18]. The wave function is expanded on the grid points  $[(r_i, \Omega_{jk}) = (r_i, \theta_j, \phi_k)]$  as

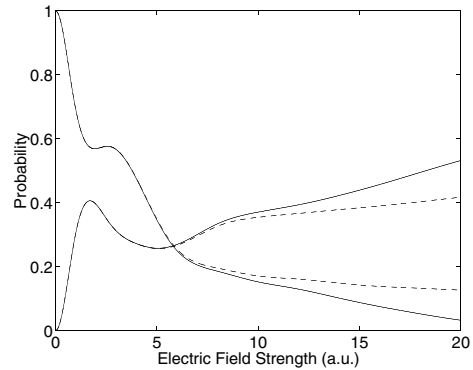


FIG. 1. Ionization and ground state probability for a two-dimensional model atom [16] in the nondipole (solid curve) and dipole (dashed curve) descriptions vs electric field strength for a 5 cycle pulse with  $\omega = 1$  a.u.

$$\Psi(r_i, \Omega_{jk}, t) = \sum_{l,m}^{l_{\max}, m_{\max}} f_{l,m}(r_i, t) Y_{l,m}(\Omega_{jk}), \quad (6)$$

and the initial field-free  $H(1s)$  state is obtained from the exact analytical expression. Reflection at the edges  $r = r_{\max} = 200$  a.u. is avoided by imposing an absorbing boundary. For convergence, we include harmonics up to  $l_{\max} = 29$ , check for gauge invariance, use propagation time step  $\Delta t = 0.01$  a.u., and set  $\Delta r = 0.2$  a.u.. Doubling  $r_{\max}$  only led to minor changes in the results. This confirms that in the present frequency regime Rydberg states are not dynamically involved [19]. Photoelectron probability distributions are calculated by projecting the wave function onto the field-free (discretized) continuum states. We note that the presence of non-dipole terms will lead to a population of different  $m$  values in (6).

In Fig. 2 total ionization and ground state probabilities are shown for the fully three-dimensional case in the non-dipole and dipole limits for two different frequencies. We observe that the dipole approximation remains valid up to field strengths of the order of 10 a.u., and we find in general only a small effect of the nondipole terms on stabilization.

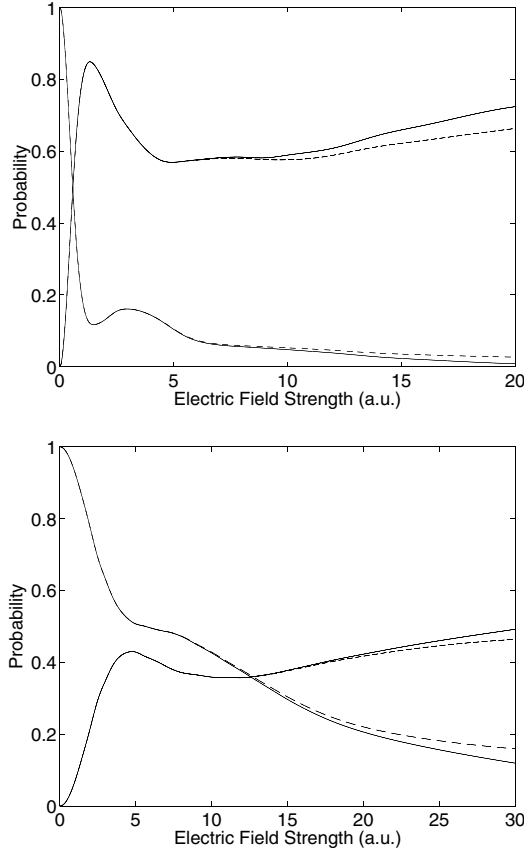


FIG. 2. Upper panel: As Fig. 1, but for the fully three-dimensional case with the system initially prepared in the  $H(1s)$  state. Lower panel: Corresponding results for  $\omega = 2$  a.u..

We now turn to the central question of how stabilization can most efficiently be experimentally detected. Measurement of absolute probabilities will require control of all parameters of the experiment: atom density, pulse characteristics, repetition rates, electron counts, etc.. We therefore suggest measuring the energy-differential photo-electron spectrum. Figure 3 shows the ionization probability density  $dP/dE$  vs electric field strength and energy  $E$  of the ionized electron with the full interaction potential (upper panel) and with the time-averaged Kramers-Henneberger potential (middle panel) [10],

$$V_0(\alpha_0; \mathbf{r}) = \frac{1}{T} \int_0^T V(\mathbf{r} + \boldsymbol{\alpha}) dt, \quad (7)$$

where  $\alpha_0 \equiv E_0/\omega^2$  is the quiver amplitude. The dipole and nondipole results are practically identical, and only the

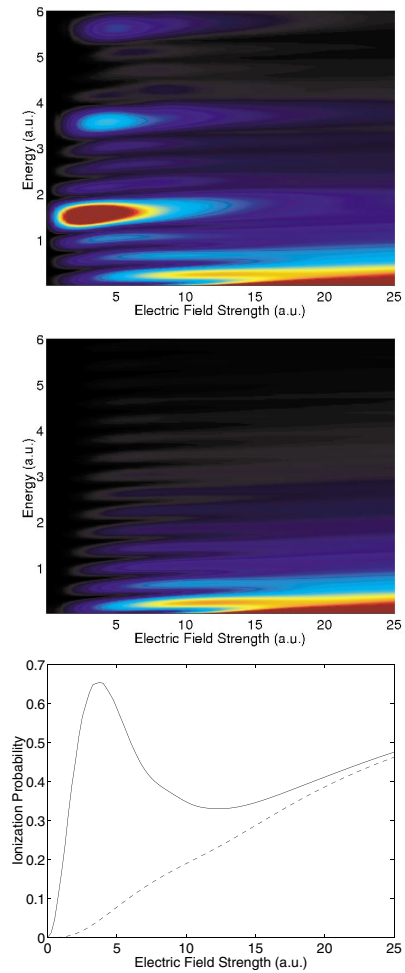


FIG. 3 (color). Upper panel: Ionization probability density  $dP/dE$  for  $H(1s)$  vs electric field strength and energy of the ionized electron for a squared shaped 5-cycle pulse (380 as) with  $\omega = 2$  a.u. (23 nm) by fully three-dimensional calculations. Middle panel: Results from the time-averaged potential (7). Lower panel: Total ionization probability in the dipole approximation (solid curve) and for the time-averaged potential (7) (dashed curve).

dipole results are shown in Fig. 3. In addition, the characteristic features observed in the figure are insensitive to the actual shape of the pulse. For lower field strengths a regular pattern of multiphoton resonances corresponding to absorption of  $1\omega$ ,  $2\omega$ , or  $3\omega$  from the field is present. However, the multiphoton ionization process weakens at higher intensities as the stabilization sets in. Simultaneously, there is a steady growth in the portion of low-energy photoelectrons in the spectrum which can be assigned to  $V_0$  of (7). That  $V_0$  is responsible for the growth in the low-energy spectrum is readily seen by comparison of the upper and middle panels. The processes leading to ionization effectively divide into two competing classes: The multiphoton ionization superimposed on a monotonically increasing “background” ionization process due solely to  $V_0$ . This is explicitly illustrated in the lower panel of Fig. 3, where the total ionization probability vs electric field strength is shown [20]. Multiphoton ionization dominates at lower field strengths, whereas the picture is the opposite at higher values of  $E_0$ . The ionization due to the  $V_0$  potential reflects to what extent the laser pulse is turned on and off adiabatically, and in a “sudden approximation” picture it represents the lack of overlap between the field-free and the field-dressed states. Common in both photoelectron spectra is the presence of peaks in the probability density which cannot be attributed to multiples of  $\omega$ . Instead, they are a result of the nonadiabatic turn-on and turn-off of the field and can be associated with the higher-order Fourier components of the pulse.

In summary, we have presented a new formulation of the interaction between atoms and light maintaining full spatial dependence of the fields. We have analyzed the terms in the interaction Hamiltonian and argued, supported by numerical evidence, that certain terms can be neglected. For the present field parameters, the main nondipole effects come from  $A(\eta)^2$ . As an application, we have considered the phenomenon of dynamic stabilization in intense high-frequency fields. We have shown by full three-dimensional wave packet simulations that the nondipole terms do not destroy the stabilization effect, and most importantly that the photoelectron spectra in the stabilization regime shows very characteristic features: After onset of stabilization all ionized electrons have very low kinetic energy. Thus, by simply measuring the energy of the released electrons stabilization can be detected.

We thank Thomas K. Kjeldsen for discussions and for critically reading the manuscript. This work was supported by the Norwegian Research Council through the NANOMAT program, the Nordic Research Board NordForsk and by the Danish Natural Science Research Council.

[1] T. Brabec and F. Krausz, Rev. Mod. Phys. **72**, 545 (2000).

- [2] M. Hentschel, R. Kienberger, Ch. Spielmann, G. A. Reider, N. Milosevic, T. Brabec, P. Corkum, U. Heinzmann, M. Drescher, and F. Krausz, Nature (London) **414**, 509 (2001).
- [3] R. Kienberger, E. Goulielmakis, M. Uiberacher, A. Baltuska, V. Yakovlev, F. Bammer, A. Scrinzi, Th. Westerwalbesloh, U. Kleineberg, U. Heinzmann, M. Drescher, and F. Krausz, Nature (London) **427**, 817 (2004).
- [4] H. Wabnitz, L. Bittner, A. R. B. de Castro, R. Döhrmann, P. Gürtler, T. Laermann, W. Laasch, J. Schulz, A. Swiderski, K. von Haeften, T. Möller, B. Faatz, A. Fateev, J. Feldhaus, C. Gerth, U. Hahn, E. Saldin, E. Schneidmiller, K. Sytchev, K. Tiedtke, R. Treusch, and M. Yurkov, Nature (London) **420**, 482 (2002).
- [5] R. Santra and C. H. Greene, Phys. Rev. Lett. **91**, 233401 (2003); C. Siedschlag and J. M. Rost, Phys. Rev. Lett. **93**, 043402 (2004).
- [6] C. Cohen-Tannoudji, J. Dupont-Roc, and G. Grynberg, *Introduction to Quantum Electrodynamics* (Wiley, New York, 1997); R. Loudon, *The Quantum Theory of Light* (Clarendon Press, Oxford, 1983).
- [7] K. J. Meharg, J. S. Parker, and K. T. Taylor, J. Phys. B **38**, 237 (2005).
- [8] A. V. Lugovskoy and I. Bray, J. Phys. B **37**, 3427 (2004).
- [9] W. Pauli and M. Fierz, Nuovo Cimento **15**, 167 (1938); H. A. Kramers, *Collected Scientific Papers* (North-Holland, Amsterdam, 1956), p. 866; W. C. Henneberger, Phys. Rev. Lett. **21**, 838 (1968).
- [10] M. Gavrila, J. Phys. B **35**, R147 (2002); A. M. Popov, O. V. Tikhonova, and E. A. Volkova, J. Phys. B **36**, R125 (2003).
- [11] E. A. Power and S. Zienau, Phil. Trans. R. Soc. A **251**, 427 (1959); R. G. Wooley, Proc. R. Soc. A **321**, 557 (1971).
- [12] For Hermitian operators  $A$  and  $G$  and a real parameter  $\lambda$  this lemma states that  $\exp(iG\lambda)A\exp(-iG\lambda) = A + i\lambda[G, A] + (i^2\lambda^2/2!)[G, [G, A]] + \dots + (i^n\lambda^n/n!) \times [G, [G, [G, \dots [G, A]]] \dots] + \dots$ . See, e.g., J. J. Sakurai, *Modern Quantum Mechanics* (Addison-Wesley, Reading, 1994).
- [13] M. P. de Boer, J. H. Hoogenraad, R. B. Vrijen, L. D. Noordam, and H. G. Muller, Phys. Rev. Lett. **71**, 3263 (1993).
- [14] M. Boca, H. G. Muller, and M. Gavrila, J. Phys. B **37**, 147 (2004); M. Dondera, H. G. Muller, and M. Gavrila, Phys. Rev. A **65**, 031405(R) (2002).
- [15] A. Bugacov, M. Pont, and R. Shakeshaft, Phys. Rev. A **48**, R4027 (1993).
- [16] N. J. Kylstra, R. A. Worthington, A. Patel, P. L. Knight, J. R. Vázquez de Aldana, and L. Roso, Phys. Rev. Lett. **85**, 1835 (2000).
- [17] M. D. Feit, J. A. Fleck, Jr., and A. Steiger, J. Comput. Phys. **47**, 412 (1982).
- [18] J. P. Hansen, T. Sørevik, and L. B. Madsen, Phys. Rev. A **68**, 031401(R) (2003); T. Birkeland, M. Førre, J. P. Hansen, and S. Selstø, J. Phys. B **37**, 4205 (2004).
- [19] Y. Komninos, T. Mercouris, and C. A. Nicolaides, Phys. Rev. A **71**, 023410 (2005).
- [20] Note that the difference between the full curve in the lower panel of Fig. 3 and the ionization curve in Fig. 2 is due to the different pulse forms used.

# Paper III

Sølve Selstø, Morten Førre, Jan Petter Hansen and Lars Bojer Madsen

**Strong Orientation Effects in Ionization of  $\text{H}_2^+$  by Short, Intense, High-Frequency Light Pulses**

*Physical Review Letters* **95**, 093002 (2005).



# Strong Orientation Effects in Ionization of $H_2^+$ by Short, Intense, High-Frequency Light Pulses

S. Selstø,<sup>1</sup> M. Førre,<sup>1</sup> J. P. Hansen,<sup>1</sup> and L. B. Madsen<sup>2</sup>

<sup>1</sup>*Department of Physics and Technology, University of Bergen, N-5007 Bergen, Norway*

<sup>2</sup>*Department of Physics and Astronomy, Aarhus University, DK-8000 Aarhus C, Denmark*

(Received 16 February 2005; published 26 August 2005)

We present three-dimensional time-dependent calculations of ionization of arbitrarily spatially oriented  $H_2^+$  by attosecond, intense, high-frequency laser fields. The ionization probability shows a strong dependence on both the internuclear distance and the relative orientation between the laser field and the internuclear axis. The physical features are explained in terms of two-center interference effects.

DOI: [10.1103/PhysRevLett.95.093002](https://doi.org/10.1103/PhysRevLett.95.093002)

PACS numbers: 33.80.Rv

The ionization dynamics of one- and two-electron processes in diatomic molecules in short, strong laser fields are at present under intense experimental investigation [1–3]. A part of these investigations also focus on the sensitivity of such processes to molecular orientation with respect to the light polarization [4]. This is again related to the ultimate goal of controlling chemical reactions by aligning the reactive molecules with respect to each other prior to the intermolecular interaction [5].

From a theoretical viewpoint such studies are extremely complex in the strong-field regime and have been of continuous interest for nearly two decades (for reviews, see, e.g., [6]). In general, only results based on approximate theories such as the molecular strong-field approximation [7,8] and tunneling [9] models have been applied to calculate effects related to molecular orientation with respect to the light polarization vector. Such approximate theories are, however, often gauge dependent [8,10] and limited in their applicability to describe complex processes. The “slowness” of past and present computers, combined with computational challenges related to Coulombic multicenter problems, has restricted exact theoretical calculations including both electronic and nuclear degrees of freedom to cases where the internuclear axis is parallel with the linear polarization direction [11,12] or models of reduced dimensionality [13–15]. These studies have given insight into the fascinating interplay between electronic and nuclear degrees of freedom, phenomena which at present are beyond reach of full-dimensional computations.

In this Letter, we present the first full time-dependent three-dimensional calculations for the electronic degrees of freedom in  $H_2^+$  exposed to a short, strong, attosecond laser pulse. The purpose is to follow the behavior of the system with internuclear distance and in particular to display the dependence of the dynamics on the angle between the internuclear axis and the linear polarization of the field. Calculations are performed for 6 cycle pulses with  $\omega = 2$  a.u. (23 nm) central frequency. This corresponds to pulse durations about 450 asec, which have already been demonstrated [16]. The ionization probability for  $H(2p)$  atoms

exposed to similar light pulses [17] showed a factor 10 stronger modulation with changing orientation than what was measured with femtosecond pulses [4]. Similar effects in diatomic molecules can thus indicate that attosecond pulses may be sensitive probes of the internal nuclear quantum state as well as its orientation. The calculations indeed display that the ionization probability depends strongly on these parameters. Specifically, it is found that for polarization parallel with the internuclear axis the ionization probability oscillates strongly as the internuclear separation increases, whereas these oscillations are absent at perpendicular polarization. Consequently, a strong dependence on the angle between the internuclear axis and the polarization direction is observed. Atomic units ( $\hbar = m_e = e = 1$ ) are applied throughout.

As the nuclear vibrational period is approximately  $10^3$  times larger than the pulse duration, the nuclear degrees of freedom can be considered frozen during the attosecond pulse. Postpulse interplay between nuclear and electronic degrees of freedom, which are important for weaker fields, is also found to be unimportant here as direct electronic ionization dominates.

The vector potential for the light pulse is given by

$$\mathbf{A}(t) = \frac{E_0}{\omega} \sin^2\left(\frac{\pi}{T}t\right) \sin(\omega t + \phi) \mathbf{u}_p, \quad (1)$$

where  $\mathbf{u}_p$  is a unit vector defining the orientation of the linearly polarized field with maximum amplitude  $E_0$ , and  $\phi$  is the carrier envelope phase. The validity of the dipole approximation was investigated in detail very recently for the present intensity and frequency regime, and was found to be well-justified for ionization [18]. The vector potential determines the electric field,  $\mathbf{E}(t) = -\partial_t \mathbf{A}(t)$ , and the translation,  $\mathbf{a}(t) = \int_0^t \mathbf{A}(t') dt'$ , which enter the length  $H_l$  and the Kramers-Henneberger  $H_{KH}$  form [19] of the interaction Hamiltonian, respectively,

$$H_l = \frac{p^2}{2} - \frac{1}{|\mathbf{r} + \mathbf{R}/2|} - \frac{1}{|\mathbf{r} - \mathbf{R}/2|} + \mathbf{E}(t) \cdot \mathbf{r}, \quad (2)$$

$$H_{\text{KH}} = \frac{p^2}{2} - \frac{1}{|\mathbf{r} + \mathbf{R}/2 + \boldsymbol{\alpha}(t)|} - \frac{1}{|\mathbf{r} - \mathbf{R}/2 + \boldsymbol{\alpha}(t)|}, \quad (3)$$

with  $\mathbf{R}$  the internuclear distance. Both versions of the Hamiltonian have been applied here to secure invariant results.

For fixed nuclei, we solve the time-dependent Schrödinger equation numerically based on a split-step operator approximation on a spherical grid. The method was described in detail elsewhere [20,21]. It should be noted, however, that this is its first application to a molecular system. Converged results have been obtained using a basis of spherical harmonics including up to  $l_{\max} = 15$  as shown in the upper panel of Fig. 1.

After the pulse a fraction of the wave function has been removed by the absorber, enabling us to find the ionization probability. However, since excitation is found to be a minor channel at moderate intensities, the ionization probability can be calculated as  $P_{\text{ion}} = 1 - |\langle \Psi_0 | \Psi(T) \rangle|^2$  in these cases. It is found that the ionization probability is unaltered by a change in the carrier envelope phase  $\phi$ .

The ionization probability versus internuclear separation and electric field strength is displayed in Fig. 1 for field polarization parallel with the internuclear axis. Two striking maxima are observed, one for small internuclear separation,  $R \sim 1$  a.u., and another for  $R \sim 3$  a.u.. When the field strength is further increased, the ionization probability decreases; i.e., the molecule is partly stabilized in the intense field. This rather counterintuitive mechanism has

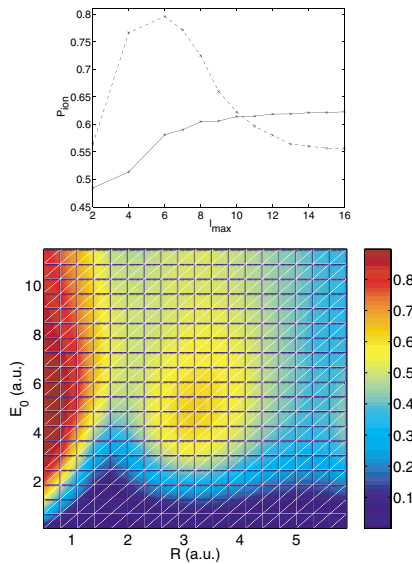


FIG. 1 (color). Lower panel: Ionization probability in the parallel geometry ( $\theta = 0^\circ$ ) as a function of the internuclear separation  $R$  and the electric field strength  $E_0$  with  $\omega = 2$  a.u. and  $T = 6\pi$  a.u.. Upper panel: Convergence of the ionization probability versus  $l_{\max}$  for  $E_0 = 4$  a.u. and  $R = 3$  a.u. (solid curve) and for  $E_0 = 8$  a.u. and  $R = 4$  a.u. (dashed curve).

been studied in detail for atoms [22]. What happens is that for increasing intensity the probabilities for single-photon and multiphoton ionization increase to a maximum value, followed by a steady decrease to zero. In this strong-field limit the Hamiltonian effectively becomes time independent in the Kramers-Henneberger picture, and shakeoff ionization dynamics, i.e., direct projection from the initial field-free state on the continuum eigenstates of the Kramers-Henneberger Hamiltonian, becomes the dominating ionization mechanism. At the ground state equilibrium distance,  $R \sim 2$  a.u. and  $R \sim 5$  a.u., the ionization probability is significantly smaller than the peak regions at  $R \sim 1$  a.u. and  $R \sim 3$  a.u., indicating a strong dynamic self-interference effects of the electronic charge clouds associated with each scattering center.

From Fig. 1 we see that the variation in the ionization signal is most pronounced for  $E_0 \sim 3$  a.u.. At this field strength, Fig. 2 exposes the ionization probability as a function of internuclear separation and as a function of the angle  $\theta$  between the internuclear axis and the polarization direction of the field. An oscillatory behavior of the ionization probability in the parallel geometry ( $\theta = 0^\circ$ ) is seen. As  $\theta$  increases, the oscillations gradually decrease, and in the perpendicular geometry ( $\theta = 90^\circ$ ), the ionization probability drops monotonically with  $R$ . In the figure, we also observe opposite functional dependence with  $\theta$ : At  $R \sim 2$  a.u. the ionization probability increases with  $\theta$ , while at  $R \sim 3$  a.u. it decreases.

We now turn to the detailed dynamics underlying the phenomena observed in Fig. 2. Figure 3 shows snapshots of the wave function in the  $xz$  plane at various times for parallel and perpendicular polarization (the molecule has its internuclear axis directed along the  $z$  axis). In general, the photoelectron is ionized in the directions of the field. For  $\theta = 0^\circ$  the initial charge cloud is partly dragged back and forth along the field, and this gives rise to a strong interference between various momentum components of the wave function and hence the oscillatory dependence with  $R$  in Fig. 1. This effect is absent at  $\theta = 90^\circ$  where the two atomiclike charge clouds pertaining to each nucleus

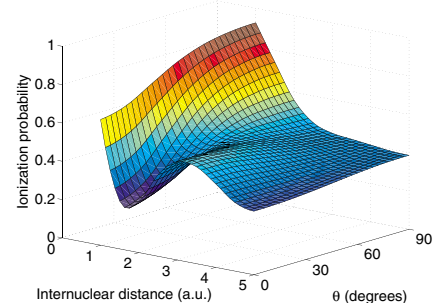


FIG. 2 (color online). Ionization probability as a function of the internuclear separation  $R$  and of the angle  $\theta$  between the polarization direction and the internuclear axis with  $\omega = 2$  a.u.,  $E_0 = 3$  a.u., and  $T = 6\pi$  a.u..

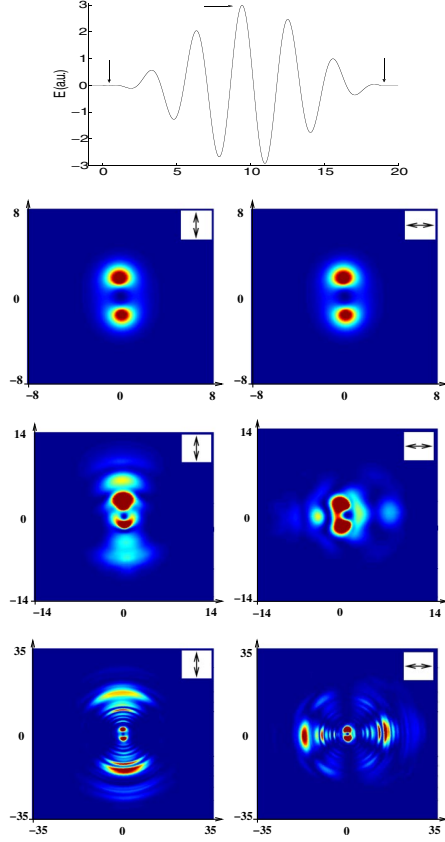


FIG. 3 (color online). Upper panel: The electric field  $E(t)$  of duration  $T = 6\pi$  a.u. (450 asec) and frequency  $\omega = 2$  a.u.. The arrows indicate the instants of time at which the snapshots of the lower part of the figure are made. Snapshots of the wave function in the  $xz$  plane at times corresponding to the beginning (top row), the middle (middle row), and the end (bottom row) of the pulse for parallel (left column) and perpendicular (right column) orientation. In all cases the internuclear separation is  $R = 3$  a.u.. Both the polarization direction and the internuclear axis lie in the  $xz$  plane.

oscillate in phase back and forth with the electric field. In the lower right panel, secondary intensity maxima appear at  $30^\circ$  and  $150^\circ$  with respect to the internuclear axis.

The following simple ansatz offers an explanation of the oscillations at  $\theta = 0^\circ$  and their absence at  $\theta = 90^\circ$ : Assume that the outgoing wave is a superposition of two outgoing spherical waves, one from each of the scattering centers,

$$\psi_{\text{out}} = f_1(\Omega_1) \frac{e^{ik|\mathbf{r}+\mathbf{R}/2|}}{|\mathbf{r} + \mathbf{R}/2|} + f_2(\Omega_2) \frac{e^{ik|\mathbf{r}-\mathbf{R}/2|}}{|\mathbf{r} - \mathbf{R}/2|}. \quad (4)$$

If we take the two scattering amplitudes to be equal,  $f_1(\Omega_1) = f_2(\Omega_2)$ , the differential ionization probability can be brought to the form

$$\frac{dP_{\text{ion}}}{d\Omega} \propto |f_1(\Omega)|^2 [1 + \cos(k\hat{\mathbf{r}} \cdot \mathbf{R})] \quad (5)$$

for  $r \gg R$ . As seen from Fig. 3, the main part of the outgoing wave follows the orientation of the field. Hence we expect that for parallel polarization the main contributions will be for  $\hat{\mathbf{r}}$  parallel to  $\mathbf{R}$ . This gives raise to oscillations in  $R$  with wave number  $k \approx \sqrt{2(\omega - I_p)}$  for one photon processes, where  $I_p(R)$  is the ionization potential. The periodicity is seen to be consistent with the results in Figs. 1 and 2, and we have also confirmed these findings for other values of  $\omega$ . The absence of oscillations in the case of perpendicular polarization is understood accordingly: The wave is sent out mainly in the direction given by  $\theta = 90^\circ$ , and since the outgoing waves will have no phase difference due to the separation of the scattering centers in this direction, this interference will not cause any  $R$  dependence in the ionization probability ( $\hat{\mathbf{r}} \cdot \mathbf{R} = 0$ ). The monotonic decrease in  $P_{\text{ion}}$  with  $R$  at  $\theta = 90^\circ$  is due to the decrease in the ionization potential which leads to an effective higher final state electronic momentum.

The angular distribution of the ionization probability can be calculated from the time integral of the radial current density through the solid angle element  $d\Omega$  at a chosen distance  $a$  from the origin

$$\frac{dP_{\text{ion}}}{d\Omega} = \int_0^\infty dt \mathbf{j}(a, t) \cdot \hat{\mathbf{r}} = \int_0^\infty dt \text{Im}\left(\Psi^* \frac{\partial \Psi}{\partial r} \Big|_a\right), \quad (6)$$

where the distance  $a$  is chosen large enough to exclude contribution to the current from the quiver motion of an electron close to the nucleus and small enough to avoid effects induced by the absorber.

The application of this procedure to the outgoing waves of the lower panels of Fig. 3 results in the intensity spectra of Fig. 4. In this figure, the predictions of the above two-center scattering model is also shown based on the following assumptions: Since the ground state of  $H_2^+$  has a dominating  $s$ -wave configuration, we may safely assume that a central part of the photoelectron is represented by a  $p$  wave when one photon ionization is the dominating process [23]. Since the scattering amplitude should have its maximum value in the direction of the polarization, we further assume that  $f_1 \propto Y_{10}$  and  $f_1 \propto Y_{1x} = (Y_{1-1} - Y_{11})/\sqrt{2}$  for parallel and perpendicular polarization, respectively. We see that the existence of the local maxima at intermediate angles is fully described based on this model. A small asymmetry is visible in the differential full numerical calculation. This is due to the relatively low number of optical cycles. The angular distribution is slightly modified by a change in the carrier envelope phase  $\phi$ . For a smaller number of cycles, it is well known that the asymmetry can be very large [24]. It is also interesting to note that in a very recent calculation of high harmonic generation (HHG) in a reduced model with respect to the electronic degrees of freedom, this interference phenomenon giving rise to local maxima does not occur [25]. In that work it is pointed out that orientational effects are very important for HHG.

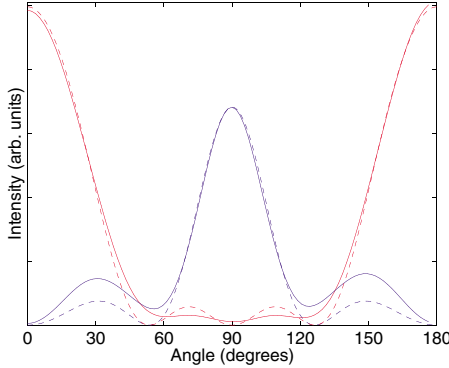


FIG. 4 (color). Angular photoelectron spectra in the scattering plane for parallel (red lines) and perpendicular (blue lines) geometry as a function of the polar angle for a 6 cycle field with  $E_0 = 3$  a.u. and  $\omega = 2$  a.u.. The solid curve is obtained using Eq. (6) and the dashed one by using Eq. (5) with a “best fit” obtained for a wave number of  $k = 1.77$  a.u.. The carrier envelope phase  $\phi$  is here zero. In all cases, the angle denotes the direction of the outgoing electron with respect to the internuclear axis.

In conclusion, fully nonperturbational calculations of the ionization dynamics of  $H_2^+$  molecules in intense attosecond light pulses have been carried out. Very strong orientation effects have been found, demonstrating that, in order to obtain a full understanding of the molecular ionization dynamics, all three electronic degrees of freedom must be included. The geometrical effects are determined by interference related to double-center scattering and the distinct features in the electron spectra show that intense attosecond pulses can resolve the instantaneous vibrational and orientational quantum state of diatomic molecules.

It is a pleasure to thank Thomas K. Kjeldsen for useful discussions and for critically reading the manuscript. The present research was supported by the Norwegian Research Council through the NANOMAT program and the Nordic Research Board NordForsk and by the Danish Natural Science Research Council.

- 
- [1] E. Eremina, X. Liu, H. Rottke, W. Sandner, M.G. Schätzel, A. Dreischuh, G.G. Paulus, H. Walther, R. Moshammer, and J. Ullrich, Phys. Rev. Lett. **92**, 173001 (2004).
  - [2] A.S. Alnaser, X.M. Tong, T. Osipov, S. Voss, C.M. Maharjan, P. Ranitovic, B. Ulrich, B. Shan, Z. Chang, C.D. Lin, and C.L. Cocke, Phys. Rev. Lett. **93**, 183202 (2004).

- [3] X. Urbain, B. Fabre, E.M. Staicu-Casagrande, N. de Ruette, V.M. Andrianarijaona, J. Jureta, J.H. Posthumus, A. Saenz, E. Baldit, and C. Cornaggia, Phys. Rev. Lett. **92**, 163004 (2004).
- [4] I.V. Litvinyuk, K.F. Lee, P.W. Dooley, D.M. Rayner, D.M. Villeneuve, and P.B. Corkum, Phys. Rev. Lett. **90**, 233003 (2003).
- [5] C.Z. Bisgaard, M.D. Poulsen, E. Peronne, S.S. Viftrup, and H. Stapelfeldt, Phys. Rev. Lett. **92**, 173004 (2004).
- [6] *Molecules in Laser Fields*, edited by A.D. Bandrauk (Marcel Dekker, New York, 1994); *Molecules and Clusters in Intense Laser Fields*, edited by J.H. Posthumus (Cambridge University Press, Cambridge, 2001).
- [7] J. Muth-Böhm, A. Becker, and F.H.M. Faisal, Phys. Rev. Lett. **85**, 2280 (2000).
- [8] T.K. Kjeldsen and L.B. Madsen, J. Phys. B **37**, 2033 (2004).
- [9] Z.X. Zhao, X.M. Tong, and C.D. Lin, Phys. Rev. A **67**, 043404 (2003).
- [10] L.B. Madsen, Phys. Rev. A **65**, 053417 (2002).
- [11] D. Dundas, Phys. Rev. A **65**, 023408 (2002).
- [12] M. Plummer and J. McCann, J. Phys. B **30**, L401 (1997).
- [13] B. Rotenberg, R. Taïeb, V. Veniard, and A. Maquet, J. Phys. B **35**, L397 (2002).
- [14] B. Feuerstein and U. Thumm, Phys. Rev. A **67**, 063408 (2003).
- [15] V. Roudnev, B.D. Esry, and I. Ben-Itzhak, Phys. Rev. Lett. **93**, 163601 (2004).
- [16] A. Baltuska, T. Udem, M. Uiberacker, M. Hentschel, E. Goulielmakis, C. Gohle, R. Holzwarth, V.S. Yakovlev, T.W.H.A. Scrinzi, and F. Krausz, Nature (London) **421**, 611 (2003); M. Drescher, M. Hentschel, R. Kienberger, M. Uiberacker, V. Yakovlev, A. Scrinzi, T. Westerwalbaslo, U. Kleineberg, U. Heinzmann, and F. Krausz, Nature (London) **419**, 803 (2002).
- [17] T. Birkeland, M. Førre, J.P. Hansen, and S. Selstø, J. Phys. B **37**, 4205 (2004).
- [18] M. Førre, J.P. Hansen, S. Selstø, and L.B. Madsen, Phys. Rev. Lett. **95**, 043601 (2005).
- [19] W. Pauli and M. Fierz, Nuovo Cimento **15**, 167 (1938); H.A. Kramers, *Collected Scientific Papers* (North-Holland, Amsterdam, 1956), p. 866; W.C. Henneberger, Phys. Rev. Lett. **21**, 838 (1968).
- [20] M.R. Hermann and J.A. Fleck, Jr., Phys. Rev. A **38**, 6000 (1988).
- [21] J.P. Hansen, T. Sørevik, and L.B. Madsen, Phys. Rev. A **68**, 031401(R) (2003).
- [22] M. Gavrila, J. Phys. B **35**, R147 (2002).
- [23] P. Lambropoulos, P. Maragakis, and Jian Zhang, Phys. Rep. **305**, 203 (1998).
- [24] H.M. Nilsen and J.P. Hansen, Phys. Rev. A **63**, 011405(R) (2001).
- [25] M. Lein, Phys. Rev. Lett. **94**, 053004 (2005).

# Paper IV

Jan Petter Hansen, Morten Førre, Sølve Selstø and Ingrid Sundvor

## **Atoms and Molecules in Strong, High-frequency Fields**

*Proceedings, 2nd International Conference on Developments in Atomic, Molecular and Optical Physics with Applications, Delhi, India 2006.*



# ATOMS AND MOLECULES IN STRONG, HIGH-FREQUENCY FIELDS

*J. P. Hansen, M. Førre, S. Selstø, I. Sundvor*

Dept. of Physics and Technology, University of Bergen, Allégt. 55, N-5007 Bergen, Norway

## ABSTRACT

A method for solving the time dependent Schrödinger equation in three dimensions based on a split operator method in spherical coordinates has been developed. This method is used to study photo-ionisation of atoms and molecules in the presence of intense, high-frequency, ultra-short laser pulses. We have investigated how the ionisation dynamics of  $H(2p)$  and  $H_2^+$  depend on geometrical factors. In general, it is found that the relative orientation of the linearly polarised laser field and the initial orientation of the system is crucial. Furthermore, effects of atomic stabilisation is studied. From a generalisation of the Kramers-Henneberger formulation of the Hamiltonian, the laser ionisation of  $H(1s)$  is investigated without applying the dipole approximation.

## INTRODUCTION AND METHOD

Laser technology has gone through continuous improvements ever since the beginning. By now, ultra intense lasers pulses with photon energies as high as 100 eV and with duration on the atto second time scale has been demonstrated [1,2]. The interaction between such fields and matter is a highly non perturbative one which calls for accurate, ab initio modelling methods on the theoretical side.

The method for solving the Schrödinger equation that we apply, is an extension of the original scheme of Hermann and Fleck [3]. Through a uniformly distributed spherical quadrature made public by Wommersley and Sloan [4], the approach is able to treat the electron dynamics in all three spatial dimensions [5]. The reduced wave function is expanded in Spherical Harmonics,

$$\Theta(\vec{r}, t) = \sum_{l,m} f_{l,m}(r, t) Y_{l,m}(\hat{\vec{r}}), \quad (1)$$

and the Schrödinger equation (in atomic units),

$$\left\{ -\frac{1}{2} \frac{\partial^2}{\partial r^2} + \frac{L^2}{2r^2} + V_s(r) + W(\vec{r}, t) \right\} \Theta(\vec{r}, t) = i \frac{\partial}{\partial t} \Theta(\vec{r}, t),$$

(2)

is solved by writing the time propagator as

$$\begin{aligned}\Theta(\vec{r}, t + \Delta t) &= e^{-iA\Delta t/2} e^{-iB\Delta t/2} e^{-iC\Delta t} e^{-iB\Delta t/2} e^{-iA\Delta t/2} \Theta(\vec{r}, t) + O(\Delta t^2), \\ A &\equiv -\frac{1}{2} \frac{\partial^2}{\partial r^2}, \\ B &\equiv l(l+1)/(2r^2) + V_s(r), \\ C &\equiv W(\vec{r}, t)\end{aligned}\tag{3}$$

The spatial differentiations are carried out through fast Fourier transforms. While the spherical part of the potential amounts to a straight forward multiplication of the spherical components of the wave function, it is necessary to construct and afterwards decompose the entire wave function to propagate the anisotropic, time-dependent potential  $W$ .

In principle any effective one electron dynamic system may be described by this method. In atomic and molecular physics, the most obvious applications would be collisions [6] and interaction with light. In the following we will focus on three examples of the latter.

## APPLICATIONS

In general we will take the field to be of the form:

$$\vec{A}(t) = \frac{\vec{E}_0}{\omega} \sin^2\left(\frac{\pi t}{T}\right) \sin(\omega t + \varphi)\tag{4}$$

where  $E_0$  is the maximum field strength,  $\omega$  is the central frequency,  $T$  is the pulse duration and  $\varphi$  is carrier envelope phase.

In the following we will focus on the dependence of geometry in the interaction between the laser pulse and anisotropic systems. Furthermore, we will study non dipole effects and its importance to atomic stabilisation.

### Laser Ionisation of the Hydrogen Molecular Ion

This most simple of molecular systems has been subject to intense theoretical investigation. Still, no ab initio, non perturbative description of this system including all spatial variables has been achieved. This has to do with the system's high number of degrees of freedom. In addition to the three spatial dimensions for the electronic, the internuclear separation  $R$  and the relative orientation  $\theta$  between the internuclear axis and the polarisation of the field need to be considered, making the description far more complex than the corresponding atomic one.

## Validity of the Fixed Nuclei Approach

Due to the long rotational period of the molecule it is usually quite safe to assume the orientation of the internuclear axis to be fixed during the time of interaction. In our case, we are focusing on pulses as short as 500 as. Therefore it seems reasonable to assume that also the internuclear separation  $R$  may be held fixed. Figure 1 confirms this [7]. It shows the total ionisation probability for a one dimensional electron with fixed internuclear separation, with classical internuclear dynamics and with full quantum mechanical internuclear dynamics.

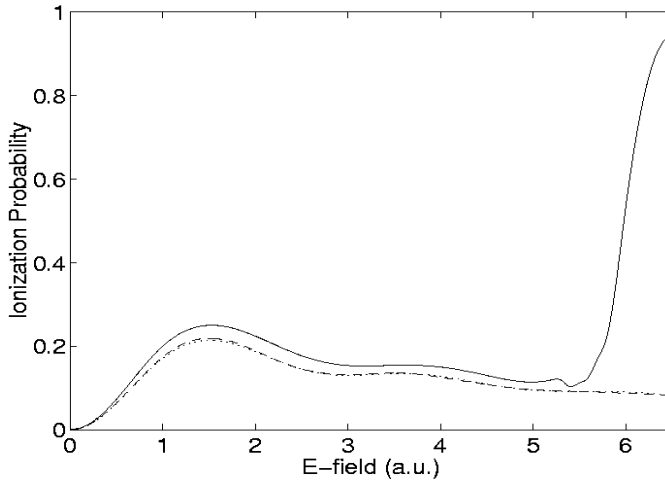


Figure 1: Ionisation probability with fixed nuclei (dotted curve), classical internuclear dynamics (dashed curve) and full quantum mechanical description (full curve). The laser has a central frequency of  $\omega = 1$  a.u. (about 27 eV), and the pulse duration  $T$  is 2 fs.

## Results

The Schrodinger equation is solved with the Hamiltonian

$$H_l = -\frac{1}{2} \nabla^2 - \frac{1}{|\vec{r} + \vec{R}/2|} - \frac{1}{|\vec{r} - \vec{R}/2|} + \vec{E}(t) \cdot \vec{r} \quad (6)$$

in the length gauge. The electric field  $E(t)$  defines the angle  $\theta$  with the internuclear axis. Figure 2 shows the total ionisation probability  $P_I$  as a function of both the internuclear distance  $R$  and the orientation  $\theta$  [8].

The ionisation probability exhibits strong dependence on both  $R$  and  $\theta$ . In particular, for  $\theta=0^\circ$  the ionisation probability  $P_I$  oscillates with  $R$ . For  $\theta=90^\circ$  these oscillations are absent, however. This phenomenon can be understood in terms of interference between outgoing waves originating from each of the scattering centres. Assuming that each of the outgoing waves essentially travels in the direction of the field, two outgoing waves in the direction parallel to the internuclear axis will have an initial phase difference depending on their separation  $R$  making the total outgoing wave subject to destructive interference. In the direction perpendicular to the internuclear axis, there is no initial

phase difference, and hence no such interference effect either.

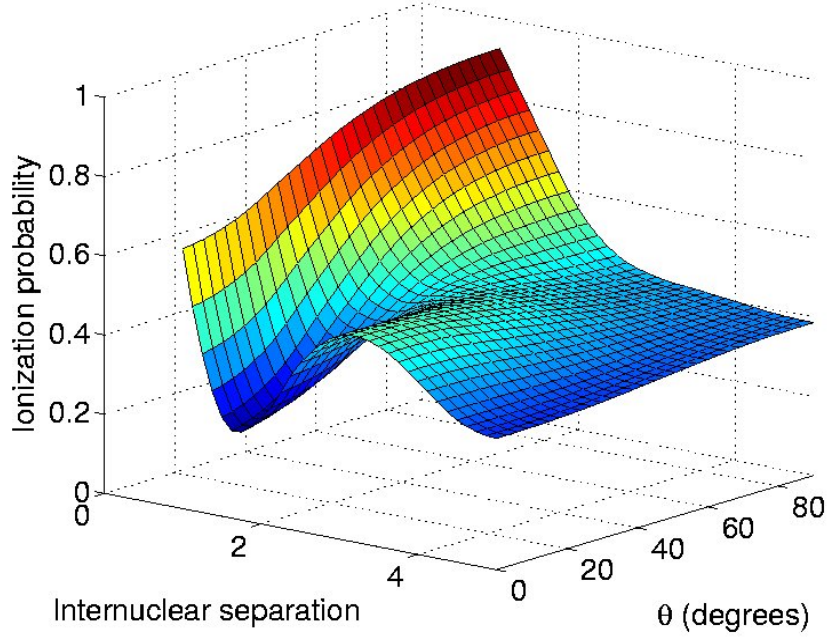


Figure 2: Ionisation probability as a function of internuclear distance  $R$  and the angle between the field and the internuclear axis. The laser field is given by  $\omega=2$  a.u.,  $E_\theta=3$  a.u. and the field duration  $T$  corresponds to 6 optical cycles.

Also the angular distribution of the photo electron can be understood within the same idea. Figure 3 shows the probability of ionisation as a function of direction for parallel ( $\theta=0^\circ$ ), intermediate ( $\theta=45^\circ$ ) and perpendicular ( $\theta=90^\circ$ ) polarisation. The first two rows correspond to  $R=2$  and  $3$ , respectively, whereas the third row represents an average over  $R$  corresponding to the vibrational ground state.

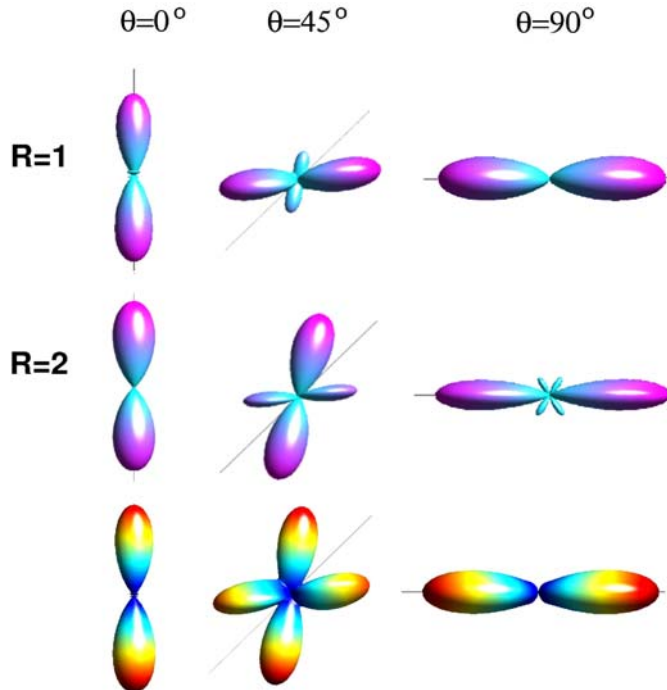


Figure 3: Angular distributions of the photo electron for various orientations and internuclear separations. The lowest row of figures corresponds to an initial  $R$ -distribution given by the vibrational ground state. The field parameters are the same as in Fig. 2.

## Orientational Dependence in Photo-Ionisation of $H(2p)$

We may expect that the relative orientation  $\theta$  will influence the ionisation probability also in the case of non isotropic atomic states. We have investigated this influence for a hydrogen atom initially prepared in the  $n=2$ ,  $l=1$ ,  $m=0$ -state exposed to laser field of energy  $\omega=1$  a.u. [9]. Results are displayed in Fig. 4. This time  $\theta$  refers to the angle between the field and the quantisation axis. We find a rather strong dependence on this angle.

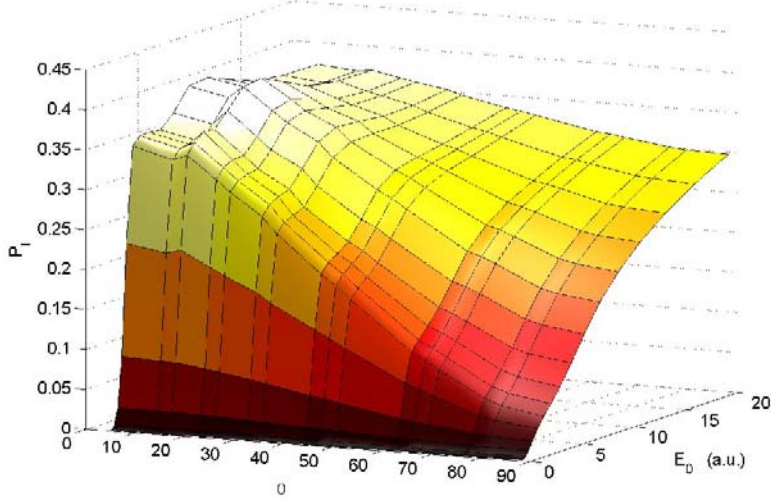


Figure 4: Probability of ionizing  $H(2p)$  as a function of the orientation of the electric field ( $\theta$ ) and the maximum field strength ( $E_0$ ). The central frequency is  $\omega=1$  a.u., and the pulse duration corresponds to 5 optical cycles.

It is well known that the multi photon ionisation channels close as the photon energy becomes very large compared to the effective ground state binding energy [10]. For  $\theta=90^\circ$ , the  $1s$ -state is not accessible through a one photon transition ( $\Delta m=1$ ) causing the effective binding energy to be lower than in the  $\theta=0^\circ$ -case. Consequently, the perpendicular ionisation is suppressed compared to the parallel one. Furthermore, as the intensity of the field increases, the effective binding energy decreases and the multi photon channels close for all values of  $\theta$ . Due to this phenomena, the ionisation probability ceases to increase with the field intensity, and the system is *stabilised*. These phenomena explains the behaviour in Fig. 4 at higher field intensities.

## Atomic Stabilisation and None-Dipole Effects

The effect of stabilisation has also been studied in more detail for a hydrogen atom initially in the ground state. In the stabilisation limit, the effective ionisation potential is small compared to the photon energy. This is manifested in the fact that only the zeroth order Floquet term in the potential in the Kramers Henneberger formulation of the Hamiltonian [11-13] contributes to the interaction,

$$V_{KH}(\vec{r}, t) = -\frac{1}{|\vec{r} + \vec{\alpha}(t)|} \rightarrow V_{KH}^0(\vec{r}) = -\frac{1}{T} \int_0^T \frac{1}{|\vec{r} + \vec{\alpha}(t)|} dt. \quad (7)$$

This potential represents the time average of the field. Thus, the dynamics in this limit arises as a consequence of the non-adiabatic turn on and off of the laser pulse. We expect that as the intensity of the field increases, the energy spectra of the photo electron loose the peaks corresponding integer numbers of the photon energy, and only the strong maximum near the threshold survives. This is exactly what we find, as demonstrated in Fig. 5 [14].

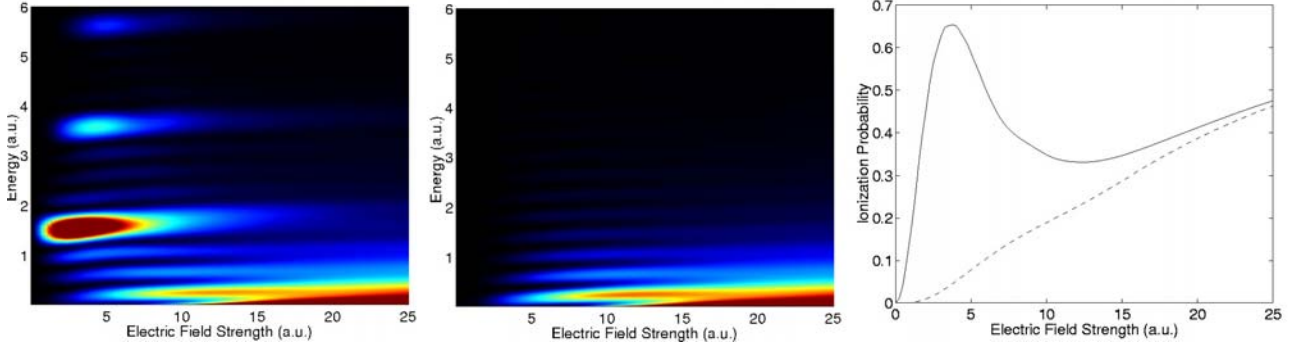


Figure 5: The figure to the left and in the middle show the energy distribution of the ionisation probability for various field strengths with the full interaction with the field and with the time averaged potential, respectively. We see that they coincide as  $E_0$  becomes large. The figure to the right shows the total ionisation probability in the same two cases (full curve and dotted curve, respectively). Here we have  $\omega=2$  a.u. and  $T$  corresponds to 5 optical cycles. The shape of the pulse is slightly different from Eq. 4.

It has been claimed that atomic stabilisation is an artefact of the dipole approximation and that the effect will be strongly reduced by inclusion of the magnetic field [15]. This claim can be checked using the non-dipole version of the Kramers Henneberger Hamiltonian:

$$H_{KH}^{ND} = -\frac{1}{2} \nabla^2 + V(\vec{r} + \vec{\alpha}(\eta)) + \frac{1}{2} (\vec{A}(\eta))^2, \\ \eta \equiv \vec{k} \cdot \vec{r} - \omega t. \quad (8)$$

This formula is valid as long as the condition

$$\frac{E_0}{\omega c} \ll 1 \quad (9)$$

where  $E_0$  is given in atomic units, is fulfilled. From Fig. 6 we see that as long as  $E_0$  stays below 20 a.u. (corresponding to an intensity of about  $10^{19}$  W/cm<sup>2</sup>), the total ionisation probability is essentially unaltered by the inclusion of the magnetic field. The figure shows the ionisation probability and the survival probability of the ground state within and without the dipole approximation. It should be noted, however, that other quantities, such as e.g. the angular distribution of the photo electron, may be influenced by the spatial variation of the field, even though the total ionisation probability is not.

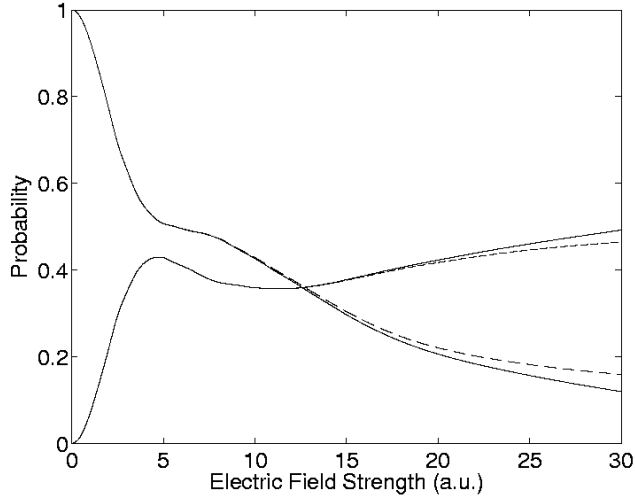


Figure 6: Ionisation probability and survival probability of the ground state with  $\omega=2$  a.u. and  $T=380$  a.s.. The full curve corresponds to the full interaction, and the dashed one to the dipole approximation.

## CONCLUDING REMARKS

We have demonstrated that for non-isotropic molecular and atomic systems, geometry is crucial, and hence any adequate description of the dynamics should include all three spatial degrees of freedom of the electron. Furthermore, the effect of atomic stabilisation is found to sustain inclusion of the magnetic field of the laser. It has been demonstrated that the phenomena is a consequence of the closing down of multi photon ionisation channels. Consequently, photo electrons are found to have a very low energy after being ionized. The effect of the magnetic field on the photo electron, in particular its angular distribution, is currently being investigated. Furthermore, methods to include more particles in the scheme is being developed.

## REFERENCES

- [1] A. Baltuska, Th. Udem, M. Uiberacker, M. Hentschel, E. Goulielmakis, Ch. Gohle, R. Holzwarth, V. S. Yakovlev, A. Scrinzi, T. H. Hänsch, F. Kraysz, *Nature (London)* **412**, 611 (2003).
- [2] R. Kienberger, E. Goulielmakis, M. Uiberacker, A. Baltuska, V. Yakovlev, F. Bammer, A. Scrinzi, Th. Westerwalbesloh, U. Kleinberg, U. Heinzmann, M. Drescher, F. Krausz, *Nature (London)* **427**, 817 (2004).
- [3] M. R. Hermann, J. A. Fleck, *Phys. Ref. A* **38**, 6000 (1988).
- [4] I. H. Sloan, R. S. Womersley, *Adv. Comput. Math.* (2003), <http://www.maths.unsw.edu.au/rsw/Sphere>.
- [5] J. P. Hansen, T. Matthey, T. Sørevik, “A parallel split operator method for the time dependent Schrödinger equation”, *10th Euro PVM/MPI* (2003).
- [6] J. P. Hansen, T. Sørevik, L. B. Madsen, *Phys. Rev. A* **68**, 031401(R) (2003).
- [7] I. Sundvor, J. P. Hansen, R. Taïeb, submitted to *Phys. Rev. A*.

- [8] S. Selstø, M. Førre, J. P. Hansen, L. B. Madsen, *Phys. Rev. Lett.* **95**, 093002 (2005).
- [9] T. Birkeland, M. Førre, J. P. Hansen, S. Selstø, *J. Phys. B* **37**, 4205 (2004).
- [10] M. Gavrila, “Atoms in Intense Laser Fields” ed Gavrila (San Diego: Academic), 1992.
- [11] W. Pauli, M. Fierz, *Nuovo Cimento* **15**, 167 (1938).
- [12] H. A. Kramers, “Collected Scientific Papers” (Amsterdam: North Holland), 1956.
- [13] W. C. Hennebeberger, *Phys. Rev. Lett.* **21**, 838 (1968).
- [14] M. Førre, S. Selstø, J. P. Hansen, L. B. Madsen, *Phys. Rev. Lett.* **95**, 043601 (2005).
- [15] A. Bugacov, M. Pont, R. Shakeshaft, *Phys. Rev. A* **48**, R4027 (1993).

# Paper V

Sølve Selstø, James F. McCann, Morten Førre, Jan Petter Hansen and Lars Bojer Madsen

**Geometrical dependence in photoionization of  $\text{H}_2^+$  in high-intensity, high-frequency, ultrashort laser pulses**

*Physical Review A*, **73**, 033407 (2006).



# Geometrical dependence in photoionization of $H_2^+$ in high-intensity, high-frequency, ultrashort laser pulses

S. Selstø,<sup>1</sup> J. F. McCann,<sup>2</sup> M. Førre,<sup>1</sup> J. P. Hansen,<sup>1</sup> and L. B. Madsen<sup>3</sup>

<sup>1</sup>Department of Physics and Technology, University of Bergen, N-5007 Bergen, Norway

<sup>2</sup>Department of Applied Mathematics and Theoretical Physics, Queen's University Belfast, Belfast, BT7 1NN, Northern Ireland, United Kingdom

<sup>3</sup>Department of Physics and Astronomy, Aarhus University, DK-8000 Aarhus C, Denmark

(Received 10 January 2006; published 6 March 2006)

The ionization dynamics of  $H_2^+$  exposed to high-intensity, high-frequency, ultrashort laser pulses is investigated with two theoretical approaches. The time-dependent Schrödinger equation is solved by a direct numerical method, and a simple two-center interference-diffraction model is studied. The energy and angular distributions of the photoelectron for various internuclear distances and relative orientations between the internuclear axis of the molecule and the polarization of the field are calculated. The main features of the photoelectron spectrum pattern are described well by the interference-diffraction model, and excellent quantitative agreement between the two methods is found. The effect of quantal vibration on the photoelectron spectrum is also calculated. We find that vibrational average produces some broadening of the main features, but that the patterns remain clearly distinguishable.

DOI: [10.1103/PhysRevA.73.033407](https://doi.org/10.1103/PhysRevA.73.033407)

PACS number(s): 33.80.Rv, 33.60.-q, 31.15.Qg

## I. INTRODUCTION

The creation of light sources in the X-ray and extreme ultraviolet (euv) regions has seen rapid developments in recent years [1]. This generation of sources offers the possibility of focusing coherent light to a spot size  $\sim 10$  nm or less, with ultrashort pulse durations  $10^{-17}$  s, and extremely high intensities. This technology provides a tool for microscopic analysis in space, time, and the interaction strength with applications in high-resolution imaging, ultrafast spectroscopy, biomicroscopy, and nanofabrication. The generation of pulses on the attosecond time scale and with photon energies as high as 100 eV have been demonstrated [2,3]. These improvements have paved the way for the possibility of resolving electronic processes in materials. For simple molecular systems, the degree of control means it is now possible to align both diatomic and polyatomic molecules [4], with various possible applications, such as optical control of molecular energy transfer [5].

The coupling between the external field of a laser and a molecule is sensitive to the frequency and intensity of the light, but also to its polarization. Since the molecular symmetry, and hence its polarizability tensor is a critical factor, the alignment and orientation of the molecule is very significant. For example, the field ionization of molecules is exponentially sensitive to the potential barrier and consequently the orientation of the field relative to the molecule [6–9]. Hence, an improved understanding of the molecule-light interaction should include geometrical effects. The nonspherical symmetry of a molecule means the effect of the interaction is far more complex than that for atoms. This is the reason why so far no nonperturbative *ab initio* calculation, including all degrees of freedom, has been performed for any diatomic molecule—including the simplest of all; the hydrogen molecular ion. Only within the last ten years has it been feasible to perform intensive simulations that can be com-

pared with detailed experimental studies of the system. Although  $H_2^+$  has been under intense theoretical investigation [10], calculations tend to be limited to some particular geometry [11] or some reduced electronic dimensionality [12].

Recently, we presented a numerical method for solving the time-dependent Schrödinger equation for  $H_2^+$  in an ultrashort, intense, high-frequency field including all three spatial dimensions of the electron [13]. The main focus was the total ionization probability  $P_I$  and its dependence on orientation and internuclear separation. In this paper, we investigate the energy and angular distributions of the photoelectrons at various orientations and internuclear separations. The angular distribution for ionization by high-frequency light is investigated by the time-dependent method for a short (few cycle) pulse and compared with a simple model describing the process as an interference-diffraction effect. For short high-frequency pulses the interaction time is of the order of a few femtoseconds or less. Thus rovibrational relaxation can be neglected. However, the initial state of vibration determines the distribution of the nuclei and can play a role. We will briefly investigate the influence of vibration on the photoelectron spectra.

The paper is organized as follows: In Sec. II, we outline the method used in the *ab initio* calculations including a discussion of the transformation to obtain the energy and angular distributions of the photoelectron. Also in Sec. II, the two-center interference model is developed. Finally we consider the effect of the quantal vibration state. The results are presented and interpreted in Sec. III, and the conclusions are drawn in Sec. IV. Atomic units ( $m_e = \hbar = e = 1$ ) are used throughout.

## II. THEORY

In Fig. 1 the coordinate notation and system geometry is illustrated. The internuclear vector  $\mathbf{R}$  is taken to be the polar

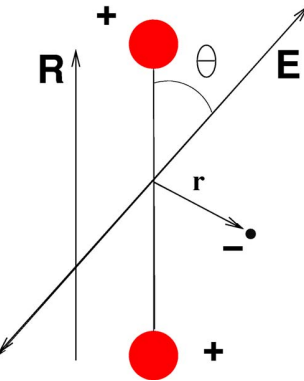


FIG. 1. (Color online) Coordinates (molecular frame); The protons are at a fixed distance  $R$  with the molecular axis defining the polar axis ( $z$  direction). The  $xz$ -plane is chosen so that it contains the polarization vector which defines an angle  $\theta$  with respect to the  $z$  axis. The electron coordinate, with its origin at the midpoint between the nuclei, is denoted by  $\mathbf{r}$ .

axis in the molecular frame. Suppose the angular frequency of the light is  $\omega$ , and the duration of the pulse is  $T$ . Then a simple representation of the vector potential ( $\mathbf{A}$ ) is

$$\mathbf{A}(t) = \frac{E_0}{\omega} \sin^2\left(\frac{\pi t}{T}\right) \sin(\omega t + \varphi) \hat{\mathbf{u}}_P, \quad (1)$$

where  $E_0$  is the electric field amplitude, the polarization direction  $\hat{\mathbf{u}}_P$  is given by the angle  $\theta$  relative to the internuclear

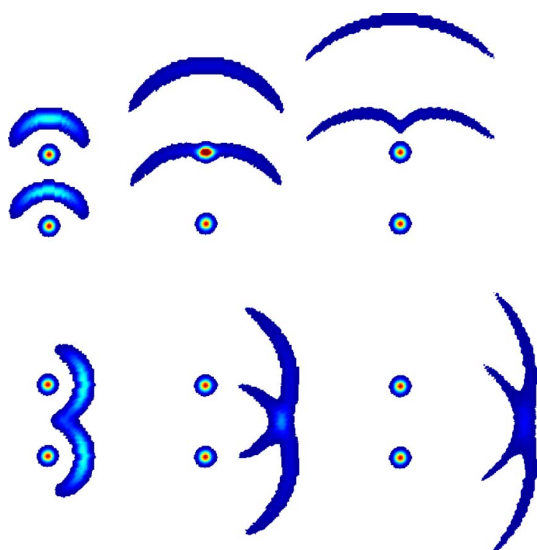


FIG. 2. (Color online) Outgoing waves from each of the scattering centers at three different instants of time (from left to right:  $t=4, 7$ , and  $10$  a.u.). The central energy of the wave packets is 1.1 a.u., and the internuclear separation is 3 a.u. The upper panels correspond to ionization in the direction parallel to the internuclear axis, and the lower ones correspond to perpendicular ionization direction. The scattering centers are shown as circular dots. In the upper case, one of the two outgoing waves is distorted by the upper scattering center, whereas no such interaction takes place in the lower case.

axis, and  $\varphi$  is the phase of the pulse. The calculations presented in this paper are representative of generic strong fields at high frequency. The parameters chosen to illustrate the ionization process are  $E_0=3$  a.u., with central frequency  $\omega=2$  a.u. and pulse duration six optical cycles, that is  $\sim 450$  as. This is far shorter than both the typical vibrational and rotational period of the molecule (15 and 396 fs, respectively). Furthermore, from a classical consideration with an initial internuclear separation 1 a.u., in the extreme case of immediate ionization, the nuclei would move less than 0.2 a.u. during the interaction. Thus we may safely neglect changes in the orientation and the internuclear distance of the molecule during the interaction with the pulse. For a pulse lasting several cycles, the results of the calculations are rather insensitive to the carrier-envelope phase  $\varphi$ . The dipole approximation is well justified for the field applied [14].

### A. Ab Initio calculations

For fixed internuclear distance,  $R$ , and with  $r_1$  and  $r_2$  denoting the distances of the electron from the nuclei, the electronic Hamiltonian in the length gauge is

$$H_L = -\frac{1}{2} \nabla^2 - \frac{1}{r_1} - \frac{1}{r_2} + \frac{1}{2} \mathbf{E}(t) \cdot (\mathbf{r}_1 + \mathbf{r}_2) = -\frac{1}{2} \nabla^2 - \frac{1}{|\mathbf{r} - \mathbf{R}/2|} - \frac{1}{|\mathbf{r} + \mathbf{R}/2|} + \mathbf{E}(t) \cdot \mathbf{r}, \quad (2)$$

or, alternatively, in the Kramers-Henneberger frame (acceleration gauge),

$$H_{KH} = -\frac{1}{2} \nabla^2 - \frac{1}{|\mathbf{r} - \mathbf{R}/2 + \boldsymbol{\alpha}(t)|} - \frac{1}{|\mathbf{r} + \mathbf{R}/2 + \boldsymbol{\alpha}(t)|}, \quad (3)$$

with  $\boldsymbol{\alpha}(t) \equiv \int_0^t \mathbf{A}(t') dt'$ .

The wave function is expanded in spherical coordinates as follows:

$$\Psi(\mathbf{r}, t) = \sum_{l=0}^{l_{\max}} \sum_{m=-l}^l f_{lm}(r, t) Y_{lm}(\Omega), \quad (4)$$

where  $Y_{lm}$  are spherical harmonics, and  $f_{lm}(r, t)$  are the radial functions that are discretized on a grid of evenly-spaced points. The time-dependent Schrödinger equation is propagated by the split-step method [15,16]. Convergent results were obtained using 2048 radial grid points ranging up to  $r_{\max}=150$  a.u. including  $l_{\max}=15$  in the expansion Eq. (4). We used this method to construct the ground state  $\Psi_0$  by propagating in “imaginary time” ( $t \rightarrow \tau = -it$ ). The eigenenergy can be found from the decay rate of the norms of the wave function, namely,

$$E_0 = -\frac{1}{2\Delta\tau} \ln\left(\frac{\langle \Psi_0(\tau + \Delta\tau) | \Psi_0(\tau + \Delta\tau) \rangle}{\langle \Psi_0(\tau) | \Psi_0(\tau) \rangle}\right). \quad (5)$$

Comparing this value with the exact result provides a good measure of the accuracy of the calculations. For instance, for  $R=2$  a.u., we find that  $E_0=-1.100$  a.u., compared with the exact value—1.103 a.u. [18]. In order to avoid unphysical reflections at the outer boundary of the spherical grid, the wave function is smoothly attenuated at each time step by

multiplying by the factor  $g(r)=1-\sin^M[\pi r/(2r_{\max})]$  with  $M=20$ . The calculations were performed mainly in the length gauge, but also the Kramers-Henneberger formulation of the Hamiltonian was used in order to check for gauge invariance.

We now turn to our method of distinguishing between the bound and the continuum part of the spectrum, and the extraction of the energy spectrum of the photoelectrons. We partition the wave function as the sum of a bound and continuum part,  $\Psi=\Psi_{\text{bound}}+\Psi_{\text{out}}$ . The separation of the spatial wave function into the two parts is accomplished by allowing the wave packet to propagate some additional time after the pulse is over. At some point  $t_f$  after the interaction, the wave packet corresponding to fast photoelectrons will have separated from the bound states, and the bound states are contained within a finite radius  $r \leq a$ . We determine  $a$  and  $t_f$  by direct inspection of the radial density of the wave function as a function of time. In the present calculations we have allowed the wave packet to propagate for about 13 a.u. after the interaction with the laser pulse has finished ( $t_f=T+13$  a.u.). It is important to bear in mind that the distance  $a$  must be large enough so that the effect of the Coulomb potential on the kinetic energy of the outgoing electron can be neglected, that is  $a \gg 2/k^2$ . The continuum function is then transformed to the momentum representation by a Fourier transform

$$\tilde{\Psi}_{\text{out}}(\mathbf{k}) \equiv \mathcal{F}\{\Psi_{\text{out}}(\mathbf{r})\}. \quad (6)$$

From  $\tilde{\Psi}_{\text{out}}(\mathbf{k})$  the energy and angular spectra can be obtained. Since we are free to chose the size of the grid, and we can propagate as long as desired, this method should in principle work in any case except for  $k \approx 0$ . Thus, we expect this method to work best for photon energies well above the ionization potential, as is the case here ( $\omega=2$  a.u.).

The Fourier transform of the ionized part is calculated from Eq. (4) as

$$\tilde{\Psi}_{\text{out}}(\mathbf{k}) = \sum_{l=0}^{l_{\max}} \sum_{m=-l}^l g_{lm}(k) Y_{lm}(\Omega_k) \quad (7)$$

with

$$g_{lm}(k) = \sqrt{\frac{2}{\pi}} (-i)^l \int_a^\infty j_l(kr) f_{lm}(r, t_f) r^2 dr, \quad (8)$$

where  $j_l$  is the spherical Bessel function of the first kind.

The momentum and angular probability distributions can be calculated directly from the momentum space densities as follows:

$$\frac{dP_I}{dk} = \int_{4\pi} k^2 |\tilde{\Psi}_{\text{out}}(\mathbf{k})|^2 d\Omega_k \quad (9)$$

and

$$\frac{dP_I}{d\Omega_k} = \int_0^\infty k^2 |\tilde{\Psi}_{\text{out}}(\mathbf{k})|^2 dk, \quad (10)$$

The energy spectrum can be derived through the relation  $dP/dE=(1/k)dP/dk$ .

If the photon energy is high and the pulse is long enough, the spectrum will have well-defined peaks associated with absorption of a certain number  $N$  of photons. Restricting the integration in Eq. (10) to this  $k$  interval, the angular distribution corresponding to absorption of  $N$  photons is found.

## B. Model

In [13] both the dependence of  $P_I$  on  $\theta$  and  $R$  and the angular distribution is a consequence of interference between two isotropic point sources located on the protons. This follows from the fact that it is a good approximation to assume that the initial state, for intermediate and large values of  $R$ , is an even-parity superposition of single-center spherical functions,  $\Psi_0 \sim \phi_s(r_1) + \phi_s(r_2)$ . The agreement between this model and the results from solving the Schrödinger equation is rather good. The model may be further improved by including polarization of the single-center orbitals [17,18] or by including a two-center function reflecting the elliptic symmetry [19].

Applying the same reasoning to the continuum function, we assume the outgoing wave to be of the asymptotic ( $t, r \rightarrow \infty$ ) form

$$\psi_{\text{out}} = f_p(\Omega_1) \exp(ikr_1)/r_1 + f_p(\Omega_2) \exp(ikr_2)/r_2. \quad (11)$$

For one-photon absorption, the scattering amplitude  $f_p$  corresponds to an atomic  $p$  wave rotated along the polarization axis. With  $\mathbf{R}$  parallel to the  $z$  axis and  $\hat{\mathbf{u}}_p$  in the  $xz$  plane we have

$$\begin{aligned} f_p(\Omega_i) &\propto \hat{\mathbf{u}}_p \cdot \mathbf{r}_i \propto \cos \theta Y_{10}(\Omega_i) \\ &+ \sin \theta \frac{1}{\sqrt{2}} [Y_{1-1}(\Omega_i) - Y_{11}(\Omega_i)]. \end{aligned} \quad (12)$$

From this, the differential ionization probability is found to be

$$\frac{dP_I}{d\Omega_k} \propto |f_p(\Omega_k)|^2 \cos^2\left(\frac{1}{2}\mathbf{k} \cdot \mathbf{R}\right), \quad (13)$$

where  $\Omega_k = \{\theta_k, \phi_k\}$  is the direction of the ionized electron with respect to the polar axis  $\mathbf{R}$ . We take the value of  $k$  to be the one corresponding to the kinetic energy at  $r \rightarrow \infty$ ,  $k(R) = \sqrt{2[\omega - I_p(R)]}$ .

Comparing the predictions of this simple model with our *ab initio* calculations gives broad agreement for the angular distribution. A simple refinement of the initial state allows for the polarization of the orbital, so that the single-center has  $p$  wave terms giving angular distributions with additional  $s$  and  $d$  wave terms. Furthermore, the simple two-center model, while including the interference effect, neglects the scattering effect of the other center; the final state (outgoing spherical waves) can be diffracted by the potential corresponding to the other proton. This effect will be most pronounced when the polarization axis is aligned with the molecular axis. On the other hand, for orthogonal axis and polarization, this refinement should not have much effect. The phenomenon is illustrated in Fig. 2. In effect, all waves passing through the area close to the other scattering center

will be Coulomb shifted. The magnitude of the shift depends on how close to the center it passes, and it is maximal for  $\theta_k=0^\circ$  and  $180^\circ$ . In order to capture this effect, the ansatz Eq. (11) should be modified accordingly. The eikonal approximation is one way of realizing this [20,21]

$$\begin{aligned} \psi'_{\text{out}} = & f_p(\Omega_1) \exp \left( i \int_0^{r_1} \sqrt{2[E - V(\mathbf{r}_1')]} \hat{\mathbf{k}}_1 \cdot d\mathbf{r}'_1 \right) / r_1 \\ & + f_p(\Omega_2) \exp \left( i \int_0^{r_2} \sqrt{2[E - V(\mathbf{r}'_2)]} \hat{\mathbf{k}}_2 \cdot d\mathbf{r}'_2 \right) / r_2, \end{aligned} \quad (14)$$

where  $E=\omega-I_P$ , and the unit vectors  $\hat{\mathbf{k}}_{1,2}$ , parallel to the line segments  $d\mathbf{r}'_{1,2}$ , point radially outwards from their respective scattering centers.  $V(\mathbf{r}_{1,2})$  is the Coulomb potential expressed in coordinates with the respective protons as origins

$$V(\mathbf{r}_{1,2}) = -\frac{1}{r_{1,2}} - \frac{1}{|\mathbf{r}_{1,2} \pm \mathbf{R}|}, \quad (15)$$

where the plus sign corresponds to proton one and the minus sign to proton two. The differential ionization probability is found by letting  $r$  become large. It is important to maintain the distinction between  $r_1$  and  $r_2$  in the upper integration limits in Eq. (14), also for large  $r$ .

Unfortunately, the singularities in the Coulomb potential cannot be treated adequately within this approximation. The divergences at  $\mathbf{r}=\pm\mathbf{R}/2$  are manifested as discontinuities in the derivative of  $dP_I/d\Omega_k$ . For this reason we have “softened” the potential;  $V \rightarrow V' \equiv -1/\sqrt{r_1^2+s^2}-1/\sqrt{r_2^2+s^2}$ . The parameter  $s$  is chosen as small as possible while removing the cusps. Outside these regions, the results are not very sensitive to this parameter.

This approach amounts to a differential ionization probability given by

$$\begin{aligned} \frac{dP_I}{d\Omega_k} \propto & |f_p(\Omega_k)|^2 \lim_{r \rightarrow \infty} \left| e^{i \int_0^{r-R/2} \cos \theta_k \sqrt{2[E-V'(\mathbf{r}_1)]} \hat{\mathbf{k}} \cdot d\mathbf{r}_1} \right. \\ & \left. + e^{i \int_0^{r+R/2} \cos \theta_k \sqrt{2[E-V'(\mathbf{r}_2)]} \hat{\mathbf{k}} \cdot d\mathbf{r}_2} \right|^2. \end{aligned} \quad (16)$$

In the limit  $s \rightarrow \infty$ , Eq. (13), is reobtained.

### C. The $R$ -averaged spectra

As already pointed out, we do not expect any interference between the dynamics of the direct ionization and the molecular vibration. However, it should be taken into account that the initial state does not have a well defined  $R$  value. Neglecting rotation, the initial state is, within the Born-Oppenheimer approximation, the product of an electronic ground state that depends parametrically on  $R$  and an internuclear state

$$\Phi_0(R, \mathbf{r}) = F(R) \Psi_0(R; \mathbf{r}). \quad (17)$$

The internuclear part may be written as a coherent linear combination of vibrational states up to some  $\nu_{\max}$ ,

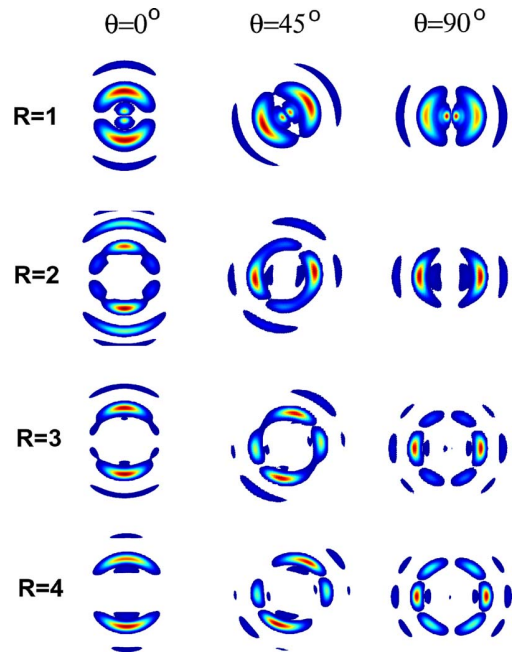


FIG. 3. (Color online) The momentum wave function in the scattering plane,  $|\tilde{\Psi}_{\text{out}}(k_x, k_y=0, k_z)|^2$ , for various internuclear distances  $R$  and relative orientations between the linearly polarized field and the vertical internuclear axis.  $R$  increases from top to bottom. To the left, the field and the molecule are parallel ( $\theta=0^\circ$ ) to each other, to the right they are perpendicular to each other ( $\theta=90^\circ$ ), and in the middle we have  $\theta=45^\circ$ . The internuclear axis points in up/down direction, and the momenta  $k_x$  and  $k_z$  span from -3 to 3 a.u.

$$F(R) = \sum_{\nu=0}^{\nu_{\max}} c_{\nu}(t_0) e^{-i\epsilon_{\nu} t_0} \chi_{\nu}(R). \quad (18)$$

From this expression, and the linearity of the Schrödinger equation, we assume that a realistic final state may be obtained from our numerical calculations as  $\Phi_{\text{final}}(R, t_f) = F(R) \Psi_R(\mathbf{r}, t_f)$  where  $\Psi_R(\mathbf{r}, t_f)$  is the solution of the electronic Schrödinger equation with the internuclear distance fixed at  $R$  and  $t_f > T$ . The spectra can then be found in the same manner as before using the “ $R$ -averaged” final electronic wave function

$$\begin{aligned} \bar{\Psi}_{\text{final}}(\mathbf{r}) \equiv & \frac{1}{R_{\max} - R_{\min}} \int_{R_{\min}}^{R_{\max}} F(R) \Psi_R(\mathbf{r}, t_f) dR \\ \approx & \sum_n w_n F(R_n) \Psi_{R_n}(\mathbf{r}, t_f), \end{aligned} \quad (19)$$

where the weights  $w_n$  depend on the set of  $R_n$ -s chosen.

The coefficients  $c_{\nu}$  in Eq. (18) are determined by the mechanism involved in producing  $\text{H}_2^+$ . When the molecular ion is made by ionizing  $\text{H}_2$ -molecules by electron impact, they are usually approximated by the well-known Franck-Condon factors. The amplitudes are also proportional to a dynamic phase factor given by the energy  $\epsilon_{\nu}$  of the particular vibrational state  $\nu$ . Consequently, the vibrational state is sub-

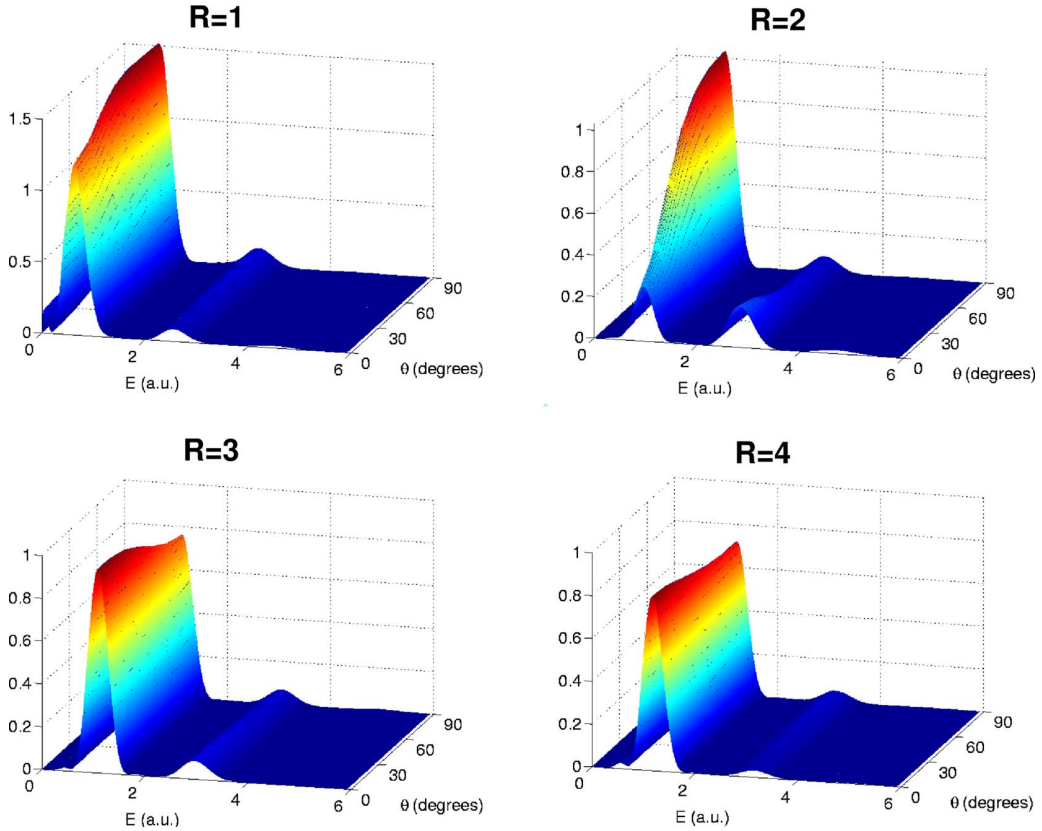


FIG. 4. (Color online) The energy distribution of the photoelectron as a function of kinetic energy of the outgoing electron and the angle  $\theta$  between the internuclear axis and the field. The distributions correspond to  $R=1, 2, 3$ , and  $4$  a.u. Peaks are seen at  $E \approx \omega - I_p$  and  $E \approx 2\omega - I_p$  [ $\omega = 2$  a.u., and  $I_p(R) = 1.45, 1.1, 0.91$ , and  $0.80$  a.u., respectively]. The one-photon ionization signal dominates the spectrum, and therefore it also governs the dependence of the ionization probability on the relative orientation  $\theta$ .

ject to a coherent time evolution, which causes a strong variation on the femtosecond time scale. Hence the actual  $R$  distribution at the instant the interaction begins, is very sensitive to the time delay  $t_0$  of the pulse [22].

Recently a method based on the strong field approximation was shown to give better agreement with the experiment [23] than the Franck-Condon factors [24]. In this paper it is also suggested that producing a pure ground vibrational state should be quite feasible. Such a state would not give rise to any time-dependent  $R$  distribution.

### III. RESULTS AND DISCUSSION

In Fig. 3 we display sections of the momentum distribution of the photoelectron in the plane spanned by the field polarization and the internuclear axis, i.e., we consider  $|\tilde{\Psi}_{\text{out}}(k_x, k_y=0, k_z)|^2$  as a function of  $k_x$  and  $k_z$ . The distributions are shown for the internuclear distances  $R=1, 2, 3$ , and  $4$  a.u., and the linear polarization is parallel, perpendicular, and intermediate ( $\theta=45^\circ$ ) relative to  $\mathbf{R}$ . The internuclear axis is oriented in the vertical direction. Both the  $k_x$  and the  $k_z$  axis extend from  $-3$  a.u. to  $3$  a.u. in all cases. These figures demonstrate clearly which ionization directions and energies are most probable. The contributions from one- and two-photon ionization are seen as parts of concentric rings in

the probability densities. For  $R=2$ ,  $\theta=0^\circ$  also probability density stemming from three-photon ionization is observed. For polarization parallel and perpendicular to the internuclear axis, the wave packets have clear maxima in the directions of the field. This is not the case at intermediate polarization directions. This behavior is a signature of interference. At internuclear separation  $R=1$  a.u., the distribution seems to be atomiclike, i.e., a rotation of the field seems to simply amount to a corresponding rotation of the wave packet. But this is in fact not the case; the principal direction of ionization is *not*  $45^\circ$  for the intermediate polarization direction, and, as we will see, the overall ionization probability is strongly  $\theta$ -dependent. For  $R=2$  a.u., the probability of two-photon ionization is comparable to the probability of one-photon ionization for  $\theta=0^\circ$ , whereas the one-photon ionization dominates more and more as  $\theta$  increases towards  $90^\circ$ . For  $R=3$  and  $4$  a.u., the maxima tend to be more localized, and some local maxima appear in addition to the global ones at perpendicular polarization.

The dependence on the orientation of the field relative to the internuclear axis is shown in Fig. 4. Here we see the energy spectrum  $dP_I/dE$  as a function of the polarization angle  $\theta$  in addition to the energy  $E$ . The plots are made for the same internuclear distances as in Fig. 3. All four figures have clear maxima for  $E \sim \omega - I_p$ , corresponding to the absorption of one photon with energy  $\omega$ . Peaks corresponding

to two-photon ionization ( $E \sim 2\omega - I_p$ ) can also be seen. The position of the maxima are independent of the polarization angle  $\theta$ , but the magnitude of the ionization probability exhibit strong  $\theta$  dependence—in particular for  $R=2$  a.u. For  $R=1$  and 2 a.u., the ionization probability is highest at the perpendicular polarization, whereas the situation is the contrary for  $R=3$  and 4 a.u. These effects can be related to the oscillatory behavior of the total ionization probability  $P_I(R)$  as a function of internuclear distance. The oscillations are strong for  $\theta=0^\circ$  and absent at  $\theta=90^\circ$ . This can be understood within the simple model of Eq. (13), as explained in [13]. The probability of ionization by two photons is rather independent of the polarization direction for all internuclear distances at hand. For  $R=1$  and 2 a.u., also three-photon ionization is visible on this scale.

Figure 5 shows three-dimensional polar plots of the differential ionization probability,  $dP_I/d\Omega_k$ , for the same internuclear distances and orientations as in Fig. 3. The radial distance of these surfaces indicates the probability density of ionization in that particular direction. In all figures, the internuclear axis is oriented vertically, and the polarization, indicated by a black line, also lies in the plane of the paper. It should be noted that the figures are not scaled equally. They show, as does Fig. 3, that for parallel and perpendicular orientation, the photoelectron is most likely ionized in the direction of the field. In addition to these global maxima, some local maxima at intermediate angles are observed. These “side lobes” are most clearly visible at  $\theta=90^\circ$ . They increase in magnitude as  $R$  increases, whereas the maxima in the directions of the field become more and more narrow. At intermediate polarization,  $\theta=45^\circ$ , the polarization direction is *not* the most likely direction of ionization. All of these features clearly indicate that the signal is built up from interfering contributions from the two centers.

The differential ionization probability for one-photon ionization has been calculated and compared with the predictions of the models in Eqs. (13) and (16). The results are shown in Fig. 6. The differential probability is shown in half of the scattering plane as functions of the angle between the ionization direction and the polarization of the field. The full curves show the results obtained from the *ab initio* calculation, whereas the others show the predictions of the models. Due to the rather sharp peaks corresponding to one-photon absorption seen in Fig. 4, the idea of using one well-defined asymptotic  $k$  value is justified. We find that our model is able to reproduce the differential one-photon ionization probability quite well. We are therefore confident that the assumption of interfering nonconcentric spherical waves is the adequate one. The approach based on the eikonal approximation in general compensates for the discrepancies between the *ab initio* results and the seemingly naive model, where the anisotropy of the molecular Coulomb potential is not fully accounted for. In general, the two models agree rather well for the polarization angle  $\theta=90^\circ$ , whereas the deviations can be quite large for  $\theta=0^\circ$  and  $45^\circ$ —in particular for  $R=2$  and 3 a.u. For small internuclear separations, the system is similar to  $\text{He}^+$ , for which no diffraction takes place. In the other extreme case, i.e., when  $R$  becomes large, a smaller angular range of the outgoing wave passes through the vicinity of the other proton. In both cases, the effect of diffraction is less

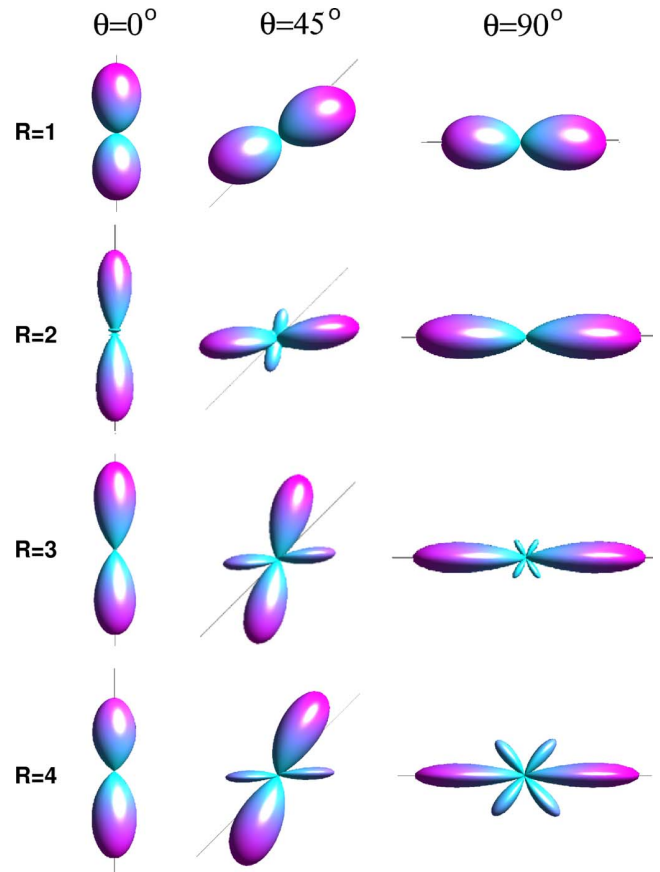


FIG. 5. (Color online) The differential ionization probability at various polarization directions and internuclear separations. The figures are displayed in the same manner as in Fig. 3. The line indicates the direction of the field. The overall scaling varies from figure to figure.

pronounced than is the case for intermediate internuclear separations, which explains the rather high level of agreement between the two models for  $R=1$  and 4 a.u.

The influence of the initial vibrational state on the final angular distributions of the total differential probability has been investigated for two initial  $R$ -distributions, namely the vibrational ground state  $\chi_{v=0}(R)$ , and another state chosen to be a Gaussian centered at  $R=2.5$  a.u. with a standard deviation 0.7 a.u. The integration in Eq. (19) has been done by the trapezoidal rule including final electronic wave functions with internuclear separations 1, 1.5, 2, 2.5, 3, and 4 a.u. The results are displayed for both cases along with the corresponding  $R$ -distributions in Fig. 7. They should be compared with Fig. 4. We find that taking the vibrational state into account does not wipe out the signatures of the different orientations completely. In the case of the vibrational ground state, all three distributions are clearly distinguishable. With the wider distribution in the lower panels, the  $\theta=0^\circ$  and  $\theta=45^\circ$  spectra are not that easily distinguished, and we expect that for such a broad distribution of  $R$  values and smaller values of  $\theta$ , the orientation of the molecule cannot be decided as precisely as in the case of a more localized internuclear wave function.

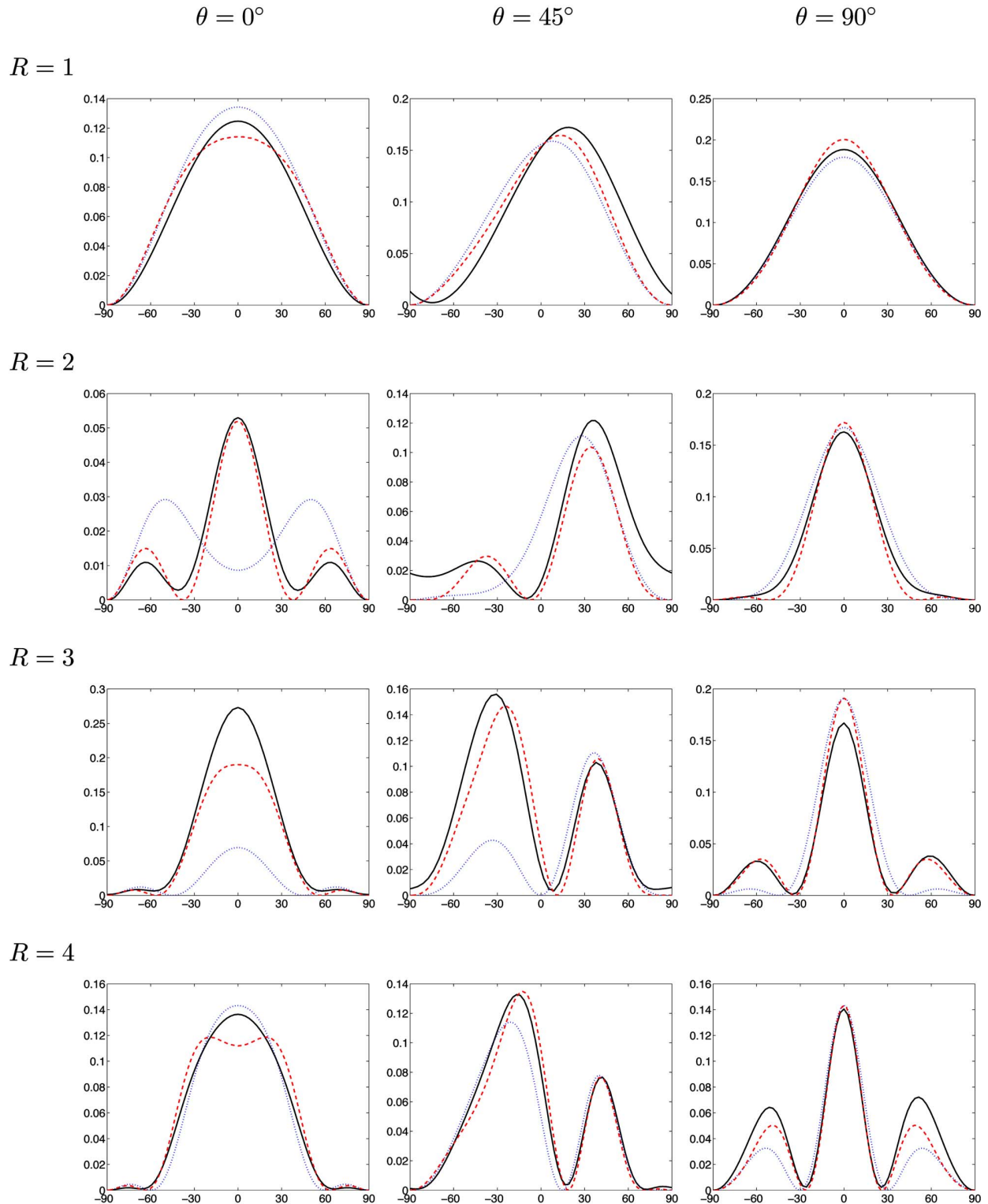


FIG. 6. (Color online) The differential ionization probability for one-photon ionization plotted in the scattering plane. The ordinate is the angle of the outgoing electron relative to the direction of the field. The full curves are the results obtained from solving the Schrödinger equation, the dotted curves are the prediction of the simple interference model, Eq. (13), while the dashed curves are the predictions of the model including diffraction, Eq. (16). The panels are displayed according to geometry in the same manner as Figs. 3 and 5.

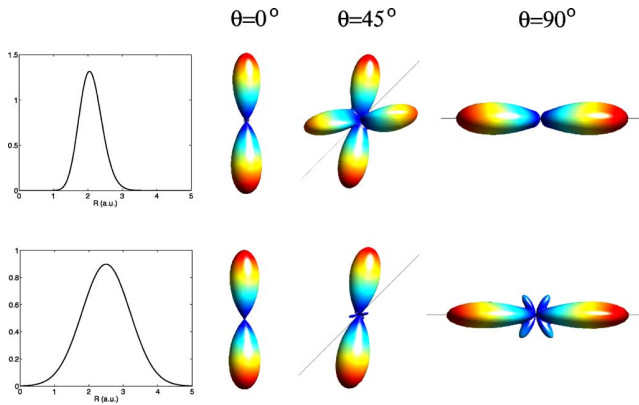


FIG. 7. (Color online) The total differential ionization probability with the initial vibrational state taken into consideration. The upper panels correspond to the vibrational ground state, and the lower ones correspond to a Gaussian distribution centered at  $R = 2.5$  a.u. with a standard deviation of 0.7 a.u. These vibrational wave functions are shown to the left. As in Fig. 4, the direction of the polarization with respect to the vertical internuclear axis is given by  $\theta = 0^\circ$ ,  $45^\circ$ , and  $90^\circ$ , respectively.

#### IV. CONCLUSIONS

We have investigated the dynamics of high-intensity, high-frequency ionization of  $\text{H}_2^+$  by laser fields based on

*ab initio* methods as well as simple models. The energy and the angular distributions of the photoelectron have been calculated for various geometries by investigating the ionized part of the wave function. These spectra have been explained as an interference effect between outgoing nonconcentric spherical waves, where the waves are diffracted by the other scattering center.

It was found that the features of the different orientations survive when the vibrational motion is taken into account. This demonstrates that information about the initial molecular orientation is obtainable experimentally from investigating the photoelectron of the molecule after interaction with a laser pulse.

#### ACKNOWLEDGMENTS

The present research was supported by the Norwegian Research Council through the NANOMAT program and the Nordic Research Board NordForsk. I.B.M. is supported by the Danish Natural Science Research Council (Grant No. 21-03-0163). Finally, we would like to thank Professor Ladislav Kocbach for fruitful discussions and Dr. Alicia Palacios at la Universidad Autónoma de Madrid for her help.

- 
- [1] U. Keller, *Nature (London)* **424**, 831 (2003).  
[2] A. Baltuška, Th. Udem, M. Uiberacker, M. Hentschel, E. Goulielmakis, Ch. Gohle, R. Holzwarth, V. S. Yakovlev, A. Scrinzi, T. W. Hänsch, and F. Krausz, *Nature (London)* **421**, 611 (2003).  
[3] R. Kienberger, E. Goulielmakis, M. Uiberacker, A. Baltuska, V. Yakovlev, F. Bammer, A. Scrinzi, Th. Westerwalbesloh, U. Kleineberg, U. Heinzmann, M. Drescher, and F. Krausz, *Nature (London)* **427**, 817 (2004).  
[4] C. Z. Bisgaard, M. D. Poulsen, E. Peronne, S. S. Viftrup, and H. Stapelfeldt, *Phys. Rev. Lett.* **92**, 173004 (2004).  
[5] H. Stapelfeldt and T. Seideman, *Rev. Mod. Phys.* **75**, 543 (2003).  
[6] R. Dörner, H. Bräuning, O. Jagutzki, V. Mergel, M. Achler, R. Moshammer, J. M. Feagin, T. Osipov, A. Bräuning-Demian, L. Spielberger, J. H. McGuire, M. H. Prior, N. Berrah, J. D. Bozek, C. L. Cocke, and H. Schmidt-Böcking, *Phys. Rev. Lett.* **81**, 5776 (1998).  
[7] T. K. Kjeldsen, C. Z. Bisgaard, L. B. Madsen, and H. Stapelfeldt, *Phys. Rev. A* **68**, 063407 (2003).  
[8] T. K. Kjeldsen and L. B. Madsen, *Phys. Rev. A* **71**, 023411 (2005).  
[9] T. K. Kjeldsen, C. Z. Bisgaard, L. B. Madsen, and H. Stapelfeldt, *Phys. Rev. A* **71**, 013418 (2005).  
[10] J. H. Posthumus and J. F. McCann, in *Molecules and Clusters in Intense Laser Fields* (Cambridge Press, Cambridge 2001).  
[11] D. Dundas, *Phys. Rev. A* **65**, 023408 (2002).  
[12] B. Rotenberg, R. Taïeb, V. Veniard, and A. Maquet, *J. Phys. B* **35**, L397 (2002).  
[13] S. Selstø, M. Førre, J. P. Hansen, and L. B. Madsen, *Phys. Rev. Lett.* **95**, 093002 (2005).  
[14] M. Førre, S. Selstø, J. P. Hansen, and L. B. Madsen, *Phys. Rev. Lett.* **95**, 043601 (2005).  
[15] M. R. Hermann and J. A. Fleck, Jr., *Phys. Rev. A* **38**, 6000 (1988).  
[16] J. P. Hansen, T. Sørevik, and L. B. Madsen, *Phys. Rev. A* **68**, 031401(R) (2003).  
[17] B. N. Dickinson, *J. Chem. Phys.* **1**, 317 (1933).  
[18] F. Weinhold, *J. Chem. Phys.* **54**, 530 (1971).  
[19] A. Dalgarno and G. Poots, *Proc. Phys. Soc., London, Sect. A* **67**, 343 (1954).  
[20] L. D. Landau and E. M. Lifschitz, in *Quantum Mechanics*, 3rd ed. (Pergamon Press, Oxford, 1977), Section 131.  
[21] R. J. Glauber, in *Lectures in Theoretical Physics*, edited by W. E. Brittin and L. G. Dunham (Interscience, New York, 1959), Vol. I, p. 315.  
[22] L.-Y. Peng, I. D. Williams, and J. F. McCann, *J. Phys. B* **38**, 1727 (2005).  
[23] X. Urbain, B. Fabre, V. M. Andrianarijaona, J. Jureta, J. H. Posthumus, A. Saenz, E. Baldit, and C. Cornaggia, *Phys. Rev. Lett.* **92**, 163004 (2004).  
[24] T. K. Kjeldsen and L. B. Madsen, *Phys. Rev. Lett.* **95**, 073004 (2005).

# Paper VI

Morten Førre, Jan Petter Hansen, Ladislav Kocbach, Sølve Selstø and Lars Bojer Madsen

**Strong Nondipole Effects in Angular Photoelectron Spectra of Atoms in Super-  
Intense, High-Frequency, Attosecond Pulses**

*To appear in Physical Review Letters.*



# Nondipole Ionization Dynamics of Atoms in Super-Intense, High-Frequency, Attosecond Pulses

M. Førre,<sup>1</sup> J. P. Hansen,<sup>1</sup> L. Kochbach,<sup>1</sup> S. Selstø,<sup>1</sup> and L. B. Madsen<sup>2</sup>

<sup>1</sup>Department of Physics and Technology, University of Bergen, N-5007 Bergen, Norway

<sup>2</sup>Department of Physics and Astronomy, University of Aarhus, 8000 Aarhus, Denmark

The ionization of H(1s) in super-intense, high-frequency, attosecond pulses is studied beyond the dipole approximation. We identify a unique nondipole 3rd lobe in the angular distribution of the ejected electron and show that this lobe has a well-defined classical counterpart. The ionization is likely to occur in the direction opposite to the laser propagation direction, which is fully understood from an analysis of the classical dynamics.

PACS numbers: 42.50.Hz, 32.80.Rm, 32.80.Fb

The production of short, high-intensity, high-frequency electromagnetic pulses is currently being pursued along two different avenues. First, large-scale free-electron (FEL) and X-ray FEL laser projects aim at producing pulses of hard radiation of  $\sim 100$  fs duration. Second, advances in laser technology have led to the production of isolated XUV pulses of a duration of only 250 attoseconds [1]. These developments mean that the counterintuitive high-intensity, high-frequency phenomena of atomic stabilization with decreasing ionization probability/rate for increasing intensity [2] may become subject to experimental investigations. Naturally, these prospects have revived the theoretical interest in the study of nonperturbative driving of atomic and molecular systems by high-intensity, high-frequency fields [3–5].

In fully three-dimensional nondipole wave packet calculations [3], we identified the onset of stabilization by a transition from multiphoton-like ionization to ionization dominated by nonadiabatic shake-off as represented by a lack of overlap between the field-free and field-dressed states and with the emergence of characteristic low-energy electrons. In this work, we consider the first fully three-dimensional angular distributions in the high-frequency nondipole regime. In particular, we show that the distributions, which typically have a  $p$ -like structure for low intensities, have a characteristic 3-lobed shape in intense fields. Furthermore, in the nondipole regime, the ionization is likely to occur antiparallel with the laser propagation direction, which is opposite to what is predicted in intense low-frequency fields [6]. Supported by classical calculations we develop a model that explains the emergence of the unique extra lobe in the angular distributions.

The nonrelativistic dynamics of atoms interacting with a classical electromagnetic field is governed by the time-dependent Schrödinger equation [atomic units (a.u.),  $m_e = e = \hbar = a_0 = 1$  are used throughout],  $i\partial_t\Psi(\mathbf{r},t) = [\frac{1}{2}(\mathbf{p} + \mathbf{A})^2 + V(\mathbf{r})]\Psi(\mathbf{r},t)$ , with the vector potential  $\mathbf{A}(\eta)$ ,  $\eta = \omega t - \mathbf{k} \cdot \mathbf{r}$  and potential  $V$ . We consider a linearly polarized laser pulse with wave vector  $\mathbf{k} = k\hat{z}$ , corresponding to the vector potential

$$\mathbf{A}(\eta) = \frac{E_0}{\omega} f(\eta) \sin(\eta + \phi) \hat{x}, \quad (1)$$

with  $E_0$  the electric field amplitude,  $\omega$  the laser frequency,  $f(\eta)$  the laser pulse envelope,  $\phi$  the carrier-envelope phase, and  $\hat{x}$  the polarization direction.

The Kramers-Henneberger (KH) form of the light-atom interaction Hamiltonian is useful for numerical ionization studies of atoms in intense, high-frequency fields. We apply the nondipole KH transformation [3, 7],  $\Psi_{KH} = \exp(i\alpha \cdot \mathbf{p})\Psi$ , to the wave function and impose the Coulomb gauge restriction  $\nabla \cdot \mathbf{A} = 0$  on the field. The vector  $\alpha(\eta) \equiv \frac{1}{\omega} \int_{\eta_i}^{\eta} d\eta' \mathbf{A}(\eta')$  represents the position relative to the laboratory frame of a classical free electron in the field. The transformation results in the Hamiltonian [3]

$$H_{KH} = \frac{1}{2}\mathbf{p}^2 + \frac{1}{2}A^2 + V(\mathbf{r} + \alpha) + \frac{1}{2c^2}(\mathbf{A} \cdot \mathbf{p})^2 - \frac{i}{2c^2} \mathbf{E} \cdot \mathbf{p} + \frac{1}{c}(\mathbf{A} \cdot \mathbf{p})(\hat{z} \cdot \mathbf{p}), \quad (2)$$

where  $\mathbf{E} = -\partial_t \mathbf{A}$  is the electric field. The last three terms stem from the transformation of the kinetic energy operator and are of relativistic order and vanish in the dipole approximation. The last two oscillate with alternating sign and are expected to have a negligible effect on the electron dynamics. The first is quadratic in  $A$  and  $p$  and hence always positive, but nevertheless we also expect the effect of this term to be small: it plays the role of a kinetic energy operator in the dynamics and is less than a factor  $E_0^2/(\omega^2 c^2)$  as important as the ordinary  $p^2$  operator in (2). Furthermore, for very high intensities the electron essentially follows the motion of a free electron in the field, which, within the KH frame of reference, means that the momentum distribution of the electronic wave packet is strongly centered about zero in the polarization direction. Therefore (2) can be approximated by

$$H_{KH} = \frac{1}{2}\mathbf{p}^2 + \frac{1}{2}A^2(\eta) + V(\mathbf{r} + \alpha(\eta)), \quad (3)$$

which is valid provided  $E_0^2/(\omega^2 c^2) \ll 1$ , i.e., in the nonrelativistic case. We confirmed the validity of (3) for three different laser frequencies,  $\omega = 0.5, 1$ , and  $2$  a.u., by numerical integration of the time-dependent Schrödinger equation for 5 periods of the field with and without the last three terms of (2). The overlaps of the wave functions were more than 99 %, for field strengths up to  $E_0 = 10, 30$ , and  $100$  a.u., respectively, for the three frequencies. The spatial dependence of  $\alpha$  was also examined, and we confirmed that for the present field parameters all nondipole effects are, in effect, incorporated via the  $A^2$  term. Accordingly, we apply the Hamiltonian (3) in our

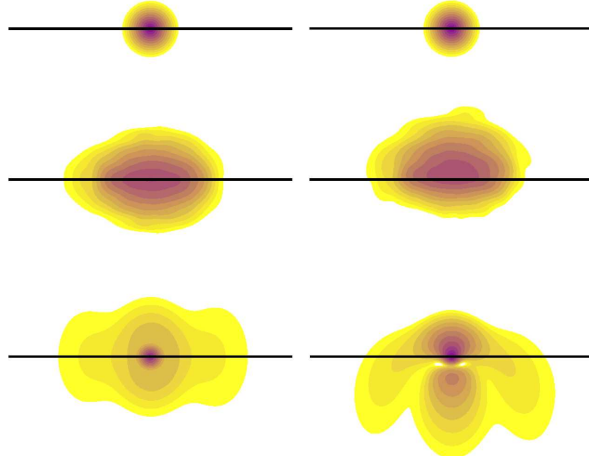


FIG. 1: (Color online). Dipole (left) and nondipole (right) probability densities of the KH wave function in the  $x - z$  plane for a  $\hat{x}$ -polarized, 10-cycle pulse propagating in the positive  $z$  direction (upward), with  $E_0 = 30$  a.u.,  $\omega = 2$  a.u. and  $\phi = 0$ . The snapshots are taken at  $t = 0$ ,  $t = T/2$ , and  $t = T + 25.1$  a.u. with  $T = 31.4$  a.u.. The length of the horizontal line corresponds to 50 a.u.. The scale is logarithmic with four contours per decade.

present study of the nondipole ionization dynamics of H, with focus on the angular distribution of the photoelectron. The ground state is exposed to a 3–15–cycle laser pulse of the form (1) with  $f(\eta) = \sin^2\left(\frac{\pi\eta}{\omega T}\right)$ , and central frequency  $\omega = 2$  a.u. (23 nm), i.e., pulse durations between 228 and 1140 attoseconds. For the frequency considered here, nondipole effects become important when the electric field strength exceeds 20 a.u. [3, 8].

Figure 1 shows a typical example of the probability density distribution of the wave function in the dipole and nondipole descriptions. The snapshots are taken before the pulse, in the middle of the pulse, and at 25 a.u. after the end of the pulse. The displacement in the nondipole case of the wave packet in the propagation direction during the pulse is a manifestation of the classical "figure-eight" motion of a free electron in the nondipole field. This motion is composed of a velocity component in the propagation direction, superimposed on the ordinary wiggle motion along the laser polarization direction. The drift in the propagation direction can be associated with the action of the magnetic field on the quivering electron. To see this, consider the Lorentz forces on a free electron in the electromagnetic field. To lowest order in  $z/c$  the magnetic force acting along the propagation direction becomes  $F_z(t) = -A_x(t)E_x(t)/c$ . Then, for an electron that is initially at rest the velocity in this direction is  $v_z(t) = A_x^2(t)/(2c)$ , which is indeed never negative. For this reason, one might expect that the ionized electron has a velocity component along the positive  $z$  axis after the pulse has

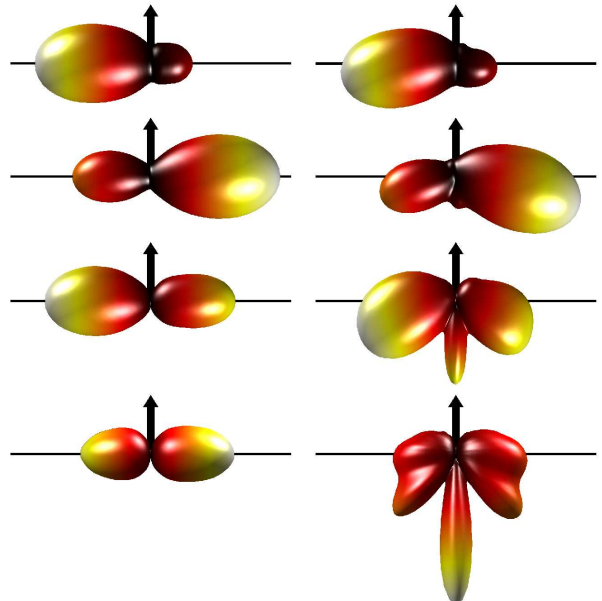


FIG. 2: (Color online). Dipole (left) and nondipole (right) electron angular distributions for a 3- (upper), 5- (second), 10- (third), and 15-cycle pulse (lower panel) linearly polarized in the horizontal direction, with  $\omega = 2$  a.u.,  $E_0 = 30$  a.u. and  $\phi = 0$ . The propagation direction, marked with an arrow, is along the positive  $z$  axis. In all cases the total ionization probability lies between 0.4 and 0.5, and the ratios of probability of ionization between the nondipole and dipole cases are 1.00, 1.06, 1.17, and 1.16 for the four different pulses.

passed. This is, however, not necessarily the case since  $v_z = 0$  at the end of the pulse. In fact, the electron is most likely ejected oppositely to the propagation direction. The last snapshot in Fig. 1 clearly shows this trend. The up/down asymmetry follows from the interplay between the electromagnetic and Coulombic forces during the pulse. The electromagnetic forces alone do not change the electron momentum along the propagation direction at the end of the pulse, since  $v_z(T) = 0$ . On the other hand, the net effect of the Coulomb forces on the polarized charge cloud is a momentum component along the negative  $z$  axis: the electron, which is most probably situated in the upper hemisphere during the pulse, gets a momentum kick in the negative  $z$  direction each time it passes close to the nucleus.

To clarify this point further, we have plotted the dipole and nondipole angular distributions of the continuum electron in Fig. 2. The data are taken for  $E_0 = 30$  a.u. and pulses with 3, 5, 10 and 15 cycles, respectively. The horizontal axis ( $x$  axis) indicates the laser polarization direction, and the pulse propagates in the positive  $z$  direction (upwards). The left/right asymmetry in the angular distributions reveals that the dynamics is strongly nonadiabatic even for the longest pulse considered here. This means that the shape of the distributions is sensitive to the value of the carrier-envelope phase,  $\phi$ . The data in Fig. 2 were obtained for  $\phi = 0$ . Figure 3 shows similar spectra for a 5-cycle pulse with  $E_0 = 20, 30$  and 45 a.u., respec-

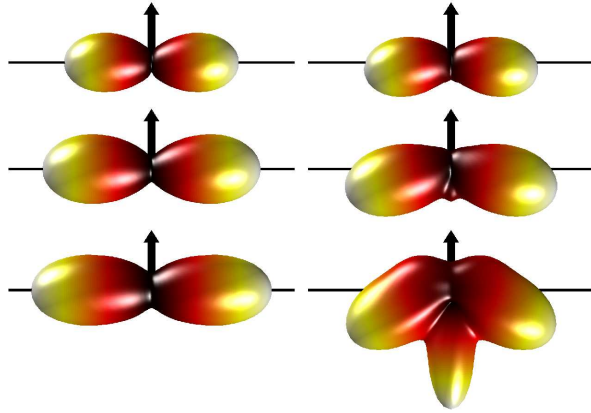


FIG. 3: (Color online). As Fig. 2, but for a 5-cycle pulse and for three different field strengths,  $E_0 = 20$  (upper),  $E_0 = 30$  (middle) and  $E_0 = 45$  a.u. (lower panel). The data are averaged over the carrier-envelope phase. The total ionization probability is between 0.41 and 0.63, and the ratios of probability of ionization between the nondipole and dipole cases are 1.01, 1.06, and 1.20 for the three different pulses.

tively, but here the data are averaged over the phase  $\phi$ . Both the distributions in Figs. 2 and 3 confirm the features exhibited in Fig. 1. The differential spectra are indeed bent downwards in the nondipole regime, i.e., in the direction opposite to the laser propagation direction. The more intense the pulse, the greater the degree of deflection. In one-photon ionization, this bending of the  $p$ -like distribution (see Fig. 2) is a well-known consequence of the nondipole terms proportional to  $\mathbf{k} \cdot \mathbf{r}$ . But now the ionization mechanism is completely different: the electron is mainly released into the continuum due to a nonadiabatic adjustment to the time-averaged KH potential,  $V_0(\alpha_0; \mathbf{r}) = 1/T \int_0^T V(\mathbf{r} + \alpha) dt$  [3], where  $\alpha_0 \equiv E_0/\omega^2$  is the quiver amplitude. Also, this very different ionization mechanism leads to a new strong-field and nondipole feature, that is manifested by a characteristic 3-lobed shape of the angular distributions. The third lobe in the direction antiparallel to the propagation direction is not present in the weak-field nondipole regime [9], neither is it present in the dipole limit of strong-field ionization. The extra lobe becomes most distinct for the longest and most intense pulses. For  $E_0 = 30$  a.u. it is not visible for the 3-cycle pulse, whereas it is prominent for the 10 and 15-cycle pulses. Furthermore, for the case of a 5-cycle pulse it becomes important for  $E_0 > 30$  a.u.. The 3-lobe structure is present for any value of the carrier-envelope phase, but the relative size of the two side-lobes can vary a lot for different choices of  $\phi$ .

In order to get a deeper insight into the physical processes governing the observed features, we have performed a classical trajectory Monte Carlo analysis of the problem. The classical angular distributions were obtained from the solutions of the Newtonian equations of motion for a large number ( $\sim 100\,000$ ) of individual electron trajectories with initial conditions taken from a microcanonical ensemble [10]. Fig-

ure 4 (upper) shows the final angular distribution corresponding to those classical electron orbits that are unbound in the nondipole limit but remain bound within the dipole picture. The figure should be compared with the lower right figure in Fig. 3. The 1-lobed shape of the distribution is striking. Hence, the classical calculation reveals that the fraction of the wave packet that remains bound within the dipole approximation but is ionized in the nondipole regime contributes to the creation of a third lobe in the spectra.

Both the deflection of the two side-lobes and the creation of a new lobe in the angular distributions can in fact be attributed to the very same physical process which is of purely classical origin. In the nondipole regime the intensity of the laser is so high that the electron essentially follows the motion of a classical free electron in the field. However, the electron will accumulate momentum from a series of Coulomb scattering events during the pulse. The momentum kicks imparted to the electron from these events may eventually lead to ionization. Although the electron receives momentum kicks both in the dipole and nondipole cases there is one important difference in the nondipole situation: because of the "figure-eight" motion, the electron's orbit is displaced in the propagation direction during the laser pulse, and a classical electron will typically spend more time in the upper hemisphere than in the lower hemisphere. The average effect of the Coulomb forces on the electronic motion in the up/down direction are, accordingly, a net momentum transfer to the electron in the direction opposite to the propagation direction. This explains the up/down asymmetry of the angular distributions in the nondipole regime.

Orbits that contribute to the extra lobe in the angular distributions have one thing in common: they are ionized as a result of an intimate interplay between magnetic, electric and Coulomb forces during the pulse. Due to the magnetic drift motion, the ionizing trajectories very early become confined to the upper hemisphere and the electron will remain there until the end of the pulse, even though it receives momentum kicks in the opposite direction from successive encounters with the nucleus. However, at the end of the pulse, when the magnetic drift motion ceases, the electron is left with a velocity component along the negative  $z$  direction. It is this momentum component, which roughly equals the algebraic sum of all such momentum kicks imparted to the electron during the pulse, that finally enables the electron to escape. The creation of the third lobe and the dependence of the 3-lobed structure on the pulse duration (see Fig. 3) is understood accordingly. In Fig. 4 (middle and lower panels) we follow one of the single classical trajectories that contributes to the third lobe in the angular distributions in the nondipole case. The differences between the nondipole (middle panel) and the dipole (lower panel) are striking. Within the dipole approximation the electron is transferred to an excited closed orbit by the electric field, whereas the electron is ionized when the spatial dependence of the field is included. This particular example illuminates essentially all the fundamental aspects of the dynamics, i.e., the "figure-eight" motion, the drift motion

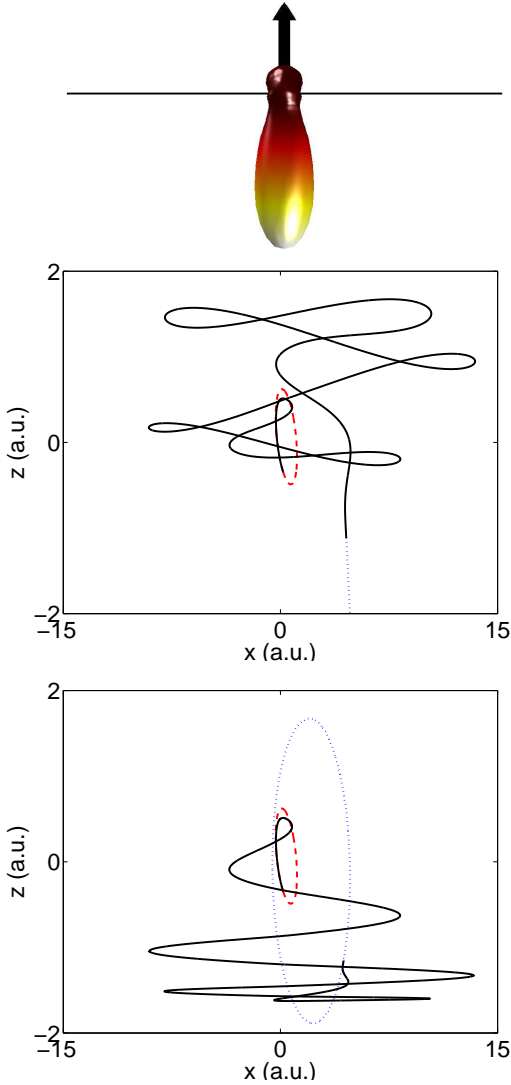


FIG. 4: (Color online). Upper panel: Classical angular distribution corresponding to those classical trajectories that remain closed orbits within the dipole approximation but are unbound in the nondipole description. The data, which are averaged over the carrier-envelope phase  $\phi$ , are taken for a 5-cycle pulse with  $E_0 = 45$  a.u. and  $\omega = 2$  a.u.. Middle panel: A single classical trajectory that contributes to the third lobe in angular distribution. Lower panel: The same trajectory in the dipole approximation. The dashed (red) and dotted (blue) curves indicate the initial and final orbits, respectively, and the full curve (black) shows the trajectories during the pulse. The linear polarization is along the  $x$  axis and the pulse propagates in the positive  $z$  direction.

and the quivering motion of the electron.

In contrast to the present dynamics, optical laser frequencies cannot be expected to produce the same 3rd lobe for two reasons. First, the excursion is in this case so large that the intimate interplay between the magnetic and the nuclear force will be much less pronounced. Second, for low-frequency fields the substantial ionization occurs in a fraction of or af-

ter only a few optical cycles, so that the "3-lobe ionization mechanism", which is a relatively slow process in the sense that it needs several cycles to be efficient, becomes much less important. In addition, in the stabilization regime the ionized electron typically has very low kinetic energy and is, therefore, effectively steered by the Coulomb kicks imparted to it. We remark, however, that the ionization mechanism that is responsible for the 3rd lobe also is present for lower frequencies, but that its relative importance very rapidly decreases as the frequency is decreased. Although the effect is strongly suppressed in the ionization of H(1s), it should in principle be possible to measure the 3rd lobe in weakly bound systems with optical laser frequencies, but now the additional nondipole effect, due to the extended size of the system compared to the central pulse wavelength, may become important [11].

In conclusion, we obtained the first angular distributions for the photoelectron in the ionization of H(1s) in super-intense, high-frequency, attosecond pulses. Our treatment went beyond the dipole approximation, and we identified a unique signature for the onset of nondipole effects in the spectra. We showed that the common 2-lobed shape of the angular distributions in the dipole regime develops gradually into a deflected 3-lobed shape in the high-frequency nondipole regime. A detailed classical analysis of the spectra revealed the classical nature of the underlying dynamics.

The present research was supported by the Norwegian Research Council through the NANOMAT program, the Nordic Research Board NordForsk, the Danish Natural Science Research Council, and the Danish Research Agency.

- [1] R. Kienberger *et al.*, *Nature (London)* **427**, 817 (2004); A. Scrinzi, M. Yu. Ivanov, R. Kienberger, and D. M. Villeneuve, *J. Phys. B* **39**, R1 (2006).
- [2] See, e.g., M. Gavrila, *J. Phys. B* **35**, R147 (2002); A. M. Popov, O. V. Tikhonova, and E. A. Volkova, *J. Phys. B* **36**, R125 (2003).
- [3] M. Førre, S. Selstø, J. P. Hansen, and L. B. Madsen, *Phys. Rev. Lett.* **95**, 043601 (2005).
- [4] S. Selstø, M. Førre, J. P. Hansen, and L. B. Madsen, *Phys. Rev. Lett.* **95**, 093002 (2005).
- [5] A. Staudt, C. H. Keitel, and J. S. Briggs, *J. Phys. B* **39**, 633 (2006); A. D. Bandrauk and H. Z. Lu, *Phys. Rev. A* **73**, 013412 (2006).
- [6] Y. I. Salamin, S. X. Hu, K. Z. Hatsagortsyan, and C. H. Keitel, *Phys. Rep.* **427**, 42 (2006).
- [7] W. Pauli and M. Fierz, *Nuovo Cimento* **15**, 167 (1938); H. A. Kramers, *Collected Scientific Papers* (Amsterdam: North-Holland, 1956) p. 866; W. C. Henneberger, *Phys. Rev. Lett.* **21**, 838 (1968).
- [8] N. J. Kylstra *et al.*, *Phys. Rev. Lett.* **85**, 1835 (2000).
- [9] O. Hemmers, R. Guillemin, and D. W. Lindle, *Rad. Phys. Chem.* **70**, 123 (2004).
- [10] J. P. Hansen, J. Lu, L. B. Madsen, and H. M. Nilsen, *Phys. Rev. A* **64**, 033418 (2001); H. M. Nilsen, L. B. Madsen, and J. P. Hansen, *ibid.* **66** 025402 (2002).
- [11] T. Mercouris, Y. Komninos, and C. A. Nicolaides, *J. Phys. B*





# Paper VII

Valentin N. Ostrovsky, Michail V. Volkov, Jan Petter Hansen and Sølve Selstø

## Four-State (Two-Spin) Non-Stationary Models

*Submitted to Physical Review.*



# FOUR-STATE (TWO-SPIN) NON-STATIONARY MODELS

V. N. Ostrovsky,<sup>1</sup> M. V. Volkov,<sup>1</sup> J. P. Hansen,<sup>2</sup> and S. Selstø<sup>2</sup>

<sup>1</sup>*V. Fock Institute of Physics, St. Petersburg State University, 198504 St. Petersburg, Russia*

<sup>2</sup>*Department of Physics and Technology, University of Bergen, N-5007 Bergen, Norway*

Quantum dynamical non-stationary 4-state systems with potential curve crossings are analyzed. Special emphasis is made on the semi-classical description in terms of transition paths that join initial and final states. Exact solutions (when available), approximate approaches and numerical results are considered. It is shown that the Multi-state Landau-Zener theory (MLZ) accounts very well for the time-dependent state populations and final transition probabilities even in cases when multiple crossings appear in close vicinity of each other. This is also true for multiple paths systems when the adiabatic and dynamic phases are accounted appropriately for. It is found that transitions may take place also between diabatic states that do not couple directly and that the dynamics of such crossings may be accurately described within the multichannel Landau-Zener theory.

PACS numbers: 03.65.-w, 75.10.Jm, 32.80.Bx, 34.50.-s

## I. INTRODUCTION

Transitions in composite systems of interacting spins exposed to time-dependent magnetic fields are considered in an immense number of publications. The demagnetization of magnetic molecules and nanomagnets is one of the physical realizations, see, for instance, [1–9]. Mathematically similar problems emerge in the theory of quantum logic operations with very different physical realizations such as ion traps or coupled Josephson junctions [13]. From a more general perspective the matter concerns solving the time-dependent Schrödinger equation in a finite basis of  $N$  states, which is one of generic problems in quantum mechanics.

The dynamics of 4 state (two spin- $\frac{1}{2}$ ) systems was considered in early applications to nuclear magnetic resonance problems, see, e.g. Ref. [14]. They became particularly important as two coupled two-state systems serve as a basic model of entanglement in spin  $\frac{1}{2}$  systems [15]. In the theory of quantum computation such systems are needed to obtain logic quantum gates such as, e.g., the Cnot gate [16]. Their analytic are especially significant with respect to long time dispersion [17] or decoherence which are sources to reduce the efficiency of the quantum processor. Various aspects of two-spin systems were studied intensively, see, e.g., Ref. [10–12, 18].

Very often linear time dependence of the magnetic field is presumed, which links the problem to the well-known two-state Landau-Zener (LZ) model and its multi-state generalizations. For systems of non-interacting spins the non-stationary quantum problem is effectively factorized, which makes the solution simple. The case of interacting spins corresponds to a special realization of the generalized Multi-state Landau-Zener model (MLZ). It is appropriate now to introduce the major notions and concepts of this model which are extensively used in the present paper.

In the MLZ model the  $N \times N$  Hamiltonian matrix has linear dependence on time

$$\mathbf{H}(t) = \mathbf{A} + \mathbf{B}t . \quad (1.1)$$

The basis of states in which this representation holds is called *diabatic basis*. It is presumed to be time-independent. Without loss of generality one can presume that the matrix  $\mathbf{B}$  is diagonal,  $\mathbf{B} = \text{diag}\{\beta_j\}$ . The diagonal and non-diagonal elements of matrix  $\mathbf{A}$  have different status. This is stressed by new notations:  $A_{jj} = \varepsilon_j$ ,  $A_{jk} = V_{jk}$ . The diagonal elements of the  $\mathbf{H}(t)$  matrix,  $\mathcal{E}_j(t) = \beta_j t + \varepsilon_j$ , are known as *diabatic potential curves* and  $V_{jk}$  are *couplings* between the diabatic states  $j$  and  $k$ . The diabatic potential curves form a rectilinear network. One can consider propagation along this network as following diabatic potential curves with hopping from one curve to another at the instances of time when the two curves cross. In this way the propagation path is introduced; it is implied that the propagation proceeds only forward in the time variable. In general several paths join prechosen initial and final states. The contributions are coherent, which implies summation of the amplitudes. In turn, this means interference and oscillations in the state-to-state transition probabilities as the parameters of the problem ( $\varepsilon_j$ , for instance) are varied. Along with such *multi-path* transitions, *single-path* transitions are always present. The obvious examples correspond to survival in the initial diabatic state  $j$  in the case when the latter has extremal (maximum or minimum) slope  $\beta_j$ ; other single-path transitions are also possible.

The description in terms of propagation paths is approximate and has heuristic significance; but it could be easily put in a more quantitative form. Below, in Section III, we provide a brief overview of the two-state Landau-Zener model (Section III A) and then describe how it is generalized and applied to systems of many states in the MLZ model (Section III B).

*Exact* solutions of the  $N$ -state MLZ model has been obtained for some special cases: the SO(3) model [19], the Demkov-Osherov model [20], the bow-tie model [21] and its generalization [22]. Among numerical studies of three- and four-state models we indicate Refs. [23, 24].

The objective of this paper is to analyze the relation between four-state models that allow exact analytical solution and the cases when such solutions are not available and apparently do not exist. The important issue here is the distinction between single-path and multiple-path transitions. In most cases when exact solutions exist they describe single-path transitions although some exceptions are known. On the other hand, not all single-path models allow exact solution. We reveal the reason for this by demonstrating that the single-path property is not absolute because analytical continuation over model parameters may link single-path and multiple-path models.

In Section II we start with formulating the theory of two spin  $\frac{1}{2}$ -particles in separate magnetic fields, at first for noninteracting particles (Section II A) and then with allowance for interaction in some restricted form (Section II B). The MLZ theory of Section III is applied to the two-spin model in Section IV; the results are compared with direct numerical solutions of the Schrödinger equation. Single- and multi-path transitions and exactly solvable four-state models are considered. Another object of interest is the case of second-order interaction, i.e. when potential curves  $i$  and  $j$  cross, but direct coupling is absent ( $V_{ij} = 0$ ). Some mathematical derivations are provided in Appendix A. The conclusions are drawn in Section V. Atomic units ( $\hbar = e = m_e = 1$ ) are used throughout.

## II. FOUR-STATE MODEL OF TWO SPIN- $\frac{1}{2}$ PARTICLES

### A. Model of non-interacting spins

We start by considering a simple case of a system of two non-interacting spins. To a significant extent we follow the ideas suggested originally by Majorana [25] and Hioe [19] and recently reformulated by Sinitzyn [26]. However, our context is somewhat different.

Consider a particle  $a$  with spin  $s_a = 1/2$  in a time-dependent magnetic field  $\mathbf{B}(t)$ . The two-state matrix Hamiltonian is

$$\mathbf{H}_a(t) = \frac{1}{2} \mathbf{B}(t) \cdot \mathbf{s}_a = \frac{1}{2} \begin{pmatrix} B_z(t) & B_x(t) + iB_y(t) \\ B_x(t) - iB_y(t) & -B_z(t) \end{pmatrix}. \quad (2.1)$$

We re-parameterize this Hamiltonian in an apparently general form

$$\mathbf{H}_a(t) = \begin{pmatrix} E_{1a}(t) & V_a(t) \\ V_a^*(t) & E_{2a}(t) \end{pmatrix}, \quad (2.2)$$

where  $E_{1a}(t)$ ,  $E_{2a}(t)$ ,  $V_a(t)$  are some functions of time.

Consider now the system consisting of two particles  $a$  and  $b$  with spin  $\frac{1}{2}$  and denote the spin operators as  $\mathbf{s}_a$  and  $\mathbf{s}_b$ . The one-particle basis states are

$$|\alpha_j\rangle = \begin{pmatrix} 1 \\ 0 \end{pmatrix}, \quad |\beta_j\rangle = \begin{pmatrix} 0 \\ 1 \end{pmatrix}, \quad (2.3)$$

where subscript  $j = a, b$  labels the particles. Assume that the second particle interacts with a magnetic field which generally *differs* from the magnetic field acting on the first particle. The interaction Hamiltonian  $\mathbf{H}_b(t)$  is parameterized similarly to  $\mathbf{H}_a(t)$ , Eq. (2.2):

$$\mathbf{H}_b(t) = \begin{pmatrix} E_{1b}(t) & V_b(t) \\ V_b^*(t) & E_{2b}(t) \end{pmatrix}. \quad (2.4)$$

Suppose at first that there are no interaction between the particles. Then the Hamiltonian of the two-particle system is  $H(t) = H_a(t) \oplus H_b(t)$ . It is operative on the two-particle states. The two-particle basis states are obtained as products of one-particle basis states; we label them as

$$\begin{aligned} |1\rangle &= |\alpha_a\rangle |\alpha_b\rangle, & |2\rangle &= |\alpha_a\rangle |\beta_b\rangle, \\ |3\rangle &= |\beta_a\rangle |\alpha_b\rangle, & |4\rangle &= |\beta_a\rangle |\beta_b\rangle. \end{aligned} \quad (2.5)$$

In this basis the matrix of the two-particle Hamiltonian is

$$\mathbf{H}(t) = \begin{pmatrix} E_{1a} + E_{1b} & V_b & V_a & 0 \\ V_b^* & E_{1a} + E_{2b} & 0 & V_a \\ V_a^* & 0 & E_{2a} + E_{1b} & V_b \\ 0 & V_a^* & V_b^* & E_{2a} + E_{2b} \end{pmatrix}, \quad (2.6)$$

where time-dependence is implicit in the right hand side. Since each particle is subject to its own magnetic field  $\mathbf{B}^{(a)}(t)$  and  $\mathbf{B}^{(b)}(t)$ , the total spin  $S$  and its projection  $S_z$  ( $\mathbf{S} = \mathbf{s}_a + \mathbf{s}_b$ ) are not integrals of motion, in distinction to the commonly met case in which both magnetic fields are identical. The relations between  $V_i$ ,  $\mathcal{E}_{ij}$  and  $\mathbf{B}^{(a)}(t)$ ,  $\mathbf{B}^{(b)}(t)$  reads

$$\begin{aligned} V_a &= \frac{1}{2} \left( B_x^{(a)} + i B_y^{(a)} \right), & E_{1a} = -E_{2a} &= \frac{1}{2} B_z^{(a)}, \\ V_b &= \frac{1}{2} \left( B_x^{(b)} + i B_y^{(b)} \right), & E_{1b} = -E_{2b} &= \frac{1}{2} B_z^{(b)}. \end{aligned} \quad (2.7)$$

The diagonal elements of the matrix  $H$ , Eq. (2.6), satisfy the condition

$$H_{11} - H_{22} = H_{33} - H_{44}. \quad (2.8)$$

This implies that by a simple common phase transformation one can always achieve  $H_{11} = -H_{44}$ ,  $H_{22} = -H_{33}$ .

One possible physical realization of the situation of different fields appears for a hydrogen Rydberg atom treated within the pseudo-spin approach, see, e.g., [27][28]. A dynamical problem emerges when such an atom is subject to external (generally time-dependent) electric and magnetic fields. Linear combinations of these fields can be equivalently considered as two different effective magnetic fields (it is presumed here that the fields are treated in the linear approximation). The role of the spin of the total system is played by the atom orbital momentum  $\mathbf{L}$ . This magnitude is generally not conserved under combined action of the fields.

Another realization of a four-state system emerges in the theory of two coupled superconducting flux qubits. The structure of the Hamiltonian provided in [13] is similar to Eq. (2.6) although condition Eq. (2.8) is not satisfied.

The matrix  $\mathbf{H}$  has zeroes on the *cross-diagonal*, which goes via elements  $\{1, 4\}$ ,  $\{2, 3\}$ ,  $\{3, 2\}$  and  $\{4, 1\}$ . The matrix is symmetrical under reflection in the cross diagonal. This is due to the fact that the two spins are not coupled to each other, so that there is no interaction responsible for simultaneous spin flip. The presence of terms bilinear in components of  $\mathbf{s}_a$  and  $\mathbf{s}_b$  in the Hamiltonian would in general eliminate these special properties of the  $\mathbf{H}$  matrix.

When both magnetic fields coincide, the following relations hold:  $E_{1a} = E_{1b}$ ,  $E_{2a} = E_{2b}$ ,  $V_a = V_b$ , and the total spin  $\mathbf{S} = \mathbf{s}_a + \mathbf{s}_b$  is integral of motion. Therefore the four-dimensional Hilbert space with the basis Eq. (2.5) is split into two invariant subspaces: a one-dimensional subspace corresponding to  $S = 0$  and a three-dimensional subspace with  $S = 1$ . All this is embedded into well-known SO(3) model ascending to Majorana [19, 25]. If different magnetic field acts on each of the two particles, we obtain what could be named *generalized SO(3) model*. In the latter, the total spin  $S$  is not integral of motion. In fact such a generalized SO(3) model was considered by Sinitzyn [26] in the context of condensed matter physics.

If we know the one-particle time-propagators  $U_a(t, t')$  and  $U_b(t, t')$ , the two-particle propagator is straightforwardly obtained as  $U_a(t, t') \otimes U_b(t, t')$ . In particular, if we know the probabilities of non-adiabatic transitions (or spin-flips)  $p_a$ ,  $p_b$  (i. e. probabilities of diabatic evolution), the related probabilities of adiabatic development are  $q_a = 1 - p_a$ ,  $q_b = 1 - p_b$ . Then the probabilities  $P_{ij}$  of transitions from  $i$ th to  $j$ th two-particle basis states comprise to a  $4 \times 4$  matrix [26]:

$$\mathbf{P} = \begin{pmatrix} p_a p_b & p_a q_b & q_a p_b & q_a q_b \\ p_a q_b & p_a p_b & q_a q_b & q_a p_b \\ q_a p_b & q_a q_b & p_a p_b & p_a q_b \\ q_a q_b & q_a p_b & p_a q_b & p_a p_b \end{pmatrix}. \quad (2.9)$$

The element  $P_{jk}$  gives probability of transition from the initial state  $j$  to the final state  $k$ . Note that this matrix is symmetrical not only with respect to its principal diagonal, but also with respect to its cross-diagonal.

## B. Model of two interacting spins

Now we turn to a model of spins that interact with the external fields and with each other, albeit the latter interaction is not of the most general form.

Non-zero elements on the cross-diagonal of matrix  $H$  are obtained if one includes the bilinear terms  $s_{a+} s_{b-} + s_{a-} s_{b+}$  where we use the standard definitions  $s_{a\pm} = s_{ax} \pm i s_{ay}$ ,  $s_{b\pm} = s_{bx} \pm i s_{by}$ . Such terms lead to simultaneous flip of both the spins. In the following we will not consider such terms, but allow for bilinear terms of the form

$$W_{\text{int}} = 4(c_1 s_{az} s_{bx} + c_2 s_{az} s_{by} + c_3 s_{bz} s_{ax} + c_4 s_{bz} s_{ay} + b s_{az} s_{bz}), \quad (2.10)$$

with some coefficients  $c_j$ . In the basis Eq. (2.5) the matrix of this interaction reads

$$\mathbf{W}_{\text{int}} = \begin{pmatrix} b & c_1 - ic_2 & c_3 - ic_4 & 0 \\ c_1 + ic_2 & -b & 0 & -c_3 + ic_4 \\ c_3 + ic_4 & 0 & -b & -c_1 + ic_2 \\ 0 & -c_3 - ic_4 & -c_1 - ic_2 & b \end{pmatrix}. \quad (2.11)$$

This leads to the *generalized four-state model* with the Hamiltonian [29]

$$\mathbf{H}_g(t) = \begin{pmatrix} \tilde{\mathcal{E}}_1(t) & V_{12} & V_{13} & 0 \\ V_{12}^* & \tilde{\mathcal{E}}_2(t) & 0 & V_{24} \\ V_{13}^* & 0 & \tilde{\mathcal{E}}_3(t) & V_{34} \\ 0 & V_{24}^* & V_{34}^* & \tilde{\mathcal{E}}_4(t) \end{pmatrix} \quad (2.12)$$

with the following relations between  $V_{ij}$ ,  $V_i$  and  $c_i$ :

$$\begin{aligned} V_{12} &= V_b + c_1 - ic_2, & V_{13} &= V_a - c_3 + ic_4, \\ V_{24} &= V_a + c_3 - ic_4, & V_{34} &= V_b - c_1 + ic_2, \\ \tilde{\mathcal{E}}_1(t) &= \mathcal{E}_1(t) + b, & \tilde{\mathcal{E}}_2(t) &= \mathcal{E}_2(t) - b, \\ \tilde{\mathcal{E}}_3(t) &= \mathcal{E}_3(t) - b, & \tilde{\mathcal{E}}_4(t) &= \mathcal{E}_4(t) + b. \end{aligned} \quad (2.13)$$

Compared to the Hamiltonian Eq. (2.6),  $\mathbf{H}_g$  retains zeroes on the cross-diagonal, albeit the symmetry with respect to it is lifted.

### III. GENERAL LANDAU-ZENER THEORY

For multi-state systems featuring crossing *diabatic* potential curves, the generic case is the situation of pairwise crossing when only two curves cross at a time. In the *adiabatic* representation one has to consider the instantaneous eigenvalues  $\epsilon_j(t)$  of the Hamiltonian  $\mathbf{H}(t)$ , which depends parametrically on time. It is well known from the Neumann-Wigner theorem that crossing of diabatic potential curves correspond to pseudo-crossings (or avoided crossings) of *adiabatic potential curves*  $\epsilon_j(t)$ . Exceptions to this generic correspondence may occur for special sparse structures of Hamiltonian when adiabatic curves cross.

The LZ model provides a very attractive way of finding the probability of transitions between the two states involved in a pairwise crossing. Furthermore, the amplitudes of the crossing states are subject to a phase-shift, which is also known analytically in the LZ case. If we assume that the dynamics in the vicinity of a crossing, or rather an avoided crossing, only involves the two (almost) crossing states, these expressions may, in principle, be used to estimate the dynamics of any system of arbitrary number of states with arbitrary number of crossings. Such ideas are used in quasi-molecular theory of atomic collisions, see, e.g., [30]. In the following, we will briefly outline this theory and also elaborate on the validity of the approach employed.

The presence of several paths gives raise to interference effects. The importance of one path compared to the others is governed not only by the transition probabilities, but also the phase differences between the relevant states. These phases may be divided into three categories: the adiabatic phase  $\int^t \epsilon_j(t') dt'$ , the instantaneous (Stokes) phase shift experienced at each crossing and finally signs arising from "book keeping" arguments. All of these are crucial, and must be considered carefully.

In outlining the theory, it is useful to define the relevant concepts and parameters of the LZ model in its original two state form.

#### A. The two state Landau-Zener case

Within some diabatic basis  $\mathcal{B}_D = \{|1\rangle, |2\rangle\}$ , the Hamiltonian may be expressed as

$$H_D = \begin{pmatrix} -\frac{1}{2}bt & V \\ V^* & \frac{1}{2}bt \end{pmatrix}, \quad (3.1)$$

where the constant  $b$  is the difference in the slopes of the diagonal energies of state 1 and 2, and the coupling  $V$  is assumed to be constant and real. We label the diabatic diagonal energies (potential curves) as  $\mathcal{E}_{1,2} = \mp \frac{1}{2}bt$ . For a

spin  $\frac{1}{2}$ -particle in a magnetic field, this situation may be realized with  $B_z = -bt$ ,  $B_x = V$  and  $B_y = 0$ , referring to Eq. (2.2). In this form the problem was solved by Majorana [25] in the same year as by Landau [31], Zener [32] and Stueckelberg [33]. A comparative discussion of physical motivations and the technical treatments used was provided recently by Di Giacomo and Nikitin [34]. However, the author's claim that "the Majorana name is never mentioned in connection with formula" (3.10) is an exaggeration; some of counter-examples are given by Refs. [21, 22, 35, 36].

The adiabatic basis  $\mathcal{B}_A = \{|\chi_1\rangle, |\chi_2\rangle\}$  is defined by the eigenvectors of the matrix Eq. (3.1). We order them corresponding to increasing energy, and choose the signs such that

$$\begin{aligned} |\chi_1\rangle &\equiv C \left\{ \left( bt/2 + \sqrt{(bt/2)^2 + V^2} \right) |1\rangle - V |2\rangle \right\}, \\ |\chi_2\rangle &\equiv C \left\{ V |1\rangle + \left( bt/2 + \sqrt{(bt/2)^2 + V^2} \right) |2\rangle \right\}, \end{aligned} \quad (3.2)$$

where  $C$  is a positive normalization factor. Note that the signs of the coefficients  $\langle 2|\chi_1\rangle$  and  $\langle 1|\chi_2\rangle$  depend on the sign of the coupling  $V$ , whereas the other ones,  $\langle 1|\chi_1\rangle$  and  $\langle 2|\chi_2\rangle$ , are always positive.

The Hamiltonian  $H_D$ , Eq. (3.1), being transformed to the adiabatic basis, becomes a diagonal matrix. The diabatic basis states are considered as time-independent, while time-dependence of the adiabatic states (3.2) generates coupling through the matrix element  $\langle \chi_1|(d/dt)|\chi_2\rangle$ . The effective Hamiltonian in the adiabatic basis reads:

$$H_A = \begin{pmatrix} -\sqrt{(bt/2)^2 + V^2} & i \frac{bV}{b^2 t^2 + 4V^2} \\ -i \frac{bV}{b^2 t^2 + 4V^2} & \sqrt{(bt/2)^2 + V^2} \end{pmatrix}. \quad (3.3)$$

The adiabatic diagonal energies (potential curves),

$$\epsilon_j = \mp \sqrt{(bt/2)^2 + V^2}, \quad (3.4)$$

coincide with the diabatic ones in the limit  $|t| \rightarrow \infty$ . At the instant when the diabatic curves cross, the splitting of the adiabatic ones gives the magnitude of the coupling:

$$\Delta\epsilon(t=0) = 2|V|. \quad (3.5)$$

From the above expressions of the effective Hamiltonian matrices in the two bases, Eqs. (3.1) and (3.3), it is evident that the adiabatic basis is more stable in the sense that the state-to-state couplings are localized in time. The coupling has a Lorentzian shape in this basis, whereas it is constant in the diabatic one. We may estimate the length of the time interval in which transitions take place in the adiabatic basis as the width of the Lorentzian in Eq. (3.3) at 1/10 of its maximal value. We label this time  $\tau$ , and define it by  $1/(b^2\tau^2 + 4V^2) = \frac{1}{10} \cdot 1/(4V^2)$ , which gives

$$\tau = 6 \left| \frac{V}{b} \right|. \quad (3.6)$$

In the adiabatic basis we are able to describe the dynamics through propagators in the form of  $2 \times 2$  matrices:

$$\mathbf{c}(t_f) = J(t_f, 0) S J(0, t_i) \mathbf{c}(t_i), \quad (3.7)$$

where  $\mathbf{c}(t) = (c_1, c_2)^T$  is defined by  $|\Psi(t)\rangle = c_1(t)|\chi_1(t)\rangle + c_2(t)|\chi_2(t)\rangle$ . The initial and final times,  $t_i$  and  $t_f$ , are to be chosen well separated from the crossing.

Intuitively, we may think of the system as undergoing an instantaneous transition at the time the diabatic potential curves cross ( $t = 0$ ). Before and after the crossing, the only time-evolution is the one corresponding to the adiabatic phase, given by the  $J$ -matrices:

$$J(t_2, t_1) \equiv \text{diag} \left\{ \int_{t_1}^{t_2} \epsilon_1(t') dt', \int_{t_1}^{t_2} \epsilon_2(t') dt' \right\}. \quad (3.8)$$

The "instantaneous" transition matrix  $S$  reads

$$S^{(\pm)} = \begin{pmatrix} \sqrt{1-p} e^{i\alpha} & \pm \sqrt{p} \\ \mp \sqrt{p} & \sqrt{1-p} e^{-i\alpha} \end{pmatrix}, \quad (3.9)$$

where  $p$  is the probability of a non-adiabatic transition [25, 30–33],

$$p \equiv \exp(-2\pi\delta), \quad \delta \equiv V^2/|b|, \quad (3.10)$$

and  $\alpha$  is the Stokes (instantaneous) phase [30]:

$$\alpha \equiv \frac{1}{4}\pi + \delta(\ln \delta - 1) - \arg[\Gamma(1 + i\delta)] . \quad (3.11)$$

The sign in Eq. (3.9) is far from arbitrary; care must be taken when choosing the right expression. When both the parameters  $b$  and  $V$  are positive,  $S^{(+)}$  applies. By considering the expressions of the adiabatic basis vectors, Eq. (3.2), and the form of the Schrödinger equation in the diabatic basis, Eq. (3.1), we find that when the product  $bV$  is positive, one should use  $S^{(+)}$ , and  $S^{(-)}$  is to be used when  $bV$  is negative.

The picture is complicated further when multi-path transitions are operative. In this case it may not be possible to insist on our adiabatic basis to follow the same sign convention as in Eq. (3.2) in all (avoided) crossings; we must make sure that our basis vectors are continuous in time. One is easily convinced that when one – and only one – of the basis vectors differ from Eq. (3.2), the  $S$ -matrix must be transposed.

In summary,  $S^{(+)}$  applies when the product  $bV$  is positive and both basis vectors have the same sign relative to Eq. (3.2) or when  $bV$  is negative and one of the basis vectors differs by a sign. If this is not the situation,  $S^{(-)}$  applies.

## B. The multi state Landau-Zener case

The expression Eq. (3.7) is easily generalized to a system of more than two states with more than one crossing. Suppose a system of  $N$  states is subject to  $m$  crossings:

$$\begin{pmatrix} c_1(t_f) \\ c_2(t_f) \\ \vdots \\ c_N(t_f) \end{pmatrix} = J(t_f, t_m) S_m J(t_m, t_{m-1}) S_{m-1} \cdots J(t_3, t_2) S_2 J(t_2, t_1) S_1 J(t_1, t_i) \begin{pmatrix} c_1(t_i) \\ c_2(t_i) \\ \vdots \\ c_N(t_i) \end{pmatrix} \quad (3.12)$$

with

$$t_i \leq t_1 \leq t_2 \leq \dots t_{m-1} \leq t_m \leq t_f . \quad (3.13)$$

The  $S$ -matrices are constructed by inserting the elements of the  $2 \times 2$  matrix Eq. (3.9) in the entries corresponding to the adiabatic states involved in the avoided crossing. It is imperative to maintain the ordering of the adiabatic basis vectors such that the energy order is unchanged. The rest of the matrix should correspond to the identity matrix. The  $J$ -matrices are constructed by a straightforward generalization of Eq. (3.8). Alternatively, through the Dirac-picture formulation,  $|\chi_k\rangle \rightarrow \exp\left(-i \int_{t_i}^{t_f} \epsilon_k(t') dt'\right) |\chi_k\rangle$ , the dynamics may be expressed as a pure product of  $S$ -matrices. In this case, a phase shift originating from the adiabatic phases must be imposed on the off-diagonal elements.

The simplest way to obtain the adiabatic diagonal energies that enter into the  $J$ -matrix, is usually numerical solution of the eigenvalue equation with the diabatic Hamiltonian matrix. Of course, in doing so, the model is no longer purely analytical. Alternatively one may try and find approximate eigenenergies analytically. One way of doing this would be to use the two state energies given by Eq. (3.4) in the vicinity of a crossing and diabatic energies elsewhere.

As mentioned, the underlying assumption is that in the vicinity of an avoided crossing, the multi-state system may be treated as a two level system. Equation (3.6) may serve as a criterion for this; the time separation between two consecutive crossings must be such that their Lorentzian couplings does not overlap considerably. In other words,

$$t_{n+1} - t_n > \frac{1}{2}(\tau_{n+1} + \tau_n) \quad \forall n . \quad (3.14)$$

Logically, we have assumed that the system locally may be considered a two level system in order to justify that very same idea, so technically it is a necessary condition, not a sufficient one. Still, the criterion should serve at least as an estimate.

From Eq. (3.12) we may predict the dynamical *evolution* of the system – not just the final state – by only multiplying by the propagators corresponding to crossings that have taken place at the instant in question. Of course, such a prediction should be compared with the actual evolution expressed in the adiabatic basis rather than the diabatic one. Although the diabatic and adiabatic basis vectors coincide when well separated from crossings, there are oscillations in the populations of states undergoing a crossing or an avoided crossing, which obviously die out much faster in the adiabatic basis than in the diabatic one [37].

### C. Second order crossings

From Eq. (3.10) it seems reasonable to assume that no transition will occur between two diabatic states that do not couple. To some extent this is true – but not completely. When there are more than two states, there may be a finite coupling between two adiabatic states for which the corresponding diabatic states does not couple directly. This manifests itself in the fact that the adiabatic potential curves do exhibit an avoided crossing rather than an exact one. With the Hamiltonian Eq. (2.12), we may find a diabatic "pseudo-coupling"  $\tilde{V}$  as

$$|\tilde{V}_{k\ell}| = \left| \sum_{j \neq k, \ell} \frac{V_{kj} V_{j\ell}}{\mathcal{E}_j(t_{k\ell}) - \mathcal{E}_k(t_{k\ell})} \right|, \quad (3.15)$$

where  $\mathcal{E}_j$  is the potential curve of the diabatic state  $j$ , and  $k\ell$  label a set of two diabatic, uncoupled states ( $V_{k\ell} = 0$ ) that cross at time  $t = t_{k\ell}$  [that means  $\mathcal{E}_k(t_{k\ell}) = \mathcal{E}_\ell(t_{k\ell})$ ]. This formula, which has been checked numerically by comparing it to half the energy splitting at avoided crossings, is derived in Appendix A. In this way, also second order transition may be studied. Seen from a "diabatic point of view", this phenomenon is quite puzzling; the transition takes place through instantaneous hops to states that do *not* take part in the crossing, then, at the same instant, onto the other crossing state that and no shifts in the populations of the "intermediate" states are seen. Similar dynamical phenomenon in the theoretical description of two-level atoms in an ion trap was described as "mindboggling" [15].

## IV. APPLICATION OF LANDAU-ZENER THEORY TO THE TWO SPIN- $\frac{1}{2}$ SYSTEM

In Section II we have made no assumption about the time dependence of the elements of the Hamiltonian matrices Eqs. (2.6), (2.12) of the system of the two spin particles. In the following we will assume that the couplings are constant and the diagonal energies are linear in time. Hence, our basis, Eq. (2.5), coincides with the time-independent basis of the LZ model. This situation is certainly physically realizable. Moreover, it may be considered as an approximation to systems of more complex time dependence.

In the following, we wish to investigate the applicability of the MLZ model to various situations met in the case of the Hamiltonian Eq. (2.12). We start out with the simple case of two non-interacting spins Eq. (2.12).

### A. Dynamics in the case of non interacting particles

The formula Eq. (2.9) remains valid for any time-dependence in the matrix elements of the Hamiltonian  $H$ , Eq. (2.6). The specific character of this time dependence governs the values of  $p_a$  and  $p_b$  but the general form remains the same. In the particular choice of time-dependence corresponding to the LZ model, expressions for the two-state transition probabilities  $p_a$  and  $p_b$  are known, Eq. (3.10).

The diabatic potential curves for the Hamiltonian  $H$  are identified with the diagonal elements of the matrix Eq. (2.6)

$$\begin{aligned} \mathcal{E}_1(t) &= E_{1a}(t) + E_{1b}(t) , & \mathcal{E}_2(t) &= E_{1a}(t) + E_{2b}(t) , \\ \mathcal{E}_3(t) &= E_{2a}(t) + E_{1b}(t) , & \mathcal{E}_4(t) &= E_{2a}(t) + E_{2b}(t) . \end{aligned} \quad (4.1)$$

Referring to the adiabatic basis, the non-adiabatic transitions are located in the vicinities of crossings between the diabatic potential curves. Four types of crossings are located at the instants of time where the single-particle diabatic potential curves cross, namely:

$$\begin{aligned} \mathcal{E}_1(t) &= \mathcal{E}_2(t) \Rightarrow E_{1b}(t) = E_{2b}(t) , \\ \mathcal{E}_3(t) &= \mathcal{E}_4(t) \Rightarrow E_{1b}(t) = E_{2b}(t) , \\ \mathcal{E}_1(t) &= \mathcal{E}_3(t) \Rightarrow E_{1a}(t) = E_{2a}(t) , \\ \mathcal{E}_2(t) &= \mathcal{E}_4(t) \Rightarrow E_{1a}(t) = E_{2a}(t) . \end{aligned} \quad (4.2)$$

We denote the time of the crossing of the diabatic potential curves  $\mathcal{E}_i(t)$  and  $\mathcal{E}_j(t)$  as  $t_{ij}$ . From Eq. (4.2) one sees that two pairs of diabatic potential curves,  $\{\mathcal{E}_1(t), \mathcal{E}_2(t)\}$  and  $\{\mathcal{E}_3(t), \mathcal{E}_4(t)\}$ , cross at the same instant of time denoted as  $t_1$  in Fig. 1 ( $t_1 = t_{12} = t_{34}$ ). Similarly, two other pairs of diabatic potential curves,  $\{\mathcal{E}_1(t), \mathcal{E}_3(t)\}$  and  $\{\mathcal{E}_2(t), \mathcal{E}_4(t)\}$ , cross simultaneously at some other instant of time  $t_2 = t_{13} = t_{24}$ . Note that for the crossing discussed above the couplings are non-zero,  $V_{ij} \equiv H_{ij} \neq 0$  (see Fig. 1).

The conditions for two other types of crossing cannot be reduced to single-particle crossings:

$$\begin{aligned}\mathcal{E}_1(t) &= \mathcal{E}_4(t) \Rightarrow E_{1a}(t) + E_{1b}(t) = E_{2a}(t) + E_{2b}(t) , \\ \mathcal{E}_2(t) &= \mathcal{E}_3(t) \Rightarrow E_{1a}(t) + E_{2b}(t) = E_{2a}(t) + E_{1b}(t) .\end{aligned}\quad (4.3)$$

Note however that here the crossing potential curves are not coupled directly, which corresponds to the zero elements of the Hamiltonian matrix Eq. (2.6),  $V_{14} = V_{23} = 0$ . As discussed in Section III C, in the general case, such *second-order* crossings manifest a typical pseudo-crossing pattern of adiabatic potential curves, although with small splitting ( $\sim V^2$  as compared to  $\sim V$  splittings in the generic case, see Eq. (3.5) and Appendix A). However, in the special case of the Hamiltonian Eq. (2.6), due to its specific structure, the adiabatic curves cross exactly. This correlates with the fact that formula (A12) gives zero second-order splitting in this case. For the generalized Hamiltonian Eq. (2.12) the splittings are non-zero.

The remarkable features of the model of non-interacting spins is that only *single path* connects any initial state to any final state via two-state crossings of the type in Eqs. (4.2) with non-zero couplings; it is assumed that the crossings with zero couplings, Eqs. (4.3), do not lead to transitions. It is worthwhile to remind here that, as discussed in the Introduction, by definition, a *path* is composed of segments of diabatic potential curves; it can switch from one curve to the other at the point where diabatic potential curves cross, *provided* there is a non-zero direct coupling between these two curves. A path always corresponds to propagation in positive direction of time  $t$ .

When checking the single-path property, it is convenient to assume that, in the spirit of the MLZ model, the diabatic potential curves are linear functions of time, with some constants  $\beta_{1j}$ ,  $\beta_{2j}$ ,  $\alpha_{1j}$ ,  $\alpha_{2j}$ ,

$$\begin{aligned}E_{1a}(t) &= \beta_{1a}t + \alpha_{1a} , & E_{2a}(t) &= \beta_{2a}t + \alpha_{2a} , \\ E_{1b}(t) &= \beta_{1b}t + \alpha_{1b} , & E_{2b}(t) &= \beta_{2b}t + \alpha_{2b} ,\end{aligned}\quad (4.4)$$

and the couplings  $V_a$  and  $V_b$  are time independent. Within this assumption, the pairwise transition probabilities are given by Eq. (3.10) as

$$p_j = \exp\left(-\frac{2\pi|V_j|^2}{|\beta_{1j} - \beta_{2j}|}\right) , \quad q_j = 1 - p_j , \quad (4.5)$$

where  $j = a, b$ . The path-following arguments lead to the state-to-state probability matrix (2.9) which is exact for the non-interacting spins model. We emphasize once again that the validity of formula (2.9) does not necessarily require presumption (4.4).

Figure 2 shows the solution of the Schrödinger equation using the Hamiltonian of Eq. (2.6) with diagonal energies given by Eq. (4.4) and constant couplings. In this particular case, we have in atomic units  $\beta_i = \{-2.0, -0.50, 0.50, 2.0\}$ ,  $\alpha_i = \{0.0, -7.0, 7.0, 0.0\}$ , ( $i = 1, 2, 3, 4$ ),  $V_{12} = V_{34} = 0.5$ , and  $V_{24} = V_{13} = 0.3$ . The figure shows the population of each of the diabatic states as a function of time along with the MLZ prediction. The inset shows diabatic potential curves, and the horizontal lines are the predictions of the LZ model. One can clearly see that redistribution of populations is localized in time around the crossings, Eq. (4.2) (of course, at least one of two interacting states is to be populated prior to the crossing). The exact crossings, Eq. (4.3) (that are not replaced by pseudo-crossings in the adiabatic picture) do not lead to any redistribution of population. The final LZ probabilities are given by the second column of the matrix in Eq. (2.9). We find that they agree rather well with the numerical solution of the Schrödinger equation.

## B. Dynamics within the interacting spins model

In the following we will refer to the more general Hamiltonian of Eq. (2.12). This model also normally has 4 crossings of diabatic potential curves with non-zero coupling (first-order crossings) and 2 crossings with zero couplings (second-order crossings). One can again suggest linear time-dependence of the diabatic potential curves  $\tilde{\mathcal{E}}_j(t)$  with some constants  $A_j$  and  $B_j$ :

$$\tilde{\mathcal{E}}_j(t) = B_j t + A_j , \quad (4.6)$$

and time-independence of the couplings  $V_{jk}$ .

In general, all crossings occur at different instants of time  $t_{ij}$ . Two qualitatively different situations are met. In case of the time ordering

$$t_{34} < t_{12} < t_{14} < t_{24} < t_{13} < t_{23} , \quad (4.7)$$

the generalized model has single-path property, as seen from Fig. 3a. In case of the time ordering

$$t_{24} < t_{12} < t_{14} < t_{13} < t_{34} < t_{23}, \quad (4.8)$$

the single-path property is absent, as seen in Fig. 3b. These conclusions can be drawn through direct inspection of the generic Figures 3.

In the single-path case, when the ordering Eq. (4.7) is valid, by considering paths that connect initial and final states, one obtains a matrix of all state-to-state transition probabilities

$$\mathbf{P} = \begin{pmatrix} p_{12}p_{13} & p_{24}q_{12} & p_{12}q_{13} & q_{12}q_{24} \\ p_{13}q_{12} & p_{12}p_{24} & q_{12}q_{13} & p_{12}p_{24} \\ p_{34}q_{13} & q_{24}q_{34} & p_{13}p_{34} & p_{24}q_{34} \\ q_{13}q_{34} & p_{34}q_{24} & p_{13}q_{34} & p_{24}p_{34} \end{pmatrix}. \quad (4.9)$$

Here  $p_{jk}$  is the probability of non-adiabatic transition at the crossing between the  $j$ th and the  $k$ th diabatic potential curves, i.e. the probability of remaining in the same diabatic state. Within the Landau-Zener model one has

$$p_{jk} = \exp\left(-\frac{2\pi|V_{jk}|^2}{|B_j - B_k|}\right). \quad (4.10)$$

Note that the matrix in Eq. (4.9) generally is non-symmetrical.

The formula (2.9) is exact within the related 'generalized SO(3)' model. In distinction, the formula (4.9) for the model Eq. (2.12) is derived from 'path-following' arguments of semi-classical type. As numerical calculation shows, this formula is not valid within the general model Eq. (2.12). As an example one can consider the model with the diabatic potential curves as drawn in Fig. 1. By rotating potential curve 4 around the point of its crossing with the potential curve 1 and keeping all other parameters unchanged we thereby turn from Hamiltonian (2.6) to the more general model of Eq. (2.12). Let us consider a transition probability  $P_{32}$  as a function of the slope  $B_4$  as obtained by the rotation described. Other Hamiltonian parameters used in numerical calculations are, in atomic units:  $B_1 = -4$ ,  $B_3 = 2 = -B_2$ ,  $A_1 = A_4 = 0$ ,  $A_3 = 1 = -A_2$ , with the couplings  $V_{12} = V_{34} = 0.65$ ,  $V_{13} = V_{24} = 0.8$ ,  $V_{23} = V_{14} = 0$ .

At  $B_4 < -2$  the transition  $3 \rightarrow 2$  can be realized via two different paths, while at  $B_4 > -2$  only a single path is available. Formula (4.9) suggests that the probability  $P_{32}$  does not depend on  $B_4$  at all. Figure 4 shows that it is not true not only when several transition paths exist, but also when there is only one path connecting the initial and final states.

Some special cases of the generalized model Eq. (2.12) are known in which exact solutions are available.

The first case appears when the model Eq. (2.12) reduces to the model Eq. (2.6). In this case  $V_{12} = V_{34}$ ,  $V_{31} = V_{42}$  and  $\tilde{\mathcal{E}}_1 - \mathcal{E}_2 = \tilde{\mathcal{E}}_3 - \mathcal{E}_4$ . From the latter property it follows that  $B_1 - B_2 = B_3 - B_4$ ,  $B_3 - B_1 = B_1 - B_2$  and formula (4.10) leads to  $p_{12} = p_{34} \equiv p_b$ ,  $p_{13} = p_{24} \equiv p_a$ . The transition probabilities, Eq. (4.9), are reduced to (2.9), which are *exact*.

Generally, four linear adiabatic curves experience 6 avoided crossings, although at some crossings the couplings would turn zero, as in the case of model Eq. (2.12). In the special case when three diabatic curves are parallel, they are crossed by the fourth one at 3 points. This is the well known Demkov-Osherov model [20]. In the following, we will consider some special cases with 5 (section IV B 1) and 4 (section IV B 3) crossings, and finally we will study the general case including interference effects and second order crossings.

### 1. Four-state generalized bow-tie model

The case when semi-classical considerations are exact stems from the generalized bow-tie model [22]. Exact solution of this model is available for any  $N$ , but the simplest case,  $N = 4$ , was not yet considered in detail. The original bow-tie model [21] is covered by the generalized one as a special case. Our four-state model, Eq. (2.12), is reduced to the generalized bow-tie model provided that some restrictions on its parameters are imposed. One claim is that two diabatic potential curves are parallel; by an appropriate phase transformation they could be made horizontal. Let these curves have labels 2 and 3. Then one has  $B_2 = B_3 = 0$ . The state 1 interacts with 2 and 3 so that the couplings are identical, i.e.  $V_{12} = V_{13}$ . The same refers to the state 4, namely,  $V_{24} = V_{34}$ . Besides this, the generalized bow-tie model presumes that within the pairs 2, 3 and 1, 4 the couplings are absent:  $V_{23} = V_{32} = 0$ ,  $V_{14} = V_{41} = 0$ . The latter properties are intrinsic in the Hamiltonian operator in Eq. (2.12). The additional condition is that the diabatic potential curves cross half-way between the curves 2 and 3. Denoting the instant of crossing as  $t_0$  we obtain

$$B_1 t_0 + A_1 = B_4 t_0 + A_4 = \frac{1}{2}(A_2 + A_3). \quad (4.11)$$

By choosing  $t_0 = 0$  and the energy zero half-way between the horizontal potential curves 2 and 3, we have  $A_1 = A_4 = 0$  without any loss of generality. Within these conventions the model Hamiltonian is

$$\mathbf{H}_{\text{gb}}(t) = \begin{pmatrix} B_1 t & V_{12} & V_{12} & 0 \\ V_{12}^* & A_2 & 0 & V_{24} \\ V_{12}^* & 0 & -A_2 & V_{24} \\ 0 & V_{24}^* & V_{24}^* & B_4 t \end{pmatrix}. \quad (4.12)$$

At first we consider the case when the slopes  $B_1$  and  $B_4$  have opposite signs (for definiteness we assume below that  $B_1 < 0$  and  $B_4 > 0$ , see Fig. 5a). For a special symmetric case of matrix (4.12) with  $B_4 = -B_1$ ,

$$\mathbf{H}_{\text{gb1}}(t) = \begin{pmatrix} B_1 t & V_{12} & V_{12} & 0 \\ V_{12}^* & A_2 & 0 & V_{24} \\ V_{12}^* & 0 & -A_2 & V_{24} \\ 0 & V_{24}^* & V_{24}^* & -B_1 t \end{pmatrix}, \quad (4.13)$$

it is particularly easy to write down the related spin-Hamiltonian:

$$H_{\text{gb1}}(t) = B_1 t(s_{az} + s_{bz}) + A(s_{az} - s_{bz}) + 2G_1(s_{ax} + s_{bx}) + 2G_2(s_{ay} + s_{by}) + 4c_1(s_{az}s_{bx} + s_{bz}s_{ax}) + 4c_2(s_{az}s_{by} + s_{bz}s_{ay}), \quad (4.14)$$

with  $V_{12} = G_1 - iG_2 + c_1 - ic_2$ ,  $V_{24} = G_1 - iG_2 - c_1 + ic_2$ . Note that the Hamiltonian (4.14) is symmetric under permutation of spins  $a$  and  $b$ , except for the term  $A(s_{az} - s_{bz})$ . The case when this term turns zero, i.e.  $A \rightarrow 0$ , corresponds to transition from the generalized bow-tie model [22] to the original one [21], as described in detail in [22].

According to the results of *exact* analytical calculations (carried out in [22] for an arbitrary number of states  $N$ ), the matrix of transition probabilities reads

$$\mathbf{P} = \begin{pmatrix} p_1^2 & p_1 q_1 & p_4 q_1 & q_1 q_4 \\ p_4 q_1 & p_1 p_4 & q_4^2 & p_4 q_4 \\ p_1 q_1 & q_1^2 & p_1 p_4 & p_1 q_4 \\ q_1 q_4 & p_1 q_4 & p_4 q_4 & p_4^2 \end{pmatrix}, \quad (4.15)$$

where

$$p_1 = \exp\left(-\frac{2\pi|V_{12}|^2}{|B_1|}\right), \quad p_4 = \exp\left(-\frac{2\pi|V_{24}|^2}{|B_4|}\right), \quad q_1 = 1 - p_1, \quad q_4 = 1 - p_4. \quad (4.16)$$

The matrix of Eq. (4.15) is generally non-symmetrical. This is a special case of formula (4.9) (with  $p_{13} = p_{12} = p_1$ ,  $p_{24} = p_{34} = p_4$ ). Only single-path transitions are operative in this case.

Figure 6 shows the dynamics of a system with Hamiltonian of the form Eq. (4.12) with parameters  $B_1 = -0.5$ ,  $B_4 = 1$ ,  $B_2 = B_3 = A_1 = A_4 = 0$ ,  $A_2 = 5 = -A_3$ ,  $V_{12} = V_{13} = 0.2$ ,  $V_{24} = V_{34} = 0.15$ . Initially, the system is prepared in state 1 (see Fig. 5 a), so the diabatic populations should converge towards the probabilities in the first column of the matrix in Eq. (4.15). This is the case to a high degree of accuracy. The remaining small discrepancy is a measure of precision of the numerical procedure employed.

We now turn to the case when the slopes  $B_1$  and  $B_4$  have the same sign; for definiteness we assume that  $B_4 > B_1 > 0$ , see Fig. 5b. Again we use the *exact* results of [22], which give the matrix of transition probabilities

$$\mathbf{P} = \begin{pmatrix} (1 - p_4 q_1)^2 & p_4 q_1 & \underline{\underline{p_1 p_4^2 q_1}} & \underline{\underline{q_1 q_4 p_4}} \\ \underline{\underline{q_1 p_1 p_4^2}} & p_1 p_4 & (1 - p_1 p_4)^2 & \underline{\underline{p_1 p_4 q_4}} \\ p_4 q_1 & 0 & p_1 p_4 & q_4 \\ \underline{\underline{q_1 q_4 p_4}} & q_4 & \underline{\underline{p_1 p_4 q_4}} & \underline{\underline{p_4^2}} \end{pmatrix}. \quad (4.17)$$

This matrix does not have form of Eq. (4.9). In this case both single- and multi-path transitions are operative. Actually above *multi-* means *double-*; such transition probabilities are underlined in the matrix in Eq. (4.17). The doubly underlined matrix elements correspond to transitions that in principle could be multi-path ones in the generalized bow-tie model for an arbitrary  $N$  (cf. [22]), but in fact are single-path in the particular  $N = 4$  realization considered here.

Figure 7 shows the dynamics for the same system as in Fig. 6 except for the sign of  $B_1$ , which now is positive. The initial state is still diabatic state number 1. Once again, we find that the final probabilities coincide rather well with the phase independent LZ-prediction given in the first row of the matrix in Eq. (4.17).

The intermediate case emerges when  $B_1 = 0$ . Here we obtain the single-path Demkov-Osherov model [20] with three parallel horizontal diabatic potential curves (1, 2, 3) crossed by a slanted curve (4) under the particular condition  $V_{14} = 0$ . The state-to-state transition probability matrix reads ( $B_4 > 0$ )

$$\mathbf{P} = \begin{pmatrix} 1 & 0 & 0 & 0 \\ 0 & p_4 & q_4^2 & p_4 q_4 \\ 0 & 0 & p_4 & q_4 \\ 0 & q_4 & p_4 q_4 & p_4^2 \end{pmatrix}. \quad (4.18)$$

The condition  $V_{14} = 0$  means that the state 1 is completely decoupled from all other states, i.e.  $p_1 \rightarrow 1$ ,  $q_1 \rightarrow 0$ . Both the matrices in Eqs. (4.15), (4.17) tends to Eq. (4.18) in this limit. Although the transition from Eq. (4.15) via Eq. (4.18) to Eq. (4.17) is continuous, it is not smooth and analytical, i.e. there is no analytical formula that embraces all these expressions.

Thus, a change of sign of the slopes  $B_1$ ,  $B_4$  alters the character of the model (from single- to multiple- path) and drastically changes the expressions for the state-to-state transition probabilities. For instance, if  $B_1$  and  $B_4$  are both positive, transition  $2 \rightarrow 3$  becomes impossible,  $P_{23} \equiv 0$ . The generalized bow-tie model provides a so far unique case in which exact solutions are available also in the situation when multi-path transitions are operative. The important specific feature of the model is that the multi-path transitions do not result in interference oscillations, as discussed in detail in Ref. [22].

## 2. Survival on a diabatic curve with extreme slope

Consider now the case when all the slopes  $B_j$  are different. Let  $B_1$  be largest of all the slopes  $B_j$ , and  $B_4$  be the smallest of all the slopes  $B_j$

$$B_1 = \max\{B_j\}, \quad B_4 = \min\{B_j\}. \quad (4.19)$$

Then, according to conjecture of Brundobler and Elser [38], recently proved by Shytov [39] and Volkov and Ostrovsky [35], some transition probabilities are known exactly

$$P_{11} = p_{12}p_{13}p_{14}, \quad P_{44} = p_{14}p_{24}p_{34}. \quad (4.20)$$

For our particular model with  $V_{14} = 0$  one has to put  $p_{14} = 1$ . For the generalized bow-tie model additional relations are  $p_{12} = p_{13} = p_1$  and  $p_{24} = p_{34} = p_4$ . This reduces formulas (4.20) to

$$P_{11} = p_1^2, \quad P_{44} = p_4^2, \quad (4.21)$$

in agreement with Eqs. (4.15), (4.17).

## 3. Crossing of two parallel bands of diabatic states

Usuki [40] considered crossing of two parallel bands of diabatic states [41]. The case of two states in each band corresponds in our terms to  $B_1 = B_4$ ,  $B_2 = B_3$ . With an appropriate choice of zeroes on the energy and time axes the Hamiltonian takes the form

$$\mathbf{H}_{\text{band}}(t) = \begin{pmatrix} B_1 t + A_1 & V_{12} & V_{13} & 0 \\ V_{12}^* & B_2 t + A_2 & 0 & V_{24} \\ V_{13}^* & 0 & B_2 t - A_2 & V_{34} \\ 0 & V_{24}^* & V_{34}^* & B_1 t - A_1 \end{pmatrix}. \quad (4.22)$$

Within each band coupling is absent, but inter-band coupling persist. For definiteness we assume  $B_1 > 0$ ,  $B_2 < B_1$ .

Again, only some state-to-state transition probabilities are known exactly [36, 40, 42]

$$\begin{aligned} P_{11} &= p_{12}p_{13}, & P_{44} &= p_{24}p_{34}, \\ P_{22} &= p_{24}p_{12}, & P_{33} &= p_{34}p_{13}, \end{aligned} \quad (4.23)$$

Two more probabilities have exact expressions, depending on sign of  $A_1$  and  $A_2$

$$P_{41} = 0, \quad A_1 > 0; \quad P_{14} = 0, \quad A_1 < 0; \quad (4.24)$$

$$P_{23} = 0, \quad A_2 > 0; \quad P_{32} = 0, \quad A_2 < 0; \quad (4.25)$$

#### 4. Degenerate cases

Within the general MLZ, Eq. (1.1), one can distinguish the case of degenerate slopes, where  $\beta_i = \beta_j$  and the case of complete degeneracy, where in addition  $\varepsilon_i = \varepsilon_j$ . A number of cases of slope degeneracy appeared above: Demkov-Osherov model, bow-tie model, band-crossing model. The situation with complete degeneracy generally requires a special treatment, to be carried out elsewhere. As an illustrative example we consider here only the limit of band-crossing model with complete pairwise degeneracy of diabatic potential curves. Presuming additionally that the couplings are pairwise equal we obtain Hamiltonian matrix for *degenerate band* case as

$$\mathbf{H}_{\text{db}}(t) = \begin{pmatrix} B_1 t & V_a & V_b & 0 \\ V_a^* & B_2 t & 0 & V_a \\ V_b^* & 0 & B_2 t & V_b \\ 0 & V_a^* & V_b^* & B_1 t \end{pmatrix}. \quad (4.26)$$

There is only one, albeit degenerate crossing of diabatic potential curves at  $t = 0$ . To simplify the problem we introduce new orthonormal basis set:

$$\begin{aligned} |I\rangle &= \frac{1}{\sqrt{2}}(|1\rangle - |4\rangle), \\ |II\rangle &= \frac{1}{\sqrt{2}}(|1\rangle + |4\rangle), \\ |III\rangle &= \frac{1}{h}(V_a|2\rangle + V_b|3\rangle), \\ |IV\rangle &= \frac{1}{h}(V_b|2\rangle - V_a|3\rangle) \end{aligned} \quad (4.27)$$

with  $h = \sqrt{|V_a|^2 + |V_b|^2}$ . In the new basis the Hamiltonian (4.26) is transformed to

$$\tilde{\mathbf{H}}_{\text{db}}(t) = \begin{pmatrix} B_1 t & 0 & 0 & 0 \\ 0 & B_1 t & \sqrt{2}h & 0 \\ 0 & \sqrt{2}h & B_2 t & 0 \\ 0 & 0 & 0 & B_2 t \end{pmatrix}. \quad (4.28)$$

Thus the states  $|I\rangle$  and  $|IV\rangle$  are fully decoupled while the remaining pair of states  $|II\rangle$  and  $|III\rangle$  provide standard two-state Landau-Zener model. Accordingly, S-matrix (i.e. matrix of state-to-state transition amplitudes) is

$$\tilde{\mathbf{S}}_{\text{db}} = \begin{pmatrix} 1 & 0 & 0 & 0 \\ 0 & s_{22} & s_{23} & 0 \\ 0 & s_{32} & s_{33} & 0 \\ 0 & 0 & 0 & 1 \end{pmatrix}, \quad (4.29)$$

where

$$s_{22} = s_{33}^* = p_0 e^{i\varphi}, \quad s_{23} = s_{32}^* = e^{i\theta} \sqrt{1 - p_0^2}, \quad (4.30)$$

$$p_0 = \exp\left(-\frac{2\pi h^2}{|B_1 - B_2|}\right), \quad (4.31)$$

where the phase  $\theta$  is insignificant (see below), and the phase of the diagonal elements,  $\pm\varphi$ , vanishes when the interaction time before and after the crossing is about the same. Note that the effective coupling in the Hamiltonian (4.28) is  $\sqrt{2}h$  which is responsible for extra factor of 2 in the exponent (4.31) [cf. expression (4.10)]. Returning to the original basis of states we get

$$\mathbf{S}_{\text{db}} = \begin{pmatrix} \frac{1}{2}(s_{22} + 1) & (V_a/\sqrt{2}h)s_{23} & (V_b/\sqrt{2}h)s_{23} & \frac{1}{2}(s_{22} - 1) \\ (V_a/\sqrt{2}h)s_{32} & (V_a^2/h^2)s_{33} + V_b^2/h^2 & (V_a V_b/h^2)(s_{33} - 1) & (V_a/\sqrt{2}h)s_{32} \\ (V_b/\sqrt{2}h)s_{32} & (V_a V_b/h^2)(s_{33} - 1) & (V_b^2/h^2)s_{33} + V_a^2/h^2 & (V_b/\sqrt{2}h)s_{32} \\ \frac{1}{2}(s_{22} - 1) & (V_a/\sqrt{2}h)s_{23} & (V_b/\sqrt{2}h)s_{23} & \frac{1}{2}(s_{22} + 1) \end{pmatrix} \quad (4.32)$$

that corresponds to the transition probabilities

$$\mathbf{P}_{\text{bd}} = \begin{pmatrix} \frac{1}{4}(1 + p_0)^2 & (V_a/2h^2)(1 - p_0^2) & (V_b/2h^2)(1 - p_0^2) & \frac{1}{4}(1 - p_0)^2 \\ V_a^2(1 - p_0^2)/(2h^2) & (V_a^2 p_0 + V_b^2)^2/h^4 & V_a^2 V_b^2(1 - p_0)^2/h^4 & V_a^2(1 - p_0^2)/(2h^2) \\ V_b^2(1 - p_0^2)/(2h^2) & V_a^2 V_b^2(1 - p_0)^2/h^4 & (V_b^2 p_0 + V_a^2)^2/h^4 & V_b^2(1 - p_0^2)/(2h^2) \\ \frac{1}{4}(1 - p_0)^2 & V_a^2(1 - p_0^2)/(2h^2) & V_b^2(1 - p_0^2)/(2h^2) & \frac{1}{4}(1 + p_0)^2 \end{pmatrix}. \quad (4.33)$$

This result does not depend on the phase  $\theta$  in formula (4.30); nor  $\varphi$  when  $|t_i| \sim t_f$ . No state-to-state transition probability coincides with that from the matrix (4.9).

### C. The general multiple path case

In the general case systems are subject to both interference effects and possibly also second order transitions. The question of exact solutions remains a difficult one, but we do expect that if the crossings are separated well enough, the MLZ model should give satisfactory predictions.

When the couplings are very strong, and when the crossings are not very well separated in time, the LZ model may not describe the dynamics very well. This may be attributed to the fact that the populations oscillate with decreasing amplitude after an avoided crossing. It should be re-emphasized, however, that figures demonstrated here do not give a very accurate idea of these oscillations; in the MLZ model we are always referring to the adiabatic basis, in which the oscillations die out much faster than in the diabatic one. The figures, however, display the populations in the diabatic basis. Hence, the actual situation is not as unstable as suggested by the figures, and the agreement between the final transition probabilities and the LZ prediction is far from as coincidental as it may seem.

Figure 8 shows the dynamics corresponding to the Hamiltonian of Eq. (2.12) with parameters  $B_i = \{-3, 0.5, 5, 0\}$ ,  $A_i = \{0, 4, -5, 1.5\}$  ( $i = 1, 2, 3, 4$ ),  $V_{12} = 0.5$ ,  $V_{13} = 0.3$ ,  $V_{24} = 0.1$  and  $V_{34} = 0.4$ . This is a realization of the system displayed generically in Fig. 3b. The initial state is the diabatic state 2. Referring to the diabatic basis, the transitions to e.g. the final state 4 can take place through various paths, and hence the transition probabilities are strongly phase-dependent. If second order transitions are considered, the picture becomes even more complex. Even though the crossings appear rather close, the condition (3.14) is satisfied, and, as we see, the MLZ model describes the dynamics quite well.

Figure 9 shows essentially the same as Fig. 8 but with parameters corresponding to a slightly longer time scale. In this case we have  $B_i = \{-3, 1, 5, 0\}$ ,  $A_i = \{0, 50, -80, 16\}$ ,  $V_{12} = 0.6$ ,  $V_{13} = 0.5$ ,  $V_{24} = 0.45$  and  $V_{34} = 0.4$ . Again we find that the agreement between the numerical calculations and Eq. (3.12) is rather good. Furthermore, by focusing on what happens at  $t_3 \approx -5$ , we discover a rather striking phenomena; there is a significant shift in the populations at the time of the crossing between two states that do not couple directly. This is quite surprising considering the very low probability of an adiabatic transition. In this particular case, the LZ model, Eq. (3.15), predicts this probability to be  $1 - p_3 < 10^{-4}$ , which leads us to suspect that the populations of the crossing diabatic states are practically unaltered. However, when both diabatic states are initially populated, the shift in population may be orders of magnitude larger. In order to trace this amplification effect, consider the transition matrix  $S_3$  corresponding to  $t = t_3$ :

$$S_3 = \begin{pmatrix} 1 & 0 & 0 & 0 \\ 1 & \sqrt{1-p_3}e^{i\alpha_3} & \sqrt{p_3} & 0 \\ 0 & -\sqrt{p_3} & \sqrt{1-p_3}e^{-i\alpha_3} & 0 \\ 0 & 0 & 0 & 1 \end{pmatrix}. \quad (4.34)$$

Suppose that the state immediately before the crossing is given by  $(0, 1, e^{i\varphi}, 0)/\sqrt{2}$ . Then the populations of adiabatic states 2 and 3 immediately after the crossing are  $1/2 \pm \sqrt{p_3(1-p_3)} \cos(\alpha_3 - \varphi)$ . This amounts to a maximum shift of populations of  $\sqrt{p_3(1-p_3)}$ , which may be orders of magnitude larger than  $1 - p_3$ . Consequently, second order transitions may be quite significant – even for very small diabatic transition probabilities. This is demonstrated in Fig. 10 in which the particular case treated above is demonstrated using the same parameters as in Fig. 9.

## V. CONCLUSIONS

In this paper we have studied in detail the analytic properties of quantum mechanical four-state systems. The particular case of crossings of time dependent diagonal elements of the Hamiltonian leads to semi-analytical expressions for the state probabilities determined by the LZ model. We have demonstrated that the MLZ model in many cases gives accurate transition probabilities tested by parallel numerical solution of the four-state system. Furthermore, it has been demonstrated that by carefully taking phase interference effects into account, the general case in which multiple paths are encountered may also be treated adequately within the Landau-Zener model.

It is found that transitions may take place also between diabatic states that does not couple directly. These transitions, which are induced by the presence of the states that are not involved directly in the (avoided) crossing, can strongly influence the dynamics. An analytical expression for such effective coupling strengths has been derived and verified by numerical calculations.

The known analytically solvable four-state models have been analyzed with focus on their single- and multi-path properties. In particular, the four-state generalized bow-tie model has been explored in detail for two qualitatively different realizations. Transition between the two cases has been shown to go through the Demkov Osherov model.

## APPENDIX A: SECOND-ORDER PSEUDO-CROSSINGS

### 1. Four-state model

At first we consider the special case of our four-state model by analyzing the characteristic equation for the eigenvalues  $\lambda$  of the Hamiltonian matrix  $\mathbf{H}_g$  of Eq. (2.12)

$$(\mathcal{E}_1 - \lambda)(\mathcal{E}_2 - \lambda)(\mathcal{E}_3 - \lambda)(\mathcal{E}_4 - \lambda) - (\mathcal{E}_3 - \lambda)(\mathcal{E}_4 - \lambda)V_{12}^2 - (\mathcal{E}_2 - \lambda)(\mathcal{E}_4 - \lambda)V_{13}^2 \\ - (\mathcal{E}_1 - \lambda)(\mathcal{E}_3 - \lambda)V_{24}^2 - (\mathcal{E}_1 - \lambda)(\mathcal{E}_2 - \lambda)V_{34}^2 + (V_{13}V_{24} - V_{12}V_{34})^2 = 0. \quad (\text{A1})$$

The special case of the Hamiltonian of Eq. (2.6) is obtained by putting  $V_{13} = V_{24} = V_a$ ,  $V_{12} = V_{34} = V_b$ ,  $\mathcal{E}_4 = -\mathcal{E}_1$ ,  $\mathcal{E}_3 = -\mathcal{E}_2$ . In this case, the characteristic equation (A1) reduces to

$$(\mathcal{E}_1^2 - \lambda^2)(\mathcal{E}_2^2 - \lambda^2) - (\mathcal{E}_2 + \lambda)(\mathcal{E}_1 + \lambda)V_b^2 + (\mathcal{E}_2 - \lambda)(\mathcal{E}_1 + \lambda)V_a^2 \\ + (\mathcal{E}_1 - \lambda)(\mathcal{E}_2 + \lambda)V_a^2 - (\mathcal{E}_1 - \lambda)(\mathcal{E}_2 - \lambda)V_b^2 + (V_a^2 - V_b^2)^2 = 0. \quad (\text{A2})$$

It could be rewritten as bi-quadratic equation

$$\mathcal{E}_1^2\mathcal{E}_2^2 + 2\mathcal{E}_1\mathcal{E}_2(V_a^2 - V_b^2) + (V_a^2 - V_b^2)^2 - (\mathcal{E}_1^2 + \mathcal{E}_2^2 + 2V_a^2 + 2V_b^2)\lambda^2 + \lambda^4 = 0. \quad (\text{A3})$$

Now we consider the second-order crossing of a pair of potential curves 2 and 3; at the crossing of diabatic curves one obtains  $\mathcal{E}_2 = \mathcal{E}_3 \equiv \mathcal{E}$ . Assuming  $(\mathcal{E} - \lambda) \sim V_{ij}^2 \ll 1$  and retaining terms of order  $\sim V_{ij}^4$ , we reduce Eq. (A1) to

$$(\mathcal{E}_1 - \mathcal{E})(\mathcal{E}_4 - \mathcal{E})(\mathcal{E} - \lambda)^2 - (\mathcal{E} - \lambda)[(\mathcal{E}_4 - \mathcal{E})(V_{12}^2 + V_{13}^2) + (\mathcal{E}_1 - \mathcal{E})(V_{24}^2 + V_{34}^2)] \\ + (V_{13}V_{24} - V_{12}V_{34})^2 = 0. \quad (\text{A4})$$

This is a quadratic equation over  $(\mathcal{E} - \lambda)$  with discriminant

$$D = [(\mathcal{E}_4 - \mathcal{E})(V_{12}^2 + V_{13}^2) + (\mathcal{E}_1 - \mathcal{E})(V_{24}^2 + V_{34}^2)]^2 - 4(\mathcal{E}_1 - \mathcal{E})(\mathcal{E}_4 - \mathcal{E})(V_{13}V_{24} - V_{12}V_{34})^2 \\ = [(\mathcal{E}_4 - \mathcal{E})(V_{12}^2 - V_{13}^2) - (\mathcal{E}_1 - \mathcal{E})(V_{24}^2 - V_{34}^2)]^2 + 4[(\mathcal{E}_4 - \mathcal{E})V_{12}V_{13} + (\mathcal{E}_1 - \mathcal{E})V_{24}V_{34}]^2 \quad (\text{A5})$$

presented as a sum of two squared (i.e. positive) quantities. The first of these quantities turns zero upon adjustment of the system parameters (in our case this parameter is the time  $t$ ). Then splitting of the two eigenvalues governed by Eq. (A4) equals

$$\Delta\lambda = 2 \left| \frac{V_{12}V_{13}}{\mathcal{E}_1 - \mathcal{E}} + \frac{V_{24}V_{34}}{\mathcal{E}_4 - \mathcal{E}} \right|. \quad (\text{A6})$$

We remind that this is splitting at the second-order pseudo-crossing of potential curves 2 and 3; it is quadratic over  $V_{ij}$ . It can be compared with the splitting at conventional (or the first-order) pseudo-crossing of curves  $i$  and  $j$ ; it is linear over  $V_{ij}$ , Eq. (3.5):

$$\Delta\lambda = 2|V_{ij}|. \quad (\text{A7})$$

The formula (A6) has structure typical for the second-order quantities in the perturbation theory: the states 2 and 3 are coupled via intermediate states 1 and 4, with the characteristic energy denominators. By fitting of parameters, the expression (A6) can be made equal zero. Then the splitting  $\Delta\lambda$  is of higher order over  $V_{ij}$ . In special cases it might turn zero exactly; this occurs in the model of non-interacting spins.

## 2. Model with an arbitrary number of states

Consider now an  $N \times N$  Hamiltonian matrix  $\mathbf{H}_t$  with diagonal elements  $\mathcal{E}_j$  and non-diagonal elements  $V_{ij}$  (for brevity we assume that matrix  $\mathbf{H}_t$  is real). We consider the second-order crossing of potential curves 2 and 3:  $\mathcal{E}_2 = \mathcal{E}_3 \equiv \mathcal{E}$ ,  $V_{23} = 0$ . Let  $\lambda$  be eigenvalue of  $\mathbf{H}_t$ , and column vector  $\mathbf{c}$  be an eigenvector. Then the standard set of equations is

$$\begin{aligned} \sum_{k \neq 2, 3}^N (\mathbf{h} - \lambda \mathbf{I})_{jk} c_k + V_{j2} c_2 + V_{j3} c_3 &= 0, \\ \sum_{k \neq 2, 3}^N V_{2k} c_k + (\mathcal{E}_2 - \lambda) c_2 &= 0, \\ \sum_{k \neq 2, 3}^N V_{3k} c_k + (\mathcal{E}_3 - \lambda) c_3 &= 0, \end{aligned} \quad (\text{A8})$$

where  $\mathbf{h}$  is an  $(N-2) \times (N-2)$  submatrix of  $\mathbf{H}_t$ , and  $\mathbf{I}$  is the  $(N-2) \times (N-2)$  unit matrix. Denote  $\mathbf{R}(\lambda) = (\mathbf{h} - \lambda)^{-1}$  the resolvent for the matrix  $\mathbf{h}$ . Then the first equation of Eqs. (A8) gives  $c_k = -\sum_{k \neq 2, 3}^N R_{kj}(V_{j2} c_2 + V_{j3} c_3)$  and two other equations are reduced to

$$\begin{aligned} - \sum_{j, k \neq 2, 3}^N V_{2k} R_{kj}(\lambda) V_{j2} c_2 - \sum_{j, k \neq 2, 3}^N V_{2k} R_{kj}(\lambda) V_{j3} c_3 + (\mathcal{E} - \lambda) c_2 &= 0, \\ - \sum_{j, k \neq 2, 3}^N V_{3k} R_{kj}(\lambda) V_{j2} c_2 - \sum_{j, k \neq 2, 3}^N V_{3k} R_{kj}(\lambda) V_{j3} c_3 + (\mathcal{E} - \lambda) c_2 &= 0. \end{aligned} \quad (\text{A9})$$

We approximately put  $\lambda = \mathcal{E}$  in the argument of the resolvent and obtain for the splitting of two eigenvalues of interest (which are degenerate in the limit  $V \rightarrow 0$ ):

$$\Delta\lambda = 2 \left| \sum_{j, k \neq 2, 3}^N V_{2k} R_{kj}(\mathcal{E}) V_{j3} \right|. \quad (\text{A10})$$

In the particular case when  $N = 4$ , a simple analytical expression for the resolvent is available that allows to rewrite expression (A10) as

$$\begin{aligned} \Delta\lambda &= \frac{2}{|(h_{11} - \mathcal{E})(h_{44} - \mathcal{E}) - h_{14}^2|} |V_{21}(h_{44} - \mathcal{E})V_{13} + V_{24}(h_{11} - \mathcal{E})V_{43} - 2V_{21}h_{14}V_{43}| \\ &= \frac{2}{|(\mathcal{E}_1 - \mathcal{E})(\mathcal{E}_4 - \mathcal{E}) - V_{14}^2|} |V_{21}(\mathcal{E}_4 - \mathcal{E})V_{13} + V_{24}(\mathcal{E}_1 - \mathcal{E})V_{43} - 2V_{21}V_{14}V_{43}|, \end{aligned} \quad (\text{A11})$$

where we have simply switched to alternative notations in the second line. In this paper we considered  $4 \times 4$  Hamiltonian matrices, Eq. (2.12), with zeroes on the cross-diagonal, i.e. with  $V_{14} = 0$ . Then

$$\begin{aligned} \Delta\lambda &= \frac{2}{|(\mathcal{E}_1 - \mathcal{E})(\mathcal{E}_4 - \mathcal{E})|} |V_{21}(\mathcal{E}_4 - \mathcal{E})V_{13} + V_{24}(\mathcal{E}_1 - \mathcal{E})V_{43}| \\ &= 2 \left| \frac{V_{21}V_{13}}{\mathcal{E}_1 - \mathcal{E}} + \frac{V_{24}V_{43}}{\mathcal{E}_4 - \mathcal{E}} \right|, \end{aligned} \quad (\text{A12})$$

which coincides with Eq. (A7).

If the submatrix  $\mathbf{h}$  is diagonal, the formula (A10) reduces to

$$\Delta\lambda = 2 \left| \sum_{k \neq 2, 3}^N \frac{V_{3k}V_{k2}}{\mathcal{E}_k - \mathcal{E}} \right|. \quad (\text{A13})$$

[1] H. De Raedt, S. Miyashita, K. Saito, D. García-Pablos, and N. García, Phys. Rev. B **56**, 11761 (1997); S. Miyashita and N. Nagaosa, Progr. Theor. Phys. **106**, 533 (2001); S. Miyashita, K. Saito, H. Nakano, and M. Nishino, Mol. Cryst. Liq.

- Cryst. **379**, 475 (2002); H. De Raedt, S. Miyashita, K. Michelsen, and M. Machida, Phys. Rev. B **70**, 064401 (2004); I. Chiorescu, W. Wernsdorfer, A. Müller, S. Miyashita, and B. Barbara, Phys. Rev. B **67**, 020402(R) (2003).
- [2] D. A. Garanin and R. Schilling, Phys. Rev. B **66**, 174438 (2002); **69**, 104412 (2004); D. A. Garanin, Phys. Rev. B **70**, 212403 (2004); C. Calero, E. M. Chudnovsky, and D. A. Garanin, Phys. Rev. B **72**, 024409 (2005).
- [3] D. A. Garanin, Phys. Rev. B **68**, 014414 (2003).
- [4] D. A. Garanin and R. Schilling, Phys. Rev. B **71**, 184414 (2005); cond-mat/0312030.
- [5] V. G. Benza, C. M. Canali, and G. Strini, Phys. Rev. B **70**, 184426 (2004).
- [6] H. Nojiri, T. Taniguchi, Y. Ajiro, A. Müller, and B. Barbara, Physica B **346-347**, 216 (2004); S. Maegawa and M. Ueda, Physica B **329-333**, 1144 (2003); M. Nishino, K. Saito, and S. Miyashita, Physica B **329-333**, 1170 (2003).
- [7] I. Rousochatzakis, Y. Ajiro, H. Mitamura, P. Kögerler, and M. Luban, Phys. Rev. Lett. **94**, 147204 (2005).
- [8] J.-M. Hu, Z.-D. Chen, and S.-Q. Shen, Phys. Rev. B **68**, 104407 (2003); Z.-D. Chen and S.-Q. Shen, Phys. Rev. B **67**, 012408 (2003).
- [9] L.-B. Fu, S.-G. Chen, and B. Hu, Phys. Lett. A **323**, 460 (2004).
- [10] D. G. Gory, M. D. Price, and T. F. Havel, Physica D **120**, 82 (1998); S. S. Somaroo, D. G. Gory, and T. F. Havel, Phys. Lett. **240**, 1 (1998); D. Gottesman, Phys. Rev. A **57**, 127 (1998).
- [11] C. H. Bennett, Phys. Today **48** (10), 24 (1995); D. P. DiVincenzo, Science **270**, 255 (1995); A. Barenco *et al* **52**, 3457 (1995); V. Scarani, Am. J. Phys. **66**, 957 (1998); P. Benioff, J. Stat. Phys. **22**, 563 (1980); Phys. Rev. Lett. **48**, 1581 (1982); Phys. Rev. A **54**, 1106 (1996).
- [12] C.-P. Yang, S.-I. Chu, S. Han, Phys. Rev. A **66**, 034301 (2002); Z. Zhou, S.-I. Chu, S. Han, Phys. Rev. B **66**, 054527 (2002).
- [13] J. B. Majer, F. G. Paauw, A. C. J. ter Haar, C. J. P. M. Harmans, and J. E. Mooij, Phys. Rev. Lett. **94**, 090501 (2005).
- [14] F. J. M. van de Ven and C. W. Hilbers, J. Magn. Res. **54**, 512 (1983).
- [15] K. Mølmer and A. Sørensen, Phys. Rev. Lett. **82**, 18351838 (1999); A. Sørensen and K. Mølmer, Phys. Rev. Lett. **82**, 19711974 (1999).
- [16] M. A. Nielsen, and I. L. Chuang, *Quantum Computation and Quantum Information* (Cambridge University Press, Cambridge, 2000).
- [17] A. Svandal, and J. P. Hansen, Phys. Rev. A, **65**, 033406 (2002).
- [18] A. R. P. Rau, Phys. Rev. A **61**, 032301 (2000); A. R. P. Rau, G. Selvaraj, and D. Uskov, Phys. Rev. A **71**, 062316 (2005).
- [19] F. T. Hioe, J. Opt. Soc. B **4**, 1327 (1987).
- [20] Yu. N. Demkov and V. I. Osherov, Zh. Exp. Teor. Fiz. **53**, 1589 (1967) [Sov. Phys.-JETP **26**, 915 (1968)].
- [21] V. N. Ostrovsky and H. Nakamura, J. Phys. A **30**, 6939 (1997).
- [22] Yu. N. Demkov and V. N. Ostrovsky, Phys. Rev. A **61**, 032705 (2000); J. Phys. B **34**, 2419 (2001).
- [23] H. Kobayashi, N. Hatano, and S. Miyashita, Physica A **265**, 565 (1999).
- [24] A. A. Rangelov, J. Piilo, and N. V. Vitanov, Phys. Rev. A **72**, 053404 (2005).
- [25] E. Majorana, Nuovo Cimento **9**, 43 (1932).
- [26] N. A. Sinitzyn, Phys. Rev. B **66**, 205303 (2002).
- [27] A. K. Kazansky and V. N. Ostrovsky, J. Phys. B **29**, L855 (1996).
- [28] M. Førre, H. M. Nilsen and J. P. Hansen, Phys. Rev. A **65**, 053409 (2002).
- [29] The  $4 \times 4$  matrices for various interaction operators were written down explicitly in Refs. [14, 18].
- [30] E. E. Nikitin and S. Ya. Umanskii, *Theory of Slow Atomic Collisions* (Springer, Berlin, 1984).
- [31] L. D. Landau, Phys. Z. Soviet Union **2**, 46 (1932).
- [32] C. Zener, Proc. Royal Society A **137**, 696 (1932).
- [33] E. C. G. Stueckelberg, Helvetica Physica Acta **5**, 369 (1932).
- [34] F. Di Giacomo and E. E. Nikitin, Usp. Fiz. Nauk **175**, 545 (2005) [Physics – Uspekhi **48**, 515 (2005)].
- [35] M. V. Volkov and V. N. Ostrovsky, J. Phys. B **37**, 4069 (2004).
- [36] M. V. Volkov and V. N. Ostrovsky, J. Phys. B **38**, 907 (2005).
- [37] N. V. Vitanov, Phys. Rev. A **59**, 988 (1999).
- [38] S. Brundobler and V. Elzer, J. Phys. A **26**, 1211 (1993).
- [39] A. V. Shytov, Phys. Rev. A **70**, 052708 (2004).
- [40] T. Usuki, Phys. Rev. B **56**, 13360 (1997).
- [41] The system of crossing between two infinite equidistant bands of potential curves was solved by Demkov and Ostrovsky and Demkov [J. Phys. B **28**, 403 (1995)] and Demkov *et al* [J. Phys. A **28**, 4361 (1995)].
- [42] N. A. Sinitzyn, J. Phys. A **37**, 10691 (2004).

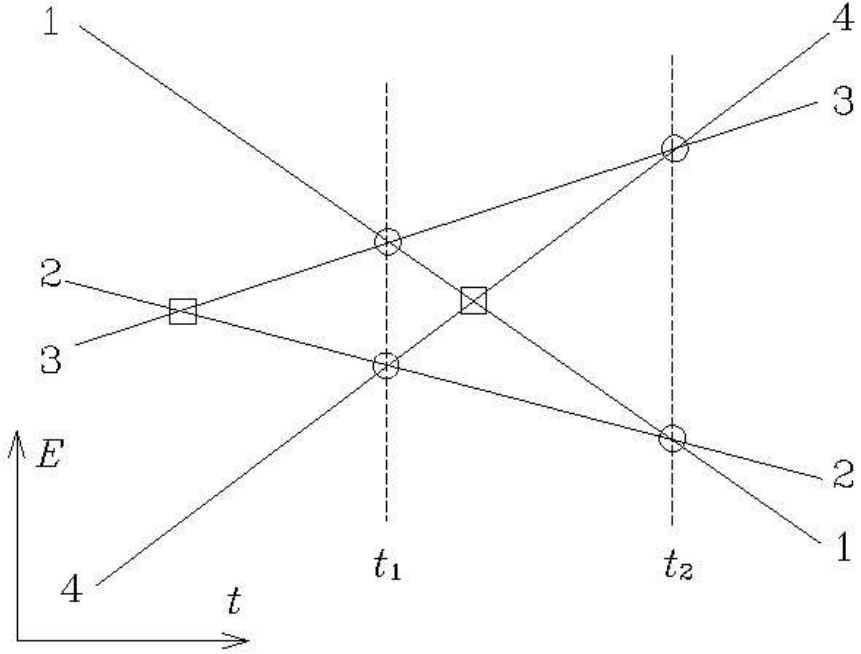


FIG. 1: Diabatic potential curves for the four-state model with the Hamiltonian of Eq. (2.6). In the generic case, there are no parallel curves. Altogether 6 curve crossings take place. Open circles mark crossings between curves  $i$  and  $j$  with non-zero couplings  $V_{ij}$ . Open boxes mark crossings between non-interacting curves,  $V_{ij} = 0$ . Due to the specific form of the model Hamiltonian  $H$  (2.6), two pairs of curves cross simultaneously at instants of time  $t_1$  and  $t_2$ .

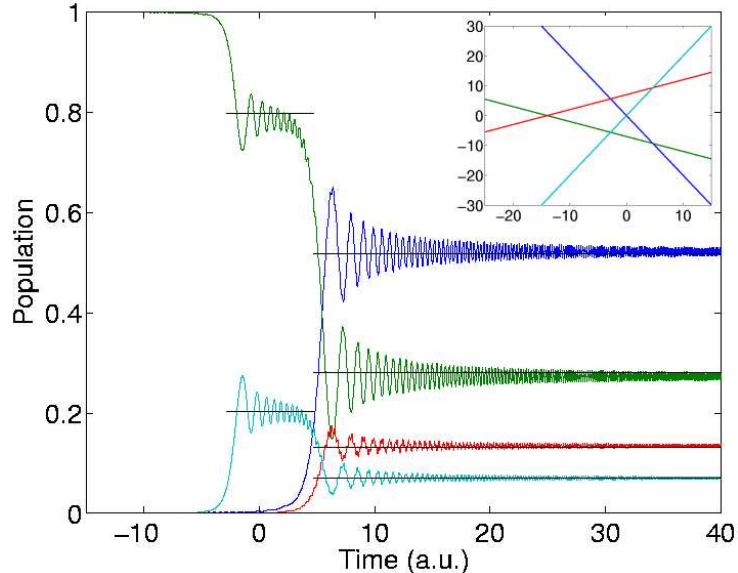


FIG. 2: (Color online) Dynamics of a particular system with the Hamiltonian of the form of Eq. (2.6), with the diabatic diagonal energies displayed in Fig. 1. The parameters are listed in the text. The initial state is diabatic state 2 (green in the color version), so the final LZ transition probabilities are given by the second column of the matrix in Eq. (2.9) with the transition probabilities at each crossing given in Eq. (4.5).

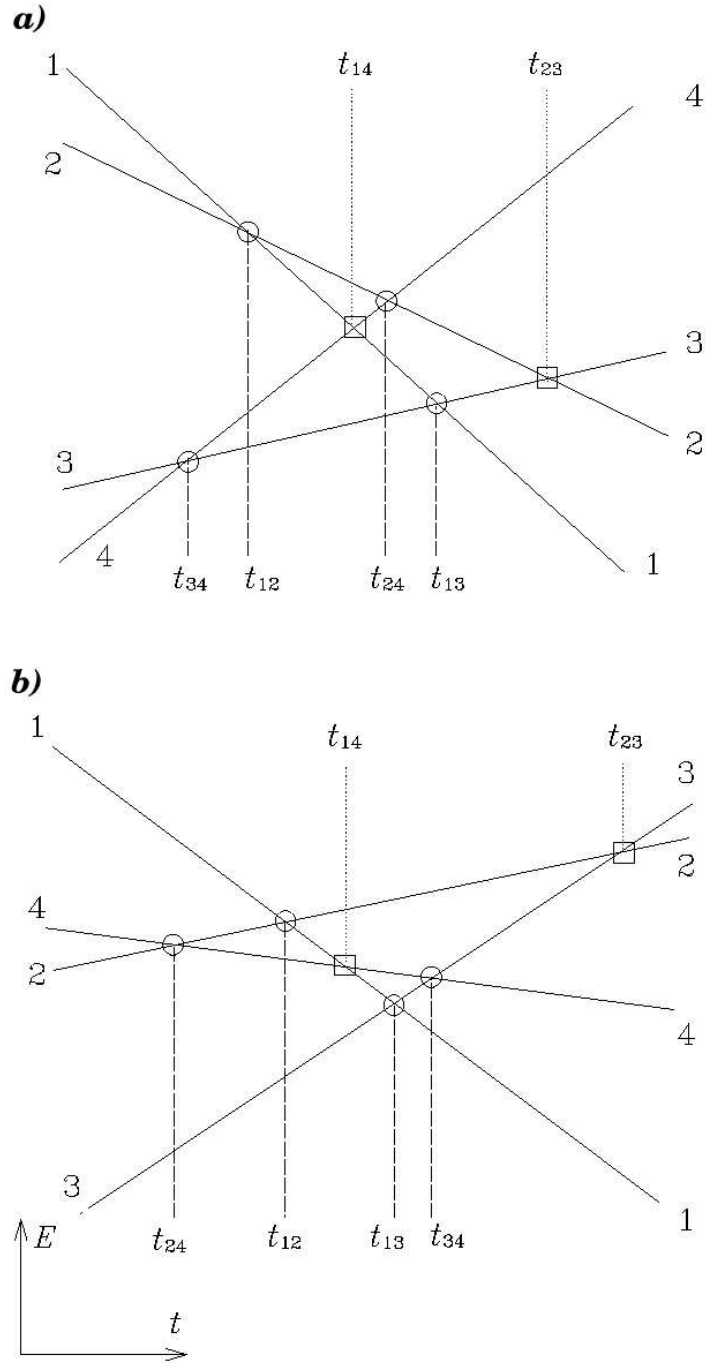


FIG. 3: Same as in Fig. 1, but for the more general model Hamiltonian  $H_g$  (2.12). All curve crossings occur at different instants of time. In case (a), neglecting second order transitions, all the state-to-state transitions occur via single paths, while in case (b), this property is absent.

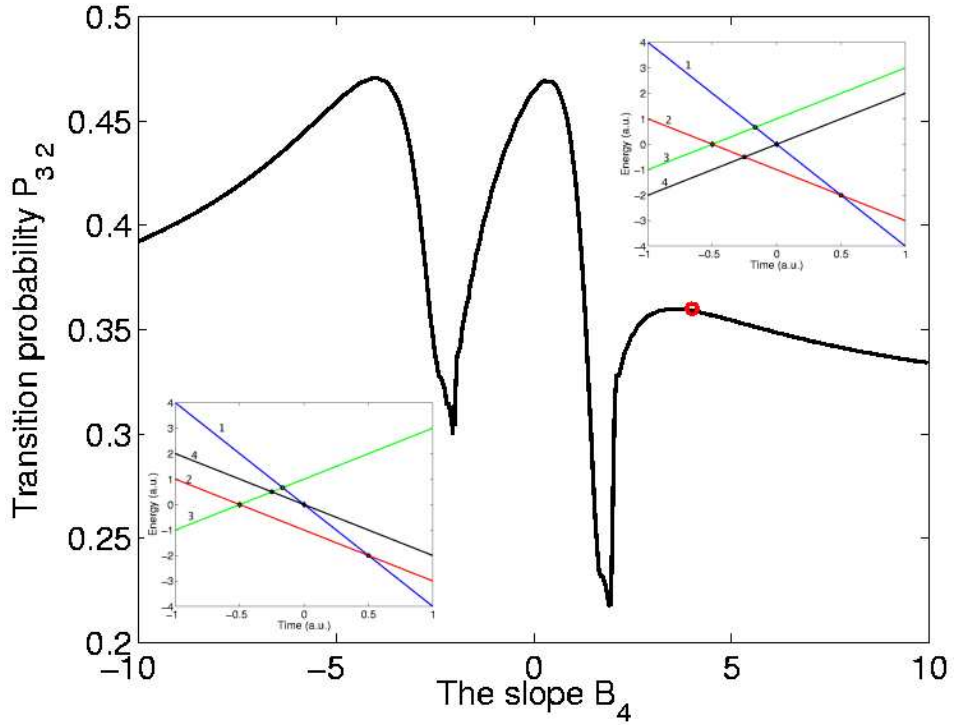


FIG. 4: (Color online) Transition probability  $P_{32}$  depending on the slope parameter  $B_4$ . It is implied that the variation of  $B_4$  is achieved by rotating the potential curve 4 in Fig. 1 around the point of its crossing with the potential curve 1. The inserted plots corresponds to the special cases  $B_4 = \pm 2$ . The Hamiltonian parameters are listed in the text. Exact result for  $P_{32}$  is available only at  $B_4 = 4$  (red circle).

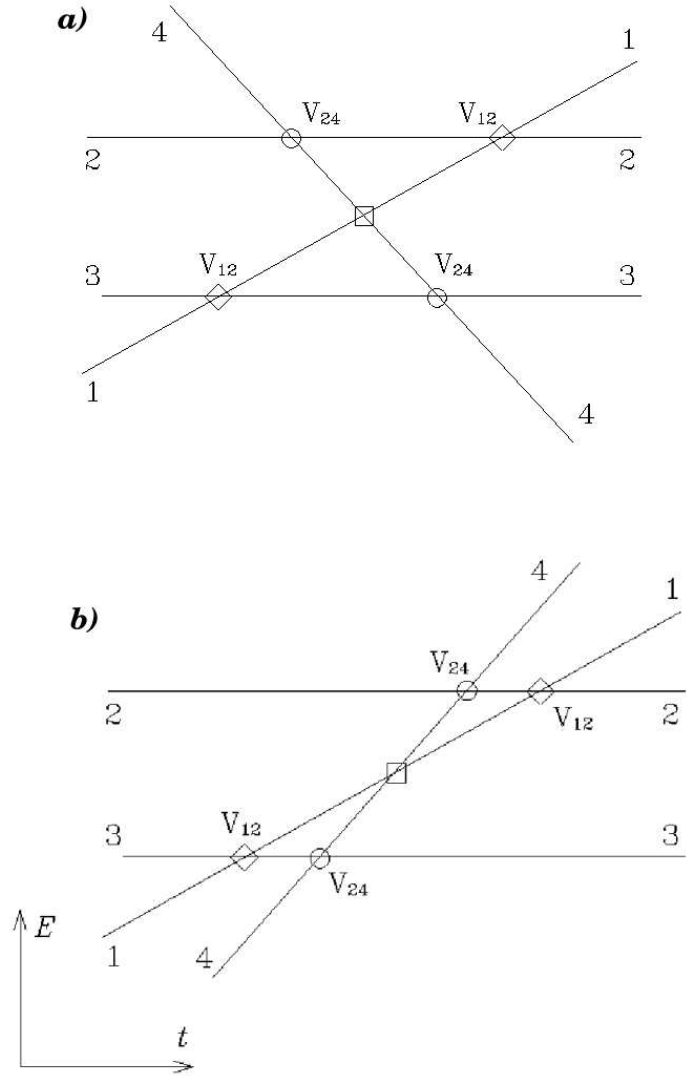


FIG. 5: Diabatic potential curves in the four-state generalized bow-tie model with the Hamiltonian (4.9). Open circles and diamonds mark crossings with pairwise identical couplings; open box marks crossing of non-interacting potential curves. In case (a) the slopes  $B_1$  and  $B_2$  have opposite signs ( $B_1 > 0, B_2 < 0$ ) and all the state-to state transitions occur via single paths, while in case (b) ( $B_4 > B_1 > 0$ ) two paths are allowed for the transitions  $1 \rightarrow 1$ ,  $1 \rightarrow 3$ ,  $2 \rightarrow 1$  and  $2 \rightarrow 3$ .

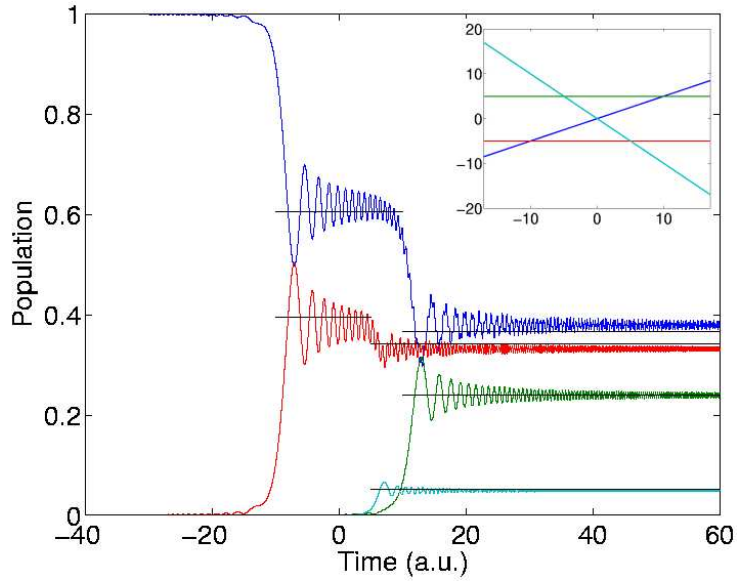


FIG. 6: (Color online) Dynamics corresponding to a Hamiltonian of the form of Eq. (4.12) where the slopes of the non-parallel potential curves have opposite signs (see Fig. 5a). The diabatic energy curves specific of this case are shown in the inserted figure. The system is initially prepared in diabatic state 1 (blue in the color version). The final probabilities coincide with the first row of the matrix in Eq. (4.15).

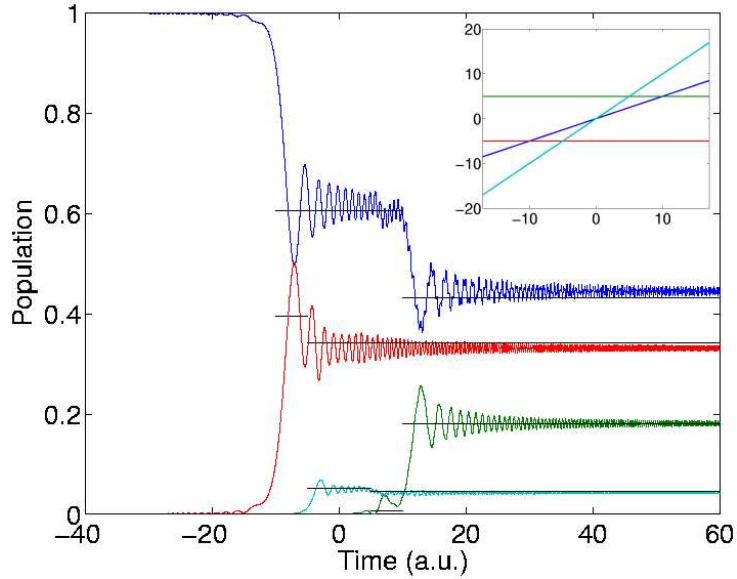


FIG. 7: (Color online) The same as in Fig. 6 except for the signs of the slopes of the non-parallel potential curves, which are the same in this case. This removes the single path nature of the system. However, in this particular case, the final transition probabilities are still independent of the adiabatic phases, as explained in detail in Ref. [22]. The final LZ-probabilities (the horizontal lines) corresponds to the first row in Eq. (4.17).

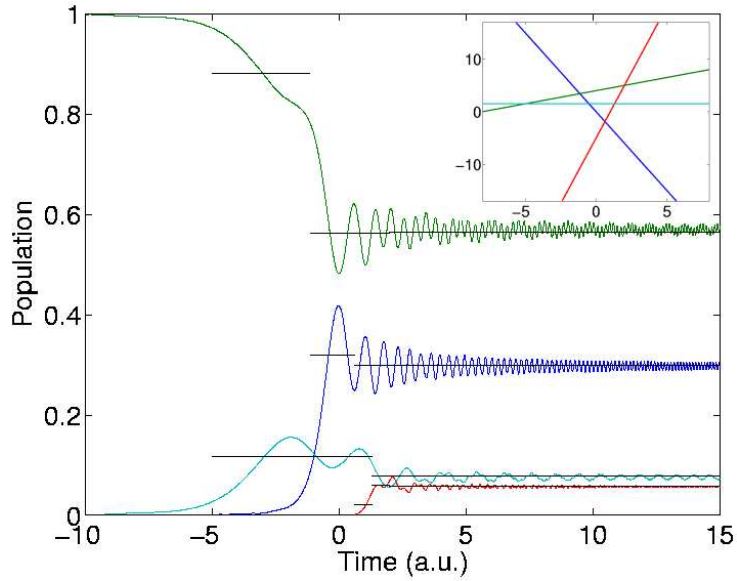


FIG. 8: (Color online) Dynamics given by the general 4-state Hamiltonian in Eq. (2.12) (see Fig. 3) when starting out in diabatic state 2 (green in the color version), which initially is adiabatic state number 2 as well. The LZ transition probabilities are found by Eq. (3.12), which includes the effect of the adiabatic phase. Furthermore, the instantaneous transition matrices at the second order crossings (crossings number 3 and 6) takes into account the possibility of transitions. The diagonal energies are indicated by the inserted figure, and the couplings are in this case  $V_{12} = 0.5$ ,  $V_{13} = 0.3$ ,  $V_{24} = 0.1$  and  $V_{34} = 0.4$ . The strong oscillations in the diabatic populations may give the impression that the agreement of the MLZ-predictions with the final probabilities is somewhat coincidental. However, if the dynamic populations of the *adiabatic* states were displayed, we would see that the oscillations would die out much more rapidly in this basis.

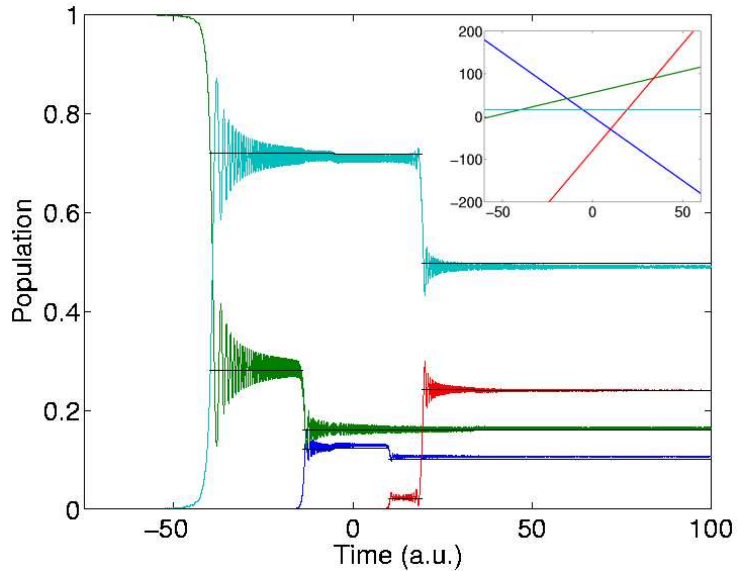


FIG. 9: (Color online) Dynamics of a system with the same generic structure as Fig. 8, but on a different time scale. Here the couplings are  $V_{12} = 0.6$ ,  $V_{13} = 0.5$ ,  $V_{24} = 0.45$  and  $V_{34} = 0.4$ . As in the prior figure, the accuracy of the model is fully relying on the inclusion of the adiabatic and dynamic phases and the use of correct signs in the S-matrices. Since the oscillations in the populations of the diabatic states following each crossings has had time to die out, second order transitions at  $t = -5.3$  can be seen in the figure.

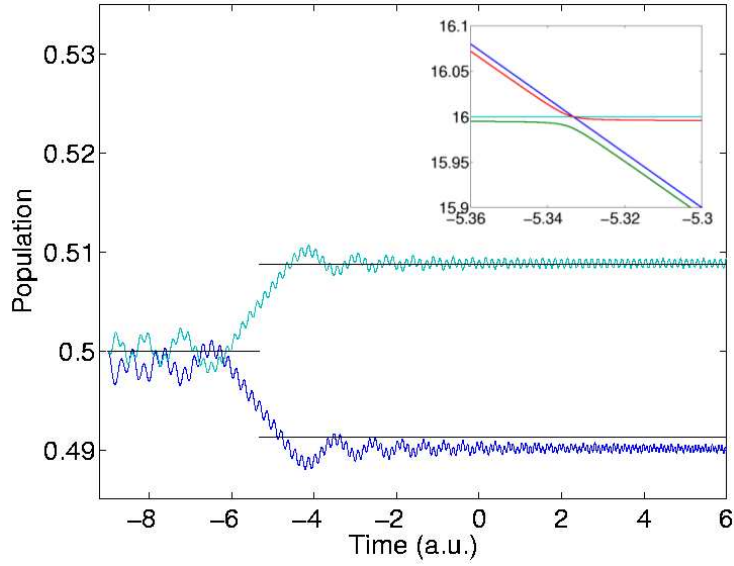


FIG. 10: (Color online) This figure demonstrates the significance of second order transitions. The parameters are the same as in Fig. 9, and the initial state is a mix of equal populations of the crossing diabatic states at a time shortly before the second order crossing. In this case, both diabatic and adiabatic diagonal energies are shown in the vicinity of the second order (avoided) crossing in the upper right corner. As we see, both populations are shifted approximately by 1 % although the probability of a diabatic transition is very low;  $1 - p_3 = 8.3 \cdot 10^{-5}$ .



# Paper VIII

Sølve Selstø and Morten Førre

**Coherent Single-Electron Transport between Coupled Quantum Dots**

*Submitted to Physical Review.*



# Coherent Single-Electron Transport between Coupled Quantum Dots

Sølve Selstø<sup>1</sup> and Morten Førre<sup>1</sup>

<sup>1</sup>*Department of Physics and Technology, University of Bergen, N-5007 Bergen, Norway*

We propose a method for a fully coherent transport of single electrons between the ground states of two anharmonic coupled quantum dots. The transition is achieved as a result of an intrinsic interplay between an external applied radio-frequency field and the interdot tunnel coupling between the single dot states. We have developed a 4-level model for the system, and full quantitative agreement with the exact solution of the time-dependent Schrödinger equation is obtained for a wide range of field parameters. The analytical model has the advantage that it can be used as guidance in the actual design of such systems.

PACS numbers: 73.21.La, 73.63.Kv, 73.23.Hk, 03.67.-a, 85.35.Bc

The ability to fabricate and operate single or few-electron solid state quantum devices of nanometer sizes will have great impact on future technology. Quantum dots are one example of such devices that have numerous potential applications in biology, chemistry and physics. They constitute one of the most potent systems for full experimental control at the quantum level [1]. Two (or more) quantum dots may be interconnected to form so-called 'artificial molecules' [2]. These systems have proved to be promising candidates for a quantum bit or 'qubit', the basic component of a quantum computer [3]. The ability to create and maintain coherence for a sufficiently long time is one of the main obstacles on the way to a physical implementation of a solid state quantum computer. Recently, coherence times of about 200 ns were observed in a double quantum dot system [4].

The possibility to address and manipulate single charge states in the quantum dot is a prerequisite for an efficient operation of solid state quantum devices. Coupled quantum dots have been the subject of extensive experimental and theoretical studies [5–10]. Several schemes for controlled transport of single electrons between such two-dimensional quantum dots have been experimentally demonstrated [4, 10], and experimental methods to determine the interdot tunnel coupling both for ground and excited state have been developed [10, 11]. New techniques for coherent manipulation of charge transport in quantum dot arrays [12] and asymmetric double quantum dots [13] have been proposed.

In this Letter we present a realistic and robust method to transfer a single electron with unit probability between the (quasi stationary) ground states of two coupled two-dimensional quantum dots. The initial coupling between the two ground states is so small that they remain stationary for times many orders of magnitude longer than the manipulation time. The driving force is an external microwave field which is in resonance with the transition between the ground state and an excited quasi stationary state in each respective well. The actual transition between the wells is accomplished by tunneling between the two coupled excited states rather than between the ground states. Under certain conditions, only four quantum states in the double well are involved in the dynamics (see Fig. 1). We have developed an analytical model for the coherent transition that coincides with exact *ab initio* cal-

culations for a wide range of field parameters. The model has general validity and could in principle be applied to other coupled systems like e.g. coupled Cooper-pair qubits in a Josephson circuit [14]. The switching is robust in the sense that the actual shape of the microwave pulse is not crucial for the efficiency of the gate, and the method is applicable to almost any symmetric anharmonic double well potential. The parameters of the gate may be optimized such that a fully coherent charge transfer can take place within only a fraction of the natural decoherence time in the dots [4]. Our starting point is the two-dimensional double well confining potential,

$$W(x, y) = \frac{1}{2}m^* \frac{\omega_0^2}{D^2} [(x - D/2)^2(x + D/2)^2 + (y^4 + 2D|y|^3 + D^2y^2)], \quad (1)$$

where  $D$  is the interdot distance, and  $\omega_0$  defines the strength of the potential barrier. In this Letter we, apply reduced atomic units (a.u.\* ) throughout, in order to maintain generality of the results. In these units  $\hbar = m^* = e = 1$ , where  $m^*$  is the effective mass of the electron. For a GaAs material  $m^* = 0.067m_e$ , with  $m_e$  being the free electron mass. If we set  $\hbar\omega_0 = 3$  meV the unit of time becomes about 0.2 ps and the unit of length about 20 nm.

The evolution of the system is governed by the time-dependent Schrödinger equation,

$$i\frac{\partial}{\partial t}\Psi = \left\{ -\frac{1}{2} \left( \frac{\partial^2}{\partial x^2} + \frac{\partial^2}{\partial y^2} \right) + W(x, y) + xE(t) \right\} \Psi, \quad (2)$$

where  $E(t)$  is the external  $\hat{x}$  polarized microwave field. Here, we simply assume that the field takes the form of a constant intensity monochromatic field, i.e.  $E(t) = E_0 \sin(\omega t)$ . The Schrödinger equation is solved numerically based on accurate Fourier transform split operator methods [15]. The wave function is initially prepared in the (pseudo) ground state of dot 1. The net population transfer to dot 2 as a function of time is shown for a particular case in Fig. 1, for a moderate value of the interdot separation ( $D = 7$ ). At the instant when this probability becomes 1 after about 1800 time units, the field is switched off. At that time practically all the population is left in the ground and 1st excited states in dot 2, with only a very small interference from the 2nd excited state. After the field

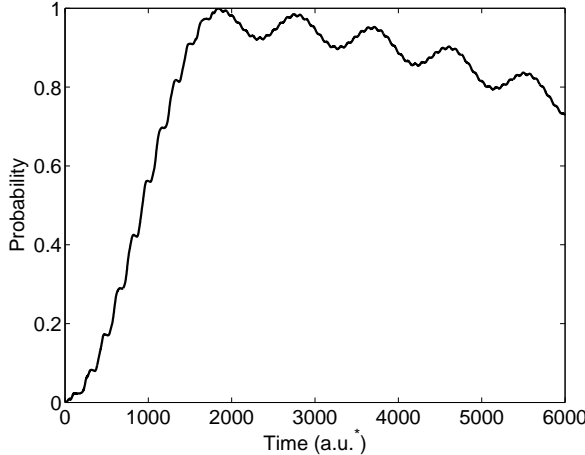


FIG. 1: The probability for electron transport from dot 1 to dot 2 versus time for a double quantum dot with  $D = 7$  and  $\omega_0 = 1$ . The microwave field is resonant with the first excited state in each dot, i.e.  $\omega = 0.906\omega_0$ , and the intensity of the field is  $E_0 = 0.05$ . In this particular example the field is turned off at an instant ( $t \sim 1800$  time units) when the population is in a superposition of the ground state and the first (and second) excited state in dot 2. The Rabi-like oscillations in the population are due to tunneling between the two 1st excited states in dot 1 and 2, and the overall decrease indicates tunneling between the quasi stationary ground states of each dot. The fast oscillations superimposed on the longer oscillations stem from the small fraction of the total population that is left in the 2nd excited state after the field is turned off.

is turned off, the population will oscillate in a Rabi-like manner between the respective quasi stationary states in dot 1 and 2 due to the tunnel coupling between them. The signatures of these Rabi oscillations are displayed in Fig. 1. The overall decay of the population stems from the tunneling between the two ground states in dot 1 and 2, respectively, and shows that the "lifetime" of these states is only a factor 10 longer than the total transition time. Therefore, in the rest of this Letter, we set  $D = 10$  in order to keep the ground states stationary for times many orders of magnitude longer than the manipulation time.

The particular example given in Fig. 1 reveals that the whole dynamics is essentially restricted to four quantum levels, i.e. to two states in each dot. These observations inspire a model given in a basis consisting of two states with their wave functions essentially contained within each of the dots. The energy of both states lies below the interdot barrier. We label the states  $|g\ i\rangle$  for the ground states and  $|e\ i\rangle$  for the excited states where  $i = 1, 2$  indicates the dot (see Fig. 2). The microwave frequency  $\omega$  is in resonance with the energy separation  $\varepsilon$  between the states. Due to the anharmonicity of the potential, we assume that the other excited states can be neglected in the model for moderate field intensities and for not too long interaction times. Now, with the basis defined in Fig. 2, the Schrödinger equation reduces to a set of four coupled equations,  $i\dot{\mathbf{c}} = H\mathbf{c}$ , where  $\mathbf{c} =$

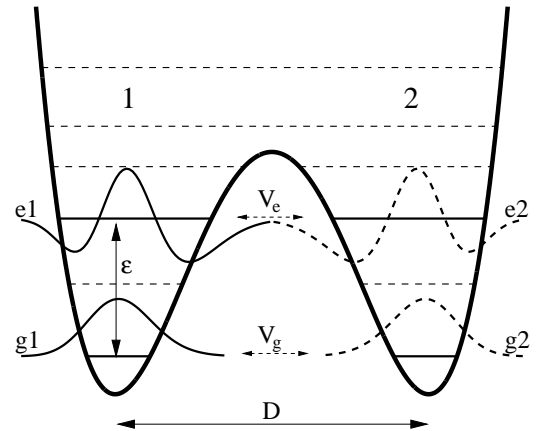


FIG. 2: The double well potential, Eq. 1, in the  $x$ -direction for  $D = 10$  and  $\omega_0 = 1$  with the single dot wave functions corresponding to the ground state and the third excited state. The tunnel coupling between the two excited states and the ground states of the two dots are given by  $V_e$  and  $V_g$ , respectively.

$(\langle g1|\Psi\rangle, \langle e1|\Psi\rangle, \langle e2|\Psi\rangle, \langle g2|\Psi\rangle)$ , and the Hamiltonian

$$H = \begin{pmatrix} -\frac{\varepsilon}{2} & d \sin(\omega t) & 0 & V_g \\ d \sin(\omega t) & \frac{\varepsilon}{2} & V_e & 0 \\ 0 & V_e & \frac{\varepsilon}{2} & d \sin(\omega t) \\ V_g & 0 & d \sin(\omega t) & -\frac{\varepsilon}{2} \end{pmatrix}. \quad (3)$$

The coupling between the lower and the upper states are induced by the microwave field, and  $d = E_0 \langle g1|(x + D/2)|e1\rangle$ . The constant coupling  $V_e$  ( $V_g$ ) is given by the Rabi frequency of the oscillations between the excited states (ground states). Typically, the tunnel coupling  $V_g \ll V_e$ , and  $V_g$  can be neglected for  $D > 7$ .

The 4-state system may be decoupled to two 2-level systems by defining a new basis set given by the sum (*gerade*) and difference (*ungerade*), respectively, of corresponding single-well states. In the adiabatic representation, this transformation casts the Hamiltonian into the decoupled form,

$$H_A = \begin{pmatrix} H_+ & \mathbf{0} \\ \mathbf{0} & H_- \end{pmatrix}, \quad (4)$$

where

$$H_{\pm} = \begin{pmatrix} -\zeta_{\pm} \pm \frac{V_e + V_g}{2} & i \frac{d\omega V_{\pm} \cos(\omega t)}{2(d^2 \sin^2(\omega t) + V_{\pm}^2)} \\ -i \frac{d\omega V_{\pm} \cos(\omega t)}{2(d^2 \sin^2(\omega t) + V_{\pm}^2)} & \zeta_{\pm} \pm \frac{V_e + V_g}{2} \end{pmatrix}. \quad (5)$$

Here,  $\zeta_{\pm}(t) \equiv \sqrt{d^2 \sin^2(\omega t) + V_{\pm}^2}$  and  $V_{\pm} \equiv [\varepsilon \pm (V_e - V_g)]/2$ . For high field strengths, i.e. when  $(d/V_{\pm})^2 \gg 1/2$ , each of these sub-systems coincides with the well known Landau-Zener model [16, 17]. However, here we consider only weak fields, and the probability of transition at resonance by absorption or emission of single photons becomes [17, 18]

$$p_{\pm} = \left( \frac{\pi d}{4V_{\pm}} \right)^2,$$

which is valid for  $(d/V_{\pm})^2 \ll 1$ . In the adiabatic basis, the evolution of each sub-system over a half cycle of the field is given by the propagator

$$S_{\pm} = \begin{pmatrix} \sqrt{1-p_{\pm}}e^{i\gamma_{\pm}} & \sqrt{p_{\pm}} \\ -\sqrt{p_{\pm}} & \sqrt{1-p_{\pm}}e^{-i\gamma_{\pm}} \end{pmatrix}. \quad (6)$$

The phase shifts  $\gamma_{\pm}$  arise as a consequence of the frequency being slightly off resonance. This, in turn, is due to the lifting of the degeneracy of the system induced by the tunnel couplings  $V_e$  and  $V_g$ . The shifts are  $\gamma_{\pm} = \frac{2}{\omega} \left[ \sqrt{d^2 + V_{\pm}^2} E \left( \frac{d}{\sqrt{d^2 + V_{\pm}^2}} \right) - \sqrt{d^2 + \frac{\varepsilon^2}{4}} E \left( \frac{d}{\sqrt{d^2 + \frac{\varepsilon^2}{4}}} \right) \right]$ , where  $E(k)$  is the complete elliptic integral of the second kind [19].

The total propagator after  $N$  half field-cycles is found by exponentiating the  $S_{\pm}$ -matrices by  $N$ , multiplying them with the phases  $\exp(\pm i(V_e + V_g)/2t)$ , respectively, and putting all together in a 4 by 4 matrix:

$$\mathcal{U} = \begin{pmatrix} e^{-i(V_e+V_g)/2t} S_+^N & \mathbf{0} \\ \mathbf{0} & e^{i(V_e+V_g)/2t} S_-^N \end{pmatrix} \quad (7)$$

Then, the probability of the  $g1 \rightarrow g2$  transition is found as  $|\langle g2 | \mathcal{U} | g1 \rangle|^2$ . Finally, the result may be written as

$$P(g1 \rightarrow g2) = \frac{1}{4} \left( X_+ + X_- - 2\sqrt{X_+ X_-} \cos \theta \right), \quad (8)$$

with

$$\begin{aligned} X_{\pm} &= 1 - \frac{4r_{\pm} \sin^2(N\phi_{\pm})}{(1+r_{\pm})^2} \\ r_{\pm} &= \frac{1}{p_{\pm}} [1 - (1-p_{\pm}) \cos(2\gamma_{\pm}) + \\ &\quad 2 \sin \gamma_{\pm} \sqrt{1-p_{\pm} - (1-p_{\pm})^2 \cos^2 \gamma_{\pm}}] \\ \phi_{\pm} &= \cos^{-1} \left( \sqrt{1-p_{\pm}} \cos \gamma_{\pm} \right) \\ \theta &= (V_e + V_g)t + \tan^{-1} \left[ \frac{r_- - 1}{r_+ + 1} \tan(N\phi_-) \right] - \\ &\quad \tan^{-1} \left[ \frac{r_+ - 1}{r_+ + 1} \tan(N\phi_+) \right]. \end{aligned} \quad (9)$$

Figure 3 shows the probability of populating the ground state of dot 2 when starting out in the ground state of dot 1 for three different field strengths, namely  $E_0 = 0.01, 0.05$  and  $0.1$ , respectively. The solution of the time-dependent Schrödinger equation is shown along with the prediction of the model, Eq. (8). In all cases, the *ab initio* calculations demonstrate almost complete transfer. We see that for the two lower field strengths, the coincidence with the model is practically complete, whereas discrepancies are seen for  $E_0 = 0.1$ . This is due to the breakdown of the 4-level approximation, i.e. for higher field strengths more than four states are involved in the dynamics.

In Fig. 4 snapshots of the wave function at different times during the process corresponding to Fig. 3 (intermediate) are

shown. We clearly see that the intermediate states  $|e1\rangle$  and  $|e2\rangle$  are populated during the interaction.

Concerning the transport time, we find that for the more intense microwave fields, it is about the double of the tunneling time between the excited states,  $\tau = \pi/2V_e$ , which accords fairly well with intuition. For the weaker fields, however, the transport time is mainly determined by the characteristic Rabi-flopping frequency between the ground and excited states. These observations are confirmed in the model. Since the tunnel coupling  $V_e$  (and  $V_g$ ) is weak,  $V_e/\varepsilon \simeq 0$ , Eq. (8) simplifies to

$$P(g1 \rightarrow g2) = \frac{1}{2} \left( 1 - \frac{4r_+ \sin^2(N\phi)}{(1+r_+)^2} \right) (1 - \cos \theta). \quad (10)$$

Then, the condition for transport may be formulated as

$$N\phi \simeq 0 \pmod{\pi} \quad \text{and} \quad \theta \simeq \pi \pmod{2\pi}. \quad (11)$$

As the field strength increases, the trigonometric terms of Eq. (9) become less important, and the second criterion is fulfilled for  $t \simeq \pi/V_e = 2\tau$ . In this limit,  $N\phi$  varies more rapidly than  $\theta$ , so that the first criterion does not modify the transport time much. Also for weaker fields, this criterion is less significant since the sine term in Eq. (10) vanishes in this limit. However, the importance of the trigonometric terms in Eq. (9) can not be neglected, resulting in a transport time much longer than  $2\tau$ .

In conclusion, we have presented a realistic method for coherent transfer of a single electron between the ground states of two coupled quantum dots. The transition takes place on the picosecond time scale, which is far below recently achieved coherence times in corresponding systems. We have developed an analytical model for the dynamics that can be used to optimize the parameters of the system in order to achieve the desired fidelity and operation time of the gate. We have demonstrated that the coherent charge transport between the wells can become an almost 100 % reversible process, which is an important property of a working two-qubit gate in a quantum computer.

The present research was supported by the Norwegian Research Council through the NANOMAT program, and the Nordic Research Board NordForsk.

- 
- [1] S. M. Reimann and M. Manninen, Rev. Mod. Phys. **74**, 1283 (2002).
  - [2] T. H. Oosterkamp, T. Fujisawa, W. G. van der Wiel, K. Ishibashi, R. V. Hijman, S. Tarucha, and L. P. Kouwenhoven, Nature (London) **395**, 873 (1998).
  - [3] J. R. Petta, A. C. Johnson, J. M. Taylor, E. A. Laird, A. Yacoby, M. D. Lukin, C. M. Marcus, M. P. Hanson, and A. C. Gossard, Science **309**, 2180 (2005).
  - [4] J. Gorman, D. G. Hasko, and D. A. Williams, Phys. Rev. Lett. **95**, 090502 (2005).
  - [5] W. G. van der Wiel, S. De Franceschi, J. M. Elzerman, T. Fujisawa, S. Tarucha, and L. P. Kouwenhoven, Rev. Mod. Phys. **75**, 1 (2003).

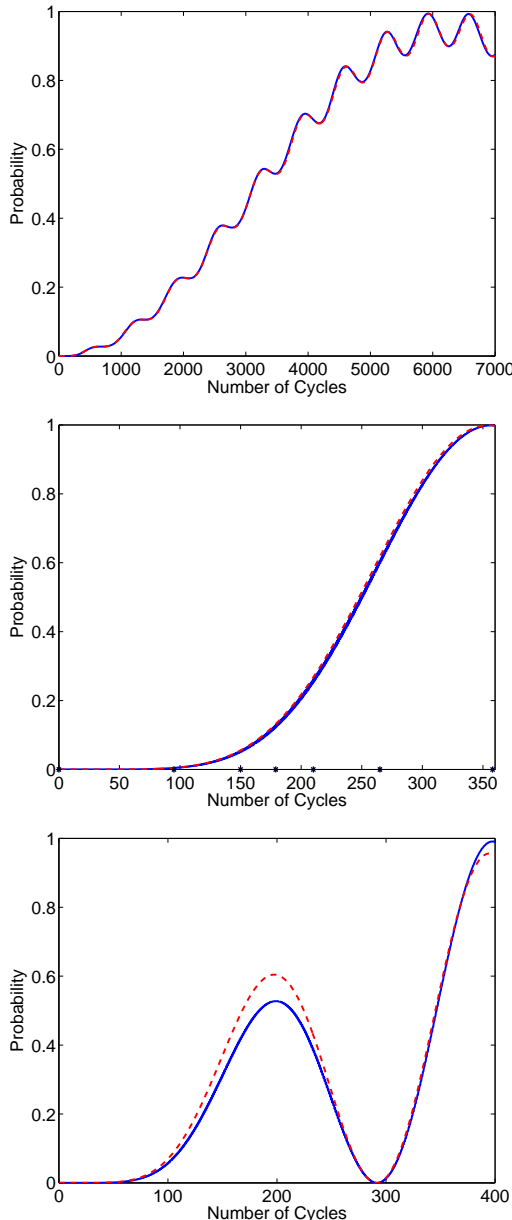


FIG. 3: (Color online). Probability of finding the electron in the ground state of dot 2 as a function of the number of field cycles for  $E_0 = 0.01$  (upper),  $E_0 = 0.05$  (intermediate), and  $E_0 = 0.1$  (lower), with  $\omega_0 = 1$  and  $\omega = \varepsilon = 1.78\omega_0$ . The wave function was initially prepared in the ground state of dot 1. The full (blue) curves stem from *ab initio* calculations, and the dashed (red) curves are the predictions of the model, Eq. 8.

- [6] F. H. L. Koppens, J. A. Folk, J. M. Elzerman, R. Hanson, L. H. Willems van Beveren, I. T. Vink, H. P. Tranitz, W. Wegscheider, L. P. Kouwenhoven, and L. M. K. Vandersypen, *Science* **309**, 1346 (2005).
- [7] M. T. Woodside and P. L. McEuen, *Science* **296**, 1098 (2002); G. Schedelbeck, W. Wegscheider, M. Bichler, and G. Abstreiter, *Science* **278**, 1792 (1997).

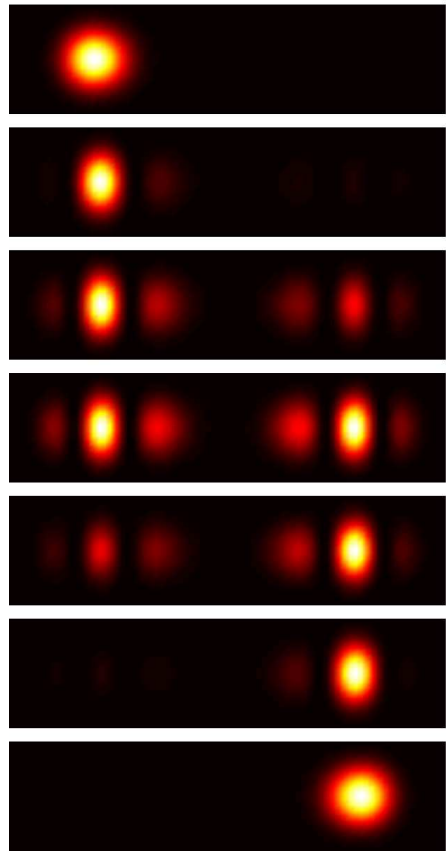


FIG. 4: (Color online). Snapshot of the electronic probability density for  $E_0 = 0.05$  and  $D = 10$  at 7 instants, after 0 (upper), 95, 150, 179, 210, 265, and 358 (lower) oscillations of the field. The times are indicated with '\*' in Fig. 3 (intermediate). The axis ranges are from  $x = -8$  to  $x = 8$  and  $y = -2$  to  $y = 2$ .

- [8] R. Aguado and L. P. Kouwenhoven, *Phys. Rev. Lett.* **84**, 1986 (2000).
- [9] J. C. Chen, A. M. Chang, and M. R. Melloch, *Phys. Rev. Lett.* **92**, 176801 (2004).
- [10] J. R. Petta, A. C. Johnson, C. M. Marcus, M. P. Hanson, and A. C. Gossard, *Phys. Rev. Lett.* **93**, 186802 (2004).
- [11] T. Hayashi, T. Fujisawa, H. D. Cheong, Y. H. Jeong, and Y. Hirayama, *Phys. Rev. Lett.* **91**, 226804 (2003).
- [12] K. Saito and Y. Kayanuma, *Phys. Rev. B* **70**, 201304(R) (2004).
- [13] A. A. Batista, *Phys. Rev. B* **73**, 075305 (2006).
- [14] Yu. A. Pashkin, T. Yamamoto, O. Astafiev, Y. Nakamura, D. V. Averin, and J. S. Tsai, *Nature (London)* **421**, 823 (2003); Y. Nakamura, Yu. A. Pashkin, and J. S. Tsai, *Nature (London)* **398**, 786 (1999).
- [15] M. D. Feit, J. A. Fleck, and A. Steiger, *J. Comput. Phys.* **47**, 412 (1982).
- [16] C. Zener, *Proc. R. Soc. A* **137**, 696 (1932).
- [17] M. Førre, *Phys. Rev. A* **70**, 013406 (2004).
- [18] J. H. Shirley, *Phys. Rev.* **138**, B979 (1965).
- [19] I. S. Gradshteyn and I. M. Ryzhik, *Table of Integrals, Series, and Products* (Academic Press Inc., New York, 1994).

# Paper IX

Sølve Selstø, Alicia Palacios, Jorge Fernández, and Fernando Martín

**Electron angular distribution in resonance enhanced two-photon ionization of  $\text{H}_2^+$  by ultrashort laser pulses**

*To be submitted to Physical Review.*



# Electron angular distribution in resonance enhanced two-photon ionization of H<sub>2</sub><sup>+</sup> by ultrashort laser pulses

S. Selstø\*, A. Palacios, J. Fernández, and F. Martín

Departamento de Química C-9, Universidad Autónoma de Madrid, 28049 Madrid, Spain.

(Dated: June 22, 2006)

We present a theoretical study of the electron angular distribution produced in resonance enhanced two-photon ionization of the H<sub>2</sub><sup>+</sup> molecular ion using ultrashort laser pulses. The method consists in solving the time dependent Schrödinger equation and includes all electronic and vibrational degrees of freedom. Differential (in proton energy and electron emission solid angle) ionization probabilities have been evaluated for various photon energies, laser intensities and pulse durations. We show that (1+1)-REMPI leads to angular distributions significantly different from those produced in direct two-photon ionization. The REMPI process is observed even at photon energies not matching the energy difference between two electronic states in a perfect vertical transition. Interestingly, there is no trace of REMPI effects when the fully differential probabilities are integrated over proton energy.

PACS numbers: 33.80.Rv, 33.80.-b,

## I. INTRODUCTION

Experimental approaches that make use of high-order harmonic generation [1, 2] or free electron lasers [3–5] are currently able to provide fs laser pulses with wave lengths in the VUV/XUV region of the electromagnetic spectrum. The use of such pulses has opened up the way to study elementary two- and three-photon ionization processes in simple atoms (He, Ne, ...) [6, 7] and molecules (H<sub>2</sub><sup>+</sup>, H<sub>2</sub>, ...) [8]. These systems are accessible to accurate theoretical descriptions, which is crucial to guide theoretical developments in strong field multiphoton ionization and to reach a deeper insight on the basic mechanisms involved in the latter process.

The study of multiphoton ionization in molecules is interesting because vibration and rotation may significantly affect the ionization process. This is the case of, e.g., resonance enhanced multiphoton ionization (REMPI), in which the molecule may have enough time to vibrate in the intermediate electronic state before it absorbs the additional photons that ultimately lead to ionization [9, 10]. Theoretical investigations of multiphoton ionization in molecules are scarce due to the difficulty to account for both electronic and nuclear degrees of freedom. Detailed investigations on H<sub>2</sub><sup>+</sup> ionization have been carried out in the infra-red (IR) regime (see [11] and references therein), mainly using low dimensional approaches. In the XUV domain, multiphoton ionization of H<sub>2</sub><sup>+</sup> has been recently studied by solving the time dependent Schrödinger equation (TDSE) within the frozen nuclei approximation (FNA) [12–15] or by including the effect of nuclear vibrations through perturbative [16] as well as non-perturbative [17, 18] approaches. The importance of the nuclear motion in the study of REMPI effects in H<sub>2</sub><sup>+</sup> by using XUV/fs pulses has been recently

investigated by Palacios et al [9, 19] (these authors have recently extended these studies to the H<sub>2</sub> molecule [10]). The results of the latter investigations have shown that, at variance with atoms, electronic resonance effects do not lead to narrow peaks in the photoelectron energy spectra. This is because the electronic resonances are diluted among the different dissociative states. In contrast, resonance effects are perfectly visible when one analyzes the kinetic energy distribution (KED) of the nuclear fragments. None of these full dimensional theoretical studies have analyzed the electron angular distribution arising with such XUV pulses.

The aim of the present work is to theoretically investigate the electron angular distributions arising in two-photon ionization of H<sub>2</sub><sup>+</sup> by XUV/fs laser pulses including all electronic and vibrational degrees of freedom. We will pay special attention to the (1+1) REMPI region. Production of H<sub>2</sub><sup>+</sup> molecules in a well defined vibrational state (e.g.  $v = 0$ ) is now possible and has in fact recently been used to study non ionizing dissociation dynamics [20] and tunnelling ionization [21]. Therefore, the present theoretical predictions should be amenable for comparison with experiment in the near future.

The paper is organized as follows. In section II we describe the theoretical methods used in the present work, in particular how the effect of the nuclear motion is introduced in our solution of the time dependent Schrödinger equation and how the electron angular distributions is extracted from this solution. The results for the angular distribution of photoelectrons, both differential in and integrated over the proton kinetic energy, are presented and discussed in section III. Conclusions are drawn in section IV. Atomic units are used throughout unless otherwise stated.

## II. THEORY

We restrict our study to two-photon ionization of H<sub>2</sub><sup>+</sup> from the  $X^2\Sigma_g^+(1s\sigma_g)$  ground state using linearly polar-

\*Present address: Department of Physics and Technology, University of Bergen, N-5007 Bergen, Norway

ized light within the dipole approximation. We only consider the case of  $\text{H}_2^+$  molecules oriented along the polarization direction of the incident light. In this particular case, the dipole selection rule implies that  $\Delta m = 0$  and, therefore, that the first photon couples the initial molecular state to intermediate states of  $\sigma_u$  symmetry and the second photon couples the latter to final states of  $\sigma_g$  symmetry according to the sequence:  $\sigma_g \rightarrow \sigma_u \rightarrow \sigma_g$ . We solve the time-dependent Schrödinger equation (TDSE)

$$i\frac{\partial}{\partial t}\Phi(\mathbf{r}, R, t) = [H + V(t)]\Phi(\mathbf{r}, R, t) \quad (1)$$

where  $H$  is the Hamiltonian of  $\text{H}_2^+$  in the body-fixed frame and  $V(t) = \mathbf{p} \cdot \mathbf{A}(t)$  is the laser-molecule interaction potential in the velocity gauge. The vector  $\mathbf{r}$  indicates all electronic coordinates and  $R$  is the internuclear distance. For a photon energy  $\omega$  and a pulse duration  $T$ , the vector potential  $\mathbf{A}(t)$ , polarized along the vector  $\mathbf{e}_z$  (the direction of the internuclear axis), is defined as

$$\mathbf{A}(t) = \begin{cases} A_0 \cos^2\left(\frac{\pi}{T}t\right) \cos(\omega t)\mathbf{e}_z; & t \in [-T/2, +T/2] \\ 0; & \text{elsewhere.} \end{cases} \quad (2)$$

The time-dependent molecular wave function  $\Phi(\mathbf{r}, R, t)$  is expanded in the basis of stationary states  $\Psi_{nv_n}(\mathbf{r}, R)$ :

$$\Phi(\mathbf{r}, R, t) = \sum_n \sum_{v_n} c_{nv_n}(t) \Psi_{nv_n}(\mathbf{r}, R) \exp[-iW_{nv_n} t] + \sum_l \int d\varepsilon \sum_{v_\varepsilon} c_{\varepsilon v_\varepsilon}^l(t) \Psi_{\varepsilon v_\varepsilon}^l(\mathbf{r}, R) \exp[-iW_{\varepsilon v_\varepsilon} t] \quad (3)$$

where the first term is a summation over bound electronic states (and their corresponding vibrational states, including the dissociation continuum) and the second one is an integral over electronic continuum states for all  $l$  (including again the corresponding vibrational states). Substituting this expansion in the TDSE and neglecting non adiabatic couplings leads to a system of coupled differential equations that must be integrated over the whole pulse duration  $T$  to obtain the unknown coefficients  $c_{nv_n}$  and  $c_{\varepsilon v_\varepsilon}^l$ .

The methods we have used to solve the TDSE and obtain the stationary states used in the above expansion of the time dependent wave function are the same as those described in detail in Ref. [19]. Here we only summarize the main ingredients, paying special attention to the extraction of angular differential ionization probabilities. Neglecting rotational effects, the stationary states are written in the Born-Oppenheimer (BO) approximation:

$$\Psi_{nv_n}(\mathbf{r}, R) = R^{-1} \chi_{v_n}(R) \psi_n(\mathbf{r}, R) \quad (4)$$

where  $\psi_n$  and  $\chi_{v_n}$  are the usual electronic and nuclear BO wave functions. For a given value of  $R$ , the electronic continuum states of energy  $\varepsilon_n(R)$  satisfy the usual boundary conditions corresponding to a single incoming (outgoing) spherical wave with a well defined value of

the angular momentum  $l$  and a combination of outgoing (incoming) spherical waves for all possible values of the angular momentum that are compatible with the molecular symmetry (see [22] for details).

In the ionization channel, the density of probability differential in both the proton kinetic energy and the solid angle of the emitted electron is given by

$$\frac{d^2 P}{dE_{\text{H}^+} d\Omega} = \int d\varepsilon \left| \sum_l i^{-l} e^{-i\sigma_l} Y_{l0}(\hat{k}_e) c_{\varepsilon v_\varepsilon}^l(t = T/2) \right|^2 \quad (5)$$

where  $E_{\text{H}^+}$  is the center-of-mass energy of the outgoing protons,  $\Omega$  is the solid angle of the ionized electron,  $\hat{k}_e$  is the corresponding wave vector direction, and  $\sigma_l$  is the Coulomb phase shift

$$\sigma_l = \arg \Gamma(l + 1 + iZ/k_e). \quad (6)$$

with  $Z = 2$ . Integrating equation (5) over the solid angle gives the density of probability differential in the proton kinetic energy,

$$\frac{dP}{dE_{\text{H}^+}} = \sum_l \int d\varepsilon |c_{\varepsilon v_\varepsilon}^l(t = T/2)|^2 \quad (7)$$

and integrating further over vibrational energy gives the total ionization probability  $P$ , which is related to the cross section  $\sigma(\text{cm}^4\text{s}) = (\omega/I)^2(C/T)P$ , where  $I$  is the laser intensity in  $\text{Wcm}^{-2}$ ,  $T$  is the pulse duration in seconds,  $\omega$  is the photon energy in joules and  $C = \frac{128}{35}$  is a dimensionless coefficient.  $T/C$  is an effective pulse duration [23] that takes into account the time dependence of the intensity.

All wave functions have been evaluated using B-spline basis sets following the procedures described in [24]. Briefly, vibrational wave functions have been expanded in a basis of 300 B-splines of order  $k = 8$ , contained in a box of 14 a.u.. Bound electronic states have been represented through a one-center expansion that includes spherical harmonics from  $l = 0$  to  $l = 12$ . The corresponding radial parts have been expanded in a basis of 140 B-splines of order  $k = 8$  in a box of radial length of 60 a.u.. By changing the box size and/or the number of basis functions, we have checked that this basis set leads to practically converged energies in the Franck-Condon (FC) region. For the final continuum states, we have used the  $L^2$  close-coupling method (see [22] and references therein) in which each channel is represented in the same B-spline basis as that used for bound states. The resulting continuum states have the correct asymptotic behavior and exactly include inter-channel coupling within the box [22].

### III. RESULTS AND DISCUSSION

We have solved the TDSE for various photon energies, laser intensities and pulse durations. We will concentrate on (1+1) REMPI processes similar to that shown

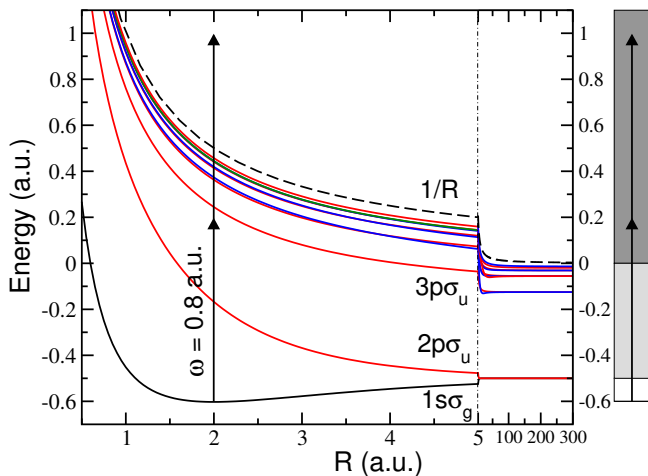


FIG. 1: *Color online:* Potential energy curves of  $\text{H}_2^+$  as functions of internuclear distance. The figure shows the ground state, the ten lowest states of  $\sigma_u$  symmetry, and the ionization threshold  $1/R$ . A typical two-photon transition leading to (1+1)-REMPI is illustrated by arrows. The two shadowed areas in the right hand side column indicate dissociation and ionization+dissociation energy regions.

in Fig. 1 and, in particular, on the resonance features induced by the two lowest  ${}^2\Sigma_u^+$  states of  $\text{H}_2^+$ . Figure 2 shows the electron angular distributions corresponding to different energies of the outgoing protons and three different photon energies,  $\omega = 0.7$ , 0.8 and 0.88 a.u.. In all cases, the laser intensity is  $10^{12} \text{ Wcm}^{-2}$  and the pulse duration 10 fs. To better understand the origin of the different structures observed in the angular distributions, the latter have been superimposed to the angle-integrated ionization probabilities differential in the proton kinetic energy. As explained in [9], the different peaks observed in the angle-integrated probability represent different physical processes: (i) direct non resonant two photon ionization (denoted by V), (ii) (1+1)-REMPI through the  ${}^2\Sigma_u^+(2p\sigma_u)$  state (denoted by  $R_1$ ), and (iii) (1+1)-REMPI through the  ${}^2\Sigma_u^+(3p\sigma_u)$  state (denoted by  $R_2$ ). It can be seen that, for proton energies lying in the non resonant region V, the photoelectron angular distribution follows the polarization direction and exhibits an almost pure  $d$  shape. This distribution is not very different to that observed in non resonant two-photon ionization of two-electron atomic systems like, e.g.,  $\text{H}^-$  [25]. In contrast, for proton energies lying in the  $R_1$  and  $R_2$  resonance regions, the angular distribution is completely different: electrons are not only ejected along the polarization direction but also in a plane perpendicular to it. This behavior results from the important mixing between the  $l = 0$  and  $l = 2$  partial waves. Similar conclusions are obtained for the three photon energies considered in Fig. 2. It is important to stress here that the signature of the (1+1)-REMPI process is observed even though the photon energy does not match a vertical transition from the  $X {}^2\Sigma_g^+$  ground state to any of the  ${}^2\Sigma_u^+$  intermediate

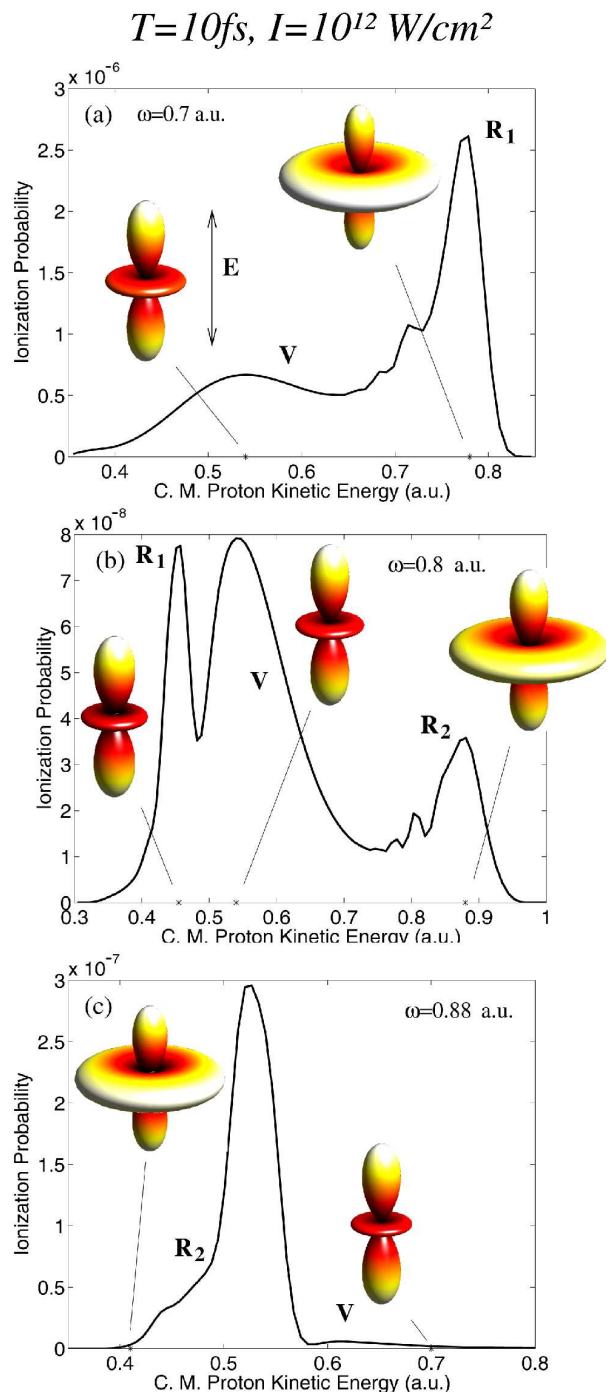


FIG. 2: *Color online:* Electron angular distributions corresponding to different energies of the outgoing protons for a laser intensity of  $10^{12} \text{ Wcm}^{-2}$  and pulse duration 10 fs. Three different photon energies have been considered: (a)  $\omega = 0.7$ , (b) 0.8 and (c) 0.88 a.u.. The angular distributions are superimposed to the angle-integrated ionization probabilities differential in the proton kinetic energy. C.M. means center of mass.

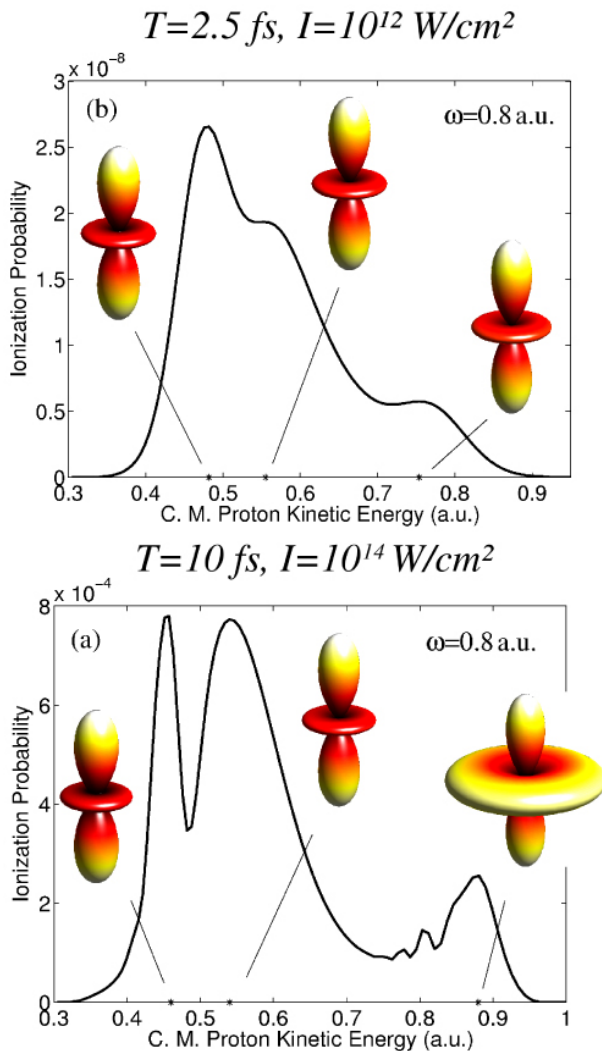


FIG. 3: *Color online:* Electron angular distributions corresponding to different energies of the outgoing protons for a laser intensity and pulse duration of (a)  $10^{14} \text{ Wcm}^{-2}$  and 2.5 fs, respectively, and (b)  $10^{12} \text{ Wcm}^{-2}$  and 10 fs. In both cases, the photon energy is  $\omega = 0.8 \text{ a.u.}$ . The angular distributions are superimposed to the angle-integrated ionization probabilities differential in the proton kinetic energy. C.M. means center of mass.

states. The reason why the REMPI process is still visible under these circumstances is that the absorbed energy is shared by the electron and the nuclei. In practice, the energy sharing is only effective in the Franck-Condon region, but provided we are in that region, there is always a particular energy sharing for which a perfectly resonant electronic transition is possible at that photon energy.

For a pulse duration of 10 fs, the molecule has enough time to vibrate in the  ${}^2\Sigma_u^+$  state resonantly populated by absorption of the first photon. This leads to the complex angular behavior shown in Fig. 2 near the  $R_1$  and  $R_2$  peaks. By reducing the pulse duration, there is less and less time to vibrate in the intermediate state and, therefore,

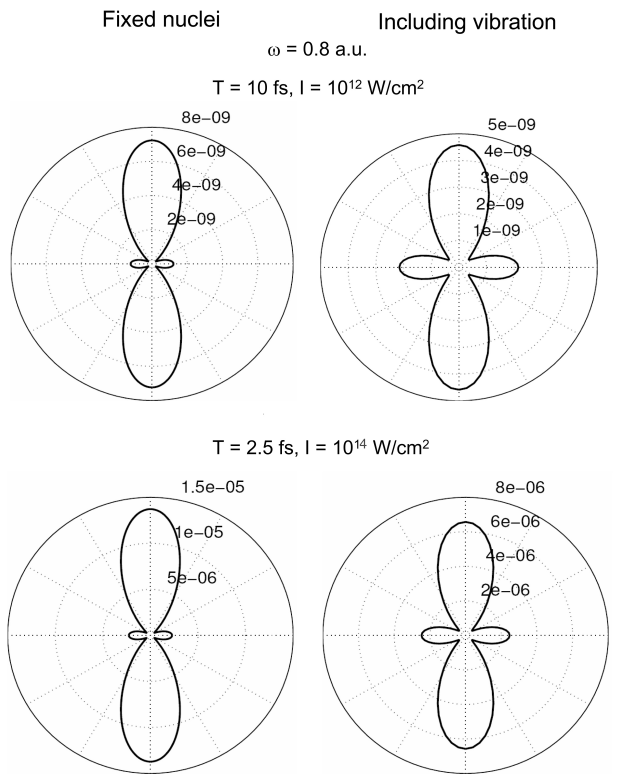


FIG. 4: Electron angular distributions integrated over proton kinetic energy. The photon energy is  $\omega = 0.8 \text{ a.u.}$ . Top:  $I = 10^{12} \text{ Wcm}^{-2}$  and  $T = 10 \text{ fs}$ . Bottom:  $I = 10^{14} \text{ Wcm}^{-2}$  and  $T = 2.5 \text{ fs}$ . The left two panels show results obtained within the fixed-nuclei approximation.

fore, one would expect, for all proton energies, an angular distribution similar to that of the non resonant process. This is illustrated in Fig. 3a where we show our results for a pulse of 2.5 fs and the same intensity. Not only are the  $R_1$  and  $R_2$  peaks diluted in the broad structure observed in the angle-integrated probability, but also the angular distribution is practically the same for all proton energies. A similar behavior is obtained when one increases the laser intensity keeping the pulse duration at 10 fs (see Fig. 3b). In this case, the higher intensity makes ionization more efficient and, therefore, there are less molecules that remain long enough in the intermediate state. As a consequence, the  $d$ -like distribution associated with the direct two-photon ionization process dominates.

It is also interesting to use the present results to check the validity of the fixed nuclei approximation (FNA), which is widely used to interpret ionization processes in molecular systems. In general, total ionization probabilities resulting from the FNA do not differ significantly from those obtained by including the nuclear motion, except in the resonance regions where the FNA leads to sharp peaks that are not physical [19]. Obviously, the FNA cannot be used to obtain probabilities that are dif-

ferential in the kinetic energy of the ionic fragments. But what about the electron angular distributions integrated over kinetic energy of these fragments? To answer this question, we show in Fig. 4 a comparison between the electron angular distributions obtained in the FNA and those resulting from the integration of the probabilities shown in Figs. 2 and 3 over proton energy. It can be seen that, apart from the absolute value of the calculated probabilities, the shapes of the angular distribution are very similar in both types of calculations and for both the longer and the shorter pulse. It is also apparent that, by integrating the angular distributions over proton energy, the signature of the REMPI effect disappears completely. We have checked that this is the case for all photon energies investigated in this work. Therefore, the only way to observe REMPI effects in the electron angular distribution is to analyze in addition the energy of the outgoing protons.

#### IV. CONCLUSION

We have theoretically studied the electron angular distribution that arises in resonance enhanced two-photon ionization of  $H_2^+$  molecules oriented along the polarization vector by using ultrashort laser pulses in the XUV frequency domain. The theoretical method includes all electronic and vibrational degrees of freedom. We have

found that the signature of the (1+1)-REMPI effect is to produce complex angular distributions that differ significantly from those observed in the direct two-photon ionization process (which have in term a marked atom-like character). The peculiar angular distributions associated with the REMPI process can only be observed by analyzing at the same time the proton kinetic energy distribution of the outgoing protons. Indeed, integration of the calculated fully differential probability over proton kinetic energy washes out the signature of the REMPI effect, thus suggesting that electron angular distributions obtained within the fixed-nuclei approximation are not appropriate to investigate this process. Interestingly, by analyzing the electron angular distributions as functions of proton energy, it is possible to observe REMPI even at photon energies that do not correspond necessarily to vertical transitions between two electronic states of the molecule. More theoretical work is needed to see if these predictions are of general validity.

#### Acknowledgments

Work supported by the DGI (Spain) project no. BFM2003-00194, the European COST action D26/0002/02, and the Norwegian Research Council. We thank the CCC-UAM (Madrid, Spain) for computer time.

- 
- [1] P. Agostini and L. F. DiMauro, *Rep. Prog. Phys.* **67**, 813 (2004).
  - [2] R. Klenberger, E. Goulielmakis, M. Uiberacker, A. Baltuska, V. Yakovlev, F. Bammer, A. Scrinzi, T. Westerwalbesloh, U. Kleineberg, U. Heinzmann, et al., *Nature* **427**, 817 (2004).
  - [3] J. Andruszkow et al., *Phys. Rev. Lett.* **85**, 3825 (2000).
  - [4] H. Wabnitz, L. Bittner, A. R. B. de Castro, R. Döhrmann, P. Gürtler, T. Laarmann, W. Laasch, J. Schulz, A. Swiderski, K. von Haeften, et al., *Nature* **420**, 482 (2002).
  - [5] V. Ayvazyan et al., *Phys. Rev. Lett.* **88**, 104802 (2002).
  - [6] N. Miyamoto, M. Kamei, D. Yoshitomi, T. Kanai, T. Sekikawa, T. Nakajima, and S. Watanabe, *Phys. Rev. Lett.* **93**, 083903 (2004).
  - [7] Y. Nabekawa, H. Hasegawa, E. J. Takahashi, and K. Midorikawa, *Phys. Rev. Lett.* **94**, 043001 (2005).
  - [8] K. Hoshina, A. Hishikawa, K. Kato, T. Sako, K. Yamamoto, E. J. Takahashi, Y. Nabekawa, and K. Midorikawa, *J. Phys. B* **39**, 813 (2006).
  - [9] A. Palacios, H. Bachau, and F. Martín, *J. Phys. B* **38**, L99 (2005).
  - [10] A. Palacios, H. Bachau, and F. Martín, *Phys. Rev. Lett.* **96**, 173201 (2006).
  - [11] A. D. Bandrauk, S. Chelkowski, and I. Kawata, *Phys. Rev. A* **67**, 013407 (2003).
  - [12] D. Dundas, J. F. McCann, J. Parker, and K. T. Taylor, *J. Phys. B* **33**, 3261 (2000).
  - [13] J. Colgan, M. S. Pindzola, and F. Robicheaux, *Phys. Rev. A* **68**, 063413 (2003).
  - [14] S. Barmaki, S. Laulan, H. Bachau, and M. Ghalim, *J. Phys. B* **36**, 817 (2003).
  - [15] S. Selstø, M. Førre, J. P. Hansen, and L. B. Madsen, *Phys. Rev. Lett.* **95**, 093002 (2005).
  - [16] A. Apalategui, A. Saenz, and P. Lambropoulos, *J. Phys. B* **33**, 2791 (2000).
  - [17] S. Barmaki, H. Bachau, and M. Ghalim, *Phys. Rev. A* **69**, 043403 (2004).
  - [18] S. Selstø, J. F. McCann, M. Førre, J. P. Hansen, and L. B. Madsen, *Phys. Rev. A* **73**, 033407 (2006).
  - [19] A. Palacios, S. Barmaki, H. Bachau, and F. Martín, *Phys. Rev. A* **71**, 063405 (2005).
  - [20] K. Sändig, H. Figger, and T. W. Hänsch, *Phys. Rev. Lett.* **85**, 4876 (2000).
  - [21] B. Fabre, J. H. Posthumus, L. Malfaire, E. M. Staicu-Casagrande, J. Jureta, C. Cornaggia, E. Baldit, and X. Urbain, *Laser Phys.* **14**, 468 (2004).
  - [22] F. Martín, *J. Phys. B* **32**, R197 (1999).
  - [23] L. B. Madsen and P. Lambropoulos, *Phys. Rev. A* **59**, 4574 (1999).
  - [24] H. Bachau, E. Cormier, P. Decleva, J. E. Hansen, and F. Martín, *Rep. Prog. Phys.* **64**, 1815 (2001).
  - [25] I. Sánchez, H. Bachau, and F. Martín, *J. Phys. B* **30**, 2417 (1997).



# Appendices



## Appendix A

# Derivation of the Non-Dipole Form of the Kramers-Henneberger Hamiltonian

We intend to show how the transition from the velocity gauge description of the Hamiltonian, Eq. 3.15), to the Karmers-Henneberger form, Eq. (3.29), can be made without neglecting the spatial dependence of the electromagnetic field. Atomic units are used throughout this appendix.

The non-dipole form of the Kramers-Henneberger Hamiltonian is defined by Eqs. (3.24), (3.27) and (3.33).

For simplicity we assume that the laser field propagates along the  $x$ -axis with the polarisation along the  $z$ -axis,

$$\mathbf{A}(x, t) = A(kx - \omega t) \hat{\mathbf{z}}, \quad (\text{A.1})$$

with  $k$  and  $\omega$  satisfying  $\omega/k = c$ . With this, the transformation is defined by

$$\begin{aligned} T &= \exp(-i\alpha p_z) \\ \alpha(\eta) &= \frac{q}{\omega m} \int_{\eta_0}^{\eta} A(\eta') d\eta' \\ \eta &= \omega t - kx, \end{aligned}$$

and the new Hamiltonian reads

$$H_{\text{KH}} = T \frac{p^2}{m} T^\dagger - T \frac{q}{m} A(x, t) p_z T^\dagger + T \frac{q}{2m} A^2 T^\dagger + T V T^\dagger - i T \dot{T}^\dagger. \quad (\text{A.2})$$

Since the vector field is independent of  $z$ , the transformation leaves the second and third term above unaltered.

This could also be seen by using the Baker-Hausdorff lemma (24),

$$e^{\lambda A} B e^{-\lambda A} = B + \frac{\lambda}{1!} [A, B] + \frac{\lambda^2}{2!} [A, [A, B]] + \frac{\lambda^3}{3!} [A, [A, [A, B]]] + \dots, \quad (\text{A.3})$$

which will prove quite useful in the following.

The last term in Eq. A.2 is calculated as

$$-i T \dot{T}^\dagger = -iT \frac{\partial}{\partial t} \sum_{n=0}^{\infty} \frac{1}{n!} (i\alpha p_z)^n = -iT \sum_{n=1}^{\infty} \frac{1}{n!} n (i\alpha p_z)^{n-1} \left( \frac{\partial}{\partial t} (i\alpha p_z) \right) =$$

$$T \sum_{n=0}^{\infty} \frac{1}{n!} (i\alpha p_z)^n \frac{q}{m} Ap_z$$

Once again, since  $\alpha p_z$  and  $Ap_z$  commute, the term is simplified to

$$\frac{q}{m} Ap_z T T^\dagger = \frac{q}{m} Ap_z,$$

which cancels the second term in Eq. (A.2).

It is well known that spatial translation can be described as

$$\exp(-i \mathbf{a} \cdot \mathbf{p}) \Psi(\mathbf{r}) = \Psi(\mathbf{r} - \mathbf{a}) \quad (\text{A.4})$$

Hence we expect the transformation of the potential to amount to a translation by  $\boldsymbol{\alpha}$ . This is indeed the case for our particular field, Eq. A.1, though one may suspect that the spatial dependence of the field may give raise to terms with derivatives of  $\boldsymbol{\alpha}$  in the expansion of  $T$ . As can be seen by mathematical induction, the  $n$ -th commutator in Eq. A.3 is  $\alpha^n \partial^n V / \partial z^n$ , so that  $TVT^\dagger$  takes the form of a Taylor expansion:

$$TV(\mathbf{r})T^\dagger = \sum_{n=0}^{\infty} \frac{1}{n!} \left. \frac{\partial^n V}{\partial z^n} \right|_{\mathbf{r}} \alpha_z^n = V(\mathbf{r} - \boldsymbol{\alpha}).$$

The kinetic energy term,

$$T p^2 T^\dagger = (T p_x T^\dagger) (T p_x T^\dagger) + T (p_y^2 + p_z^2) T^\dagger,$$

does not simplify as nicely as the other ones. Since  $\alpha$  depends on  $x$ , the  $p_x$ -contribution is modified. By Eq. (A.3) we find that  $T p_x T^\dagger = p_x - \partial\alpha/\partial x p_z$ , so that the final Hamiltonian reads

$$\begin{aligned} H_{KH} &= \frac{1}{2m} p^2 + \frac{q^2}{2m} (A(x, t))^2 + V(\mathbf{r} - \boldsymbol{\alpha}(\mathbf{r}, t)) + \\ &\quad \frac{1}{2m} \left( \left( \frac{\partial\alpha(x, t)}{\partial x} \right)^2 p_z^2 + i \frac{\partial^2\alpha(x, t)}{\partial x^2} p_z - 2 \frac{\partial\alpha(x, t)}{\partial x} p_x p_z \right). \end{aligned} \quad (\text{A.5})$$

The general Hamiltonian can be written as Eq. (3.34), which may be generalised further to elliptically polarised light of arbitrary propagation direction and to any number of particles.

In many cases the three last terms, which contain directional derivatives in the position representation of the operator, may be neglected. The first two are both proportional to  $k^2 = w^2/c^2$ , whereas the last term is of order  $2\alpha_{\max} k v^2$  where  $v$  is the velocity of the particle. We expect the last one to be the dominant. From the ratio between this term and the kinetic energy term we arrive at the following criterion for neglecting all three terms:

$$\frac{|q| E_{\max}}{\omega m c} \ll 1.$$

This also ensures the validity of a non-relativistic treatment. It may also be argued, at least for high frequencies, that the dominant term is probably the first of these three terms since it is the only term that is not zero on average. This leads to the somewhat less restrictive criterion.

$$\left( \frac{q E_{\max}}{\omega m c} \right)^2 \ll 1.$$

## Appendix B

# Separation of the Schrödinger Equation for Two Particles in a Spatially Dependent Field

In Sect. 3.3.2, we arrived at an expression for the Hamiltonian of two particles subject to the field  $\mathbf{A}(x, t)$  to first order in  $\omega x/c$ . For convenience we re-write the equations here:

$$H = H' + h' + \left( \frac{Q^2}{2M} + \frac{\tilde{q}^2}{2\mu} \right) A_0^2 - \frac{\tilde{q}}{M} \mathbf{P} \cdot \mathbf{E}_0 \frac{x}{c} - \frac{\tilde{q}}{\mu} \mathbf{p} \cdot \mathbf{E}_0 \frac{X}{c} \quad (\text{B.1})$$

$$H' \equiv \frac{1}{2M} P^2 - \frac{Q}{M} \mathbf{P} \cdot \left( \mathbf{A}_0 + \mathbf{E}_0 \frac{X}{c} \right) + \left( \frac{Q^2}{M} + \frac{\tilde{q}^2}{\mu} \right) A_0 E_0 \frac{X}{c} \quad (\text{B.2})$$

$$h' \equiv \frac{1}{2\mu} p^2 + V_C(r) - \frac{\tilde{q}}{\mu} \mathbf{p} \cdot \mathbf{A}_0 - \frac{q'}{\mu} \mathbf{p} \cdot \mathbf{E}_0 \frac{x}{c} + \left( \frac{Q\tilde{q}}{M} + \frac{\tilde{q}q'}{\mu} \right) A_0 E_0 \frac{x}{c}. \quad (\text{B.3})$$

with

$$\begin{aligned} Q &= q_1 + q_2 \\ \tilde{q} &= \frac{q_1 m_2 - q_2 m_1}{m_1 + m_2} \\ q' &= \frac{q_1 m_2^2 + q_2 m_1^2}{(m_1 + m_2)^2}. \end{aligned}$$

Equation (B.1) includes two cross terms which prohibit separation; they must be neglected in order to separate the Schrödinger equation. Of course, whether this is admissible depends on the particular system and field at hand. One special case deserves special attention.

### Systems with no reduced charge.

For systems with  $\tilde{q} = 0$ , the two terms prohibiting separation in Eq. (B.1) vanish, and separation may be done without other approximations than the first order expansion, Eqs. (3.36) and (3.37). The most obvious example of such systems are those consisting of two identical particles. However, there are also other exotic examples such as, e.g., an alpha and a deuterium particle.

### Charged systems.

A system with a total charge  $Q \neq 0$  will essentially feel the effect of the field as a whole. In the velocity gauge, the generalised momentum of the centre of mass motion is given by  $\mathbf{P} = M\dot{\mathbf{R}} + q_1\mathbf{A}(\mathbf{r}_1) + q_2\mathbf{A}(\mathbf{r}_2)$  (see Eqs. (3.11) and (3.18)). From a classical consideration, in which we neglect the spatial dependence of  $\mathbf{A}$ , we estimate that  $\langle \dot{R}_{\hat{\mathbf{E}}} \rangle \sim -Q/M A$ , where the subscript indicates the component parallel with the field. Consequently, both the expectation value,  $\langle P_{\hat{\mathbf{E}}} \rangle$ , and the width of its distribution vanish. From this we expect that first order terms involving the operator  $P_{\hat{\mathbf{E}}}$  are dominated by first order spatial terms that do not involve momentum operators.

The same reasoning may be applied to the relative motion as well – at least in the limit that the field dominates the Coulomb interaction. This argument is due to Vázquez de Aldana et al., (35), who conclude that the  $x/\mu c \mathbf{p} \cdot \mathbf{E}$  interaction in atomic hydrogen may be disregarded for strong fields. The same conclusion is reached by Buagacov et al., (61), but with a seemingly different argument. The assumption is supported by calculations made by Meharg et al. (62) and Førre et al. (paper II in this thesis). In this way also the last term of Eq. (B.1) may be neglected upon comparison to, e.g., the last term of Eq. (B.2).

### Neutral systems.

For systems with no net charge, such as the hydrogen atom, the CoM motion is little influenced by the field. Hence, the reason we used in the prior case for neglecting the second last term of Eq. (B.1) no longer applies. However, inspired by Reiss (34), we may suggest that the expectation value of the velocity is thermal so that its "root mean square" (rms) value may be estimated by the equipartition principle,  $1/2 M \dot{R}_{\hat{\mathbf{E}}} = 1/2 kT$  where  $k$  is the Boltzmann constant and  $T$  is temperature. Doing so, the ratio between this term and the time averaged rms value of the last term of Eq. (B.3) (with  $Q = 0$ ) may serve as a measure of the separability. We obtain the following criterion:

$$\frac{\mu\omega}{|q'|E_{\max}} \sqrt{\frac{kT}{M}} \ll 1, \quad (\text{B.4})$$

where the reduced mass  $\mu$  is defined in Eq. (3.21),  $\omega$  is the frequency of the field and  $E_{\max}$  is the maximal value of the electric field. For a hydrogen atom at room temperature, the criterion reads  $\omega/E_{\max} \ll 1.3 \cdot 10^3$  a.u.. We see that the separability is increasingly justified for increasing field strength. It should be pointed out that separation certainly is admissible also in the limit  $E \rightarrow 0$ .

The inequality (B.4) indicates that separation is rather difficult for systems consisting of a particle - antiparticle pair. Furthermore, for such systems, no first order contributions are present in the part of the Hamiltonian corresponding to the relative coordinate, so any non-dipole treatment of such systems should include all six spatial variables.